

Application of Surface Complexation Modeling to Selected Radionuclides and Aquifer Sediments

Application of Surface Complexation Modeling to Selected Radionuclides and Aquifer Sediments

Manuscript Completed: January 2008
Date Published: April 2008

Prepared by
J.A. Davis

U.S. Geological Survey
Menlo Park, Ca 94025

M. Fuhrmann, NRC Project Manager

NRC Job Code Y6462

**AVAILABILITY OF REFERENCE MATERIALS
IN NRC PUBLICATIONS**

NRC Reference Material

As of November 1999, you may electronically access NUREG-series publications and other NRC records at NRC's Public Electronic Reading Room at <http://www.nrc.gov/reading-rm.html>. Publicly released records include, to name a few, NUREG-series publications; *Federal Register* notices; applicant, licensee, and vendor documents and correspondence; NRC correspondence and internal memoranda; bulletins and information notices; inspection and investigative reports; licensee event reports; and Commission papers and their attachments.

NRC publications in the NUREG series, NRC regulations, and *Title 10, Energy*, in the Code of *Federal Regulations* may also be purchased from one of these two sources.

1. The Superintendent of Documents
U.S. Government Printing Office
Mail Stop SSOP
Washington, DC 20402-0001
Internet: bookstore.gpo.gov
Telephone: 202-512-1800
Fax: 202-512-2250
2. The National Technical Information Service
Springfield, VA 22161-0002
www.ntis.gov
1-800-553-6847 or, locally, 703-605-6000

A single copy of each NRC draft report for comment is available free, to the extent of supply, upon written request as follows:

Address: Office of the Chief Information Officer,
Reproduction and Distribution
Services Section
U.S. Nuclear Regulatory Commission
Washington, DC 20555-0001
E-mail: DISTRIBUTION@nrc.gov
Facsimile: 301-415-2289

Some publications in the NUREG series that are posted at NRC's Web site address <http://www.nrc.gov/reading-rm/doc-collections/nuregs> are updated periodically and may differ from the last printed version. Although references to material found on a Web site bear the date the material was accessed, the material available on the date cited may subsequently be removed from the site.

Non-NRC Reference Material

Documents available from public and special technical libraries include all open literature items, such as books, journal articles, and transactions, *Federal Register* notices, Federal and State legislation, and congressional reports. Such documents as theses, dissertations, foreign reports and translations, and non-NRC conference proceedings may be purchased from their sponsoring organization.

Copies of industry codes and standards used in a substantive manner in the NRC regulatory process are maintained at—

The NRC Technical Library
Two White Flint North
11545 Rockville Pike
Rockville, MD 20852-2738

These standards are available in the library for reference use by the public. Codes and standards are usually copyrighted and may be purchased from the originating organization or, if they are American National Standards, from—

American National Standards Institute
11 West 42nd Street
New York, NY 10036-8002
www.ansi.org

Legally binding regulatory requirements are stated only in laws; NRC regulations; licenses, including technical specifications; or orders, not in NUREG-series publications. The views expressed in contractor-prepared publications in this series are not necessarily those of the NRC.

The NUREG series comprises (1) technical and administrative reports and books prepared by the staff (NUREG-XXXX) or agency contractors (NUREG/CR-XXXX), (2) proceedings of conferences (NUREG/CP-XXXX), (3) reports resulting from international agreements (NUREG/IA-XXXX), (4) brochures (NUREG/BR-XXXX), and (5) compilations of legal decisions and orders of the Commission and Atomic and Safety Licensing Boards and of Directors' decisions under Section 2.206 of NRC's regulations (NUREG-0750).

212-642-4900

DISCLAIMER: This report was prepared as an account of work sponsored by an agency of the U.S. Government. Neither the U.S. Government nor any agency thereof, nor any employee, makes any warranty, expressed or implied, or assumes any legal liability or responsibility for any third party's use, or the results of such use, of any information, apparatus, product, or process disclosed in this publication, or represents that its use by such third party would not infringe privately owned rights.

ABSTRACT

Several different surface complexation modeling approaches exist to describe the adsorption of solutes from water onto the surfaces of mineral phases. The Generalized Composite surface complexation modeling approach considers the surfaces of a mixed mineral assemblage, such as soils or sediments, to contain generic functional groups with averaged properties (see demonstration of this approach in USNRC, 2003). The objective of the study described in this report was to extend the Generalized Composite modeling approach to other complex geomaterials and other radionuclides. The modeling approach provides the methodology to estimate K_d values and potential retardation of sorbing radionuclides (Np, U, Ni) with complex aqueous chemistry, and as a function of aqueous chemical conditions in groundwaters. Laboratory batch experiments with natural sediments illustrate that the adsorption (and K_d values) are sensitive to aqueous chemical conditions, including pH and the dissolved carbonate concentration (which equilibrates with a given partial pressure of carbon dioxide in the gas phase). Complex geomaterials in this study included aquifer sediments from: 1) the Naturita (Colorado) UMTRA site, 2) the Forty-Mile Wash (Nye County, Nevada) aquifer, and 3) the USGS research site at Cape Cod (Massachusetts).

Generalized Composite surface complexation models (GC-SCM) were developed for the following radionuclide/geomaterial pairs, as examples of the modeling approach: 1) Np(V)/Naturita aquifer sediments, 2) U(VI)/Forty-Mile Wash aquifer sediments, and 3) Ni/Cape Cod aquifer sediments. In each case the models were calibrated by fitting batch adsorption data as a function of chemical conditions. In all cases, the GC-SCM were developed without electrical double layer terms.

In the case of Np(V)/Naturita aquifer sediments, the GC-SCM was able to accurately simulate K_d values for Np(V) adsorption on the sediments over a range of pH and dissolved carbonate and Np(V) concentrations using three Np(V) surface reactions and two surface sites for each reaction (strong- and weak-binding). Unlike U(VI), the sorption of Np(V) was found to be much less sensitive to the dissolved carbonate concentration. Part of the reason for this limited dependence on dissolved carbonate may be the Np(V) forms both aqueous and surface (ternary) carbonate complexes. The effect of humic acids on Np(V) sorption was also studied. Like carbonate, Np(V) sorption was not influenced (decreased) as much by aqueous Np(V)-humic aqueous complexation as might have been expected, indicating that ternary surface-Np(V)-humic complexes may form on mineral surfaces.

In the case of the U(VI)/Forty-Mile Wash aquifer sediments, the GC-SCM produced good agreement with the experimental data for U(VI) adsorption as a function of pH, dissolved carbonate, and U(VI) concentration with only one U(VI) surface reaction with two surface sites that formed strong and weak complexes. The K_d values decreased significantly with increasing carbonate or U(VI) concentrations, but the GC-SCM was able to simulate the dependence of K_d on these variables. In the case of the Ni/Cape Cod aquifer sediments, Ni K_d values increased with increasing pH and with decreasing Ni concentration. A very simple GC-SCM was calibrated to the experimental data, with one Ni surface species and only one site type. Addition of more reactions or more sites did not improve the goodness-of-fit to the data collected. Aqueous complexation of Ni with sulfate ions in the groundwater was considered as a part of the model calculations.

The challenge in applying the surface complexation concept in the environment is to simplify the SCM, such that predicted adsorption is still calculated with mass laws that are coupled with aqueous speciation, while lumping parameters that are difficult to characterize in the environment in with other parameters. In order to be applied by solute transport modelers and within PA applications, the complexity of the

adsorption model needs to be balanced with the goal of using the simplest model possible that is consistent with observed data. This can be achieved with the semi-empirical, site-binding GC modeling approach used in this report and previously demonstrated for modeling U(VI) retardation at the Naturita UMTRA site (Curtis et al., 2006; USNRC, 2003). The GC-SCM is a compromise between the simple constant- K_d approach and more complex SCM that are difficult to apply to the environment at present. The GC modeling approach is preferable to completely empirical approaches, such as the constant- K_d model or adsorption isotherms, because the important linkage between surface and aqueous species (and associated thermodynamic data) is retained in the modeling through the coupling of mass action equations. This linkage also provides a framework for conducting uncertainty analyses that is based on process level parameters rather than on ranges of K_d values that result from lumping together multiple processes. Uncertainty in radionuclide retardation predictions may be reduced, quantified, and more completely understood in the future with the use of the GC-SCM modeling approach.

FOREWORD

The U.S. Nuclear Regulatory Commission (NRC) uses environmental transport models, describing the mass and rate of the movement of contaminants, to evaluate the migration of radionuclides released to the environment from sites that are licensed by the NRC. This report discusses the development of improved methods to describe chemical processes that control radionuclide movement in ground water.

A key process that constrains the movement of dissolved contaminants in a soil is adsorption. In this process, ions associate with solid materials through reactions at the solid surface, and as a result they move more slowly than water moving through the material. The reactions controlling adsorption can vary substantially for different contaminants and can be sensitive to parameters such as pH, ionic strength, and concentrations of other dissolved species. Adsorption is typically described by the distribution coefficient, K_d . This is the concentration of an ion adsorbed on an associated solid divided by its concentration in solution, at steady state. A variety of approaches are used to describe adsorption in models, all of which ultimately assign a K_d value. Simple, constant geochemical conditions can use an empirical K_d , determined through batch experiments with site-specific materials. For better definition of K_d , isotherms can be developed through batch experiments in which some parameter, such as contaminant concentration, is varied. Cases in which several adsorption controlling parameters may change with time or location require more sophisticated approaches. The use of surface complexation models (SCMs) allows the calculation of K_d under these complex conditions, mechanistically describing how K_d changes as conditions are altered. SCMs employ mass action laws and thermodynamics to describe speciation in solution and on the solid, as well as the reactions between them. The family of SCMs ranges from detailed calculations of surface charge and associated adsorption to the semi-empirical approach of the generalized composite SCM (GC-SCM). This latter approach is applicable to mixed mineral assemblages of natural materials and views the mineral surface sites as generic functional groups with averaged properties. This report discusses the GC-SCM.

The work described in this report developed GC-SCMs for three cases of contaminant/sediment combinations—Np(V)/Naturita aquifer sediment, U(VI)/Forty Mile Wash aquifer sediment, and Ni/Cape Cod aquifer sediment. These contaminants provide very different chemistries to test the modeling approach. The models provided good agreement with experimental data and performed satisfactorily in describing adsorption as a function of changing chemical conditions. Using this type of model as an input to performance assessment models will provide more realistic and flexible evaluations of site-specific geochemical processes, leading to better estimates of contaminant behavior.

Christiana Lui, Director
Division of Risk Analysis
Office of Nuclear Regulatory Research
U.S. Nuclear Regulatory Commission

CONTENTS

ABSTRACT.....	iii
FIGURES.....	vii
TABLES.....	xv
1. APPLICATIONS OF SURFACE COMPLEXATION MODELING: SCIENTIFIC BACKGROUND <i>by J. A. Davis</i>	
1.1 INTRODUCTION	1
1.2 SURFACE COMPLEXATION MODELING	3
1.3 PROJECT GOALS.....	4
1.4 OVERVIEW OF REPORT.....	4
2. NEPTUNIUM(V) SORPTION TO AN ALLUVIAL AQUIFER SEDIMENT: APPLICABILITY OF SURFACE COMPLEXATION MODELING <i>by P. B. Moran, B. D. Honeyman, and J. A. Davis</i>	
2.1 BACKGROUND	5
2.1.1 Neptunium Aqueous Geochemistry.....	5
2.1.2 Neptunium(V) Sorption to Pure Mineral Phases	10
2.1.3 Neptunium(V) Sorption to Complex Geomedia	21
2.1.4 Influence of Humic Acids on Neptunium(V) Sorption.....	22
2.1.5 Surface Complexation Modeling of Natural Systems	28
2.2 EFFECT OF SOLUTION COMPOSITION ON NEPTUNIUM(V) SORPTION TO AN ALLUVIAL AQUIFER SEDIMENT.....	28
2.2.1 Aquifer Sediment Sample	28
2.2.2 Materials and Methods.....	29
2.2.2.1 Np(V) Time Dependent Sorption Experiments	32
2.2.2.2 Sorption Isotherm Experiments	32
2.2.2.3 Np(V) Sorption Edge Experiments	33
2.2.2.4 Surface Charge Characterization	33
2.2.2.5 Near Infrared Spectroscopy	35
2.2.3 Results and Discussion	35
2.2.3.1 Oxidation State Confirmation	35
2.2.3.2 Liquid Scintillation Analysis	35
2.2.3.3 Np(V) Time Dependent Sorption	37
2.2.3.4 Time Dependent Sorption in the Presence of Humic Acids	37
2.2.3.5 Np(V) Sorption Isotherm Results	37
2.2.3.6 Np(V) Sorption Edge Results	43
2.2.3.7 Effect of Groundwater Constituents on Np(V) Sorption	51
2.2.4 Summary of Np(V) Sorption Results	52
2.3 SURFACE COMPLEXATION MODELING OF NEPTUNIUM(V) SORPTION IN NATURAL SYSTEMS	55
2.3.1 Introduction	55
2.3.2 Generalized Composite Modeling Approach	55
2.3.3 Effect of Humic Acids Presence	77
2.3.4 Summary of Np(V) Surface Complexation Modeling	81

3. DEVELOPMENT OF A SURFACE COMPLEXATION MODEL FOR URANIUM(VI) SORPTION ONTO FORTY-MILE WASH (NEVADA) AQUIFER SEDIMENTS <i>by M. Kohler, and J. A. Davis</i>	
3.1 MATERIALS AND METHODS.....	83
3.1.1 Sediments.....	83
3.1.2 Artificial Groundwater Solutions	83
3.1.3 Sodium Carbonate Extractions	83
3.1.4 Uranium(VI) Sorption Experiments	83
3.2 RESULTS	84
3.2.1 Uranium(VI) Sorption Kinetics onto Forty-Mile Wash Sediments	84
3.2.2 Uranium(VI) Sorption onto Forty-Mile Wash Sediments at Variable pH and Alkalinity	84
3.3 URANIUM(VI) SURFACE COMPLEXATION MODELING FOR FORTY-MILE WASH SEDIMENTS	88
3.3.1 Introduction.....	88
3.3.2 Modeling Calculations and Approach	89
4 DEVELOPMENT OF A SURFACE COMPLEXATION MODEL FOR NICKEL SORPTION ONTO CAPE COD (MASSACHUSETTS) AQUIFER SEDIMENTS <i>by J. A. Davis and J. Joye</i>	
4.1 MATERIALS AND METHODS.....	95
4.1.1 Preparation of an Aquifer Sediment Composite Sample	95
4.1.2 Nickel Sorption Experiments	95
4.2 RESULTS	95
4.3 SURFACE COMPLEXATION MODEL DEVELOPMENT FOR NICKEL ADSORPTION.....	97
5. CONCLUDING REMARKS AND SUMMARY..... <i>by J. A. Davis</i>	99
REFERENCES.....	103

FIGURES

Figure 2.1	Np(V) species distribution as a function of pH in 0.1 M NaClO ₄ with a total Np(V) concentration of 2.0x10 ⁻⁶ M under CO ₂ -free conditions.....	6
Figure 2.2	Np(V) species distribution as a function of pH in 0.1 M NaClO ₄ with a total Np(V) concentration of 2.0x10 ⁻⁶ M at atmospheric PCO ₂	6
Figure 2.3	Np(V) species distribution as a function of pH in 0.1 M NaClO ₄ with a total Np(V) concentration of 2.0x10 ⁻⁶ M at 2% PCO ₂	7
Figure 2.4	Np(V) species distribution as a function of pH in 0.1 M NaClO ₄ with a total Np(V) concentration of 2.0x10 ⁻⁶ M at 8% PCO ₂	7
Figure 2.5a	Np(V) species distribution as a function of pH in 0.1 M NaClO ₄ with a total Np(V) concentration of 2.0x10 ⁻⁶ M, 10 mg L ⁻¹ HA at atmospheric PCO ₂	9
Figure 2.5b	Np(V) species distribution as a function of pH in 0.1 M NaClO ₄ with a total Np(V) concentration of 2.0x10 ⁻⁶ M, 100 mg L ⁻¹ HA at atmospheric PCO ₂	10
Figure 2.6	Np(V) species distribution as a function of PCO ₂ in 0.1 M NaClO ₄ with 2.0x10 ⁻⁶ M Np(V) and 100 mg L ⁻¹ HA at pH 7 and pH 8	11
Figure 2.7	LSC spectrum showing activity associated with ²³⁷ Np α particle emission and activity associated with background radioactivity and residual ²³³ Pa in a 2.0x10 ⁻⁶ M Np(V) sample	36
Figure 2.8	Series of LSC spectra of 2.0x10 ⁻⁶ M Np(V) in the presence of 10-200 mg L ⁻¹ HA showing varying degrees of color quenching without a reduction in counts	36
Figure 2.9	Time dependent sorption of 5.0x10 ⁻⁷ M Np(V) to 50 g L ⁻¹ unmodified NABS in AGW-3 at pH 8.0 ± 0.1 and atmospheric PCO ₂	38
Figure 2.10	Time dependent sorption of Np(V) to 50 g L ⁻¹ treated NABS in the presence of 10 mg L ⁻¹ HA (pH 8.0 ± 0.1) at atmospheric PCO ₂ with a total Np(V) concentration of 5.0x10 ⁻⁷ M and 0.1 M NaClO ₄	38
Figure 2.11	Comparison of time dependent sorption of 5.0x10 ⁻⁷ M Np(V) with and without 10 mg L ⁻¹ HA at pH 8.0 ± 0.1 and atmospheric PCO ₂ . . .	38
Figure 2.12a	Np(V) sorption isotherms using a maximum range of Np(V) from 3.0x10 ⁻⁷ M to 5.0x10 ⁻⁶ M, 125 g L ⁻¹ unmodified NABS, in AGW-3 (pH 8) at atmospheric PCO ₂ or in AGW-6 (pH 6.8) at 8% PCO ₂	39
Figure 2.12b	K _d values for Np(V) sorption as a function of aqueous Np(V) remaining in solution using a maximum range of Np(V) from 3.0x10 ⁻⁷ M to 5.0x10 ⁻⁶ M, 125 g L ⁻¹ unmodified NABS, in AGW-3 (pH 8) at atmospheric PCO ₂ or in AGW-6 (pH 6.8) at 8% PCO ₂	39

Figure 2.13a	Np(V) sorption isotherms using a maximum range of Np(V) from 2.0×10^{-7} M to 3.0×10^{-6} M, 125 g L^{-1} treated NABS, in AGW-3 (pH 8) at atmospheric PCO_2 or in AGW-6 (pH 6.8) at 8% PCO_2	41
Figure 2.13b	K_d values for Np(V) sorption as a function of aqueous Np(V) remaining in solution using a maximum range of Np(V) from 2.0×10^{-7} M to 3.0×10^{-6} M, 125 g L^{-1} treated NABS, in AGW-3 (pH 8) at atmospheric PCO_2 or in AGW-6 (pH 6.8) at 8% PCO_2	41
Figure 2.14a	Np(V) sorption isotherms using a maximum range of Np(V) from 3.0×10^{-7} M to 5.0×10^{-6} M, 125 g L^{-1} treated and unmodified NABS, in AGW-3, pH 8, at atmospheric PCO_2	42
Figure 2.14b	Np(V) sorption isotherms using a maximum range of Np(V) from 2.0×10^{-7} M to 1.0×10^{-6} M, 125 g L^{-1} treated and unmodified NABS, in AGW-6, pH 6.8, at 8% PCO_2	42
Figure 2.14c	K_d values for Np(V) sorption as a function of aqueous Np(V) remaining in solution using a maximum range of Np(V) from 3.0×10^{-7} M to 5.0×10^{-6} M, 125 g L^{-1} treated and unmodified NABS, in AGW-3 (pH 8) at atmospheric PCO_2	42
Figure 2.14d	K_d values for Np(V) sorption as a function of aqueous Np(V) remaining in solution using a maximum range of Np(V) from 2.0×10^{-7} M to 1.0×10^{-6} M, 125 g L^{-1} treated and unmodified NABS, in AGW-6 (pH 6.8) at 8% PCO_2	42
Figure 2.15	Comparison of U(VI) and Np(V) sorption isotherms using Np(V) concentration range from 3.0×10^{-7} to 3.0×10^{-6} M on 125 g L^{-1} treated NABS and a U(VI) concentration range of 3.0×10^{-7} to 4.0×10^{-6} M on 50 g L^{-1} treated NABS in AGW-3 (pH 8) at atmospheric PCO_2	44
Figure 2.16a	Np(V) sorbed as a function of Np(V) remaining in solution using a maximum range of Np(V) from 8×10^{-7} M to 1×10^{-5} M, 125 g L^{-1} or 500 g L^{-1} unmodified NABS, in AGW-3 (pH 8) at atmospheric PCO_2	44
Figure 2.16b	Np(V) sorption isotherms using a maximum range of Np(V) from 8×10^{-7} M to 1×10^{-5} M, 125 g L^{-1} and 500 g L^{-1} unmodified NABS, in AGW-3 (pH 8) at atmospheric PCO_2	44
Figure 2.17a	Np(V) sorption edges using 5.0×10^{-7} M on 50 g L^{-1} treated NABS in AGW-A at atmospheric PCO_2	45
Figure 2.17b	Np(V) sorption edges using 5.0×10^{-7} M on 125 g L^{-1} treated NABS in AGW-A at atmospheric PCO_2	45
Figure 2.18a	Salt titrations of 500 g L^{-1} treated NABS in 0.001 M NaClO_4 within an inert atmosphere glovebox.....	46
Figure 2.18b	Concentrations of $\text{Al}_{(\text{aq})}$ and SiO_2 in the solution phase of 500 g L^{-1} treated NABS in 0.1 M NaClO_4 at atmospheric PCO_2	46
Figure 2.18c	Concentrations of Ca^{2+} in the solution phase of 500 g L^{-1} treated NABS in 0.1 M NaClO_4 at atmospheric PCO_2	46

Figure 2.19	Sorption to 1 g L ⁻¹ hematite as a function of pH using 5.0x10 ⁻⁷ M Np(V) in 0.1 M NaClO ₄ at atmospheric PCO ₂	46
Figure 2.20a	Sorption edges using 5.0x10 ⁻⁷ M Np(V), 50 g L ⁻¹ and 125 g L ⁻¹ treated NABS in AGW-A at atmospheric PCO ₂	47
Figure 2.20b	Sorption edges using 5.0x10 ⁻⁷ M Np(V) , 50, 125 and 500 g L ⁻¹ treated NABS in AGW-A at atmospheric PCO ₂	47
Figure 2.21a	Np(V) sorption edges using 5.0x10 ⁻⁷ M and 5.0x10 ⁻⁶ M, 50 g L ⁻¹ treated NABS, in AGW-A at atmospheric PCO ₂	48
Figure 2.21b	Np(V) sorption edges using 5.0x10 ⁻⁷ M and 5.0x10 ⁻⁶ M, 125 g L ⁻¹ treated NABS, in AGW-A at atmospheric PCO ₂	48
Figure 2.21c	Np(V) sorption edges using 5.0x10 ⁻⁷ M and 5.0x10 ⁻⁶ M, 500 g L ⁻¹ treated NABS, in 0.1 M NaClO ₄ at atmospheric PCO ₂	48
Figure 2.22	Comparison of U(VI) and Np(V) sorption edges using 5.0x10 ⁻⁷ M, 125 g L ⁻¹ treated NABS in AGW-A at atmospheric PCO ₂	49
Figure 2.23a	Sorption edges using 5.0x10 ⁻⁷ M Np(V), 50 or 125 g L ⁻¹ treated NABS, in 0.1 M NaClO ₄ using a N ₂ atmosphere (CO ₂ -free).....	50
Figure 2.23b	Sorption edges using 5.0x10 ⁻⁷ M Np(V), 125 g L ⁻¹ treated NABS, in 0.1 M NaClO ₄ at atmospheric PCO ₂ or using a N ₂ atmosphere (CO ₂ -free).....	50
Figure 2.24a	Sorption edges using 5.0x10 ⁻⁷ M Np(V), 500 g L ⁻¹ treated NABS, in 0.1 M NaClO ₄ at 8% PCO ₂	51
Figure 2.24b	Comparison of 5.0x10 ⁻⁷ M Np(V) sorption edges at atmospheric and 8% PCO ₂ using 500 g L ⁻¹ treated NABS in 0.1 M NaClO ₄	51
Figure 2.24c	Comparison of 5.0x10 ⁻⁷ M Np(V) sorption edges at atmospheric PCO ₂ using 50 and 125 g L ⁻¹ treated NABS in AGW-3.....	51
Figure 2.25a	Np(V) sorption edges with 5x10 ⁻⁷ M Np(V), 125 g L ⁻¹ treated NABS, in AGW-A, 0.1 M NaClO ₄ or AGW-3 at atmospheric PCO ₂	52
Figure 2.25b	Np(V) sorption edges with 5x10 ⁻⁷ M Np(V), 125 g L ⁻¹ treated NABS, in AGW-A or 0.1 M NaClO ₄ at atmospheric PCO ₂	52
Figure 2.26a	Effect of 10 mg L ⁻¹ and 100 mg L ⁻¹ HA on Np(V) sorption edges using 5.0x10 ⁻⁷ M Np(V), 500 g L ⁻¹ treated NABS, in 0.1 M NaClO ₄ at atmospheric PCO ₂	53
Figure 2.26b	Effect of 10 mg L ⁻¹ and 100 mg L ⁻¹ HA on Np(V) sorption edges using 5.0x10 ⁻⁶ M Np(V), 500 g L ⁻¹ treated NABS, in 0.1 M NaClO ₄ at atmospheric PCO ₂	53
Figure 2.27a	Comparison of HA and Np(V) sorption edges using 100 mg L ⁻¹ HA, 5.0x10 ⁻⁷ M Np(V), 500 g L ⁻¹ treated NABS in 0.1 M NaClO ₄ at atmospheric PCO ₂	54

Figure 2.27b	Comparison of HA and Np(V) sorption edges using 100 mg L ⁻¹ HA, 5.0x10 ⁻⁶ M Np(V), 500 g L ⁻¹ treated NABS in 0.1 M NaClO ₄ at atmospheric PCO ₂	54
Figure 2.28a	Model calibration with a single surface species ($\equiv\text{XOHNpO}_2^+$) and a single data set, 5x10 ⁻⁷ M Np(V), 50 g L ⁻¹ treated NABS in AGW-A at atmospheric PCO ₂	69
Figure 2.28b	Model calibration with a single surface species ($\equiv\text{XOHNpO}_2^+$) and a single data set, 5x10 ⁻⁷ M Np(V), 125 g L ⁻¹ treated NABS in AGW-A at atmospheric PCO ₂	69
Figure 2.29a	Model calibration with a single surface species ($\equiv\text{XONpO}_2$) and a single data set, 5x10 ⁻⁷ M Np(V), 50 g L ⁻¹ treated NABS in AGW-A at atmospheric PCO ₂	69
Figure 2.29b	Model calibration with a single surface species ($\equiv\text{XONpO}_2$) and a single data set, 5x10 ⁻⁷ M Np(V), 125 g L ⁻¹ treated NABS in AGW-A at atmospheric PCO ₂	69
Figure 2.30a	Model calibration with two surface species ($\equiv\text{XOHNpO}_2^+$ and $\equiv\text{XONpO}_2$) and a single data set; 5x10 ⁻⁷ M Np(V), 50 g L ⁻¹ treated NABS in AGW-A at atmospheric PCO ₂	71
Figure 2.30b	Model calibration with two surface species ($\equiv\text{XOHNpO}_2^+$ and $\equiv\text{XONpO}_2$) and a single data set, 5x10 ⁻⁷ M Np(V), 125 g L ⁻¹ treated NABS in AGW-A at atmospheric PCO ₂	71
Figure 2.31a	Model calibration including a neptunyl carbonato ternary surface complex ($\equiv\text{XONpO}_2(\text{HCO}_3)_2^{2-}$) and a single data set, 5x10 ⁻⁷ M Np(V), 50 g L ⁻¹ treated NABS in AGW-A at atmospheric PCO ₂	71
Figure 2.31b	Model calibration including a neptunyl carbonato ternary surface complex ($\equiv\text{XONpO}_2(\text{HCO}_3)_2^{2-}$) and a single data set, 5x10 ⁻⁷ M Np(V), 125 g L ⁻¹ treated NABS in AGW-A at atmospheric PCO ₂	71
Figure 2.32a	Model calibration with both AGW-A data sets, 5x10 ⁻⁷ M Np(V), 50 and 125 g L ⁻¹ treated NABS at atmospheric PCO ₂ , with a 1-site type model.....	72
Figure 2.32b	Model calibration with both AGW-A data sets, 5x10 ⁻⁷ M Np(V), 50 and 125 g L ⁻¹ treated NABS at atmospheric PCO ₂ , 2-site type model with 99% weak and 1% strong sites.....	72
Figure 2.32c	Model calibration with both AGW-A data sets, 5x10 ⁻⁷ M Np(V), 50 and 125 g L ⁻¹ treated NABS at atmospheric PCO ₂ with incorporation of surface protolysis reactions. Surface species include $\equiv\text{XOHNpO}_2^+$, $\equiv\text{XONpO}_2$ and $\equiv\text{XONpO}_2(\text{HCO}_3)_2^{2-}$	72
Figure 2.33a	Test of model performance for higher Np(V) concentration AGW-A data sets without additional parameter optimization.....	73
Figure 2.33b	Test of model performance for higher Np(V) concentration AGW-A data sets with additional log K optimization.....	73
Figure 2.34a	Test of model performance to Np(V) sorption isotherm data sets without additional parameter optimization using the best fit model (Figure 2.32b).....	75

Figure 2.34b	Test of model performance to Np(V) sorption isotherm data sets with additional log K optimization	75
Figure 2.34c	Np(V) surface species distribution for the model simulation presented in Figure 2.31b with the 5×10^{-7} M Np(V), 125 g L ⁻¹ treated NABS in AGW-A at atmospheric PCO ₂ data set.....	75
Figure 2.34d	Model calibration for the Np(V) sorption isotherms using $\equiv\text{XONpO}_2$ and $\equiv\text{XONpO}_2(\text{HCO}_3)_2^{2-}$ with a range of total Np(V) concentrations from 2×10^{-7} M to 3×10^{-6} M, 125 g L ⁻¹ treated NABS, in AGW-3 (pH 8) at atmospheric PCO ₂ or in AGW-6 (pH 6.8) at 8% PCO ₂	75
Figure 2.35a	Test of model performance to Np(V) sorption isotherm data sets without additional parameter optimization	77
Figure 2.35b	Test of model performance to Np(V) sorption isotherm data sets with additional log K optimization.	77
Figure 2.35c	Test of model performance to Np(V) sorption isotherm data sets with additional parameter optimization and exclusion of a $\equiv\text{XOHNpO}_2^+$ surface species.....	77
Figure 2.36a	Test of model performance for the 5×10^{-7} M Np(V) data sets using 50, 125 and 500 g L ⁻¹ treated NABS in 0.1 M NaClO ₄ with additional log K optimization.....	78
Figure 2.36b	Test of model performance for the 5×10^{-7} M Np(V) data set using 500 g L ⁻¹ treated NABS in 0.1 M NaClO ₄ with additional log K optimization and an additional fit showing the effect of increasing the importance of the ternary neptunyl carbonate surface species....	78
Figure 2.37a	Model simulation of 100 mg L ⁻¹ HA sorption to 500 g L ⁻¹ treated NABS at atmospheric PCO ₂ in 0.1 M NaClO ₄ without Np(V) present.....	80
Figure 2.37b	Model simulation for 100 mg L ⁻¹ HA sorption to 500 g L ⁻¹ treated NABS at atmospheric PCO ₂ in 0.1 M NaClO ₄ with 5×10^{-7} M Np(V) present.....	80
Figure 2.38	Model simulation of 5×10^{-7} M Np(V) to 500 g L ⁻¹ treated NABS in the presence of 100 mg L ⁻¹ HA sorption at atmospheric PCO ₂ in 0.1 M NaClO ₄	81
Figure 3.1.	Kinetics of U(VI) adsorption on the composite sample of Forty-Mile Wash subsurface sediments (FMW-COMP) in artificial groundwater solution (FMW-2).....	85
Figure 3.2.	U(VI) sorption data on the composite sample of Forty Mile Wash subsurface sediments (FMW-COMP) in artificial groundwater solutions at low ionic strength.	85
Figure 3.3.	U(VI) sorption data on the composite sample of Forty Mile Wash subsurface sediments (FMW-COMP) in artificial groundwater solutions at low ionic strength as a function of dissolved U(VI) and PCO ₂ . Data expressed as log K _d for U(VI) sorption versus log dissolved U(VI) concentration.....	86

Figure 3.4.	U(VI) sorption data on the composite sample of Forty Mile Wash subsurface sediments (FMW-COMP) in artificial groundwater solutions at low ionic strength as a function of dissolved U(VI) and PCO_2 . Data expressed as percent U(VI) adsorbed versus log dissolved U(VI) concentration.....	86
Figure 3.5.	U(VI) sorption data on the composite sample of Forty Mile Wash subsurface sediments (FMW-COMP) in artificial groundwater solution at ionic strength of 0.1M.....	87
Figure 3.6.	U(VI) sorption data on the composite sample of Forty Mile Wash subsurface sediments (FMW-COMP) in artificial groundwater solution at ionic strength of 0.1M as a function of dissolved U(VI) and PCO_2 . Data expressed as log K_d for U(VI) sorption versus log dissolved U(VI) concentration.....	87
Figure 3.7.	U(VI) sorption data on the composite sample of Forty Mile Wash subsurface sediments (FMW-COMP) in artificial groundwater solution at ionic strength of 0.1M as a function of dissolved U(VI) and PCO_2 . Data expressed as percent U(VI) adsorbed versus log dissolved U(VI) concentration.....	88
Figure 3.8a.	Comparison of U(VI) sorption data and surface complexation model calculations for the composite sample of Forty Mile Wash subsurface sediments (FMW-COMP) in artificial groundwater solutions at low ionic strength as a function of dissolved U(VI) and PCO_2 . Data expressed as log K_d for U(VI) sorption versus log dissolved U(VI) concentration and shown with large symbols.....	91
Figure 3.8b.	Comparison of U(VI) sorption data and surface complexation model calculations for the composite sample of Forty Mile Wash subsurface sediments (FMW-COMP) in artificial groundwater solutions at low ionic strength as a function of dissolved U(VI) and PCO_2 . Data expressed as log K_d for U(VI) sorption versus log dissolved U(VI) concentration and shown with large symbols.....	91
Figure 3.9.	Comparison of U(VI) sorption data and surface complexation model calculations for the composite sample of Forty Mile Wash subsurface sediments (FMW-COMP) in artificial groundwater solutions at an ionic strength of 0.1M as a function of dissolved U(VI) and PCO_2 . Data expressed as log K_d for U(VI) sorption versus log dissolved U(VI) concentration and shown with large symbols.....	92
Figure 3.10.	Comparison of selected U(VI) sorption data and surface complexation model calculations for the composite sample of Forty Mile Wash subsurface sediments (FMW-COMP) in artificial groundwater solutions at low ionic strength. Data expressed as percent U(VI) adsorbed versus alkalinity and shown with large symbols.....	92
Figure 4.1.	Percent Ni adsorbed as a function of pH and total Ni concentration for suspensions with 400 g/L of Cape Cod aquifer sand composite in artificial groundwater solution.....	96
Figure 4.2.	Ni adsorption isotherms for Cape Cod aquifer sand composite in artificial groundwater solution at pH 5.4 and 6.1.....	96
Figure 4.3.	Comparison of GC model simulation and experimental data for percent Ni adsorbed as a function of pH and total Ni concentration, for suspensions with 400 g/L of Cape Cod aquifer sand composite in artificial groundwater solution.....	98

Figure 4.4. Comparison of GC model simulations and experimental data for Ni adsorption isotherms for Cape Cod aquifer sand composite in artificial groundwater solution at pH 5.4 and 6.198

TABLES

Table 2.1	Equilibrium Constants for Select Np(V) Aqueous Phase Reactions	8
Table 2.2	Humic Binding Model Parameters and Best Fit Values	9
Table 2.3	Studies Of Np(V) Sorption To Pure Mineral Phases	12
Table 2.4	Np(V) Sorption Spectroscopic Studies	22
Table 2.5	Studies Of Np(V) Sorption To Complex Geomedia.....	23
Table 2.6	Studies Of Np(V) Sorption In The Presence Of Humic Substances.....	29
Table 2.7	NABS Surface Area Distributions And Weight Percent For Various Grain Size Fractions.....	31
Table 2.8	Composition Of Artificial Groundwater Solutions.....	31
Table 2.9	Np(V) Sorption Isotherm Experimental Variables	34
Table 2.10	Np(V) Sorption Edge Experimental Variables	34
Table 2.11	Humic Acid Sorption Experiment Variables	34
Table 2.12	Error Calculations Using The 95% Confidence Intervals From Regression Analysis Of Np(V) Isotherm Experimental Data.....	41
Table 2.13	Surface Complexation Modeling Studies Of Np(V) Sorption To Pure Mineral Phases....	56
Table 2.14	Plausible Np(V) Surface Reactions Considered in Models	67
Table 2.15	Summary Of Adjustable Parameters And Goodness-Of-Fit: One-Site Models.....	68
Table 2.16	Summary Of Adjustable Parameters And Goodness-Of-Fit: Two-Site Models.....	74
Table 2.17	Summary Of Adjustable Parameters And Goodness-Of-Fit: Isotherm Data	76
Table 2.18	Summary Of Adjustable Parameters And Goodness-Of-Fit: NaClO ₄ Solution.....	79
Table 2.19	Humic Acid Solution Reactions.....	80
Table 2.20	Humic Acid Surface Reactions	81
Table 3.1.	U(VI) Surface Reactions Considered for the Forty-Mile Wash GC Model	90
Table 4.1.	Ni Surface Reactions Considered for the Cape Cod GC Model	97
Table 5.1.	Characteristics of Surface Complexation Modeling Approaches for Environmental Adsorbents	101

1 APPLICATIONS OF SURFACE COMPLEXATION MODELING: SCIENTIFIC BACKGROUND

1.1 Introduction

Public and private organizations in the United States and other nations are cleaning up hundreds of sites contaminated with uranium (U) and other contaminants that were released to the environment or that remain in temporary storage facilities (Crowley and Ahearne, 2002). These wastes contain high levels of radionuclides with long half-lives, and in most cases, the wastes will be disposed of in engineered facilities constructed underground in specific types of geologic formations. The most likely pathway for radionuclides to reach the biosphere from these repositories is by transport of dissolved radionuclides in groundwater (or transport of colloidal particles with adsorbed radionuclides).

In addition to the nuclear waste disposal problem, numerous sites throughout the United States are contaminated by radionuclides, especially U and thorium (Th) and their by-products, due to mining, milling and other industrial processes (Morrison and Cahn, 1991). The United States Nuclear Regulatory Commission (USNRC) is responsible for the regulatory oversight of site remediation and clean up, and possible release of sites for public or unrestricted use. Licensing decisions are made based on performance assessment (PA) calculations that utilize numerical models to estimate the increase in radioactivity exposure to the biosphere at selected locations. Contamination is often limited to the soils, subsurface sediments, and shallow aquifers at these sites.

Prediction of the fate and transport of radionuclides is of paramount importance in evaluating remediation schemes and in quantifying the risk of contamination to human or ecosystem health. To make a calculation of radioactive exposure risk in PA, it is necessary to calculate the total amount of each radionuclide that will be present at selected locations as a function of time. A solute

transport model is typically used to describe the physical processes of advection and dispersion that may transport radionuclides in groundwater from the source location to a site of ingestion. In addition to these hydrophysical processes, the transport of many radionuclides can be strongly influenced by reactive chemical processes, including aqueous complexation, sorption, precipitation and dissolution, and redox reactions. However, in practice, many reactive transport models ignore the chemical complexity of aqueous complexation and sorption processes and utilize the distribution coefficient (constant K_d) approach to describe the retardation of radionuclide contaminants (Bethke and Brady, 2000; USEPA, 1999). Although sorption is only a part of the overall PA calculations, retardation of radionuclide transport in the far-field geosphere zone may be extremely important in reducing the risk of biosphere exposure of certain radionuclides to levels that are in compliance with regulations.

The transport of actinide elements and other radionuclides in porous media can be strongly influenced by the competitive effects of the formation of mobile solution complexes and immobile adsorbed species. These elements can form many species in natural waters as a result of hydrolysis and complexation reactions. The distribution of aqueous species can be highly dependent on chemical conditions, especially pH and the concentrations of complexing ligands, such as carbonate ions (Curtis et al., 2006; Davis et al., 2004; Clark et al., 1995). In natural waters, important complexing ligands for U(VI) and Np(V) include hydroxide, carbonate and dissolved organic carbon; such ligands may compete with adsorption sites for complexation of UO_2^{2+} (and other actinyl ions) and decrease the extent of adsorption via the formation of nonadsorbing aqueous complexes. The influence of some ligand interactions can be very complex, as demonstrated by the observed increased adsorption of metals in the presence of certain ligands (Davis and Leckie, 1978). However, in some cases, the effects of

complexing ligands can be modeled in a straightforward way by assuming that the aqueous complexes formed do not adsorb. For example, Kohler et al. (1996) showed that the adsorption of U(VI) on quartz in the presence of fluoride (F) ligands could be modeled as a competition between the quartz surface and aqueous F for complexation of U(VI).

Application of the K_d concept to inorganic contaminants can be problematic because the parameter is so sensitive to aqueous chemical conditions. For example, the K_d for U(VI) adsorption on ferrihydrite at pH 8 decreases by *four orders of magnitude* as the partial pressure of carbon dioxide gas, pCO_2 , increases from its value in air (0.032%) to 1% (Davis et al., 2004; USNRC, 2003). This is an important variation to understand, because the pCO_2 in aquifers commonly reaches values of 1-5%, while most K_d values have been determined in laboratory experiments equilibrated with or exposed to air. Moreover, pCO_2 often increases with transport after groundwater recharge, and this spatial/temporal trend in chemical conditions can greatly affect the retardation of radionuclides that form strong aqueous complexes with carbonate.

The quality of thermodynamic data for radionuclide solubilities and aqueous speciation has been steadily increasing in recent years and the data are now available in critically reviewed compilations (Guillaumont et al., 2003; Langmuir, 1997; Silva et al., 1995; Grenthe et al., 1992). In contrast, the choice of K_d values in PA modeling is generally made based on expert judgement of available experimental data for individual radionuclides and various rock materials. The expert judgement may include an evaluation of laboratory measurements of K_d values from batch or column experiments with site-specific materials in contact with solutions of varying chemical composition. In addition to measurements with site-specific materials, databases of K_d values have been assembled for the sorption of radionuclides on a variety of single mineral phases (Turner, 1995), natural materials, including soils and rock powders (USEPA, 1996; McKinley and Scholtis, 1993; Sheppard and Thibault, 1990; Looney et al.,

1987; Baes and Sharp, 1983; Isherwood, 1981), and engineered barrier materials pertinent to nuclear waste disposal (Berry, 1992; Krupka and Serne, 1996).

One of the potentially large uncertainties in PA model calculations arises from the choice of K_d values for individual radionuclides. Depending on the type and purpose of the PA modeling study, either a single K_d value may be chosen for each radionuclide or a probability distribution function (PDF) may be derived that encompasses a range of K_d values. The uncertainty in the choice of K_d values or in the PDF arises from several sources, e.g. 1) experimental error, 2) extrapolation or interpolation of values to chemical conditions or rock types other than those used in actual experimental measurements of K_d , and 3) the scaling of K_d values measured for rock powders to the values expected for intact rocks in the site-specific, geologic setting.

Constant K_d models for adsorption do not adequately account for spatial variability in the composition of adsorbing phases or for variable chemical conditions, such as pH, ionic strength, alkalinity, or concentrations of complexing ligands that may be encountered along a groundwater flow path (Curtis et al., 2006; Davis et al., 2004; Kohler et al., 2004; USNRC, 2003; Kohler et al., 1996). For a variety of reasons, the range of K_d values that may need to be considered for each radionuclide/rock combination can be quite large. One can consider spatial and temporal variability in chemical conditions in PA modeling with K_d values by separating the calculations into separate blocks of time or hydrologic units in space. Although the effects of changes in chemical conditions on the solubilities of radionuclides can usually be calculated in a straightforward manner, the effects of variable chemical conditions on adsorption and the choice of K_d values is more complex (Curtis et al., 2004; Davis et al., 2004; USEPA, 1999; Kohler et al., 1996). In order to be “conservative”, large ranges of K_d values may need to be estimated by expert judgement in order to account for possible changes in chemical conditions and for other sources of

error. The uncertainties in these ranges are difficult to assess quantitatively without doing large numbers of experiments.

1.2 Surface Complexation Modeling

Although a number of variations in the modeling approach have been developed, there are four fundamental tenets in all surface complexation models (SCM) (NEA, 2005; Davis and Kent, 1990):

- Mineral surfaces are composed of specific chemical functional groups that react with dissolved solutes to form surface species (coordinative complexes or ion pairs), in a manner analogous to complexation reactions in homogeneous solution.
- The equilibria of adsorption reactions can be described by mass action equations. If desired, correction factors to these equations may be applied to account for variable electrostatic energy, using electrical double layer theory.
- The apparent binding constants determined for the mass action equations are empirical parameters related to thermodynamic constants by the rational activity coefficients of the surface species.
- Electrical charge at the surface is determined by the chemical reactions of the mineral functional groups, including acid-base reactions and the formation of ion pairs and coordinative complexes.

In contrast to models using constant K_d , SCM have the capability of describing changes in contaminant adsorption as chemical conditions and aqueous speciation vary, and SCM can be readily incorporated within solute transport models (Curtis et al., 2006; USNRC, 2003; Kent et al., 2000). Previous investigations have shown that the SCM concept can be applied to great advantage in natural systems by employing a simple Generalized Composite (GC) approach to describe metal or radionuclide adsorption (Davis

et al., 2004; Curtis et al., 2004; Davis et al., 2002). In the GC approach, the surface of the mineral assemblage is considered too complex to be quantified in terms of the contributions of individual phases to adsorption. Instead, it is assumed that adsorption can be described by SCM equilibria written with “generic” surface functional groups, with the stoichiometry and formation constants for each SCM mass law determined by fitting experimental data for the mineral assemblage (Davis et al., 2004).

Fortunately, the uncertainty in K_d values that arises from variations in the chemical composition of groundwater or mineralogical composition of the adsorbent phases along a flow path can be reduced with the use of surface complexation modeling (SCM) to describe adsorption (Curtis et al., 2006; USNRC, 2003; Kent et al., 2000). In addition, certain large sources of uncertainty (e.g., scaling from K_d values measured for rock powders to the surfaces of a fractured rock system) can be more easily addressed with SCM, because SCM is based on defining radionuclide adsorption per unit surface area rather than per unit mass.

SCM could be of significant value to PA if it was used to determine the range of K_d values that need to be considered and provide a scientific basis for the range of values chosen (NEA, 2005). Uncertainties in SCM parameters can be less than the uncertainties in K_d values (when considered as robust over a range of chemical conditions), and SCM uncertainties may be more easily quantified. For example, a recent report on batch studies of U(VI) adsorption on montmorillonite presented K_d values that ranged by more than 4 orders of magnitude over the pH range of 6.5 to 8.5 (Pabalan and Turner, 1996). In a series of papers, Davis et al. (2004), Kohler et al. (2004), and Curtis et al. (2004) showed that the K_d values for U(VI) in an alluvial aquifer in Colorado varied by more than one order of magnitude because of variable chemical conditions in the groundwater. In each of these cases the datasets could be described by an SCM with a small number of independent parameters that remained constant and had comparatively little uncertainty in their values.

Using a range of 4 orders of magnitude in the uncertainty of K_d values (Pabalan and Turner, 1996) in PA calculations could lead to increased costs for waste cleanup at an industrial site or to rejection of an alternative waste disposal scenario. If used properly, SCM for radionuclide adsorption has the potential to increase the confidence and scientific credibility of PA transport modeling, by reducing the uncertainty in quantifying retardation and providing a means of quantifying that uncertainty. In addition, SCM has the potential to lower the estimated remediation costs of sites contaminated with radionuclides (or the feasibility of a disposal scenario) by decreasing the uncertainty of K_d values (and the associated safety factor applied in PA modeling).

The use of equilibrium geochemical models to calculate radionuclide solubilities and aqueous speciation is well established in the PA field. Surface complexation modeling is an extension of this thermodynamic modeling approach to include the reactions between dissolved species and the functional groups (ligands) present on mineral surfaces (NEA, 2005). The adsorption reactions are included as part of the network of chemical reactions that require equilibration, rather than as a condition-dependent partitioning coefficient, like K_d . Once the model is calibrated, it allows predictive calculations for a range of geochemical conditions without changing the values of the stability constants for radionuclide adsorption. The adsorption equations can be included efficiently in transport simulations in which there are chemical gradients in the subsurface environment rather than constant chemical conditions (Curtis et al., 2006; Kent et al., 2000).

1.3 Project Goals

In a previous study (USNRC, 2003), the surface complexation modeling approach was demonstrated successfully for a field site contaminated with uranium. The objective of

that project was to demonstrate that, despite the complexities inherent at field sites and in modeling sorption by natural mineral assemblages, the surface complexation concept could be utilized to great advantage to describe U(VI) sorption and retardation in a field setting.

In this report we demonstrate that the surface complexation concept can also be used to describe the sorption of other radionuclides (Np(V), Ni) on complex mineral assemblages and U(VI) sorption on other sediment samples. Generalized Composite models are developed for simulating: 1) Np(V) sorption by the subsurface sediments collected from an alluvial aquifer at the UMTRA site near Naturita, Colorado, 2) U(VI) sorption by aquifer sediments from the Forty-Mile Wash aquifer, Nye County, Nevada, and 3) Ni sorption by aquifer sediments from Cape Cod, Massachusetts.

1.4 Overview of Report

Data were collected within this project to enable development of a GC modeling approach for description of radionuclide adsorption by subsurface materials collected from three different field sites. The studies were completed under conditions of variable aqueous chemistry, which caused significant variation in the speciation of U(VI) or Np(V). The study of Np(V) sorption by Naturita (Colorado) aquifer sediments and development of a GC model to describe its sorption is presented in Section 2. The study of U(VI) sorption and modeling with Forty-Mile Wash sediments is summarized in Section 3. Ni sorption and modeling with Cape Cod aquifer sediments is described in Section 4. Section 5 summarizes the conclusions of the project and discusses the significance of the project results to PA modeling. The project impacts the evaluation of appropriate methods to determine K_d values for radionuclides, the choice of models to describe radionuclide sorption, and the extent of adsorption uncertainties on PA modeling.

2 NEPTUNIUM(V) SORPTION TO AN ALLUVIAL AQUIFER SEDIMENT: APPLICABILITY OF SURFACE COMPLEXATION MODELING

2.1 Background

Neptunium-237 (^{237}Np) is a component of spent nuclear fuel and other radioactive wastes. ^{237}Np is considered a radionuclide of significant concern due to its long half-life (2.14×10^6 years), biological toxicity, high chemical stability of the pentavalent oxidation state and low sorption affinity of the neptunyl (NpO_2^+) cation (Choppin, 1983; Dozol and Hagemann, 1993; Silva and Nitsche, 1995). The fate of Np(V) in natural systems is largely controlled by the extent NpO_2^+ and its complexes sorb to solid surfaces (Morse and Choppin, 1991). A considerable body of research has focused on the sorption of Np(V) to pure mineral phases (e.g. Girvin et al., 1991; Tochiyama et al., 1996; Bertetti et al., 1996; Del Nero et al., 1998). Np(V) sorption is shown to strongly depend on surface characteristics and variations in chemical composition such as pH, carbonate concentration, ionic strength and competing ligands. The data and text of this section are mostly taken from Moran (2007), whose thesis work was funded by this project.

2.1.1 Neptunium Aqueous Geochemistry

Np can exist in the III, IV, V, VI and VII oxidation states in aqueous solutions with the pentavalent state being the most stable under oxidizing conditions found in many aquatic systems (Dozol and Hagemann, 1993). Similar to U(VI), Np(V) exists as a linear trans dioxo cation in aqueous solutions. However, the lower effective charge density of NpO_2^+ compared to UO_2^{2+} (+2.2 and +3.3, respectively) leads to the much lower complexation strength of Np(V) compared to U(VI) (Choppin and Unrein, 1976). The unusual stability of NpO_2^+ compared to other pentavalent actinides is due to its resistance to hydrolysis, lack of polynuclear complex formation, and the fact that oxidation state disproportionation occurs only in highly acidic solutions (Burney and Harbour, 1974).

In a CO_2 -free atmosphere, the hydroxo complexes ($\text{NpO}_2\text{OH}^\circ$ and $\text{NpO}_2(\text{OH})_2^-$) dominate at high pH (Maya, 1983; Lierse et al., 1985; Neck et al., 1992). Figure 2.1 illustrates the occurrence of aqueous neptunyl hydroxo complexes at a total Np(V) concentration of 2.0×10^{-6} M, in 0.1 M NaClO_4 under CO_2 -free conditions. The thermodynamic constants applicable to this study, compiled within the NEA critical reviews of all available thermodynamic data for Np(V) complexation with inorganic ligands, are presented in Table 2.1 (Lemire et al., 2001; Guillaumont et al., 2003). It is important to note that the speciation diagrams presented here only take solution phase reactions into consideration and only show Np(V) aqueous complexes that contribute >1% to the total species distribution. Solubility calculations estimate that crystalline NpO_2OH may precipitate at $\sim \text{pH} > 8$ under the CO_2 -free conditions presented in Figure 2.1.

In the presence of carbonate ligands, aqueous carbonate complexes dominate Np(V) speciation at near-neutral pH (Clark et al., 1995). A wealth of spectroscopic (Neck et al., 1994; Runde and Kim, 1995; Clark et al., 1996) and solubility (Neck et al., 1994; Runde and Kim, 1995) data support the existence of the aqueous carbonate complexes, $\text{NpO}_2\text{CO}_3^-$, $\text{NpO}_2(\text{CO}_3)_2^{3-}$ and $\text{NpO}_2(\text{CO}_3)_3^{5-}$. A number of authors have found evidence for a mixed Np(V) hydroxo-carbonato complex, but the exact stoichiometry has yet to be determined. As Figure 2.2 demonstrates, under conditions similar to those encountered in the laboratory, 0.1 M NaClO_4 and atmospheric partial pressure of CO_2 (PCO_2), the NpO_2^+ carbonate complexes prevail over the hydroxo complexes, with a small contribution to Np(V) speciation by the mixed hydroxo carbonate complex in the alkaline pH range, assuming $\text{NpO}_2(\text{CO}_3)_2\text{OH}^{4-}$ is the correct stoichiometry. Figures 2.3 and 2.4 show how the shift towards dominance of carbonate complexes is extended as the PCO_2 increases from atmospheric to 2% PCO_2 and 8% PCO_2 , respectively.

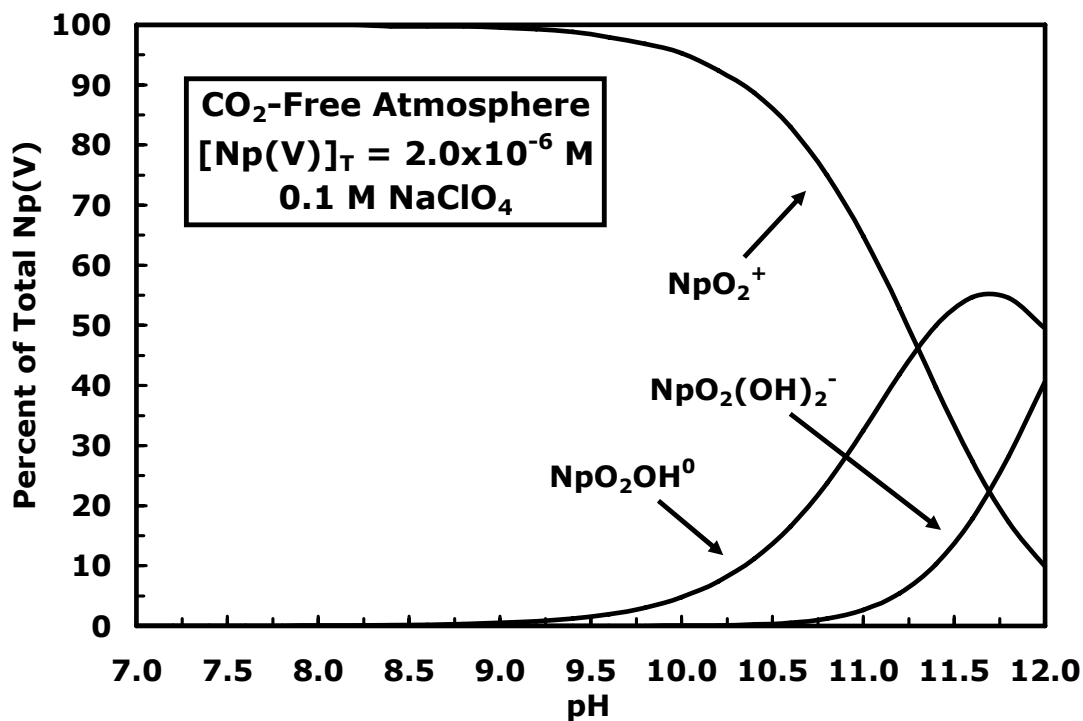


Figure 2.1. Np(V) species distribution as a function of pH in 0.1 M NaClO₄ with a total Np(V) concentration of 2.0x10⁻⁶ M under CO₂-free conditions.

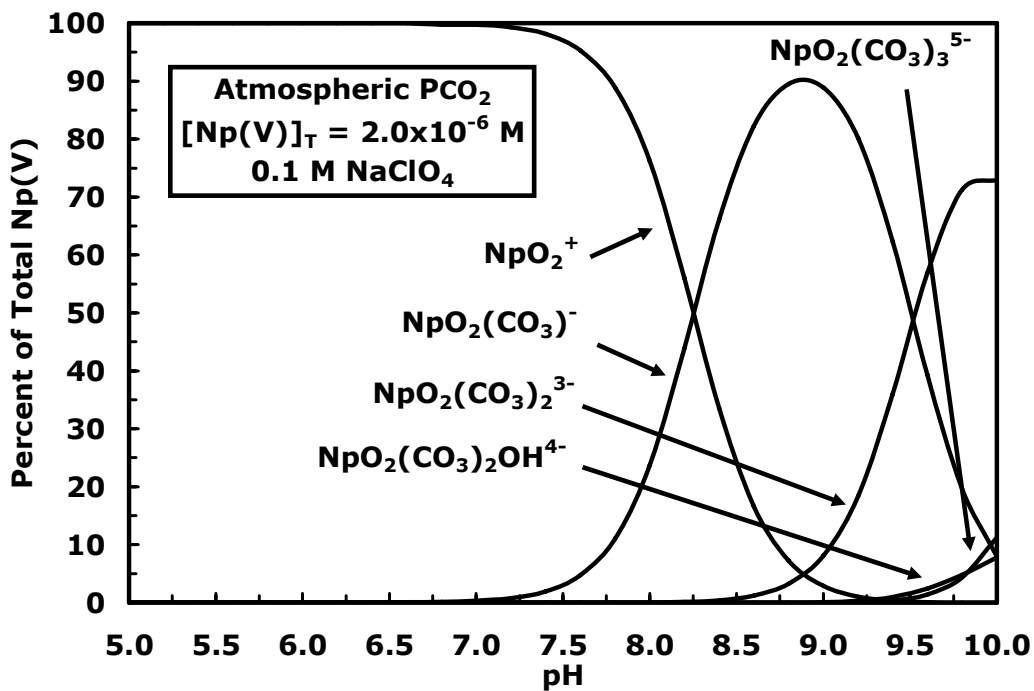


Figure 2.2. Np(V) species distribution as a function of pH in 0.1 M NaClO₄ with a total Np(V) concentration of 2.0x10⁻⁶ M at atmospheric PCO₂.

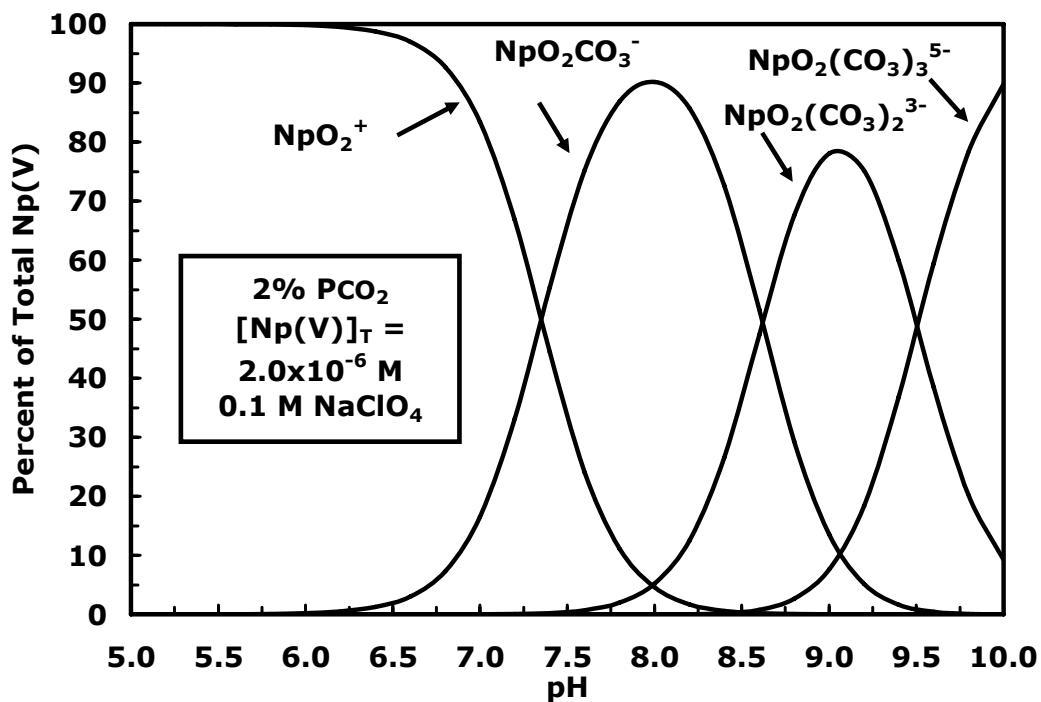


Figure 2.3. Np(V) species distribution as a function of pH in 0.1 M NaClO₄ with a total Np(V) concentration of 2.0×10^{-6} M at 2% PCO₂.

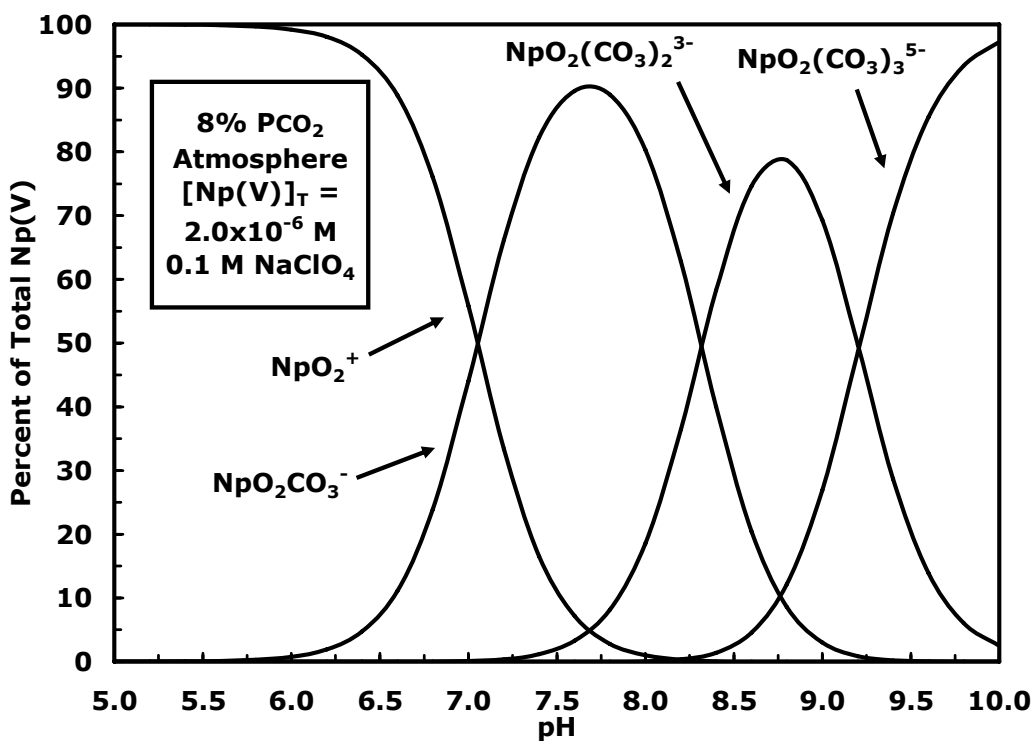


Figure 2.4. Np(V) species distribution as a function of pH in 0.1 M NaClO₄ with a total Np(V) concentration of 2.0×10^{-6} M at 8% PCO₂.

Table 2.1 Equilibrium Constants For Select Np(V) Aqueous Phase Reactions

Reactions	Log K (I = 0)
$\text{NpO}_2^+ + \text{H}_2\text{O} \leftrightarrow \text{NpO}_2\text{OH}(\text{aq})^0 + \text{H}^+$	-11.3
$\text{NpO}_2^+ + 2\text{H}_2\text{O} \leftrightarrow \text{NpO}_2(\text{OH})_2^- + 2\text{H}^+$	-23.60
$\text{NpO}_2^+ + \text{CO}_3^{2-} \leftrightarrow \text{NpO}_2\text{CO}_3^-$	4.96
$\text{NpO}_2^+ + 2\text{CO}_3^{2-} \leftrightarrow \text{NpO}_2(\text{CO}_3)_2^{3-}$	6.53
$\text{NpO}_2^+ + 3\text{CO}_3^{2-} \leftrightarrow \text{NpO}_2(\text{CO}_3)_3^{5-}$	5.47
$\text{NpO}_2^+ + 2\text{CO}_3^{2-} + \text{OH}^- \leftrightarrow \text{NpO}_2(\text{CO}_3)_2\text{OH}^{4-}$	8.70

I = 0, ionic strength corrected to zero using specific ion interaction (SIT) equations

Under CO₂-free conditions, the stable Np(V) solid phases are Np₂O₅(s) and NpO₂OH(s) (Lierse et al., 1985; Neck et al., 1992; Merli and Fuger, 1994; Efurud et al., 1998). Solid Np(V)-carbonate compounds become the stable phases with the addition of CO₂ (Maya, 1983; Grenthe et al., 1986; Neck et al., 1994; Neck et al., 1995; Novak et al., 1997; Al Mahamid et al., 1998). The stable solid phases in carbonate containing systems are MNpO₂CO₃·xH₂O(s) and M₃NpO₂(CO₃)₂(s) where M = Na⁺ or K⁺. The relatively high solubility of these Np(V) solid phases is likely to facilitate the transport of Np from underground repositories into the environment (USNRC, 2004).

In some instances, naturally occurring organic ligands, such as humic acid (HA) and fulvic acid, can compete with carbonate to form complexes with NpO₂⁺ (Leiser and Mühlenweg, 1988). Reported stability constant values vary by over two orders of magnitude. This substantial variability can be attributed to a number of factors: 1) the method used to distinguish free NpO₂⁺ from complexed NpO₂⁺; 2) the model used to determine the free HA concentration; and 3) variations in the Np(V) concentration (Moran, 2007).

In this study, the discrete log K model developed by Westall et al. (1995) was used to approximate both the acid-base character of Suwannee River humic acid (HA) and Np(V) speciation in the presence of Suwannee River HA. In this model, five discrete ligands (HL_i) are assumed to exist that can describe the macroscopic acid-base and complexation behavior of an HA sample. The discrete log K spectrum model was originally

developed to model 1:1 interactions of Co(II) with Leonardite HA. The model has since been successfully used to determine U(VI):HA and U(VI):FA stability constants with 1:1 and 1:2 uranyl-ligand complexes (Lenhart, 1997; Lenhart et al., 2000). Kantar et al. (2005) used a similar approach to obtain stability constants for U(VI):Fe(III):citrate complexation using 1:1:1 and 1:1:2 ternary complexes. The model does not explicitly account for electrostatic effects, but rather incorporates electrostatics implicitly using a counterion binding constant.

The model was applied in this study from the data and calibration of Moran (2007). Table 2.2 contains the optimized values of each hypothetical HA ligand as well as the value for K_{Na}, where one value was used for all 5 HL_i ligands. The model fits for Np(V) complexation with HA were conducted using only ligands HL₁ – HL₄ (Moran, 2007). The log β values at I = 0 and the associated errors determined by Moran (2007) are: pH 7.0, log β = 4.28 ± 0.14; pH 8.0, log β = 4.49 ± 0.11; average log β = 4.39 ± 0.13.

Using the average stability constant, distribution diagrams were developed to predict the environmental behavior of Np(V) in the presence of HA. At atmospheric PCO₂, Np(V) speciation in the presence of 10 mg L⁻¹ HA over a wide pH range (3-10) in 0.1 M NaClO₄ show little importance of HA complexation in a 2x10⁻⁶ M Np(V) solution (Figure 2.5a). Figure 2.5b illustrates a greater importance of the Np(V)-HA complex as the HA concentration increases from 10 to 100 mg L⁻¹. Under these conditions, HA complexation plays a role in Np(V) speciation below pH 9.

Table 2.2 Humic Binding Model Parameters and Best Fit Values*

Reactions	THL _i (mmol L ⁻¹)	THL _i (mmol g ⁻¹)	Log K (I = 0 M)
HL ₁ = L ₁ ⁻ + H ⁺	0.298	0.608	-2
HL ₂ = L ₂ ⁻ + H ⁺	0.807	1.65	-4
HL ₃ = L ₃ ⁻ + H ⁺	0.713	1.46	-6
HL ₄ = L ₄ ⁻ + H ⁺	0.283	0.578	-8
HL ₅ = L ₅ ⁻ + H ⁺	0.332	0.678	-10
L _i ⁻ + Na ⁺ = NaL _i			2.34

*Model fit to potentiometric data, THL_i = Total HL_i, Total HL = 4.97 mmol g⁻¹

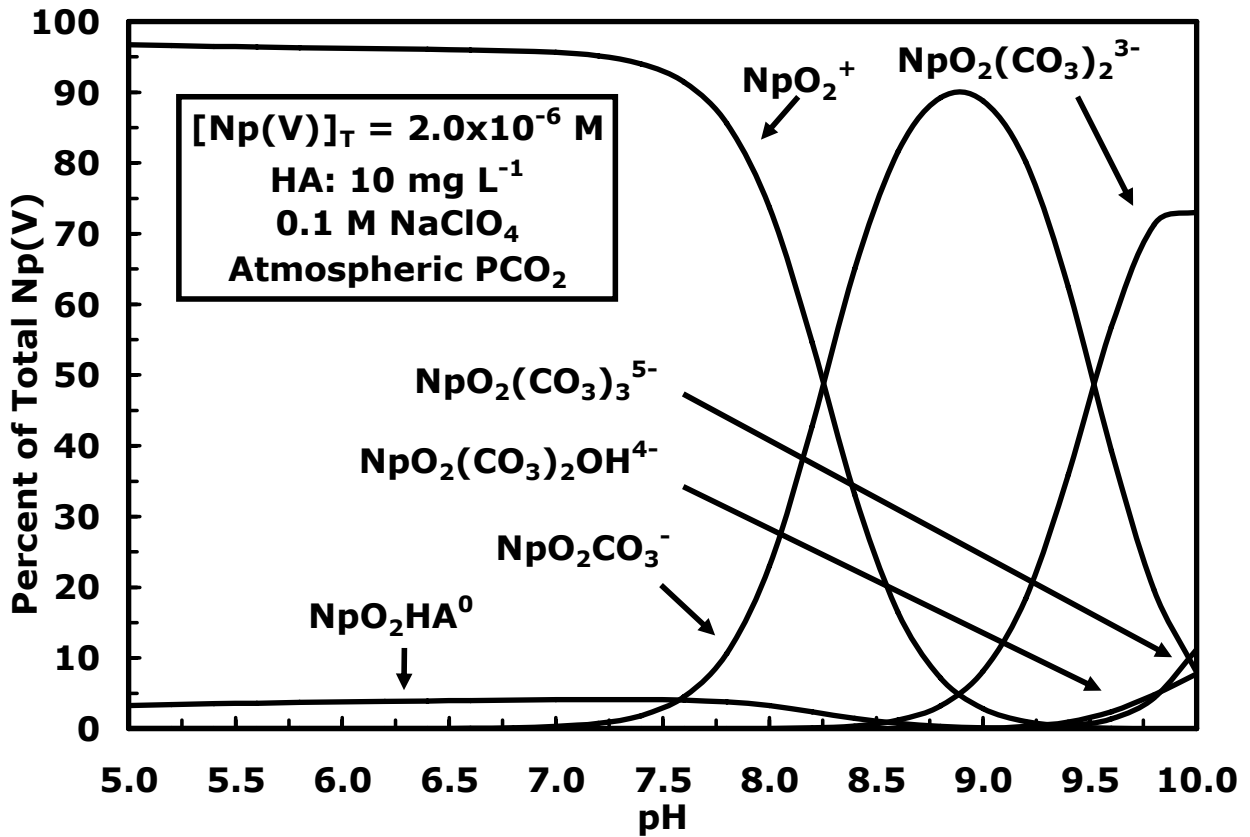


Figure 2.5a. Np(V) species distribution as a function of pH in 0.1 M NaClO₄ with a total Np(V) concentration of 2.0 × 10⁻⁶ M, 10 mg L⁻¹ HA at atmospheric PCO₂.

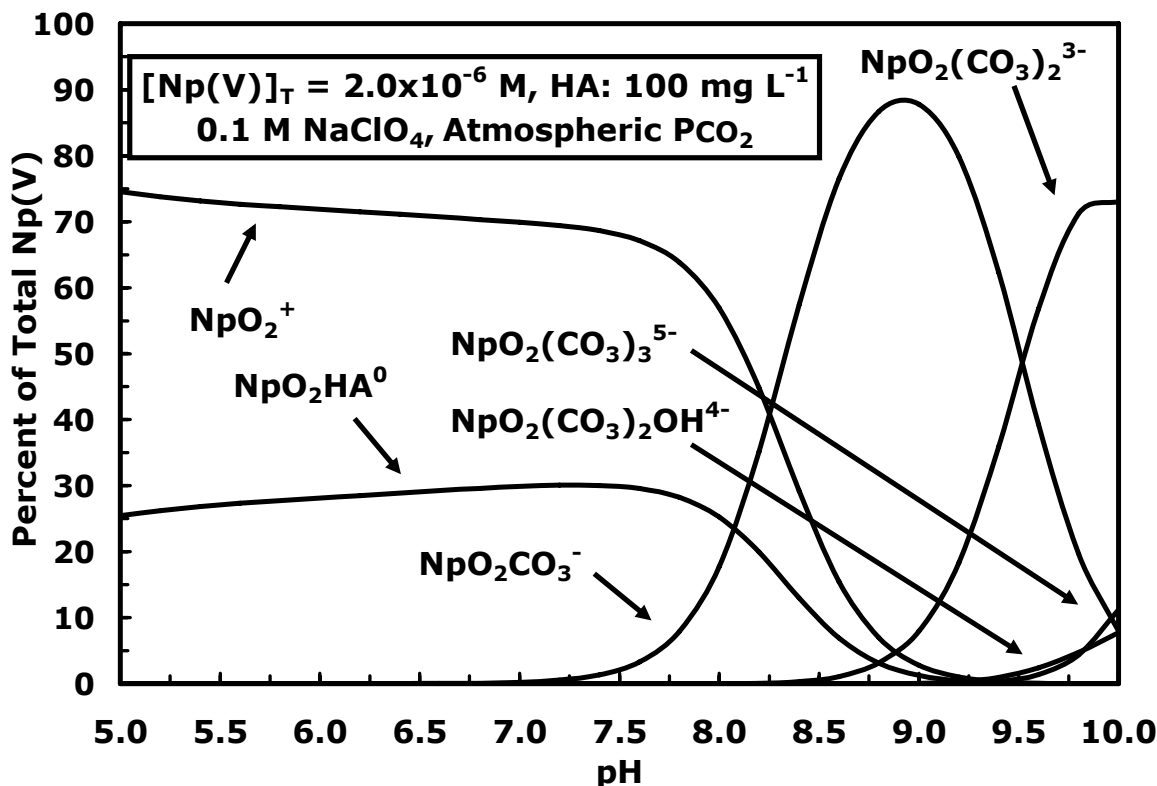


Figure 2.5b. Np(V) species distribution as a function of pH in 0.1 M NaClO₄ with a total Np(V) concentration of 2.0×10^{-6} M, 100 mg L^{-1} HA at atmospheric PCO₂.

Figure 2.6 shows an estimate of the effect of PCO₂ on 2×10^{-6} M Np(V) complexation with 100 mg L^{-1} HA at pH 7 and pH 8 in 0.1 M NaClO₄. At pH 7 and below, the Np(V)-HA complex primarily competes with the free NpO_2^+ cation over the entire PCO₂ range shown. Increasing the pH to 8 shows that the NpO_2^+ -HA complex is only significant at low PCO₂. The first NpO_2^+ carbonato complex becomes the primary Np(V) species as PCO₂ increases to levels likely to be encountered in groundwater.

The conditional stability constant ($\log \beta = 4.39$) determined by Moran (2007) is consistent with $\log \beta$ values for Aldrich HA obtained by Siebert et al. (2001) at similar Np(V) concentrations. Siebert et al. (2001) used ultrafiltration experiments to obtain values between 3.7 and 5.0 over a wide Np(V) concentration range (10^{-14} – 10^{-4} M). In the more narrow Np(V) range of 1×10^{-5} to 4×10^{-6} M, the $\log \beta$ values are between 4.1 and 4.2 at pH 7 and 8 (Siebert et al., 2001).

2.1.2 Neptunium(V) Sorption to Pure Mineral Phases

The majority of recent Np sorption studies have focused on the interaction of Np(V) with pure mineral phases. The discussion below illustrates some key features of Np(V) sorption to representative minerals using specific studies from the literature. Table 2.3 contains an overview of the literature pertaining to Np(V) sorption to pure mineral phases.

The pH dependence of Np(V) sorption to many different types of pure mineral phases is well documented. The seminal paper by Girvin et al. (1991) investigated Np(V) sorption to ferrihydrite at tracer Np(V) concentrations (4.5×10^{-13} M to 4.5×10^{-11} M) and PCO₂ slightly below $10^{-3.5}$ atm. The Girvin et al. study showed that sorption increased rapidly from about zero at pH 4 to almost 100% by pH 8. At low Np(V) concentrations the total Np(V) concentration had

little impact on sorption. In contrast, the ferrihydrite concentration (0.1, 0.4 and 1.0 g L⁻¹) had a significant effect on sorption, resulting in a shift in the sorption edge to higher pH as the solid concentration was reduced.

The Kohler et al. (1999) study of Np(V) sorption to goethite and hematite obtained results consistent with the Girvin et al. study. Kohler and coworkers also investigated the effect of PCO₂ on Np(V) sorption. At 2% PCO₂, sorption to goethite and hematite was significantly reduced above approximately pH 7.5 compared to samples obtained under atmospheric and CO₂-free conditions with the suggestion that weakly sorbing aqueous neptunyl carbonate complexes were responsible. Of interest, the experimental data collected under CO₂-free conditions was well fit using a model without carbonate species while the data collected under atmospheric and 2% PCO₂ was well simulated using a model that included a ternary neptunyl carbonate surface complex.

At Np(V) concentrations used for the Kohler et al. study (1.2x10⁻⁷ M to 1.3x10⁻⁶ M) the impact of reduced solid concentrations on sorption was

greater than observed by Girvin and coworkers. For example, at 1.1x10⁻⁶ M Np(V) and 1 g L⁻¹ hematite, sorption followed the same trend as observed by Girvin et al., while at 1.3x10⁻⁶ M Np(V) and 0.01 g L⁻¹ hematite, Np(V) sorption was less than 10% over the entire pH range studied (pH 4 to 10). This flattening of the sorption edge was indicative of hematite surface site saturation. Calculations confirmed that the Np(V) concentration was in excess of the site concentration at 1.3x10⁻⁶ M Np(V) and 0.01 g L⁻¹ hematite.

Tochiyama et al. (1995) studied sorption of ~10⁻¹³ M Np(V) to a number of naturally occurring and synthetic iron oxides at 20 g L⁻¹. The study found that Np(V) K_d values varied by 2 to 4 orders of magnitude at a given pH for the group of iron oxides investigated. Furthermore, Np(V) sorption affinity followed the trend: goethite (α-FeOOH) > ferrihydrite (Fe₂O₃·H₂O) > hematite (α-Fe₂O₃) ≈ magnetite (α-Fe₃O₄). This trend suggested that crystal structure was the primary variable controlling Np(V) sorption to iron oxides. Tochiyama et al. (1996) conducted Np(V) sorption experiments using naturally

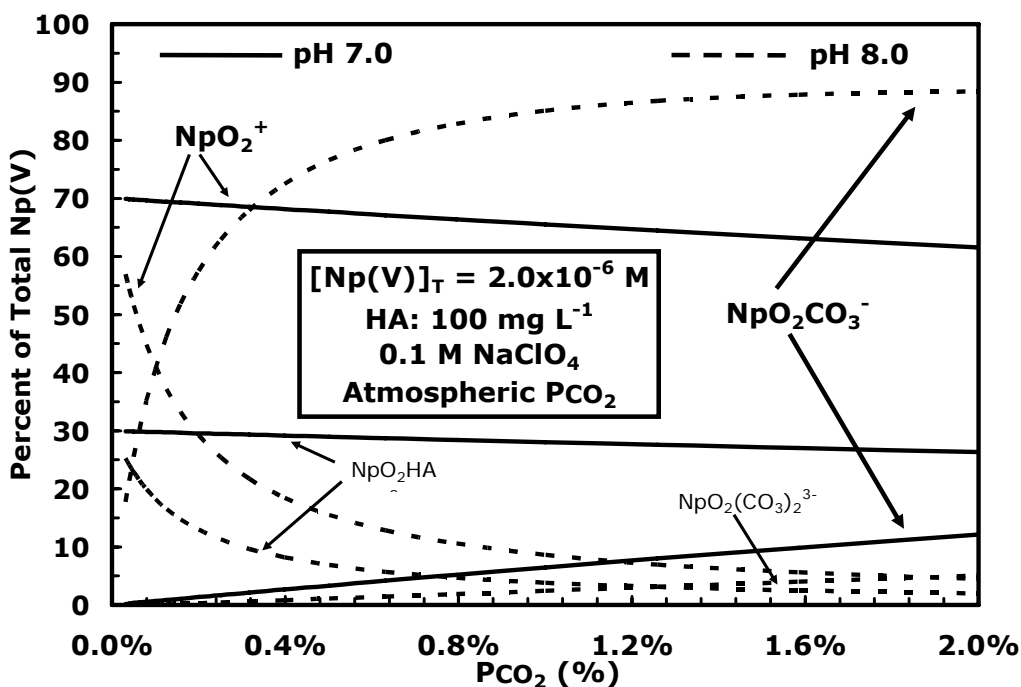


Figure 2.6. Np(V) species distribution as a function of PCO₂ in 0.1 M NaClO₄ with a total Np(V) concentration of 2.0x10⁻⁶ M, 100 mg L⁻¹ HA at pH 7 and 8.

Table 2.3. Studies of Np(V) Sorption to Pure Mineral Phases (AGW = artificial groundwater, GW = groundwater)

Sorbent (Chemical Formula)	Np(V) (^{237,239} Np) (mol L ⁻¹)	pH range	Solid Concentration (g L ⁻¹)	I (mol L ⁻¹)	PCO ₂ (Atm)	Reference
Albite (NaAlSi ₃ O ₈)	<10 ⁻⁷	1.9, 7.5 and 11.3	20	GW	10 ^{-3.5}	Torstenfelt et al. (1988)
Al silicates	6x10 ⁻⁶ – 1x10 ⁻⁹	3-10	20	0.001 and 0.1	0 and 10 ^{-3.5}	Del Nero et al. (2004)
Alumina (γ-Al ₂ O ₃)	4x10 ⁻⁷ - 6x10 ⁻⁶	4-11	1	0.1	<10 ^{-3.5} sealed vials	Nakayama and Sakomoto (1991)
Alumina	1.0x10 ⁻¹⁴	4-10	0.2	0.1	0	Righetto et al. (1991)
Alumina	1.02x10 ⁻⁶	10-13.6	12.5	1.0	10 ^{-3.5}	Yamaguchi et al. (2004)
Anorthite	<10 ⁻⁷	1.9, 7.5 and 11.3	20	GW	10 ^{-3.5}	Torstenfelt et al. (1988)
Amorphous SiO ₂	1.0x10 ⁻¹⁴	4-10	1.2	0.1	0	Righetto et al. (1991)
Apatite (group) (Ca ₅ (PO ₄) ₃ (OH,F,Cl))	2.0x10 ⁻¹¹	5-10	7.8	0.01- AGW	10 ^{-3.5}	Beall and Allard (1981)
Aragonite (CaCO ₃)	1x10 ⁻⁴ – 1x10 ⁻¹³	7.8-8.2	3.4	~0.05- 0.7	10 ^{-3.5}	Keeney- Kennicutt and Morse (1984)
Attapulgite ((Mg,Al) ₂ Si ₄ O ₁₀ (OH)·4(H ₂ O))	2.0x10 ⁻¹¹	5 and 8	7-12	0.01- AGW	10 ^{-3.5}	Beall and Allard (1981)
Bentonite (Al ₂ O ₃ ·4SiO ₂ ·H ₂ O)	6x10 ⁻⁷	2-8	10	0.01	10 ^{-3.5}	Kozai et al. (1995)

Table 2.3 (continued). Studies of Np(V) Sorption to Pure Mineral Phases

Sorbent (Chemical Formula)	Np(V) (^{237,239}Np) (mol L⁻¹)	pH range	Solid Concentration (g L⁻¹)	I (mol L⁻¹)	PCO₂ (Atm)	Reference
Bentonite	<10⁻⁷	2.3, 8.7 and 10.2	20	GW	10^{-3.5}	Torstenfelt et al. (1988)
Biotite (K(Fe, Mg)₃ AlSi₃O₁₀(F,OH)₂)	2.0x10⁻¹¹	5 and 8	7-12	0.01-AGW	10^{-3.5}	Beall and Allard (1981)
Biotite-natural and synthetic	4x10⁻⁷- 6x10⁻⁶	3-11	1.0	0.1	<10^{-3.5} Sealed vials	Nakayama and Sakomoto (1991)
Boehmite (γ-AlOOH)	4x10⁻⁷- 6x10⁻⁶	3-11	1.0	0.1	<10^{-3.5} Sealed vials	Nakayama and Sakomoto (1991)
Boehmite	2x10⁻⁷ – 2x10⁻⁶	6.2	~20	0.1 (KCl)	10^{-3.5}	Kung and Triay (1994)
Calcite (CaCO₃)	2.0x10⁻¹¹	8-10	7.8	0.01-AGW	10^{-3.5}	Beall and Allard (1981)
Calcite	1x10⁻⁴ – 1x10⁻¹³	7.8-8.2	8.3	~0.05- 0.7	10^{-3.5}	Keeney- Kennicutt and Morse (1984)
Calcite	8.84x10⁻⁶ – 9.54x10⁻⁶	Atm PCO₂= 8.0-8.5 N₂ = 9.5	250	AGWs- varied total dissolved solids	10^{-3.5} and N₂ (low O₂ < 0.5 ppm)	Ticknor (1993)
Calcite	1.6x10⁻⁶	7.25-9	3.3-15	varied with pH (~0.6 to 0.1)	10^{-3.5}	Bertetti (2002)
Calcite	not given	7.0-9.6	not given	0.1	10^{-3.5}	Zavarin et al. (2005)

Table 2.3 (continued). Studies of Np(V) Sorption to Pure Mineral Phases

Sorbent (Chemical Formula)	Np(V) (^{237, 239}Np) (mol L⁻¹)	pH range	Solid Concentration (g L⁻¹)	I (mol L⁻¹)	PCO₂ (Atm)	Reference
Chlorite (group) (Generalized: (Fe,Mg, Al)₆(Si, Al)₄O₁₀(OH)₈)	2.0x10⁻¹¹	5 and 8	7-12	0.01- AGW	10^{-3.5}	Beall and Allard (1981)
Chlorite (group)	8.84x10⁻⁶ – 9.54x10⁻⁶	Atm PCO₂= 8.0-8.5 N₂ = 9.5	250	AGWs- varied total dissolved solids	10^{-3.5} and N₂ (low O₂ < 0.5 ppm)	Ticknor (1993)
Clinoptilolite (Generalized:Na_{1.3} K_{1.2}Ca_{1.55}Al_{6.2}Si_{29.8} O₇₂•23H₂O)	1x10⁻⁶	4 -11	4 and 8	0.01 and 0.1	0, capped and 10^{-3.5}	Bertetti et al. (1996)
Clinoptilolite	≈10⁻⁶	8.6 and 9.0	50	GW	10^{-3.5}	Triay et al. (1993)
Corundum (α-Al₂O₃)	2.0x10⁻¹¹	4-10	7.2	0.01- AGW	10^{-3.5}	Beall and Allard (1981)
Corundum- natural and synthetic	≈10⁻¹² – 10⁻¹³	4-10	20	0.1	10^{-3.5}	Tochiyama et al. (1996)
Diaspore (α-AlOOH)	≈10⁻¹² – 10⁻¹³	4-10	20	0.1	10^{-3.5}	Tochiyama et al. (1996)
Epidote (Ca₂(Al,Fe)₃(SiO₄)₃ (OH))	8.84x10⁻⁶ – 9.54x10⁻⁶	Atm PCO₂= 8.0-8.5 N₂ = 9.5	250	AGWs- varied total dissolved solids	10^{-3.5} and N₂ (low O₂ < 0.5 ppm)	Ticknor (1993)

Table 2.3 (continued). Studies of Np(V) Sorption to Pure Mineral Phases

Sorbent (Chemical Formula)	Np(V) (^{237,239}Np) (mol L⁻¹)	pH range	Solid Concentration (g L⁻¹)	I (mol L⁻¹)	PCO₂ (Atm)	Reference
Fe silicates	1x10⁻⁶ – 1x10⁻⁹	3-9	20	0.01 and 0.1	0 and 10^{-3.5}	Del Nero et al. (2004)
Ferrihydrite (Fe₂O₃•H₂O)	4.5x10⁻¹¹- 4.5x10⁻¹³	4-9	0.1, 0.4 and 1.0	0.1	10^{-3.5}	Girvin et al. (1991)
Fluorite (CaF₂)	2.0x10⁻¹¹	4-9	7.4	0.01- AGW	10^{-3.5}	Beall and Allard (1981)
Gibbsite-natural and synthetic (γ- Al(OH)₃)	≈10⁻¹² – 10⁻¹³	4-10	20	0.1	10^{-3.5}	Tochiyama et al. (1996)
Goethite-natural and synthetic (α- FeOOH)	4x10⁻⁷ – 6x10⁻⁶	3-11	1.0	0.1	<10^{-3.5} sealed vials	Nakayama and Sakomoto (1991)
Goethite	1.3x10⁻⁵	7.2	1	0.08	10^{-3.5}	Combes et al. (1992)
Goethite	8.84x10⁻⁶ – 9.54x10⁻⁶	Atm PCO₂= 7.0-7.5 N₂ = 9.5	250	AGWs- varied total dissolved solids	10^{-3.5} and N₂ (low O₂ < 0.5 ppm)	Ticknor (1993)
Goethite	2x10⁻⁷ – 2x10⁻⁶	6.2	~20	0.1 (KCl)	10^{-3.5}	Kung and Triay (1994)
Goethite	4x10⁻⁷- 6x10⁻⁶	4-11	1	0.1	10^{-3.5}	Fugita et al. (1995)
Goethite-natural and synthetic	≈10⁻¹²	3-9	20	0.1	10^{-3.5}	Tochiyama et al. (1995)
Goethite	1.2x10⁻⁷	3-9	20	0.1	0,10^{-3.5} and 10^{-2.7}	Kohler et al. (1999)

Table 2.3 (continued). Studies of Np(V) Sorption to Pure Mineral Phases

Sorbent (Chemical Formula)	Np(V) (^{237,239} Np) (mol L ⁻¹)	pH range	Solid Concentration (g L ⁻¹)	I (mol L ⁻¹)	PCO ₂ (Atm)	Reference
Goethite	5.0x10 ⁻⁵	2-11	4	0.1 and ~0.004 GW	0 and 10 ^{-3.5}	Sherman et al. (2000)
Gypsum CaSO ₄ •2(H ₂ O)	8.84x10 ⁻⁶ – 9.54x10 ⁻⁶	Atm PCO ₂ = 8.0-8.5 N ₂ = 9.5	250	AGWs- varied total dissolved solids	10 ^{-3.5} and N ₂ (low O ₂ < 0.5 ppm)	Ticknor (1993)
Hausmanite (Mn ₃ O ₄)	1x10 ⁻⁶ , 1x10 ⁻⁵ and 1x10 ⁻⁴	4-11	3.3	0.1	10 ^{-3.5}	Wilk et al. (2005)
Hematite- natural and synthetic (α-Fe ₂ O ₃)	4x10 ⁻⁷ - 6x10 ⁻⁶	4-11	1	0.1	10 ^{-3.5}	Nakayama and Sakomoto (1991)
Hematite	8.84x10 ⁻⁶ – 9.54x10 ⁻⁶	Atm PCO ₂ = 8.0-8.5 N ₂ = 9.5	250	AGWs- varied total dissolved solids	10 ^{-3.5} and N ₂ (low O ₂ < 0.5 ppm)	Ticknor (1993)
Hematite-natural and synthetic	≈10 ⁻¹²	3-9	20	0.1	10 ^{-3.5}	Tochiyama et al. (1995)
Hematite	1.2x10 ⁻⁷ - 1.3x10 ⁻⁶	4-9.5	0.1 -5.75	0.005, 0.01, 0.05 and 0.1	0, 10 ^{-3.5} and 10 ^{-2.7}	Kohler et al. (1999)
Hematite	6x10 ⁻⁶	4-8	25	0.1	0 and 10 ^{-3.5}	Nakata et al. (2000 and 2002)
Hematite	1.90x10 ⁻⁷	6, 7 and 8.5	0.2	~0.004 GW	10 ^{-3.5}	Runde et al. (2002)
Hematite	≈10 ⁻⁶	8.5 and 8.7	50	GW	10 ^{-3.5}	Triay et al. (1993)

Table 2.3 (continued). Studies of Np(V) Sorption to Pure Mineral Phases

Sorbent (Chemical Formula)	Np(V) (^{237,239} Np) (mol L ⁻¹)	pH range	Solid Concentration (g L ⁻¹)	I (mol L ⁻¹)	PCO ₂ (Atm)	Reference
Hornblende (Representative: Ca ₂ (Mg,Fe, Al) ₅ (Al,Si) ₈ O ₂₂ (OH) ₂)	<10 ⁻⁷	2.5, 8.5 and 10.4	20	GW	10 ^{-3.5}	Torstenfelt et al. (1988)
Hydrargilite (α-Al(OH) ₃)	≈10 ⁻¹³	4-9	19	0.1 and 0.01	0 and 10 ⁻⁴ M HCO ₃ ⁻	Del Nero et al. (1997)
Hydrargilite	≈10 ⁻¹³	4-9	6	0.1	0 and 10 ⁻⁴ M HCO ₃ ⁻	Del Nero et al. (1998)
Illite (Generalized: (K,H)Al ₂ (Si,Al) ₄ O ₁₀ (OH) ₂ •xH ₂ O)	8.84x10 ⁻⁶ – 9.54x10 ⁻⁶	Atm PCO ₂ = 8.0-8.5 N ₂ = 9.5	250	AGWs- varied total dissolved solids	10 ^{-3.5} and N ₂ (low O ₂ < 0.5 ppm)	Ticknor (1993)
Illite	1x10 ⁻⁸ - 1x10 ⁻⁴	6	~0.1	0.01	10 ^{-3.5}	Nagasaki et al. (1998)
Illite	<10 ⁻⁷	2.5, 8.5 and 10.4	20	GW	10 ^{-3.5}	Torstenfelt et al. (1988)
Kaolinite (Al ₂ Si ₂ O ₅ (OH) ₄)	2.0x10 ⁻¹¹	5 and 8	7-12	0.01- AGW	10 ^{-3.5}	Beall and Allard (1981)
Kaolinite	9.37x10 ⁻¹⁴ - 9.48x10 ⁻¹⁴	not given	0.61	~ 0 and 0.05	10 ^{-3.5}	Keeney- Kennicutt and Morse (1984)
Kaolinite	8.84x10 ⁻⁶ – 9.54x10 ⁻⁶	Atm PCO ₂ = 6.0-6.5 N ₂ = 9.5	250	AGWs- varied total dissolved solids	10 ^{-3.5} and N ₂ (low O ₂ < 0.5 ppm)	Ticknor (1993)

Table 2.3 (continued). Studies of Np(V) Sorption to Pure Mineral Phases

Sorbent (Chemical Formula)	Np(V) (^{237,239} Np) (mol L ⁻¹)	pH range	Solid Concentration (g L ⁻¹)	I (mol L ⁻¹)	PCO ₂ (Atm)	Reference
Kaolinite	7.0x10 ⁻⁶	6-11	5.0	0.1	0	Niitsu et al. (1997)
Lepidocrocite (γ -FeOOH)	4x10 ⁻⁷ - 6x10 ⁻⁶	4-11	1	0.1	<10 ^{-3.5} sealed vials	Nakayama and Sakomoto (1991)
Mackinawite (FeS)	2.7x10 ⁻² – 2.74x10 ⁻³	7-8	8.8	no added I	0	Moyes et al. (2002)
Mackinawite	650-6500 mg L ⁻¹	buffer was initially pH 4.5	0.17 MBq g ⁻¹ – 333 MBq g ⁻¹	no added I	0	Livens et al. (2004)
Magnetite (α -Fe ₃ O ₄)	2.0x10 ⁻¹¹	5-10	7.3	0.01- AGW	10 ^{-3.5}	Beall and Allard (1981)
Magnetite- natural and synthetic	4x10 ⁻⁷ - 6x10 ⁻⁶	4-11	1	0.1	<10 ^{-3.5} sealed vials	Nakayama and Sakomoto (1991)
Magnetite	4x10 ⁻⁷ - 6x10 ⁻⁶	4-11	1	0.1	10 ^{-3.5}	Fugita et al. (1995)
Magnetite- natural and synthetic	≈10 ⁻¹²	3-9	20	0.1	10 ^{-3.5}	Tochiyama et al. (1995)
Magnetite	6x10 ⁻⁶	4-8	25	0.1	0 and 10 ^{-3.5}	Nakata et al. (2000 and 2002)
Manganese dioxide	9.42x10 ⁻¹⁴ - 9.52x10 ⁻¹⁴	not given	0.028	~ 0 and 0.05	10 ^{-3.5}	Keeney- Kennicutt and Morse (1984)
Manganite (MnOOH)	1x10 ⁻⁶ , 1x10 ⁻⁵ and 1x10 ⁻⁴	4-11	2.5	0.1	10 ^{-3.5}	Wilk et al. (2005)
Microcline (Formula)	<10 ⁻⁷	1.9, 8.4 and 10.3	20	GW	10 ^{-3.5}	Torstenfelt et al. (1988)

Table 2.3 (continued). Studies of Np(V) Sorption to Pure Mineral Phases

Sorbent (Chemical Formula)	Np(V) (^{237,239} Np) (mol L ⁻¹)	pH range	Solid Concentration (g L ⁻¹)	I (mol L ⁻¹)	PCO ₂ (Atm)	Reference
Montmorillonite (Generilized: (Na,Ca)(Al, Mg) ₆ (Si ₄ O ₁₀) ₃ (OH) ₆ • nH ₂ O))	2.0x10 ⁻¹¹	5 and 8	7-12	0.01-AGW	10 ^{-3.5}	Beall and Allard (1981)
Montmorillonite	9.31x10 ⁻¹⁴ - 9.61x10 ⁻¹⁴	not given	0.18	~ 0 and 0.05	10 ^{-3.5}	Keeney and Morse (1984)
Montmorillonite	1x10 ⁻⁶	2-10	4.0	0.1	0	Bertetti et al. (1996)
Montmorillonite	8.79x10 ⁻⁷	2-10	3.97	0.1	0-10 ^{-3.5}	Turner et al. (1998)
Montmorillonite	1x10 ⁻⁸ - 1x10 ⁻⁴	6	1	0.01	10 ^{-3.5}	Nagasaki and Tanaka (2000)
Montmorillonite	1.90x10 ⁻⁷	6, 7 and 8.5	0.2	~0.004 GW	10 ^{-3.5}	Runde et al. (2002)
Montmorillonite	5.0x10 ⁻⁵	2-11	4	0.1 and ~0.004 GW	0 and 10 ^{-3.5}	Sherman et al. (2000)
Montmorillonite	≈10 ⁻⁶	8.5 and 8.7	50	GW	10 ^{-3.5}	Triay et al. (1993)
Muscovite (KAl ₂ (AlSi ₃ O ₁₀) (F,OH) ₂)	8.84x10 ⁻⁶ - 9.54x10 ⁻⁶	Atm PCO ₂ = 8.0-8.5 N ₂ = 9.5	250	AGW solutions- varied total dissolved solids	10 ^{-3.5} and N ₂ (low O ₂ < 0.5 ppm)	Ticknor (1993)
Pyrite (FeS ₂)	2.0x10 ⁻¹¹	3-9	7.8	0.01-AGW	10 ^{-3.5}	Beall and Allard (1981)

Table 2.3 (continued). Studies of Np(V) Sorption to Pure Mineral Phases

Sorbent (Chemical Formula)	Np(V) (^{237,239}Np) (mol L⁻¹)	pH range	Solid Concentration (g L⁻¹)	I (mol L⁻¹)	PCO₂ (Atm)	Reference
Quartz (SiO₂)	2.0x10⁻¹¹	3-10	7.6	0.01- AGW	10^{-3.5}	Beall and Allard (1981)
Quartz	≈10⁻⁶	8.5 and 8.9	50	GW	10^{-3.5}	Triay et al. (1993)
Quartz	8.84x10⁻⁶ – 9.54x10⁻⁶	Atm PCO₂= 7.0-7.5 N₂ = 9.5	250	AGWs- varied total dissolved solids	10^{-3.5} and N₂ (low O₂ < 0.5 ppm)	Ticknor (1993)
Quartz	1.0x10⁻⁷- 1.0x10⁻⁶	5-11	40 and 80	0.1	<10^{-3.5} sealed vials and 10^{-3.5}	Bertetti et al. (1996)
Quartz	1.2x10⁻⁷	4-12	30	0.1	0	Kohler et al. (1999)
Serpentinite	2.0x10⁻¹¹	5 and 9	7-12	0.01- AGW	10^{-3.5}	Beall and Allard (1981)
Silica colloids	1.90x10⁻⁷	6, 7 and 8.5	0.2	~0.004 GW	10^{-3.5}	Runde et al. (2002)
Silcate gel (Ca²⁺ or Mg²⁺)	7.2x10⁻¹⁴ and 2.8 x10⁻⁴	7	not given ~ 4	not given ~ 0.25	10^{-3.5}	Paulus et al. (1992)
Sodium-Smectite (Generilized: (Ca, Na, H) (Al, Mg, Fe, Zn)₂ (Si, Al)₄O₁₀ (OH)₂•xH₂O))	6x10⁻⁷	2-8	1	0.01	10^{-3.5}	Kozai et al. (1993 and 1996)

occurring and synthetic aluminum oxides under conditions similar to those used to study Np(V) sorption to iron oxides. Similar to Np(V) sorption to iron oxides, sorption to aluminum oxides followed the order: gibbsite (α -Al(OH)₃) > diaspore (α -AlOOH) > corundum (α -Al₂O₃), with the highest Np(V) sorption occurring on the least crystalline aluminium oxides having the highest surface area.

Del Nero et al. (2004) conducted Np(V) sorption experiments using poorly ordered allophane-like (Al-rich) and hisingerite-like (Fe-rich) silicates. This study found that increasing the concentration of aluminol sites had little impact on Np(V) sorption, suggesting that the predominant surface sites were the weakly acidic silanol groups. Np(V) sorption to Fe-rich silicates was substantially higher than sorption to Al-rich silicates but the wide Fe/Si molar ratio had an unexpectedly low impact on Np(V) sorption. One explanation given was that the high solubility of the Fe silicates led to the release of silicate anions, which in turn adsorbed to the ferrinol surface sites or formed silica gel coatings.

Few spectroscopic studies have been conducted to elucidate the nature of Np(V) surface complexation (Table 2.4). Of the X-ray absorption spectroscopy (XAS) studies conducted, the majority have focused on Np(V) surface reactions with goethite and hematite likely due to the high affinity of Np(V) for iron oxides compared to other minerals (Combes et al., 1992; Sherman et al., 2000; Arai et al., 2007). The Combes et al. (1992) study of Np(V) sorption to goethite gave evidence that Np(V) formed inner- sphere mononuclear surface complexes. Arai et al. (2007) showed that EXAFS results suggest bis-carbonato inner-sphere and tris-carbonato outer-sphere ternary neptunyl surface species co-exist at the hematite-water interface at pH 7-8.8.

2.1.3 Neptunium(V) Sorption to Complex Geomedia

Most of the research on Np(V) sorption to soils and sediments has been conducted with the intent of determining K_d values for input into

transport models relevant to underground repositories. K_d values (e.g. ml g⁻¹) are defined as the ratio of the Np sorbed per mass of solid to the concentration of Np remaining in solution, where small K_d values are indicative of weak sorption. The USEPA (1999) and the USNRC (1981) offer thorough reviews of early Np(V) sorption studies. The USEPA report contains look-up tables for minimum and maximum K_d values for many radionuclides. However, look-up tables were not derived for Np(V) due to the lack of sufficient Np(V) sorption studies on complex geomedia. However, the database used by the USNRC for previous performance assessments (PA) has a K_d value of 10 ml g⁻¹ for Np(V) sorption to clay, granite, basalt and tuff (McKinley and Scholtis, 1993). Table 2.5 contains a summary of the available studies for Np(V) sorption to various sediments and soil types. Many of these studies focus on Np(V) sorption under fixed geochemical conditions (e.g. pH, PCO₂, total Np and solid concentration).

The Eckhardt (2000) review of research conducted by Los Alamos National Laboratory illustrated the variability in Np(V) sorption to different Yucca Mountain zeolitic tuff samples. Variations in Np(V) sorption was primarily attributed to variable concentrations of clay and iron oxide surface sites in the different tuff samples. However, experimental Np(V) sorption data was fairly well simulated when only clinoptilolite surface sites, a primary component of the tuffs, were considered, evidence for the surface site dependence of Np(V) sorption.

The Mincher et al. (2003) study of Np sorption to soil from the Snake River Plain in Idaho showed that sorption was well described using a Freundlich isotherm, suggesting the possible presence of multiple site types. The soil had an estimated distribution by weight of the following minerals: 50-75% quartz, 10-25% plagioclase and K-feldspar, 2-5% olivine and pyroxene, 10-20% clay as illite-smectite and kaolinite, and 2-5% calcite. The authors hypothesized that sorption was initially controlled by complexation with clay surface sites rather than iron oxides and ultimately controlled by

Table 2.4 Np(V) Sorption Spectroscopic Studies

Sorbent	Significant Findings / Comments	Reference
Goethite	EXAFS results show that Np(V) sorbs as a mononuclear species, likely neptunyl, but carbonato or hydrolysis complexes may be present; sorbs as an inner sphere complex	Combes et al. (1992)
Goethite	Preliminary XAS observations show that Np(V) is reduced to Np(IV) at low pH under inert atmosphere	Sherman et al. (2000)
Mackinawite	EXAFS and XANES results show that interaction with the sulfide surface reduces Np(V) to Np(IV) with Np(IV) coordinating directly to sulfide surface atoms	Moyes et al. (2002)
Mackinawite	EXAFS and XANES results show that direct covalent interaction of Np(V) with the sulfide surface and reduction to Np(IV) ; coordination at the surface is the same over 1 log unit of Np(V) concentration change	Livens et al. (2004)
Hausmanite and Manganite	XANES results show that solution Np(V) is reduced to Np(IV) by interaction with manganite but not hausmanite. Introduction into the X-ray beam caused Np reduction in the presence of hausmanite. EXAFS results show that Np precipitates at both mineral surfaces.	Wilk et al. (2005)
Hematite	EXAFS results show that bis-carbonato inner-sphere and tris-carbonato outer-sphere ternary surface species co-exist at the hematite-water interface at pH 7.0-8.8	Arai et al. (2007)

formation of Np oxide phases. The K_d value of $49 \pm 12 \text{ ml g}^{-1}$ in artificial groundwater was consistent with the value obtained by Grossman et al. (2001) for sorption to basalt interbedded sediments. Grossman et al. showed that Freundlich isotherms fit the experimental data for Np(V) sorption better than Langmuir isotherms. Of interest, Mincher et al. (2003) used a very short contact period of 3 hours while the Grossman et al. study was conducted over 56 days. Grossman et al. showed that sorption proceeded quickly initially, followed by a slow increase in sorption over the entire study period.

2.1.4 Influence of Humic Acids on Neptunium(V) Sorption

Humic acids (HA) can reduce, increase or have no effect on metal and radionuclide sorption to

mineral surfaces depending on the nature of the system. For example, the Niitsu et al. (1997) study of Np(V) sorption to kaolinite showed a noticeable increase in Np(V) sorption below pH 8 in the presence of HA and a marked decrease in Np(V) sorption from pH 8-11 compared to the system without HA. The increase in sorption was associated with a concomitant increase in HA sorption. Increased Np(V) affinity for the kaolinite was likely a result of the formation of ternary Np(V) complexes and the increasingly negative surface charge due to HA sorption. At pH values greater than 8, the desorption of HA and subsequent formation of a Np-HA aqueous complex was considered the cause for the reduction in Np(V) sorption. Righetto et al. (1991) observed a similar trend for Np(V) sorption to γ -alumina and amorphous silica. Righetto and co-workers also showed

Table 2.5. Studies of Np(V) Sorption to Complex Geomedia (GW = groundwater, AGW = artificial groundwater, ASW = artificial groundwater, DW = deionized water, all collected at atmospheric PCO₂ unless noted)

Sorbent	K_d (mL g⁻¹)	Solution Phase	pH	Reference
Soils :				
Sandy Washington soil (WS)	3.90	0.015 M NaNO₃	7.4 and 4.1	Routson et al. (1975, 1977)
	3.51	0.030 M NaNO₃		
	3.28	0.3 M NaNO₃		
	3.28	0.75 M NaNO₃		
	3.19	3.00 M NaNO₃		
	2.37	0.002 M Ca(NO₃)₂		
	0.93	0.02 M Ca(NO₃)₂		
	0.78	0.05 M Ca(NO₃)₂		
	0.62	0.10 M Ca(NO₃)₂		
South Carolina soil (SCS)	0.36	0.20 M Ca(NO₃)₂	7.8 and 6.2	Routson et al. (1975, 1977)
	0.66	0.015 M NaNO₃		
	0.57	0.030 M NaNO₃		
	0.51	0.3 M NaNO₃		
	0.45	0.75 M NaNO₃		
	0.43	3.00 M NaNO₃		
	0.25	0.02 M Ca(NO₃)₂		
0.16	0.20 M Ca(NO₃)₂			
Silt loam soil-clay fraction	320	5 mM Ca(NO₃)₂	6.5	Dahlman et al. (1976)
Sharpsburg silt clay loam	35	Deionized water	5.83	Nishita et al. (1981)
	95		6.85	
Malbis sandy loam	3	Deionized water	4.08	Nishita et al. (1981)
	18		5.57	

Table 2.5 (continued). Studies of Np(V) Sorption to Complex Geomedia

Sorbent	K_d (mL g ⁻¹)	Solution Phase	pH	Reference
Lyman sandy loam	32	Deionized water	4.42	Nishita et al. (1981)
Holtsville silty clay	41	Deionized water	7.29	Nishita et al. (1981)
	117		8.28	
Aiken loam	26	Deionized water	5.56	Nishita et al. (1981)
	108		6.57	
Yolo silt loam	52	Deionized water	6.13	Nishita et al. (1981)
	81		6.83	
Egbert muck	786	Deionized water	6.24	Nishita et al. (1981)
	929		7.25	
Oxidized clayey sand	180	GW	8.3 (low carb)	Bidoglio et al. (1987)
	126		8.3 (med carb)	
	68		8.3 (high carb)	
	90		9.0	
INEEL sedimentary interbed soil, representative sample: 7DS01701	58.5 ± 1.3 (7 days)	AGW	~8	Grossman et al. (2001)
	68.1 ± 4.7 (14 days)			
	80.8 ± 6.3 (28 days)			
	94.9 ± 2.9 (56 days)			
INEEL sedimentary interbed soil, representative sample: LIS-INEEL-10	195 ± 6.3 (7 days)	AGW	~8	Grossman et al. (2001)
	227 ± 13 (14 days)			
	257 ± 16 (28 days)			
	286 ± 24 (56 days)			
Idaho plains soil (quartz/feldspar/clays/Fe and Al oxides/ calcite)	49 ± 12	AGW	7.55	Mincher et al. (2003)
	63 ± 12	Deionized water	Not given	

Table 2.5 (continued). Studies of Np(V) Sorption to Complex Geomedia

Sorbent	K_d (mL g ⁻¹)	Solution Phase	pH	Reference
Calcareous soil:				Weijuan & Zuyi (2003)
Untreated soil	80-760	0.01 CaCl ₂	7.7	
Soil with CaCO ₃ removed	25-50		7.8	
Soil with organic matter removed	16-200		7.8	
Soil with CaCO ₃ and organic matter removed	27-61		7.8	
Sediments:				Kaplan and Serne (1995) and Kaplan et al. (1996)
Hanford: Touchet bed sand	2.17 (7 days)	GW	8.46	
	3.62 (77 days)			
Hanford : Silty loam	2.67 (7 days)			
	13.5 (77 days)			
Hanford : Very coarse sand	14.2 (7 days)			
	19.9 (77 days)			
Hanford: Trench 8 Sediment (TBS-1)	13.5 ± 3 (5 days)	GW	8.3	
	29.1 ± 3.6 (44 days)			
Saturated aquifer sediment- Forty Mile Wash, Nevada	10-35	GW or AGW	~ 7.0-9.0	Bertetti et al. (2006)
Aquifer sediments from Gorleben, Germany, different depths:				Leiser & Mühlenweg (1988)
S1	1.9 ± 0.5 (aerobic)	GW from same depth as sediment	6.0	
	21 ± 6 (anerobic)		6.0	
S2	1.4 ± 0.4 (aerobic)		7.1	
	1290 ± 330 (anerobic)		6.8	

Table 2.5 (continued). Studies of Np(V) Sorption to Complex Geomedia

Sorbent	K_d (mL g ⁻¹)	Solution Phase	pH	Reference
Aquifer sediments from Gorleben, Germany, different depths:				
S3	2.6 ± 0.6 (aerobic)	GW from same depth as sediment	7.9	Leiser & Mühlenweg (1988)
	168 ± 42 (anerobic)		7.3	
S4	2.7 ± 0.6 (aerobic)		7.0	
	1060 ± 260 (anerobic)		7.3	
S5	3.7 ± 0.8 (aerobic)		7.0	
	1600 ± 500 (anerobic)		6.9	
Marine sediments:				
Clay-rich & organic-rich marine sediments	Kinetic data only	Deionized water and ASW in equilibrium with calcite	7.8-8.2	Keeney-Kennicutt & Morse (1984)
Silt and clay fractions of marine particulate material	See sorption data in article	Deionized water & 0.7 M NaCl with or without 2 mM HCO ₃ ⁻ , 0.42 M NaCl & Ca ²⁺ or Mg ²⁺	6.8-11	McCubbin & Leonard (1995)
Silt and clay fractions of marine particulate material	See sorption data in article	Partial seawater	8.0	McCubbin & Leonard (1997)
Rock samples:				
Stripa granite	10	GW	1.9	Torstenfelt et al. (1988)
	60		8.5	
	70-120		10.1	
Finnsjön granite	10	GW	2.2	Torstenfelt et al. (1988)
	60-180		8.8	
	110-210		10.1	

Table 2.5 (continued). Studies of Np(V) Sorption to Complex Geomedia

Sorbent	K_d (mL g⁻¹)	Solution Phase	pH	Reference
Westerly granite	10	GW	2.0	Torstenfelt et al. (1988)
	70-90		7.5	
Granite	3000 (1.1x10⁻⁶ m s⁻¹)	GW	8.9	Kumata & Vandergraaf (1998)
	900 (3.2x10⁻⁶ m s⁻¹)			
Yucca Mountain Tuff	0-2.4 (batch)	GW and AGW	8.3-9.5	Triay et al. (1993, 1996)
	0.01-2.8 (column)			
Yucca Mountain Tuffs:				
Zeolitic	0.3	GW	7.0	Eckhardt (2000) (summary of Los Alamos Yucca Mountain project)
	1.5		8.5	
Devitrified	0.007		7.0	
	~0.04		8.5	
Vitric	0.2		7.0	
	0.3		8.5	
Vitric with 10% clay	~8		7.0	

that increasing the HA concentration (1 to 50 mg L⁻¹) accentuated the increase in Np(V) sorption to both minerals. Furthermore, the decrease in sorption at pH values >8 was greater at higher HA concentrations presumably due to an increase in the aqueous Np(V)-HA complexation. Table 2.6 summarizes the Np(V) sorption studies conducted with HA present.

2.1.5 Surface Complexation Modeling of Natural Systems

The primary geochemical mechanism that will limit the migration of ²³⁷Np away from an underground repository is the extent to which Np sorbs to solid surfaces (Eckhardt, 2000). Traditionally, quantitative descriptions of adsorption are accomplished using empirical adsorption models as suggested by the literature pertaining to Np(V) sorption to complex geomedia (see Table 2.5). Distribution coefficients, K_d , have often been used to model sorption due to the experimental simplicity (batch and column studies) and the ease of incorporation into transport models. However, factors such as solute composition, pH, PCO₂ and solid characteristics may significantly impact K_d values (USEPA, 1999). Langmuir and Freundlich isotherm constants will generally describe sorption over a wider concentration range than do single K_d values, but the constants are also system dependent (Koretsky, 2000). Therefore, K_d values and isotherms derived from a specific set of conditions may not be applicable to natural systems with geochemical conditions that vary both spatially and temporally.

Generally, the sorption behavior of Np has been incorporated into transport models using a constant distribution coefficient (K_d) or a range of K_d values (USEPA, 1999). However, K_d values can vary due to temporal and spatial variations in chemical conditions resulting in a high degree of error being incorporated into model calculations (Bethke and Brady, 2000). To address this inadequacy, surface complexation models (SCMs), which describe metal and radionuclide sorption over a range of geochemical conditions, have been incorporated into transport model simulations (Kent et al.,

2000; Curtis et al., 2006). The component additivity (CA) and generalized composite (GC) approaches are two types of SCMs capable of describing metal and radionuclide sorption to heterogeneous sediments and soils (Kent et al., 2000; Waite et al., 2000; Sanpawanitchakit, 2002; Davis et al., 2004).

The primary objective of the research described in this section was to test the appropriateness of using SCMs to describe Np(V) sorption to heterogeneous geomedia under field relevant conditions. To date, few studies have focused on Np(V) sorption to sediments and soils over a range of geochemical conditions, limiting the available experimental data (e.g. Mincher et al., 2003; Sakamoto et al., 2000; Weijuan & Zuyi, 2003). As a result, the use of SCMs to describe Np(V) sorption has been restricted to pure mineral phases (Del Nero et al., 1997; Turner et al., 1998; Kohler et al., 1999; Del Nero et al., 2004). This study expands the available experimental data for Np(V) sorption to well characterized sediments under environmentally relevant conditions. Experimental variables include: Np(V) concentration (5×10^{-8} – 1×10^{-5} M), solid concentration (50, 125 and 500 g L⁻¹) partial pressure of CO₂ (PCO₂ = 0, 10^{-3.5} and 10^{1.1} atmospheres (atm)), competing inorganic groundwater solutes (e.g. Ca²⁺, Mg²⁺, CO₃²⁻) and HA (10-200 mg L⁻¹). The effect of carbonate minerals was elucidated by conducting experiments with unmodified sediment and sediment treated to remove the carbonate minerals. The effect of variable pH (3-10) was studied using sediment treated to remove carbonate minerals. A non-electrostatic GC-SCM was assessed to determine its ability to simulate and predict the Np(V) sorption on an alluvial aquifer sediment.

2.2 Effect of Solution Composition on Neptunium(V) Sorption to an Alluvial Aquifer Sediment

2.2.1 Aquifer Sediment Sample

This section contains experimental results for Np(V) sorption to the well characterized Naturita aquifer background sediment (NABS)

Table 2.6 Studies of Np(V) Sorption in the Presence of Humic Substances

Sorbent	Organic Material (Origin and mg L ⁻¹)	Ionic Strength (mol L ⁻¹)	pH	Reference
γ -alumina and amorphous silica	Boom clay extracted HA-0 to 50 mg L ⁻¹	0.1 NaClO ₄	4-10	Righetto et al. (1991)
Yucca Mountain tuff, Al oxide and Fe oxide	Nordic aquifer FA-0.1 to 0.4 mg L ⁻¹	0.1 KCl	6.2	Kung and Triay (1994)
Kaolinite	Aldrich HA	0.1 NaClO ₄	6-11	Niitsu et al. (1997)
Sandy sediment	Gorleben groundwater DOC = 29.9 mg L ⁻¹	Unspecified-Gorleben groundwater	7.6	Artinger et al. (2000)
Sandy soil and granite media	Aldrich HA, HS from the Chalk River Laboratories (CRL-Fulvics) and from the Underground Research Laboratory (URL-Fulvics) of Atomic Energy of Canada Limited- 20 mg L ⁻¹	0.01 M NaClO ₄	5.5 and 9.5	Sakamoto et al. (2000)
Weak loess aquifer medium	Unnamed HS-10% (w/w)	Unspecified groundwater	Not given	Chunli et al. (2001)
Calcareous soil-treated to remove organic matter and/or CaCO ₃	Field site at the China Institute for Radiation Protection (CIRP) FA- 20 mg L ⁻¹	0.01 CaCl ₂	7.8	Weijuan and Zuyi (2003)

under variable geochemical conditions. Uncontaminated sediment was obtained from the Uranium Mill Tailings Remedial Action (UMTRA) site situated along the San Miguel River about 3 km downstream from the town of Naturita in Montrose County, Colorado. Sediment from the saturated zone was collected on July 16-17, 1998 from a gravel pit located up gradient of the uranium (U) contamination (USNRC, 2003). The sediment size fraction that passed through both a 64 mm and a 3 mm sieve was used for all experiments. This fraction made up roughly 15% of the total sediment collected from the field and approximately 30% of the < 64 mm fraction (Davis et al., 2004). The alluvial aquifer sediment (NABS) was utilized in its unmodified and carbonate-mineral removed forms. The unmodified sediment was largely

composed of quartz, feldspars and calcite with lesser amounts of magnetite and clay minerals (Davis et al., 2004). Treated sediment underwent carbonate destruction using 1M sodium acetate solution, adjusted to pH 5 with acetic acid. Both the unmodified and treated sediment grains exhibited illite/smectite clay coatings with occluded ferrihydrite and goethite (Davis et al., 2004). Both sediment types were previously utilized to study U(VI) sorption and have been extensively characterized (Sanpawanitchakit, 2002; USNRC, 2003; Davis et al., 2004; Kohler et al., 2004).

2.2.2 Materials and Methods

The neptunium-237 (²³⁷Np) stock solution, in secular equilibrium with its daughter

protactinium-233 (^{233}Pa), was prepared in 4 M nitric acid by Isotope Products Laboratories. With the exception of ^{233}Pa , the ^{237}Np solution was free of radioimpurities. Uranium(VI) samples were prepared from ^{238}U as uranyl nitrate, $\text{UO}_2(\text{NO}_3)_2$, spiked with ^{233}U ($t_{1/2} = 1.59 \times 10^5$ years), both purchased from Anderson Laboratories. All reagents were analytical grade or better unless noted. Standard reference grade Suwannee River humic acid (HA) was purchased from the International Humic Substances Society (IHSS) and used without further purification. Water was obtained from a Barnstead ultra-low carbon water system (EASYPure[®] UV water). Labware was soaked for approximately 24 hours in 1% w/v sodium hydroxide (NaOH), rinsed at least 3 times with UV-treated water and soaked for another 24 hours in 10% v/v hydrochloric acid (HCl) prior to a final thorough rinse with UV-treated water. Labware that contacted organic matter was scrubbed in a dilute solution of Alconox Liqui-Nox[®] detergent and rinsed with water prior to the NaOH/HCl cleaning procedure.

The stock ^{237}Np ($6 \mu\text{Ci mL}^{-1}$) and ^{233}U ($4 \mu\text{Ci mL}^{-1}$) solutions were stored in lead shielded boxes. Samples containing ^{237}Np and ^{233}U were handled in a fume hood under negative pressure or in an inert atmosphere glovebox except during sample analysis.

NABS was treated to remove carbonate minerals, primarily present as calcite, following procedures similar to Sanpawanitchakit (2002). Briefly, 500 g of sediment was added to 5 L of 1 M sodium acetate (CH_3COONa) adjusted to pH 5 with acetic acid (CH_3COOH). The slurry was placed on a shaker table for 24 hours in a large HPDE container that was left open to the atmosphere to allow CO_2 transfer. Suspended particles were allowed to settle before the supernatant was decanted and the procedure was repeated. The wet sediment was rinsed numerous times with UV-treated water following the settling/decanting procedure outlined above until conductivity measurements were constant. The treated sediment was dried at 60°C for approximately 48 hours.

The specific surface area (A_{sp}) for treated NABS was $4.47 \text{ m}^2 \text{ g}^{-1}$ as determined by BET (Brunauer, Emmett, and Teller) analysis while A_{sp} was $5.15 \text{ m}^2 \text{ g}^{-1}$ for unmodified NABS (Davis et al., 2004). Surface area measurements were also conducted for various grain size fractions of treated and unmodified NABS (Table 2.7). For all fractions, treated sediment had A_{sp} values lower than unmodified NABS suggesting that dissolution of carbonate minerals broke up the cemented fragments. An overview of NABS characterization is found in Sanpawanitchakit (2002), USNRC (2003), and Davis et al., (2004).

Artificial groundwater (AGW) solutions with major cation concentrations similar to concentrations encountered in Naturita groundwater were used for all sorption experiments with the exception of experiments conducted using sodium perchlorate (NaClO_4) solutions. AGW solution compositions varied slightly depending on the experimental PCO_2 . The composition, ionic strength and pH of each AGW are given in Table 2.8.

A Packard 2500TR liquid scintillation counting (LSC) instrument was used to analyze all ^{237}Np and ^{233}U containing samples. The LSC data analysis is discussed in detail in Section 2.2.3.2, Liquid Scintillation Analysis. A Thermo Orion Ross[™] semi-micro combination electrode calibrated with NIST certified pH buffers (4.000, 7.000 and 10.000) was used for all pH measurements. Total organic carbon (TOC) was analyzed using a Shimadzu 5000A TOC Analyzer. To confirm PCO_2 values, alkalinity titrations were conducted following Gran function plot methodology using a HACH digital titrator with 1.600 N or 0.1600 N sulfuric acid cartridges. All experiments were conducted at room temperature.

Batch sorption samples were centrifuged at 5000 g for 60 minutes and a portion of the solution phase of each sample was removed and analyzed by LSC. Gelman Acrodisc[®] syringe filters ($0.45 \mu\text{m}$) were used to ensure that separation by centrifugation was acceptable. Samples that were filtered gave consistent results with centrifuged samples.

**Table 2.7 NABS Surface Area Distributions and Weight Percent
for Various Grain Size Fractions***

Size Fractions (μm)	Unmodified		Treated	
	Surface Area (m^2/g)	Weight (%)	Surface Area (m^2/g)	Weight (%)
< 63	13.1	3.7	11.01	4.7
63-125	7.19	6.4	5.96	8.3
125-250	5.1	16.6	4.05	21.3
250-500	3.95	23.1	3.11	25.4
500-1000	5.7	15.9	4.75	15.2
1000-3000	6.31	34.2	5.20	25.1
NABS	5.15	100.0	4.47	100.0

*From USNRC, 2003; Kohler et al., 2004; and Sanpawanitchakit, 2002

Table 2.8 Composition of Artificial Groundwater Solutions

	AGW-3	AGW-A	AGW-6
Initial PCO_2	Atmospheric	Atmospheric	8%
pH	7.9	5.6	6.8
Ionic Strength	0.02	0.02	0.03
CaSO_4	2.33×10^{-3}	0	3.27×10^{-3}
MgSO_4	1.52×10^{-3}	1.52×10^{-3}	1.52×10^{-3}
Na_2SO_4	9.38×10^{-4}	3.27×10^{-3}	0
CaCl_2	2.38×10^{-3}	4.71×10^{-4}	0
KCl	6.40×10^{-5}	6.40×10^{-5}	6.40×10^{-5}
NaHCO_3	5.38×10^{-4}	0	2.41×10^{-3}
CaCO_3	0	0	3.33×10^{-3}
HCl	0	0	1.57×10^{-3}

Ionic strengths and component concentrations are in mol L^{-1}

The percent Np(V) sorbed ($\%Np_{\text{Sorbed}}$) was calculated using a mass balance approach as follows:

$$\%Np_{\text{Sorbed}} = 100\% * \left(1 - \frac{CPM_{\text{Final}}}{CPM_{\text{Initial}}} \right)$$

where CPM_{Initial} and CPM_{Final} represent the counts per minute, for solution phase samples, before and after contact with NABS, respectively. CPM and decays per minute (DPM) were considered equal due to the 100% efficiency for LSC α particle counting (Horrocks, 1976). In order to confirm that Np_{Sorbed} determined by the above approach was actually sorbed to the sediment, mass balance experiments were occasionally conducted by adding 1 M HCl, removing an aliquot of the solution phase and adjusting to pH ~ 4 prior to LSC analysis.

LSC counting times of 60 minutes gave a maximum 2σ error of $\pm 1\%$ for the α counting activity. The use of a range of humic acid (HA) concentrations resulted in varying degrees of color quenching during LSC analysis, resulting in quantifiable shifts in the LSC α spectrum. To account for color quenching, the LSC CPM data for each HA containing sample was manually analyzed (see Section 2.4.2).

2.2.2.1 Time Dependent Np(V) Sorption Experiments

The length of time needed for quasi-equilibrium conditions to be met was studied using batch sorption methodology with 5.0×10^{-7} M Np(V) and 50 g L^{-1} unmodified NABS in AGW-3 under atmospheric PCO_2 . Into each 50 ml Nalgene[®] Oak Ridge polycarbonate centrifuge tube, $19.5 \text{ ml} \pm 0.2 \text{ ml}$ AGW-3 was added to $1.000 \text{ g} \pm 0.0025 \text{ g}$ unmodified NABS. The tubes were shaken in the dark while open to atmospheric PCO_2 for a 72-hour pre-equilibration period. The purpose of this step was to allow ions dissolved from the NABS surface (e.g. Ca^{2+} , Mn^{2+} and $HSiO_4^-$) during initial contact with AGW to approach steady state concentrations (USNRC, 2003). A $500 \mu\text{l}$ aliquot of 2.0×10^{-5} M Np(V) was added to each

vial, resulting in a slight dilution ($< 3\%$) of the AGW-3 and giving a final Np(V) concentration of 5.0×10^{-7} M. Modification of pH, using unmodified NABS, was difficult under fixed PCO_2 due to the buffering effect of the carbonate minerals. Therefore, the pH of each sample was allowed to reach its final value of $\text{pH } 8.0 \pm 0.1$ without outside manipulation. Vials were removed in triplicate at specified time intervals, centrifuged, and the supernatant was analyzed by LSC.

The influence of Suwannee River HA on the time Np(V) takes to reach steady state-like concentrations in the presence of NABS was also investigated using batch sorption experiments. Two batch experiments were conducted: 1) the first studied the influence of Np(V) pre-equilibration with HA prior to conducting sorption experiments; 2) the second experiment explored the effect of contact time on Np(V) sorption to treated NABS in the presence of HA.

The stock Np(V)-HA solution, consisting of 5.0×10^{-5} M Np(V) and 1000 mg L^{-1} HA, was prepared in an autoclaved 20 ml Nalgene[®] Oak Ridge polycarbonate centrifuge tube. The sample pH was 8.0 ± 0.1 and the ionic strength was 0.02 M NaClO_4 . The stock solution was stored at 4°C in the dark except for brief periods for sample removal. To each sample vial, $1.000 \text{ g} \pm 0.0025 \text{ g}$ treated NABS was added and pre-equilibrated for 72 hours with 19.8 ml of 0.1 M NaClO_4 at $\text{pH } 8.0 \pm 0.1$. Throughout the experiment, samples were kept on a shaker table in the dark at atmospheric PCO_2 . At set time intervals, $200 \mu\text{L} \pm 2 \mu\text{L}$ of the stock pre-equilibrated Np(V)-HA solution was added to each vial in a group to be further equilibrated with NABS over separate time intervals. Each sample contained 5.0×10^{-7} M Np(V) and 10 mg L^{-1} HA. Individual vials were removed after specific time intervals, centrifuged and analyzed by LSC.

2.2.2.2 Sorption Isotherm Experiments

The effect of PCO_2 and variable Np(V) concentration on sorption to treated and

unmodified NABS was investigated using batch sorption isotherm experiments with a solid concentration of 125 and 500 g L⁻¹ at atmospheric PCO₂ (0.025% in Golden, CO) and 125 g L⁻¹ at 8% PCO₂. Sample pH was allowed to reach equilibrium with the specific PCO₂. The equilibrium pH at atmospheric PCO₂ was 8.0 ± 0.1 and 6.8 ± 0.1 at 8% PCO₂. The 8% PCO₂ conditions were carried out using 10% v/v certified primary grade CO₂ gas within a soft sided glovebox that was effectively an open system maintained at ambient pressure. To each polycarbonate tube, 19.8 ml ± 0.2 ml of AGW-3, AGW-6 or 0.1 M NaClO₄ was added to 2.5000 g ± 0.0050 g or 10.000 ± 0.0050 g treated or unmodified NABS. Tubes were shaken in the dark while open to the applicable PCO₂ atmosphere for the 72-hour pre-equilibration period. The Np(V) concentration range was varied between 2.0x10⁻⁷ M to 5.0x10⁻⁶ M for samples containing 125 g L⁻¹ and between 8.0x10⁻⁷ M and 1.0x10⁻⁵ M for the 500 g L⁻¹ samples. Following addition of the acidic Np(V) stock solution, the pH was adjusted and the total volume was brought up to 20 ml ± 0.2 ml with UV-treated water, NaOH and/or HCl. The samples were equilibrated on a shaker table in the dark for an additional 24 hours ± 1 hour before centrifugation or filtration followed by LSC analysis. Immediately following removal of a sample for LSC analysis, the final pH was measured and in some cases the total alkalinity was determined. Most samples were run in triplicate with some exceptions, including the entire 500 g L⁻¹ data set which was run in duplicate. Table 2.9 outlines the experimental variables that were examined. For comparison purposes, a U(VI) isotherm experiment was conducted at atmospheric PCO₂, using 50 g L⁻¹ and U(VI) concentrations between 1.0x10⁻⁷ M and 1.0x10⁻⁵ M.

2.2.2.3 Np(V) Sorption Edge Experiments

The protocols for determining the sorption of Np(V) as a function of pH were similar to the sorption isotherm methodology described in the previous section (2.2.2.2). The effects of pH, PCO₂, Np(V) concentration, solid-solution ratio, competing ions and HA on Np(V) sorption to

NABS were investigated using batch sorption experiments. Only treated NABS was used for sorption edge experiments due to the buffering effect of the carbonate minerals in unmodified NABS. Solid-solution ratios were held constant at 50, 125 and 500 g L⁻¹ treated NABS for each experimental data set. Most sorption edges were conducted over the pH range of 4 to 9 with some exceptions. Sorption edge experiments were conducted at Np(V) concentrations of 5.0x10⁻⁷ M and 5.0x10⁻⁶ M. For comparison purposes, several sorption edges were obtained using U(VI) = 5.0x10⁻⁷ M and solid-solution ratios of 50 and 125 g L⁻¹ treated NABS. Sorption edges with HA only (10 and 100 mg L⁻¹) were conducted at atmospheric PCO₂, using 500 g L⁻¹ treated NABS in 0.1 M NaClO₄. Table 2.10 outlines the experimental variables that were investigated without HA. Table 2.11 summarizes the experimental variables investigated with HA present.

2.2.2.4 Surface Charge Characterization

A salt titration technique based on the work by Yates and Healy (1975) was used to determine the approximate point of zero salt effect (pH_{pzse}) and obtain a reasonable estimate of the point of zero charge (pH_{pzc}) for treated NABS in NaClO₄. The ions of the indifferent electrolyte, NaClO₄, were assumed to sorb to the NABS surface non-specifically. Briefly, a series of 500 g L⁻¹ samples were prepared in triplicate following the same approach described above. The experiment was conducted in an inert (N₂) atmosphere glovebox to exclude carbonate species. Each sample was adjusted to approximately pH 5-9 using dropwise addition of dilute HCl or NaOH solutions and pre-equilibrated on a shaker table in the dark for 72 hours. The initial pH of each sample was recorded prior to addition of enough GFS Biorefined™ NaClO₄ salt to bring the NaClO₄ concentration up to 0.01 and 0.1 M. The pH of an individual sample was recorded following the first salt addition (0.01 M). The pH was recorded for an additional 10 minutes prior to the second salt addition and the final pH measurement. The samples were run in duplicate. Variations in initial pH and the change in pH due to salt addition are presented

Table 2.9 Np(V) Sorption Isotherm Experimental Variables

PCO ₂ (%)	NABS Type	Solid Concentration (g L ⁻¹)	Solution Phase
0.025	Unmodified	125	AGW-3
0.025	Unmodified	500	AGW-3
0.025	Treated	125	AGW-3
0.025	Treated	500	AGW-3
0.025	Unmodified	125	0.1 M NaClO ₄
0.025	Treated	125	0.1 M NaClO ₄
8.0	Unmodified	125	AGW-6
8.0	Treated	125	AGW-6

Table 2.10 Np(V) Sorption Edge Experimental Variables

PCO ₂ (%)	Total Np(V) (mol L ⁻¹)	Solid (g L ⁻¹)	Solution Phase
0.0	5.0x10 ⁻⁷	50	0.1 M NaClO ₄
0.0	5.0x10 ⁻⁷	125	0.1 M NaClO ₄
0.025	5.0x10 ⁻⁷	50	0.1 M NaClO ₄
0.025	5.0x10 ⁻⁷	125	0.1 M NaClO ₄
0.025	5.0x10 ⁻⁷	500	0.1 M NaClO ₄
0.025	5.0x10 ⁻⁶	500	0.1 M NaClO ₄
0.025	5.0x10 ⁻⁷	50	AGW-A
0.025	5.0x10 ⁻⁷	125	AGW-A
0.025	5.0x10 ⁻⁶	50	AGW-A
0.025	5.0x10 ⁻⁶	125	AGW-A
0.025	5.0x10 ⁻⁷	50	AGW-3
0.025	5.0x10 ⁻⁷	125	AGW-3
8.0	5.0x10 ⁻⁷	500	0.1 M NaClO ₄

Table 2.11 Humic Acid Sorption Experiment Variables*

Humic Acid (mg L ⁻¹)	NABS Type	Total Np(V) (mol L ⁻¹)
<u>Isotherm Experiments</u>		
0-200	Untreated	2.0x10 ⁻⁶
0-200	Treated	2.0x10 ⁻⁶
<u>Edge Experiments</u>		
10	Treated	No Np(V)
10	Treated	5.0x10 ⁻⁷
10	Treated	5.0x10 ⁻⁶
100	Treated	No Np(V)
100	Treated	5.0x10 ⁻⁷
100	Treated	5.0x10 ⁻⁶

*All humic acid experiments were conducted using 500 g L⁻¹ in 0.1 M NaClO₄ at atmospheric PCO₂.

as average values with the data range displayed as error bars.

2.2.2.5 Near Infrared Spectroscopy

Samples were analyzed using a Beckman Coulter DU[®] 800 UV/Vis spectrophotometer with a wavelength interval of 0.1 nm and a scanning speed of 120 nm min⁻¹. The scanning region was 600 nm to 1100 nm for oxidation state determination and 840 nm to 1100 nm for evaluation of Np(V) complexation with Suwannee River HA. Each sample cell was made of optical glass with a 10 mm path length and a septum sealable opening. Np(V) concentrations were 2x10⁻⁴ M or greater unless otherwise noted.

2.2.3 Results and Discussion

2.2.3.1 Oxidation State Confirmation

Near infrared (NIR) spectroscopic analysis showed that a dilute ²³⁷Np stock solution (2x10⁻⁴ M in 20 mM nitric acid) consists of the pentavalent oxidation state (Moran, 2007). A characteristic band at 980 nm and a small band at 617 nm confirmed the presence of the uncomplexed neptunyl (NpO₂⁺) species. The solution concentration was confirmed using the molar extinct coefficient of 395 M⁻¹ cm⁻¹ and by LSC (Hagan and Cleveland, 1966). The spectrum lacked any evidence of the characteristic absorption bands for Np(IV) at 723 and 960 nm (Burney and Harbour, 1974; Katz et al., 1986).

2.2.3.2 Liquid Scintillation Analysis

LSC is commonly used to analyze α activity associated with ²³⁷Np containing samples (Turner et al., 1998; Kohler et al., 1999; Runde et al., 2002). It is important to distinguish the α particle counts associated with ²³⁷Np from any β radiation activity. The Packard 2500TR LSC instrument used to analyze ²³⁷Np lacks the α/β discriminator that is available on some LSC instruments. Under the conditions investigated, the presence of varying amounts of the β particle emitting daughter product, ²³³Pa, must be taken

into account. To address this requirement the steps outlined below were followed.

In the case of the Np(V)-NABS system, where HA is not present, counts associated with background radiation and residual ²³³Pa are low. Figure 2.7 is a representative spectrum of 2.0x10⁻⁶ M Np(V) in a 0.1 M NaClO₄ solution that had ²³³Pa removed by passing the solution through a cation exchange column. The activity contribution of ²³³Pa in the region of the spectrum less than 75 kilo electron volts (KeV) is present as a result of its in-growth ($t_{1/2} = 23$ days) and due to a small quantity of ²³³Pa remaining in the stock solutions. In the binary system, the activity contribution of ²³³Pa and background radiation is easily removed by subtracting the total counts associated with the “ β region” of the spectra from the total α activity counts associated with ²³⁷Np in the 75 to 300 KeV region. For all experiments without HA present the distinction between the two regions is set at 75 KeV. As shown in Figure 2.7, this demarcation is located in the “trough” in the spectrum where minimal counts are detected. The error associated with the LSC analysis remains constant from sample to sample as long as the number of counts that fall within the “trough” of each spectrum remain constant. Error up to 2% beyond the LSC error ($2\sigma = 1\%$) was associated with the manual α/β discrimination. This approach was applied to a binary Np(V)-hematite system (fixed Np(V) concentration, fixed hematite concentration and variable pH), which produced sorption edge data consistent with Kohler et al. (1999) (Data not shown).

The data manipulation becomes slightly more complex when analyzing samples that contain HA due to color quenching in LSC samples. A quantifiable shift in the ²³⁷Np region of the spectra toward lower KeV results as the HA concentration increases. This phenomena is illustrated in Figure 2.8, which shows a series of Np(V)-HA samples (10-200 mg L⁻¹ HA). To locate the region in the spectra where minimum counts are observed, the LSC raw data (total counts at every 0.5 KeV from 0-300 KeV) is plotted as total counts as a function of KeV. Therefore, the α counts can be quantified even

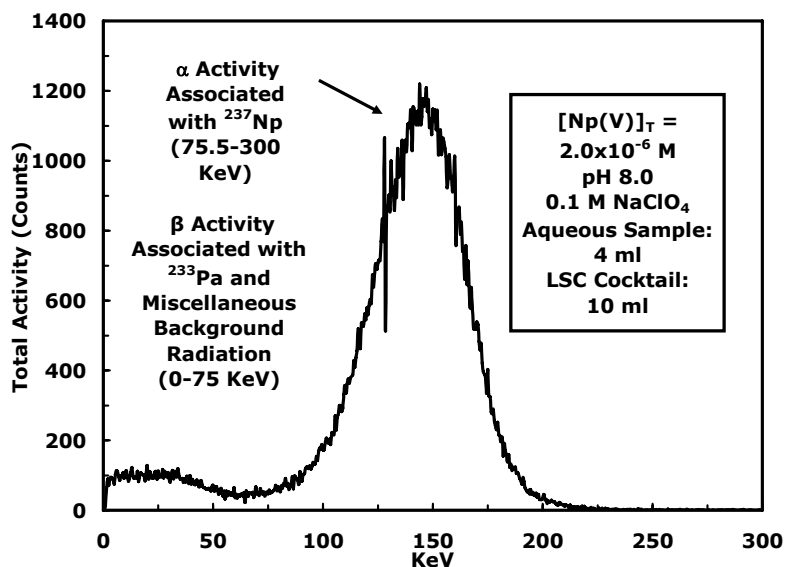


Figure 2.7. LSC spectrum showing activity associated with ^{237}Np α particle emission and activity associated with background radioactivity residual ^{233}Pa in a 2.0×10^{-6} M Np(V) sample.

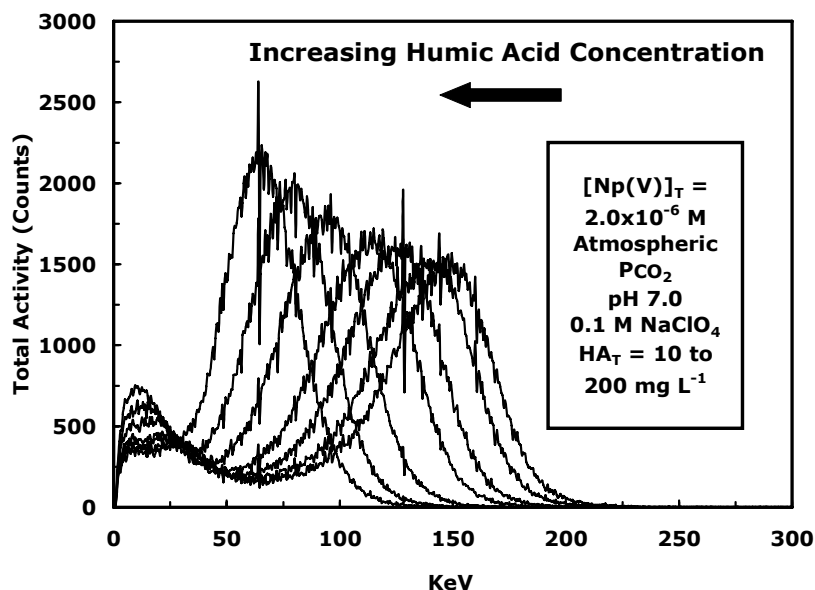


Figure 2.8. Series of LSC spectra of 2.0×10^{-6} M Np(V) in the presence of $10\text{-}200 \text{ mg L}^{-1}$ HA showing varying degrees of color quenching without a reduction in counts.

though they have shifted. Following this approach gives a relative standard deviation of 2% for the sample series containing constant Np(V) and variable HA shown in Figure 2.8. In the case of Np-HA samples, the error associated with manual α/β discrimination and color quench is limited by determining $\text{CPM}_{\text{Initial}}$ for Np-HA samples without sediment present but with CPM and degrees of spectral shift

equivalent to the samples containing NABS. This comparison is essential due to the additional error associated with the increasing number of counts within the spectral “trough” as HA concentration increases. For every Np(V)-HA dataset, several samples containing Np(V) without HA were processed in the same manner to make certain the data manipulation was consistent between sample sets.

2.2.3.3 Np(V) Time Dependent Sorption

The time dependent sorption experiment without added HA shows that Np(V) sorption to unmodified NABS is characterized by an initial rapid increase in sorption followed by a gradual slowing in rate after approximately 24 hours (Figure 2.9). Allowing the samples to equilibrate for an additional 3 days leads to an increase in sorption of approximately 10%. This type of sorption vs. time curve is characteristic of metal-ion sorption to complex geomeia. For practical reasons, a 24 hour (± 1) contact period was selected for Np(V) sorption experiments using unmodified and treated NABS without added HA. The adherence to the 24 hr equilibration time helps to reduce the error associated with the slow increase in sorption with time. All samples were run in triplicate and a relative standard deviation of 6% or less was obtained. A preliminary time dependent sorption experiment using Np(V) and treated NABS also approached steady state-like conditions within 24 hours (data not shown).

Sanpawanitchakit (2002) conducted experiments to determine the length of time for U(VI) to reach quasi-equilibrium conditions in contact with treated NABS. Similar to Np(V) sorption, U(VI) sorption to treated NABS reached steady state-like conditions within 24 hours via fast initial sorption followed by slower uptake. Davis et al. (2004) determined the time period for U(VI) sorption to unmodified NABS to occur in approximately 96 hr.

2.2.3.4 Time Dependent Sorption in the Presence of Humic Acids

The influence of pre-equilibrating Np(V) with HA prior to sorption to treated NABS was investigated using batch sorption experiments. At first glance, it appears that the addition of HA reduces the initial rapid increase regardless of how long Np(V) is in contact with HA prior to sorption to treated NABS (Figure 2.10). However, the sorption experiments with HA present were conducted over a much wider time period (24 hours to 600 hours) than the Np(V)-only time dependent experiments. Comparing

the time dependent sorption results shows that sorption with and without HA present follows the same trend with respect to time. This is best illustrated in Figure 2.11 which compares the 90 hour Np(V)-HA pre-equilibration data from Figure 2.10 and the Np(V)-only data from Figure 2.9. As a consequence of these results, all Np(V)-HA stock solutions were pre-equilibrated for 90 hours prior to sorption experiments. Clearly, extending the sorption time leads to a relatively constant slow increase in sorption regardless of the presence of HA. For example, focusing again on the 90 hour pre-equilibration results, sorption increases from 41% at 24 hours to 77% near 600 hr. This point is further illustrated by the $>90\%$ sorption observed for isotherm experiments in which Np(V) was equilibrated with 500 g L^{-1} unmodified and treated NABS in the presence of $0\text{-}200 \text{ mg L}^{-1}$ HA at pH 8.0 in 0.1 M NaClO_4 for 600 hr (results not shown). For consistency all sorption experiments with or without HA were conducted over a 24 hr (± 1) equilibration period.

2.2.3.5 Np(V) Sorption Isotherm Results

The effect of PCO_2 on Np(V) sorption to treated and unmodified NABS was investigated using isotherm experiments. An average relative standard deviation of 6% was obtained for all the isotherm experimental data at a given total Np(V) concentration. Figure 2.12a shows the sorption behavior of Np(V) under atmospheric and 8% PCO_2 using a solid-solution ratio of 125 g L^{-1} unmodified NABS, while varying the Np(V) concentration in artificial groundwater (AGW-3 and AGW-6). The pH was allowed to reach an equilibrium value specific to the particular PCO_2 . In Figure 2.12a Np(V) sorbed is presented as Γ (mol g^{-1}) as a function of Np_{Soln} , the concentration of Np(V) remaining in solution (mol L^{-1}). Figure 2.12b presents the same data in the form of K_d (mL g^{-1}) as a function of Np_{Soln} in order to easily compare the results from this study to the majority of the experimental data in the literature for Np(V) sorption to complex geomeia. These experiments show that Np(V) sorption is very similar at atmospheric and 8% PCO_2 with only a slight decrease in sorption at high PCO_2 . The

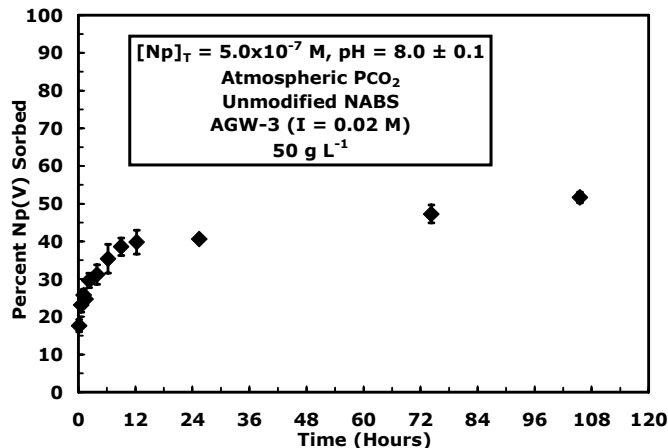


Figure 2.9. Time dependent sorption of 5.0×10^{-7} M Np(V) to 50 g L^{-1} unmodified NABS in AGW-3 at pH 8.0 and atmospheric PCO_2 .

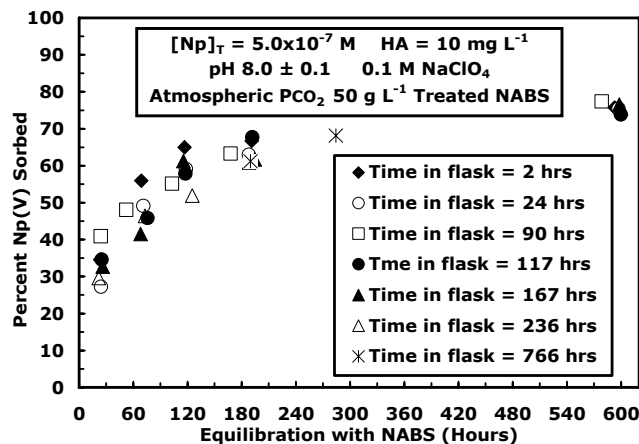


Figure 2.10. Time dependent sorption of Np(V) to 50 g L^{-1} treated NABS in the presence of 10 mg L^{-1} HA (pH 8.0) at atmospheric PCO_2 with a total Np(V) concentration of $5.0 \times 10^{-7} \text{ M}$ and 0.1 M NaClO_4 . Np(V) pre-equilibrated with HA for 2, 24, 90, 117, 167, 236 and 766 hours. Sorption times were approximately 24, 72, 120, 196, 285 and 600 hours.

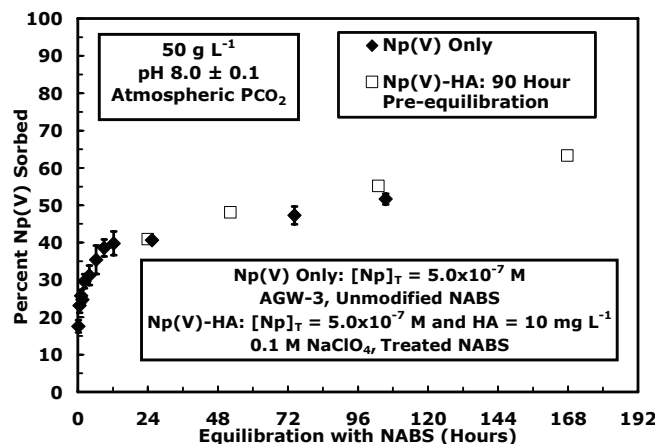


Figure 2.11. Comparison of time dependent sorption of $5.0 \times 10^{-7} \text{ M}$ Np(V) with and without 10 mg L^{-1} HA at pH 8.0 and atmospheric PCO_2 . The Np(V) only experiments were conducted with 50 g L^{-1} unmodified NABS in AGW-3. The Np(V)-HA samples shown were pre-equilibrated for 90 hours prior to sorption with 50 g L^{-1} treated NABS in 0.1 M NaClO_4 .

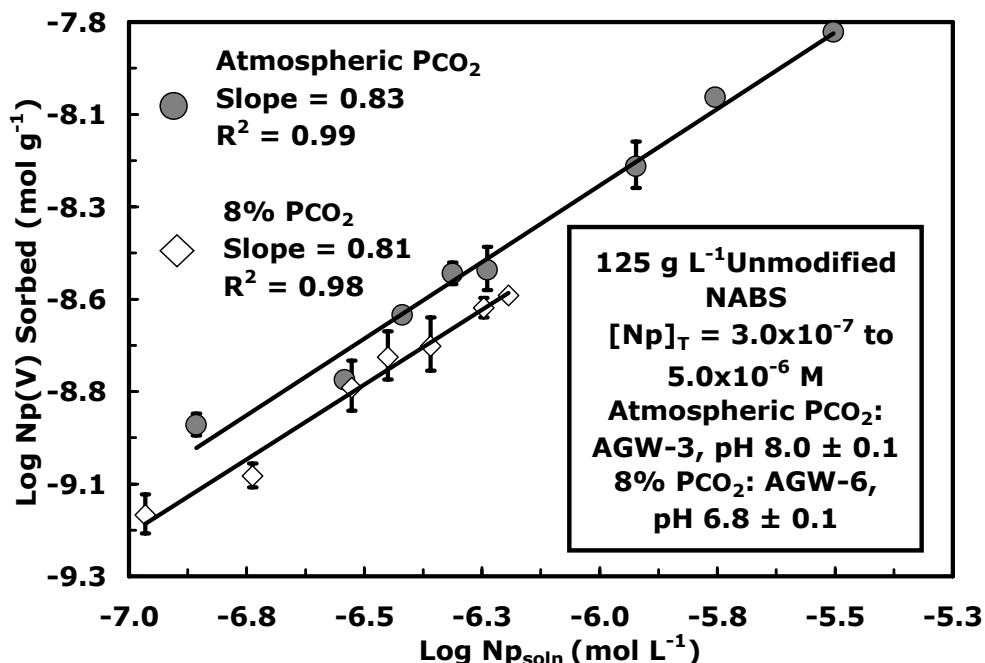


Figure 2.12a. Np(V) sorption isotherms using a maximum range of Np(V) from 3.0×10^{-7} M to 5.0×10^{-6} M, 125 g L^{-1} unmodified NABS, in AGW-3 (pH 8) at atmospheric PCO_2 or in AGW-6 (pH 6.8) at 8% PCO_2 .

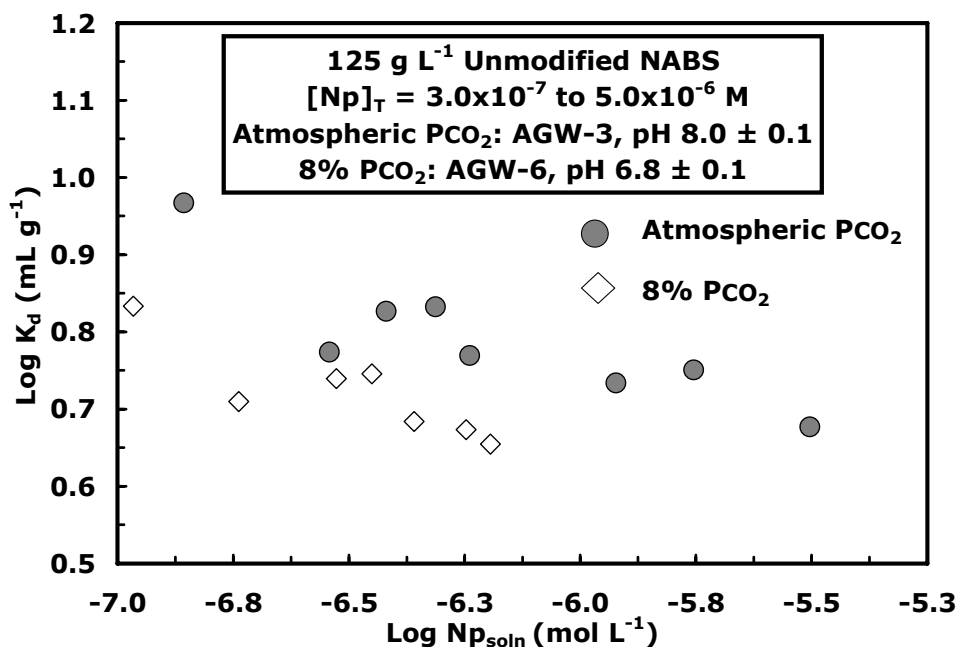


Figure 2.12b. K_d values for Np(V) sorption as a function of aqueous Np(V) remaining in solution using a maximum range of Np(V) from 3.0×10^{-7} M to 5.0×10^{-6} M, 125 g L^{-1} unmodified NABS, in AGW-3 (pH 8) at atmospheric PCO_2 or in AGW-6 (pH 6.8) at 8% PCO_2 .

error bars, which represent the 95% confidence intervals cannot be used as presented to conclusively say that the differences in the data are statistically significant. Instead, trendlines derived from the upper and lower limits of the 95% confidence intervals do not overlap, and the y-intercept values are significantly different, suggesting that the lower Np(V) uptake at 8% PCO₂ is significant. The errors associated with linear regression analysis of all Np(V) isotherm experimental data are presented in Table 2.12.

Similarities in sorption at atmospheric and 8% PCO₂ can be explained by looking at Np(V) aqueous speciation at the equilibrium pH values for each system (pH 8.0 at atmospheric and pH 6.8 at 8% PCO₂). Keep in mind that the equilibrium pH values for the two systems differ due to the presence of carbonate minerals. The calculated Np(V) aqueous speciation under atmospheric PCO₂ at pH 8.0 in AGW-3 shows that NpO₂⁺ accounts for approximately 75% of the Np(V) while NpO₂CO₃⁻ makes up approximately 25% of the species distribution. At pH 6.8, under an 8% PCO₂ atmosphere, aqueous speciation is indistinguishable from the speciation at pH 8.0 under atmospheric PCO₂.

Figures 2.13a and 2.13b show experimental data for Np(V) sorption to treated NABS under the same conditions described for Np(V) sorption to the unmodified NABS shown in Figures 2.12a and 2.12b. The systems using treated NABS were maintained at pH 8.0 under atmospheric PCO₂ and pH 6.8 under 8% PCO₂ for comparison to the systems using unmodified NABS. Np(V) sorption to treated NABS follows the same trend observed for unmodified NABS, showing what appears to be a minor reduction in sorption with an increase in PCO₂. However, error analysis of the 95% confidence interval error bars shows that the data are not significantly different.

All the isotherms under atmospheric and 8% PCO₂ exhibit Freundlich-like behavior, with slopes less than 1, over the Np(V) concentration ranges studied. The trendlines exhibited a minimum slope of 0.81 ± 0.01 and a maximum slope of 0.91 ± 0.02 (see Table 2.12). The nonlinear behavior indicates that as Np(V)

concentration increases, the sorption affinity decreases, suggesting multiple site types.

Np(V) sorption is characterized by a narrow range of K_d values, approximately 3-10 mL g⁻¹, over the large PCO₂ range. Recently, Davis et al. (2004) showed that as PCO₂ increases from atmospheric to 6.8%, the K_d values associated with U(VI) sorption to unmodified NABS cover a comparably large range. For example, near atmospheric PCO₂, with approximately 1x10⁻⁶ M U(VI) in solution, the K_d for U(VI) sorption is approximately 13 mL g⁻¹ and decreases to 1 mL g⁻¹ at 6.8% PCO₂. The K_d values for 5.0x10⁻⁷ M U(VI) sorption to 125 g L⁻¹ treated NABS varies between approximately 5 and 150 mL g⁻¹ under the conditions investigated in this study. The K_d values discussed above are low compared to values for Np(V) and U(VI) sorption to pure mineral oxides. For example, Tochiyama et al. (1991) obtained a K_d of approximately 120 mL g⁻¹ for Np(V) sorption to α-Al₂O₃ at pH 8 using 20 g L⁻¹ solid and 5.5x10⁻¹³ M Np(V) at atmospheric PCO₂. Bertetti et al. (1996) obtained a K_d = 100 mL g⁻¹ for 1x10⁻⁶ M Np(V) sorption to 4.0 g L⁻¹ montmorillonite at pH 8 without CO₂ present and at atmospheric PCO₂. The high affinity of Np(V) and U(VI) for iron oxides is illustrated by the large K_d values obtained for sorption to hematite. At pH 8 and atmospheric PCO₂, the K_d value for 1.1x10⁻⁶ M Np(V) sorption to 1 g L⁻¹ hematite is 6x10³ mL g⁻¹ and U(VI) has a K_d of 2x10⁴ at pH 8 using 1x10⁻⁶ M U(VI) and 0.9 g L⁻¹ (this study; Kohler et al., 1999; Lenhart and Honeyman, 1999).

Np(V) sorption to both unmodified and treated NABS under atmospheric PCO₂ and 8% PCO₂ suggests that carbonate mineral surface sites are only minimally important in Np(V) sorption to unmodified NABS. The isotherms presented in Figures 2.14a and 2.14b illustrate the effect of carbonate mineral removal at fixed PCO₂. The comparable results for Np(V) sorption to treated and unmodified NABS are further illustrated in Figures 2.14c and 2.14d which contain the same experimental data presented in terms of K_d as a function of Np_{Soln}. The slight decrease in the sorption affinity of Np(V) for treated NABS is most evident under the 8% PCO₂ conditions. Under high PCO₂ conditions a significant

Table 2.12 Error Calculations Using The 95% Confidence Intervals From Regression Analysis Of Np(V) Isotherm Experimental Data

PCO ₂	NABS Type	Solid-Solution	Slope	Slope Error	Y-axis Intercept	Intercept Error
Atmospheric	Unmodified	125	0.83	0.01	3.27	0.08
Atmospheric	Unmodified	500	0.91	0.02	2.90	0.11
Atmospheric	Treated	125	0.83	0.05	3.32	0.32
8%	Unmodified	125	0.81	0.01	3.51	0.03
8%	Treated	125	0.9	0.02	3.06	0.12

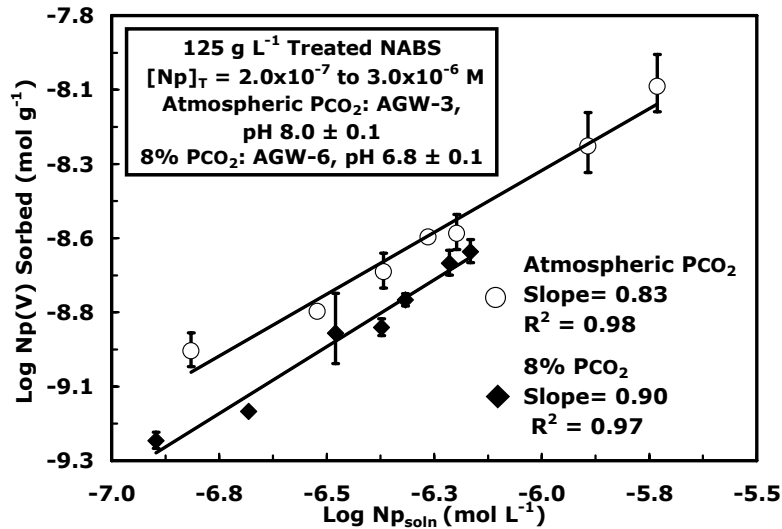


Figure 2.13a. Np(V) sorption isotherms using a maximum range of Np(V) from 2.0×10^{-7} M to 3.0×10^{-6} M, 125 g L^{-1} treated NABS, in AGW-3 (pH 8.0) at atmospheric PCO₂ or in AGW-6 (pH 6.8) at 8% PCO₂.

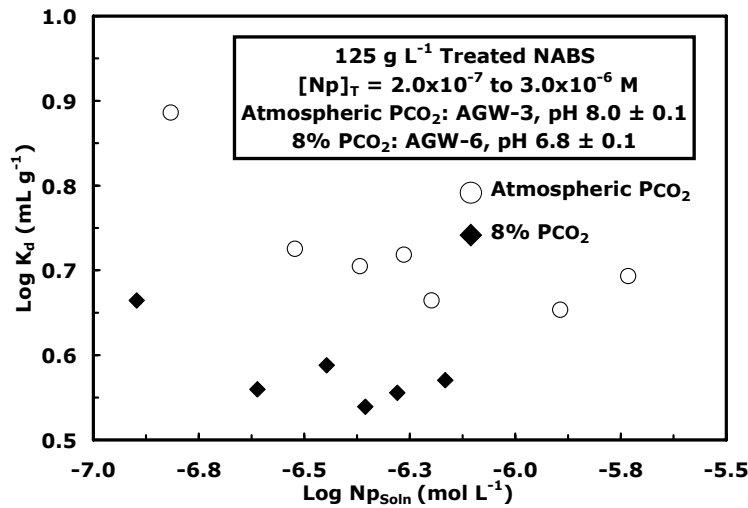


Figure 2.13b. K_d values for Np(V) sorption as a function of aqueous Np(V) remaining in solution using a maximum range of Np(V) from 2.0×10^{-7} M to 3.0×10^{-6} M, 125 g L^{-1} treated NABS, in AGW-3 (pH 8.0) at atmospheric PCO₂ or in AGW-6 (pH 6.8) at 8% PCO₂.

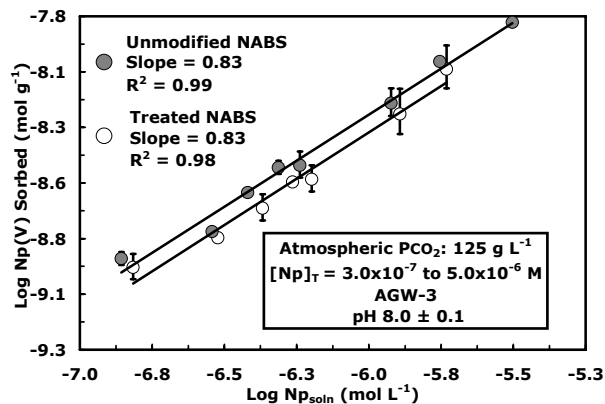


Figure 2.14a. Np(V) sorption isotherms using a maximum range of Np(V) from 3.0×10^{-7} M to 5.0×10^{-6} M, 125 g L^{-1} treated and unmodified NABS, in AGW-3, pH 8, at atmospheric PCO_2 .

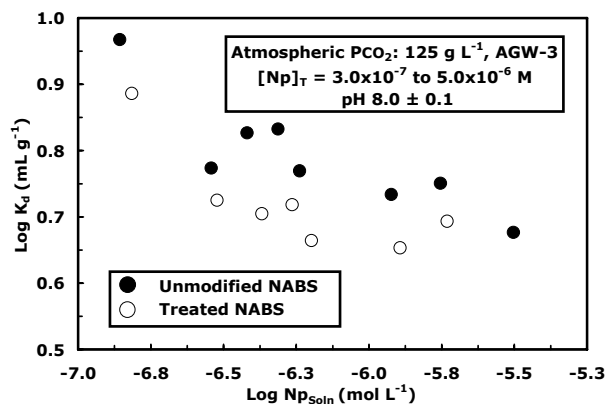


Figure 2.14c. $\text{Log } K_d$ values for Np(V) sorption as a function of aqueous Np(V) remaining in solution using a maximum range of Np(V) from 3.0×10^{-7} M to 5.0×10^{-6} M, 125 g L^{-1} treated and unmodified NABS, in AGW-3 (pH 8) at atmospheric PCO_2 .

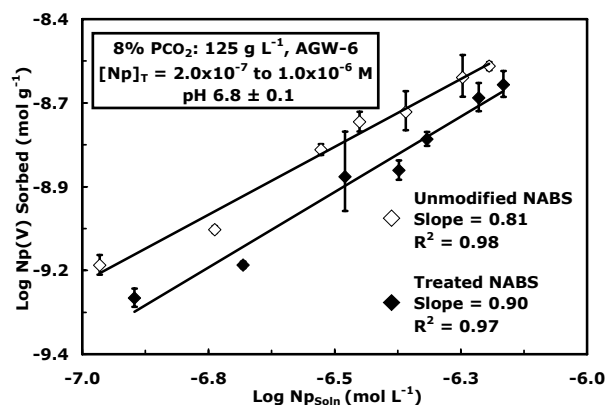


Figure 2.14b Np(V) sorption isotherms using a maximum range of Np(V) from 2.0×10^{-7} M to 1.0×10^{-6} M, 125 g L^{-1} treated and unmodified NABS, in AGW-6, pH 6.8, at 8% PCO_2 .

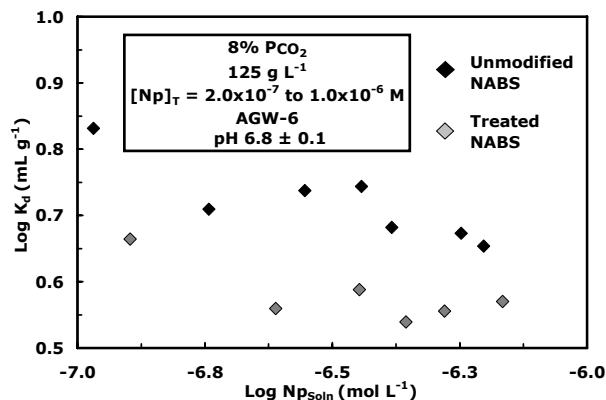


Figure 2.14d. $\text{Log } K_d$ values for Np(V) sorption as a function of aqueous Np(V) remaining in solution using a maximum range of Np(V) from 2.0×10^{-7} M to 1.0×10^{-6} M, 125 g L^{-1} treated and unmodified NABS, in AGW-6 (pH 6.8) at 8% PCO_2 .

decrease in sorption to treated NABS is observed (see Table 2.12).

The BET (Brunauer, Emmett, and Teller) specific surface area (A_{sp}) of treated NABS was $4.47 \text{ m}^2 \text{ g}^{-1}$ while the A_{sp} for unmodified NABS was $5.15 \text{ m}^2 \text{ g}^{-1}$ (Sanpawanitchakit, 2002; Davis

et al., 2004). In addition, all grain size fractions derived from unmodified NABS had higher A_{sp} values than treated NABS (Table 2.7). The higher A_{sp} values associated with treated NABS suggest that carbonate mineral dissolution resulting from NABS treatment reduces the quantity of larger cemented fragments. A more

detailed overview of NABS characterization is found in Sanpawanitchakit (2002), USNRC (2003), Kohler et al. (2004), and Davis et al., (2004).

It follows that the higher sorption affinity for unmodified NABS is in part a consequence of the higher surface area. The role surface area plays in Np(V) sorption can be examined using a distribution coefficient corrected to account for surface area, K_a , as follows:

$$K_a = \frac{K_d}{A_{sp}} \quad [2.1]$$

When surface area is taken into account, sorption to treated and unmodified sediment is equivalent under atmospheric PCO_2 . At 8% PCO_2 , the K_a values for treated and unmodified NABS are not as closely matched, but generally fall within the error associated with the data points. The minimal importance of carbonate minerals in Np(V) sorption to NABS is in contrast with the work of Keeney-Kennicutt and Morse (1984), which showed that at approximately pH 8 Np(V) had a higher affinity for calcite than iron oxides on a surface area corrected basis. However, recent work by Zavarin and Bruton (2004) suggests that Np(V) sorption affinity for calcite is considerably lower than suggested by the Keeney-Kennicutt and Morse study. For example, comparing the sorption of Np(V) to 1 g L^{-1} calcite obtained by Zavarin and Bruton (2004) and sorption to hematite obtained by Kohler et al. (1999) with similar surface areas (15.7 and 14.4 $m^2 g^{-1}$, respectively) shows that Np(V) has a much higher affinity for hematite between pH 7 and 9 at atmospheric PCO_2 . For example, the K_d for 6×10^{-6} M Np(V) sorption to calcite at pH 8 is approximately 250 $mL g^{-1}$ and 6×10^3 $mL g^{-1}$ for 1.1×10^{-6} M Np(V) sorption to hematite.

Sorption of Np(V) to 125 g L^{-1} and U(VI) to 50 g L^{-1} treated NABS at atmospheric PCO_2 at pH 8.0 show very similar behavior (Figure 2.15). This can be attributed to the similarity in the percent sorbed of Np(V) and U(VI) at pH 8.0. Of interest, under atmospheric PCO_2 , pH 8 is the only pH between 6 and 10 at which Np(V) and U(VI) have approximately the same percent sorbed.

Increasing the solid-solution ratio provides additional reactive surface sites for Np(V) complexation. This results in a substantial increase in sorption over the conditions studied. For example, Np(V) sorption increases from an average of 44% over the Np(V) concentration range studied using 125 g L^{-1} unmodified NABS to an average of 69% when the solid-solution ratio is increased to 500 g L^{-1} unmodified NABS at pH 8.0 ± 0.1 in AGW-3 under atmospheric PCO_2 (Figure 2.16a). Presenting the above experimental data in the form of a linearized isotherm plot removes much, but not all, of the dependence of sorption on the solid-solution ratio (Figure 2.16b). Error analysis of the regression lines shows that the slope and y-intercept values of the 125 and 500 g L^{-1} data sets are significantly different (see Table 2.12). In principle, presenting the data in the form of isotherm plots should eliminate the dependence on the solid-solution ratio resulting in overlapping isotherms within the error range. The lower sorption at 500 g L^{-1} suggests a particle concentration effect may be taking place. Close packing may cause particle-particle interactions that either physically block available surface sites or create electrostatic interactions that result in lower attraction of Np(V) for NABS surface sites (USEPA, 1999). Also, variability in solution composition due to mineral dissolution may increase the concentration of competitive cations and neutral or anionic species that can complex Np(V) as the solid-solution ratio increases.

2.2.3.6 Np(V) Sorption Edge Results

Sorption edge experiments were conducted between approximately pH 4 and 10, with most experiments covering pH 5-9. Several experiments contained data above pH 10. Preliminary experiments showed that samples initially adjusted to pH values below approximately pH 3 resulted in highly variable final pH values, as high as pH 7 in some cases. This is likely a result of sediment weathering which exposed carbonate minerals that otherwise were inaccessible without grinding the sediment (Miller and Gardiner, 1998). It follows that pH adjustments were conducted so as to

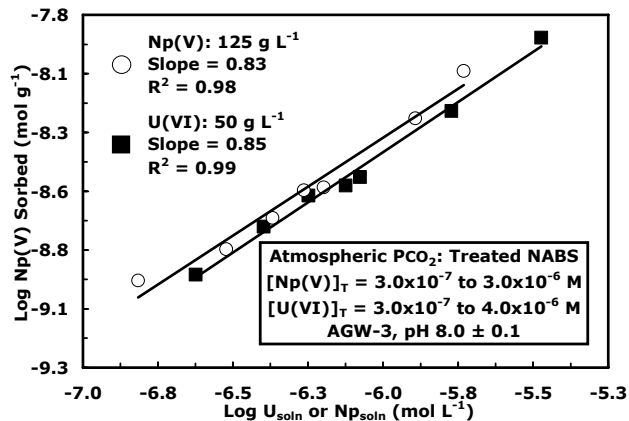


Figure 2.15. Comparison of U(VI) and Np(V) sorption isotherms (Np(V) concentration range: 3.0×10^{-7} to 3.0×10^{-6} M) on 125 g L^{-1} treated NABS and U(VI) concentration range of 3.0×10^{-7} to 4.0×10^{-6} M on 50 g L^{-1} treated NABS in AGW-3 (pH 8.0) at atmospheric PCO_2 .

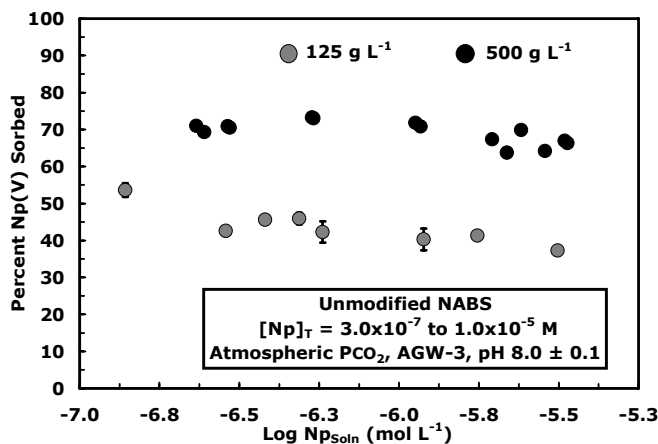


Figure 2.16a. Np(V) sorbed as a function of Np(V) remaining in solution using a maximum range of Np(V) from 8×10^{-7} M to 1×10^{-5} M, 125 g L^{-1} or 500 g L^{-1} unmodified NABS, in AGW-3 (pH 8) at atmospheric PCO_2 .

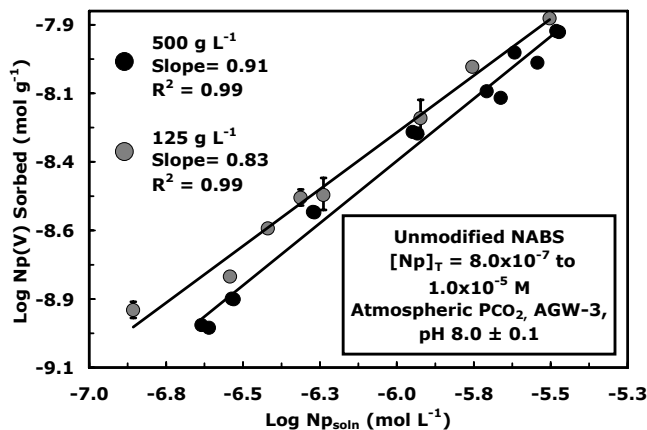


Figure 2.16b. Np(V) sorption isotherms using a maximum range of Np(V) from 8×10^{-7} M to 1×10^{-5} M, 125 g L^{-1} and 500 g L^{-1} unmodified NABS, in AGW-3 (pH 8.0 ± 0.1) at atmospheric PCO_2 .

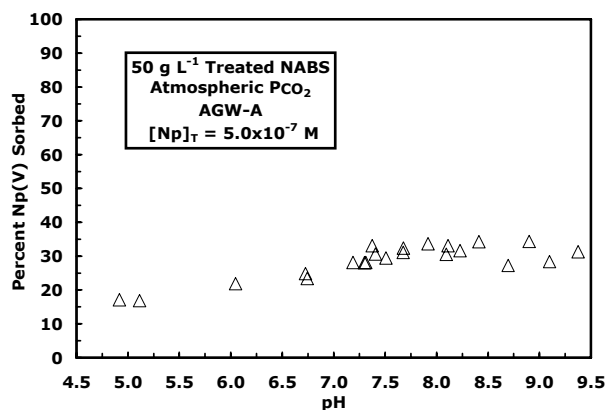


Figure 2.17a. Sorption edges using 5.0×10^{-7} M Np(V) on 50 g L^{-1} treated NABS in AGW-A at atmospheric PCO_2 .

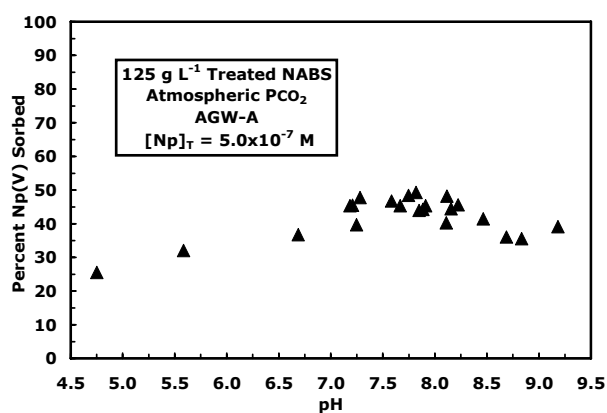


Figure 2.17b. Sorption edges using 5.0×10^{-7} M Np(V) on 125 g L^{-1} treated NABS in AGW-A at atmospheric PCO_2 .

obtain the desired pH while maintaining the sediment in the carbonate-removed form.

In AGW, Np(V) sorption to treated NABS shows weak pH dependence over the entire pH range studied. This is illustrated in Figure 2.17a, which shows the sorption of 5.0×10^{-7} M Np(V) to 50 g L^{-1} treated NABS in AGW-A at atmospheric PCO_2 . The lowest sorption (17%) is seen at approximately pH 5, which is the most acidic pH value for this data set. Low sorption in the acidic pH range is in part due to the large number of protons (e.g. $[\text{H}^+] = 10^{-5}$ M at pH 5) competing with NpO_2^+ for NABS surface sites. Similar weak pH dependence is observed for the system using 5.0×10^{-7} M Np(V) and 125 g L^{-1}

treated NABS at atmospheric PCO_2 in AGW-A (Figure 2.17b). The maximum sorption of 34% occurs over a wide pH range, specifically between pH 7.4 and 8.9. In addition, the surface charge of treated NABS plays a part in the extent to which Np(V) sorbs.

Unlike unmodified NABS, the pH_{pzsc} can be used to approximate the pH_{pzc} for treated NABS because the removal of carbonate minerals reduces the excess potential determining ions other than protons. The change in pH (ΔpH) due to salt addition as a function of pH gives an approximate $\text{pH}_{\text{pzc}} = 7$ (Figure 2.18a). Below the pH_{pzc} the surface has a net positive charge and the addition of NaClO_4 salt results in an increase in pH, above the pH_{pzc} addition of NaClO_4 causes a decrease in pH. Salt titrations for monomineralic oxide systems in an indifferent electrolyte generally lead to titration crossover points ($\Delta\text{pH}=0$) that coincide. However, the lack of a crossover point for batch titrations of treated NABS indicates the presence of variable concentrations of cationic and anionic species due to mineral dissolution. For example, analysis of the acidified NaClO_4 solution phase from 500 g L^{-1} treated NABS using inductively coupled plasma-atomic emission spectrometry (ICP-AES) shows that the concentrations of constituents such as Ca^{2+} , Mg^{2+} , $\text{Al}_{(\text{aq})}$ and SiO_2 , vary dramatically over the pH range studied. This is illustrated in Figure 2.18b, which shows the sum of the concentrations of the dissolved SiO_2 and aqueous phase Al^{3+} species in the supernatant as a function of pH. The lowest concentrations of these species (close to the concentrations found in the blank samples) are found in the circumneutral pH range, consistent with the solubility of aluminum oxyhydroxides and amorphous silica. The high variability of the SiO_2 concentration in solution at pH 6.2 and 8.3 may be a source of variability in percent $\text{Np}_{\text{sorbed}}$ in batch sorption experiments using NABS. Figure 2.18c shows the Ca^{2+} solution concentration due to mineral dissolution. The estimated Ca^{2+} concentration between approximately pH 6.5 and 8.5 is 5×10^{-4} M. Above pH ~ 8.5 the Ca^{2+} concentration drops to levels close to concentrations measured in samples without sediment present.

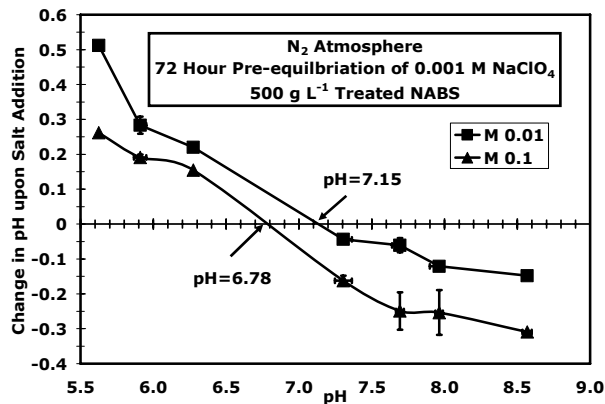


Figure 2.18a. Salt titrations of 500 g L⁻¹ treated NABS in 0.001 M NaClO₄ within an inert atmosphere glovebox.

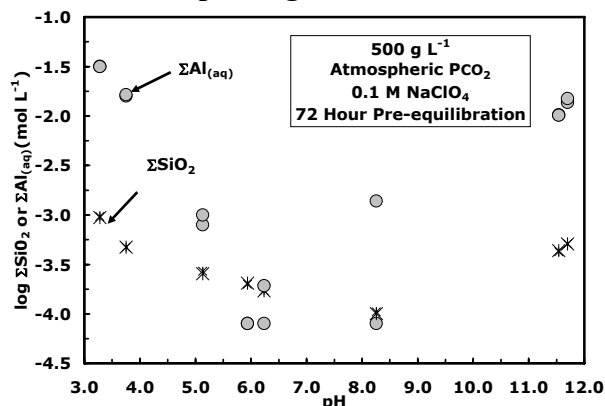


Figure 2.18b. Concentrations of Al_(aq) and SiO₂ in the solution phase of 500 g L⁻¹ treated NABS in 0.1 M NaClO₄ at atmospheric PCO₂.

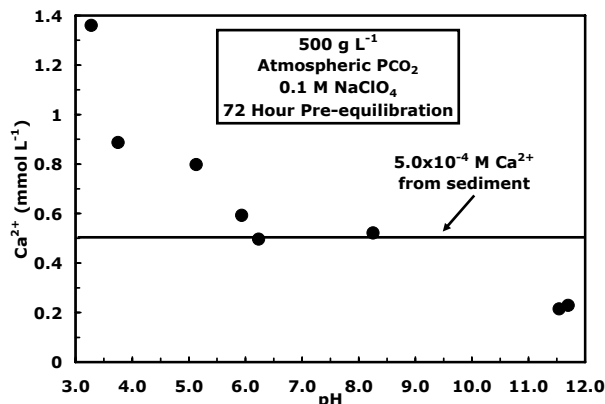


Figure 2.18c Concentrations of Ca²⁺ in the solution phase of 500 g L⁻¹ treated NABS in 0.1 M NaClO₄ at atmospheric PCO₂.

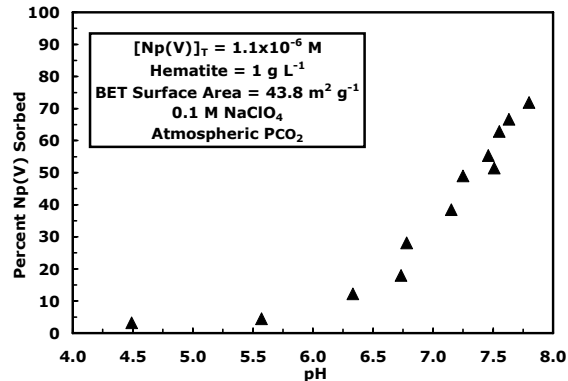


Figure 2.19. Np(V) sorption to 1 g L⁻¹ hematite as a function of pH using 5.0x10⁻⁷ M Np(V) in 0.1 M NaClO₄ at atmospheric PCO₂.

Np(V) sorption to monomineralic oxides exhibits much stronger pH dependence than seen for Np(V) sorption to treated NABS. For example, sorption of 1.1x10⁻⁶ M Np(V) to 1 g L⁻¹ hematite in 0.1 M NaClO₄ at atmospheric PCO₂ increases by 68% between pH 5.6 and 7.8 (Figure 2.19). As shown in Figure 2.19, less than 5% of the total Np(V) sorbs to hematite below approximately pH 5.5. The negligible uptake of NpO₂⁺ on hematite at low pH is to be expected given that hematite has a reported pH_{pzc} of pH 8.5 or higher (Kohler et al., 1999; Lenhart and Honeyman, 1999). In contrast, all Np(V) sorption edge experiments using treated NABS exhibit comparably high uptake in the acidic pH region. The contrast between Np(V) sorption behavior using treated NABS and hematite is a reminder of the heterogeneous nature of NABS and its clay surface coatings (Davis et al., 2004).

Figure 2.20a illustrates the impact of increasing the solid concentration from 50 g L⁻¹ to 125 g L⁻¹ in AGW-A while holding the Np(V) concentration steady at 5.0x10⁻⁷ M. In 0.1 M NaClO₄, an additional data set was collected using 500 g L⁻¹ with all other conditions the same as the AGW-A system (Figure 2.20b). An increase in Np(V) sorption is observed regardless of the solution composition. For example, between pH 7 and 8, an increase in sorption of approximately 15% was observed with a 2.5 fold increase in solid concentration in both AGW-A and 0.1 M NaClO₄. The increase

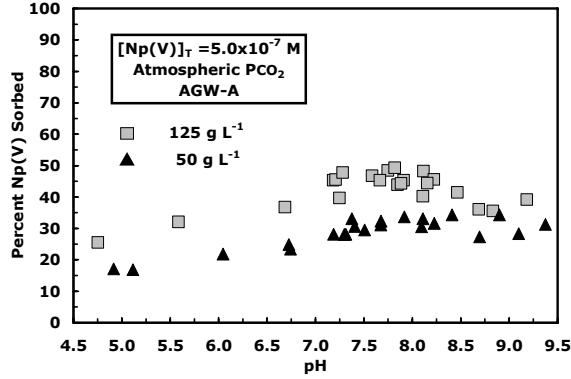
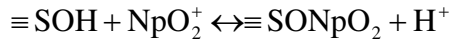


Figure 2.20a. Sorption edges using 5.0×10^{-7} M Np(V), 50 g L^{-1} and 125 g L^{-1} treated NABS in AGW-A at atmospheric PCO_2 .

was extended to slightly more than 20% when the solid concentration was increased from 125 to 500 g L^{-1} in 0.1 M NaClO_4 . The following surface reaction (Equation 2.2) and associated mass action expression give insight into the variables that play a role in the nonlinear sorption,



$$K = \frac{[\equiv \text{SONpO}_2][\text{H}^+]}{[\equiv \text{SOH}][\text{NpO}_2^+]} \quad [2.2]$$

where $\equiv \text{SOH}$ is a generic symbol for an amphoteric hydroxyl group. Rearranging the expression in terms of Np_{sorb} gives,

$$\equiv \text{SONpO}_2 = \frac{K[\equiv \text{SOH}][\text{NpO}_2^+]}{[\text{H}^+]} \quad [2.3]$$

and the fractional Np_{sorb} can be written as shown in equation 2.4.

$$\text{Fraction Np}_{\text{sorb}} = \frac{[\equiv \text{SONpO}_2]}{[\equiv \text{SONpO}_2] + [\text{NpO}_2^+]} \quad [2.4]$$

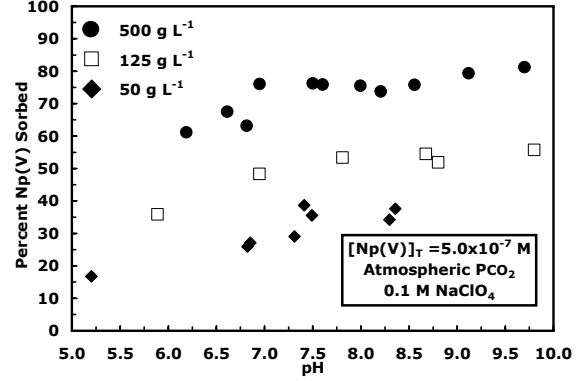


Figure 2.20b. Sorption edges using 5.0×10^{-7} M Np(V), 50 , 125 and 500 g L^{-1} treated NABS in 0.1 M NaClO_4 at atmospheric PCO_2 .

Rewriting the expression in terms of $[\text{NpO}_2^+]$, $[\equiv \text{SOH}]$, $[\text{H}^+]$ and the mass action expression, K , gives the following equation,

$$\text{Fraction Np}_{\text{sorb}} = \frac{[\text{NpO}_2^+]K \frac{[\equiv \text{SOH}]}{[\text{H}^+]}}{[\text{NpO}_2^+] \left\{ K \frac{[\equiv \text{SOH}]}{[\text{H}^+]} + 1 \right\}} \quad [2.5]$$

which reduces to an expression that is independent of $[\text{NpO}_2^+]$.

$$\text{Fraction Np}_{\text{sorb}} = \frac{K \frac{[\equiv \text{SOH}]}{[\text{H}^+]}}{K \frac{[\equiv \text{SOH}]}{[\text{H}^+]} + 1} \quad [2.6]$$

Finally, Equation 2.7 shows more clearly that Np_{sorb} will depend on the reactive surface site concentration as well as the mass action expression and protons released.

$$\text{Fraction Np}_{\text{sorb}} = \frac{[\equiv \text{SOH}]}{[\equiv \text{SOH}] + \frac{[\text{H}^+]}{K}} \quad [2.7]$$

Figures 2.21a, 2.21b and 2.21c show that fractional Np(V) sorption to NABS is largely independent of Np(V) concentration. Sorption edges using 500 g L^{-1} in 0.1 M NaClO_4 are illustrated in Figure 2.21c while Figures 2.21a

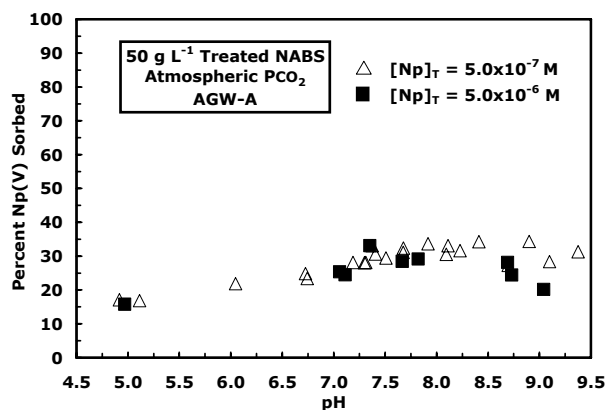


Figure 2.21a. Sorption edges with 5.0×10^{-7} M and 5.0×10^{-6} M Np(V), 50 g L^{-1} treated NABS, in AGW-A at atmospheric PCO_2 .

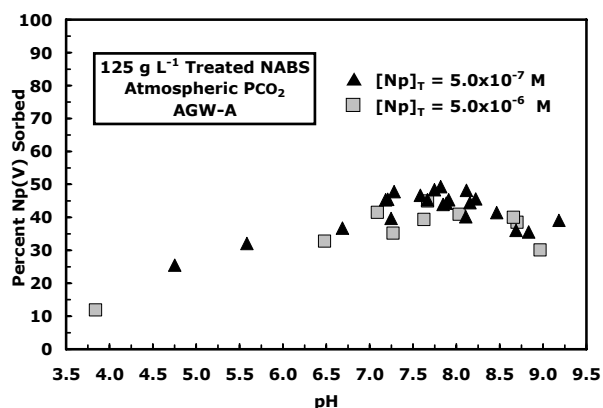


Figure 2.21b. Sorption edges with 5.0×10^{-7} M and 5.0×10^{-6} M Np(V), 125 g L^{-1} treated NABS, in AGW-A at atmospheric PCO_2 .

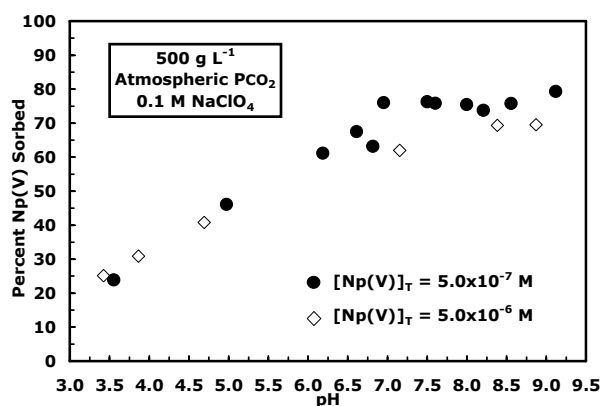


Figure 2.21c. Sorption edges with 5.0×10^{-7} M and 5.0×10^{-6} M Np(V), 500 g L^{-1} treated NABS, in 0.1 M NaClO_4 at atmospheric PCO_2 .

and 2.21b show Np(V) sorption in AGW-A using 50 and 125 g L^{-1} , respectively. The diagrams show that increasing the Np(V) concentration from 5.0×10^{-7} M to 5.0×10^{-6} M, while holding the solid-solution ratio constant, results in very similar percent Np(V) sorption. Isotherm results also suggest that percent Np_{sorb} is fairly constant over the Np(V) concentration range investigated for the edge experiments. However, a general trend towards slightly lower sorption at high Np(V) concentrations is observed when the entire Np(V) concentration range is considered at fixed pH (see Section 2.2.3.5). Agreement between the experimental data at 5.0×10^{-7} M and 5.0×10^{-6} M is evidence of excess NABS surface sites at the lowest Np(V) concentration. This can be illustrated further by considering the percent Np(V) sorbed at both Np(V) concentrations, shown in Figure 2.21a with 50 g L^{-1} treated NABS. For example, at pH 7.7 with 5.0×10^{-7} M Np(V), 30% or 3.0×10^{-9} mol of Np(V) are sorbed per gram of sediment. Increasing the Np(V) concentration to 5.0×10^{-6} M, 28% or 2.8×10^{-8} mol Np(V) are sorbed, very nearly a 10-fold increase. Therefore, the weak dependence of sorption on pH is not due to surface site saturation, which is characterized by ‘flattening’ of sorption edges (Dzombak and Morel, 1990).

The sorption of 5.0×10^{-7} M Np(V) and U(VI) to 125 g L^{-1} treated NABS in AGW-A at atmospheric PCO_2 are compared in Figure 2.22, which illustrates the key differences between the two actinides. The strong effect of carbonate complexation on U(VI) sorption is not evident in Np(V) sorption at atmospheric PCO_2 , primarily due to the predominance of NpO_2^+ over much of the pH range studied. In order to study the effect of carbonate complexation, several sorption edge experiments were conducted over an extended pH range, which included uptake between pH 9-11. For example, Np(V) sorption to 125 g L^{-1} treated NABS at atmospheric PCO_2 in 0.1 M NaClO_4 (see Figure 2.20b) displays a slow increase in sorption with increasing pH even in the alkaline pH range (pH 9-11), where the negatively charged $\text{NpO}_2\text{CO}_3^-$ and $\text{NpO}_2(\text{CO}_3)_2^{3-}$ species are expected to be the primary Np(V) aqueous complexes.

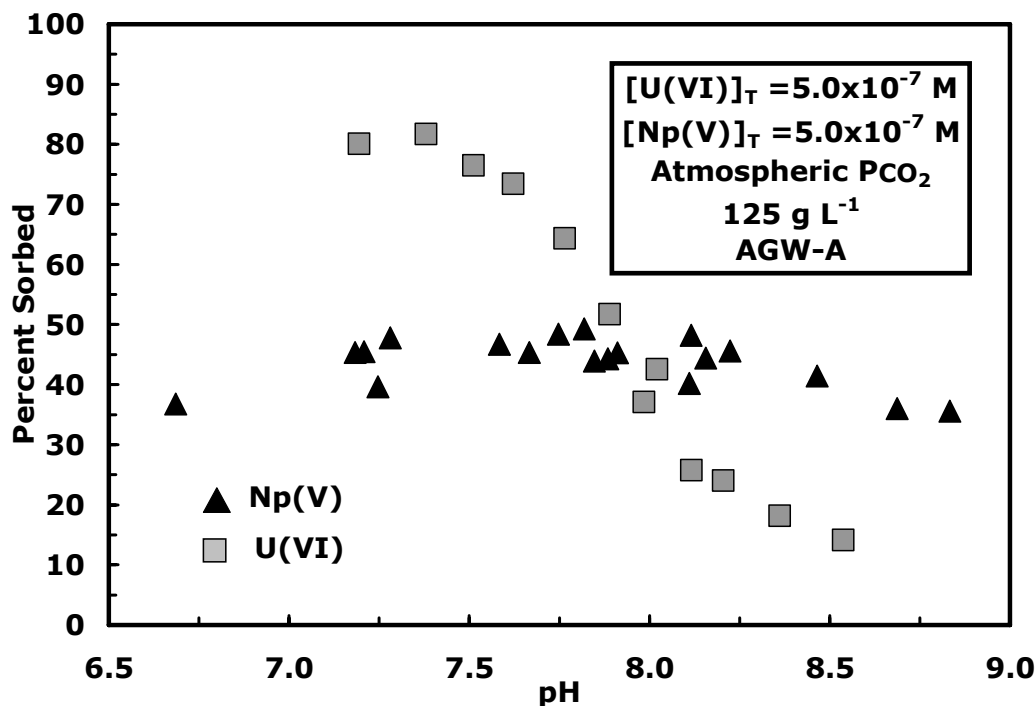


Figure 2.22. Comparison of U(VI) and Np(V) sorption edges using 5.0×10^{-7} M, 125 g L^{-1} treated NABS in AGW-A at atmospheric PCO_2 .

The findings in the current study are in agreement with numerous studies presented in the Np(V) sorption literature. For example, Del Nero et al. (2004) showed that Np(V) sorption to Al or Fe silicates steadily increased from approximately pH 3 to 10 under atmospheric conditions. Nakayama and Sakamoto (1991) found that 6×10^{-6} M Np(V) sorption to a variety of natural and synthetic Al and Fe oxides (1 g L^{-1}) continuously moved upward to the highest pH investigated (pH 11). Experiments were conducted without solid present, which confirmed that Np(V) remained soluble below pH 11. In addition, Tochiyama et al. (1996) found that 5.5×10^{-13} M Np(V) sorption onto 20 g L^{-1} natural and synthetic $\alpha\text{-Al}_2\text{O}_3$ increased relatively rapidly between pH 6 and 10. In summary, the majority of Np(V) sorption studies in the literature exhibit an increase in uptake with increasing pH at atmospheric PCO_2 . These findings as well as recent spectroscopic evidence for neptunyl-carbonato complexation at the hematite surface (Arai et al., 2007) are consistent with the possible occurrence of ternary complexes at the NABS surface.

In order to gain further insight into the role of neptunyl-carbonato aqueous and/or surface reactions in Np(V) sorption, CO_2 was excluded from the Np(V)-NABS system using a N_2 atmosphere. Figure 2.23a shows sorption of 5.0×10^{-7} M Np(V) on 50 and 125 g L^{-1} treated NABS in 0.1 M NaClO_4 using a N_2 atmosphere. At both solid concentrations, Np(V) uptake slowly increases by 60-65% between approximately pH 5 and 12. However, sorption under CO_2 -free conditions is very similar to the behavior at atmospheric PCO_2 (Figure 2.23b). Examination of the aqueous speciation under the CO_2 -free conditions shows that NpO_2^+ is the dominant aqueous species up to pH 11, at which point NpO_2OH^0 and $\text{NpO}_2(\text{OH})_2^-$ begin to become important.

Relatively few data sets are available for comparison to Figure 2.23a that are 1) maintained under CO_2 -free conditions and 2) investigated above pH 9. However, Turner et al. (1998) observed an increase in 9×10^{-7} M Np(V) sorption to 4 g L^{-1} montmorillonite up to pH 10.5, the highest pH investigated, using a N_2

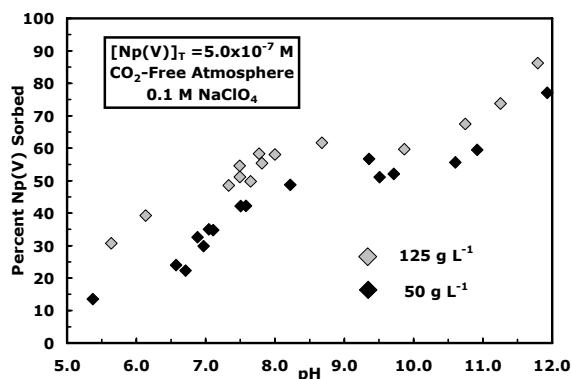


Figure 2.23a. Sorption edges using 5.0×10^{-7} M Np(V), 50 or 125 g L^{-1} treated NABS, in 0.1 M NaClO_4 using a N_2 atmosphere (CO_2 -free).

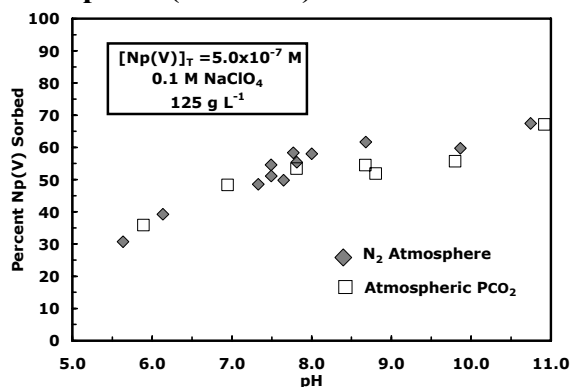


Figure 2.23b. Sorption edges using 5.0×10^{-7} M Np(V), 125 g L^{-1} treated NABS, in 0.1 M NaClO_4 at atmospheric PCO_2 or using a N_2 atmosphere (CO_2 -free).

atmosphere. Bertetti et al. (1998) studied 10^{-6} - 10^{-7} M Np(V) sorption to 4 and 40 g L^{-1} quartz, montmorillonite and α -alumina as well as 4 and 8 g L^{-1} clinoptilolite up to approximately pH 11 using CO_2 -free conditions and atmospheric PCO_2 conditions. Bertetti and coworkers showed an increase in Np(V) sorption to all the minerals investigated over the entire pH range when CO_2 -free conditions were employed.

A few studies demonstrate unambiguous decreases in percent Np_{sorb} as pH increases. For example, Turner et al. (1998) examined 9×10^{-7} M Np(V) sorption to 4 g L^{-1} montmorillonite at atmospheric PCO_2 . Unlike the system using an N_2 atmosphere, uptake decreased above pH 8.

Bertetti et al. (1998) observed the same trends for the quartz, montmorillonite and clinoptilolite systems discussed above. As a general rule, pH_{pzc} for silica and clay minerals are below pH 4 while Al and Fe oxides and oxyhydroxides have $\text{pH}_{\text{pzc}} > 7$ (Sposito, 1998). It follows that the low sorption affinity of NpO_2^+ observed by Turner et al. (1998) and Bertetti et al. (1998), beginning at pH 8, can be explained by the low pH_{pzc} of the mineral surfaces and the relatively steep decline in NpO_2^+ as the dominant aqueous species.

Figure 2.24a shows the sorption of Np(V) to 500 g L^{-1} treated NABS in 0.1 M NaClO_4 at 8% PCO_2 . The most significant feature is a sharp increase in sorption at approximately pH 7.3 followed by a 37% decrease in uptake from pH 7.6 to 8.1, the highest pH data point. The sorption edges at atmospheric and 8% PCO_2 , with all other conditions held the same, are compared in Figure 2.24b. This sorption behavior can be explained by either 1) precipitation of calcite followed by Np(V) sorption to the calcite surface sites or 2) co-precipitation of Np(V) with calcite. The dissolution of 500 g L^{-1} treated NABS leads to $5 \times 10^{-4} \text{ M Ca}^{2+}$ being released into solution between approximately pH 6.5 and 8.5 (see Figure 2.18c). Therefore, at 8% PCO_2 solubility calculations estimate that calcite oversaturation will occur at pH 7.3. Np(V) sorption or co-precipitation is substantiated by sorption edge experiments conducted at atmospheric PCO_2 in AGW-3, which show that strong Np(V) uptake takes place as pH increases (Figure 2.24c). In AGW-3, the sharp increase in sorption that occurs at approximately pH 8.2 coincides with calcite oversaturation at atmospheric PCO_2 . Aqueous speciation calculations suggest that the primary aqueous species is $\text{NpO}_2\text{CO}_3^-$ under both atmospheric and 8% PCO_2 conditions. The decrease in sorption observed above approximately pH 7.6 at 8% PCO_2 is consistent with the transition to $\text{NpO}_2(\text{CO}_3)_2^{3-}$ as the dominant aqueous complex. A possible decrease in Np(V) uptake is evident below pH 7.0-7.5 due to the increase in PCO_2 to 8%. The edge experiments show that at pH 8.0 and atmospheric PCO_2 , sorption is substantially higher than sorption at pH 6.8 and 8% PCO_2 .

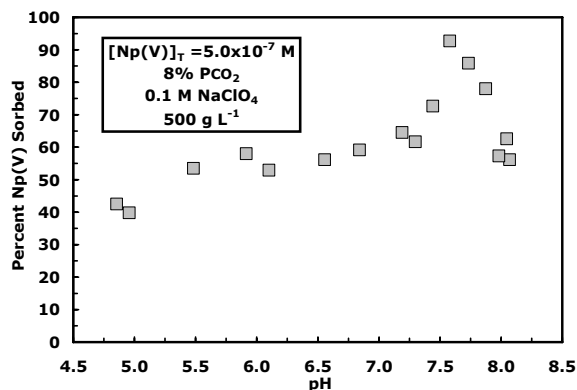


Figure 2.24a. Sorption edge using 5.0×10^{-7} M Np(V), 500 g L^{-1} treated NABS, in 0.1 M NaClO_4 at $8\% \text{ PCO}_2$.

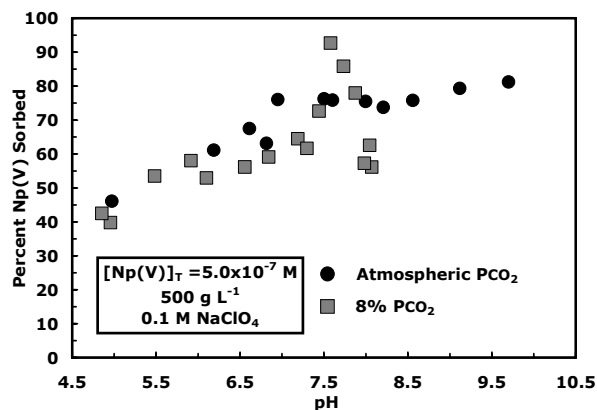


Figure 2.24b. Comparison of 5.0×10^{-7} M Np(V) sorption edges at atmospheric and $8\% \text{ PCO}_2$ using 500 g L^{-1} treated NABS in 0.1 M NaClO_4 .

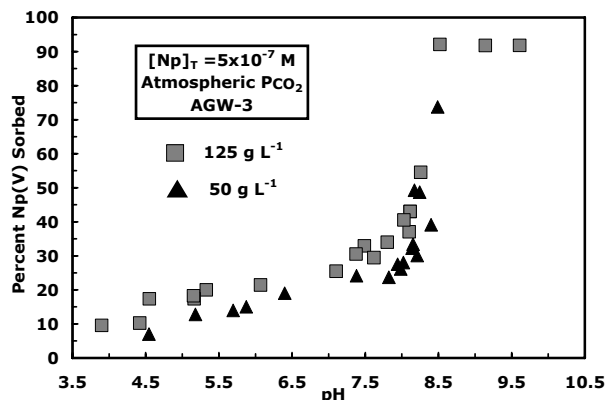


Figure 2.24c. Comparison of 5.0×10^{-7} M Np(V) sorption edges at atmospheric PCO_2 using 50 and 125 g L^{-1} treated NABS in AGW-3.

This is evidence that the decrease in sorption observed for the isotherm experiments (e.g. see Figures 2.12a and 2.12b) is significant, since the expected aqueous species distribution for both PCO_2 systems includes $75\% \text{ NpO}_2^+$ and $25\% \text{ NpO}_2\text{CO}_3^-$.

2.2.3.7 Effect of Groundwater Constituents on Np(V) Sorption

Comparing sorption edges at the same solid-solution ratio using AGW-3, AGW-A or NaClO_4 , at pH below approximately pH 8.1 (to avoid precipitation of calcite in AGW-3), suggests that changes in solution composition effect the sorption affinity of NpO_2^+ for treated NABS. A decrease in sorption was most pronounced when comparing sorption in AGW-3 and AGW-A using 125 g L^{-1} treated NABS (Figure 2.25a). NaClO_4 experiments were conducted at 0.1 M while the ionic strength of AGW-3 and AGW-A were both 0.02 M . AGW-3 included $5.4 \times 10^{-4} \text{ M}$ additional HCO_3^- while AGW-A and 0.1 M NaClO_4 had no added HCO_3^- . Np(V) sorption to 125 g L^{-1} treated NABS in 0.1 M NaClO_4 and AGW-A are compared in Figure 2.25b. The sorption edges clearly show that Np(V) sorption decreases above approximately pH 8 in AGW-A. These results are consistent with the Del Nero et al. (1998) study of Np(V) sorption to hydrargilite using a N_2 atmosphere and adding 0 , 10^{-3} M and $10^{-2} \text{ M CO}_3^{2-}$. For example, Del Nero and coworkers found that sorption at pH 8.5 decreased from approximately 75% to 43% when the carbonate concentration was increased from 0 to 10^{-2} M . Sorption using $10^{-3} \text{ M CO}_3^{2-}$ showed similar behavior to the CO_2 -free experiments.

The Ca^{2+} concentration was an order of magnitude higher in AGW-3 than AGW-A, specifically 4.7×10^{-3} and $4.7 \times 10^{-4} \text{ M}$, respectively. Given that lower Np(V) sorption to sediment was previously observed with additional Ca^{2+} (Routson et al., 1977; McCubbin and Leonard, 1995), it is reasonable to conclude that relatively high Ca^{2+} concentrations will compete with Np(V) for NABS surface sites.

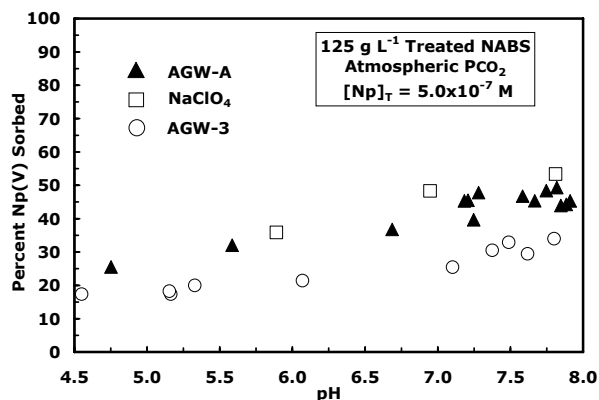


Figure 2.25a. Np(V) sorption edges with 5×10^{-7} M Np(V), 125 g L^{-1} treated NABS, in AGW-A, 0.1 M NaClO_4 or AGW-3 at atmospheric PCO_2 .

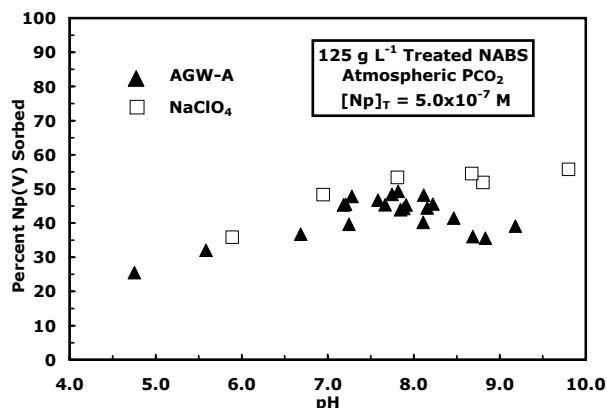


Figure 2.25b. Np(V) sorption edges with 5×10^{-7} M Np(V), 125 g L^{-1} treated NABS, in AGW-A solution or 0.1 M NaClO_4 at atmospheric PCO_2 .

Preliminary experiments using 0.1 M and 0.01 M Ca^{2+} suggest that increasing Ca^{2+} concentration by several orders of magnitude higher than in either type of AGW has no obvious impact on sorption (data not shown).

The impact of HA on Np(V) uptake to NABS was investigated over the range of conditions summarized in Table 2.11. Figures 2.26a and b show that sorption of $5.0 \times 10^{-7} \text{ M}$ or $5.0 \times 10^{-6} \text{ M}$ Np(V) to 500 g L^{-1} treated NABS at atmospheric PCO_2 is unaltered by the addition of 10 mg L^{-1} HA. However, Np(V) sorption is substantially decreased at both Np(V) concentrations over much of the pH range studied in the presence of 100 mg L^{-1} HA. These results suggest the

formation of an $\text{NpO}_2\text{-HA}$ aqueous complex. Figures 2.27a and b show that Np(V) sorption increases as sorption of 100 mg L^{-1} HA to treated NABS decreases at high pH, which suggests that HA sorption to NABS is competing with Np(V) for NABS surface sites.

2.2.4 Summary of Np(V) Sorption Results

Np(V) sorption to treated and untreated NABS was investigated over a wide range of system conditions. The most important findings follow:

1. The effect of pH is relatively weak compared to that observed for Np(V) to monomineralic oxides and oxyhydroxides as well as for U(VI) sorption to NABS (Sanpawanitchakit, 2002; this work). However, the increase in sorption even in the alkaline pH range is consistent with Np(V) sorption to many pure minerals at atmospheric PCO_2 and CO_2 -free conditions.
2. Varying PCO_2 has either a minor or no impact on Np(V) sorption to NABS. Increasing PCO_2 while allowing pH to reach equilibrium values has minimal impact on Np(V) sorption to treated and untreated NABS, due to the similarities in aqueous speciation at the equilibrium pH values. Sorption edge experiments were also minimally impacted below pH 7.5 by adjusting the PCO_2 to 8%. However, above about pH 7.5, precipitation of Np(V) is suggested by a steep increase in sorption. Sorption edge experiments conducted using CO_2 -free conditions produced similar results to experiments under atmospheric PCO_2 .
3. Sorption of carbonate species to the NABS surface appears to cause a minor reduction in Np(V) sorption. In contrast, previous studies by Sanpawanitchakit (2002), USNRC (2003) and Davis et al. (2004) show that U(VI) sorption to NABS is considerably more PCO_2 dependent.
4. Increasing the solid-solution ratio increases Np(V) sorption due to the additional surface site availability.
5. NpO_2^+ -HA aqueous complexation and HA sorption to the sediment reduces the Np(V) sorption affinity for treated NABS at high HA concentrations only.

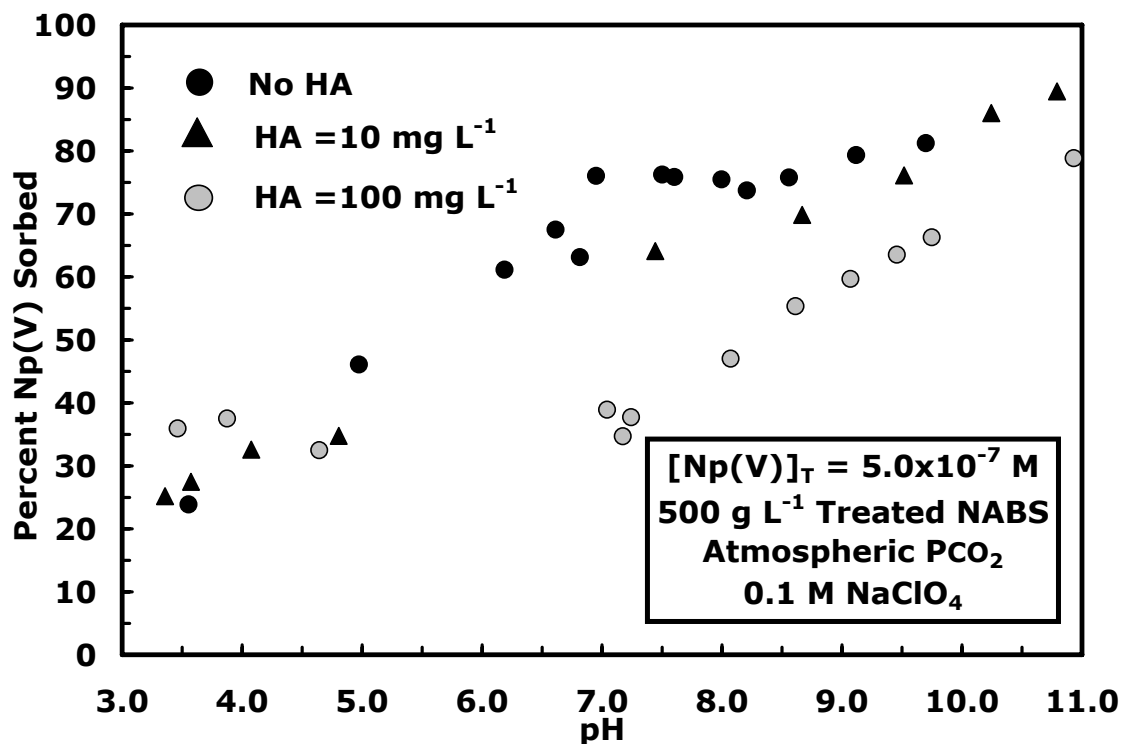


Figure 2.26a. Effect of 10 mg L⁻¹ and 100 mg L⁻¹ HA on Np(V) sorption edges using 5.0x10⁻⁷ M Np(V), 500 g L⁻¹ treated NABS, in 0.1 M NaClO₄ at atmospheric PCO₂.

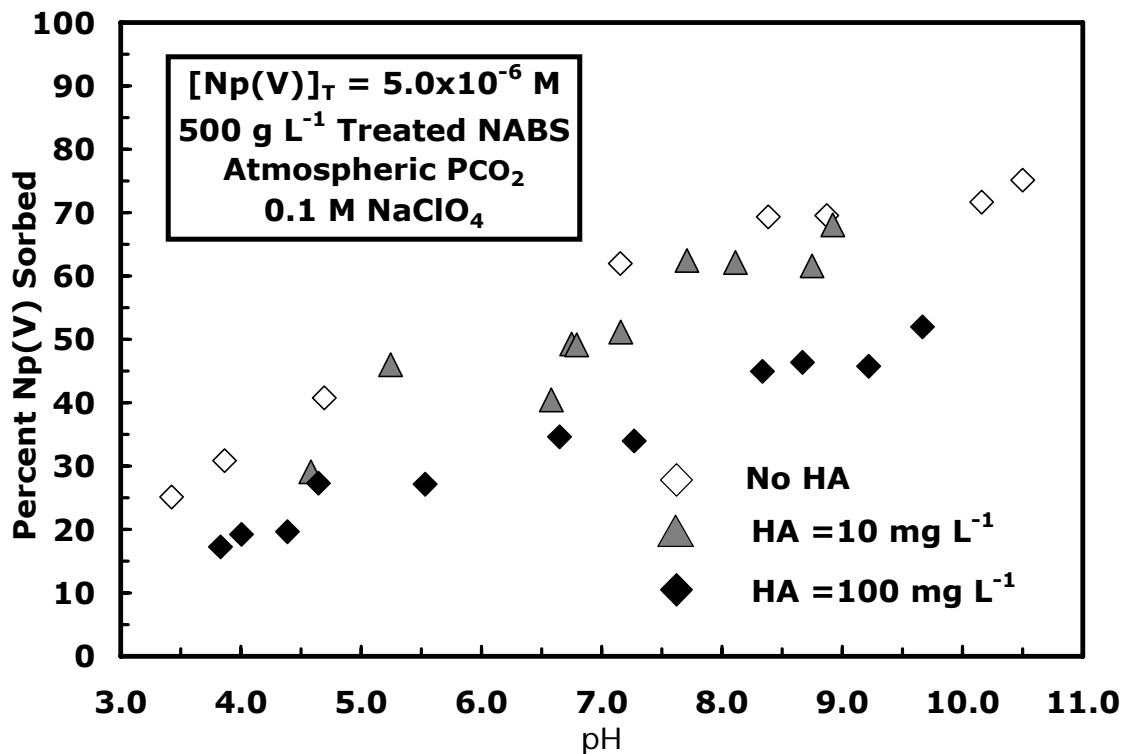


Figure 2.26b. Effect of 10 and 100 mg L⁻¹ HA on Np(V) sorption edges using 5.0x10⁻⁶ M Np(V), 500 g L⁻¹ treated NABS, in 0.1 M NaClO₄ at atmospheric PCO₂.

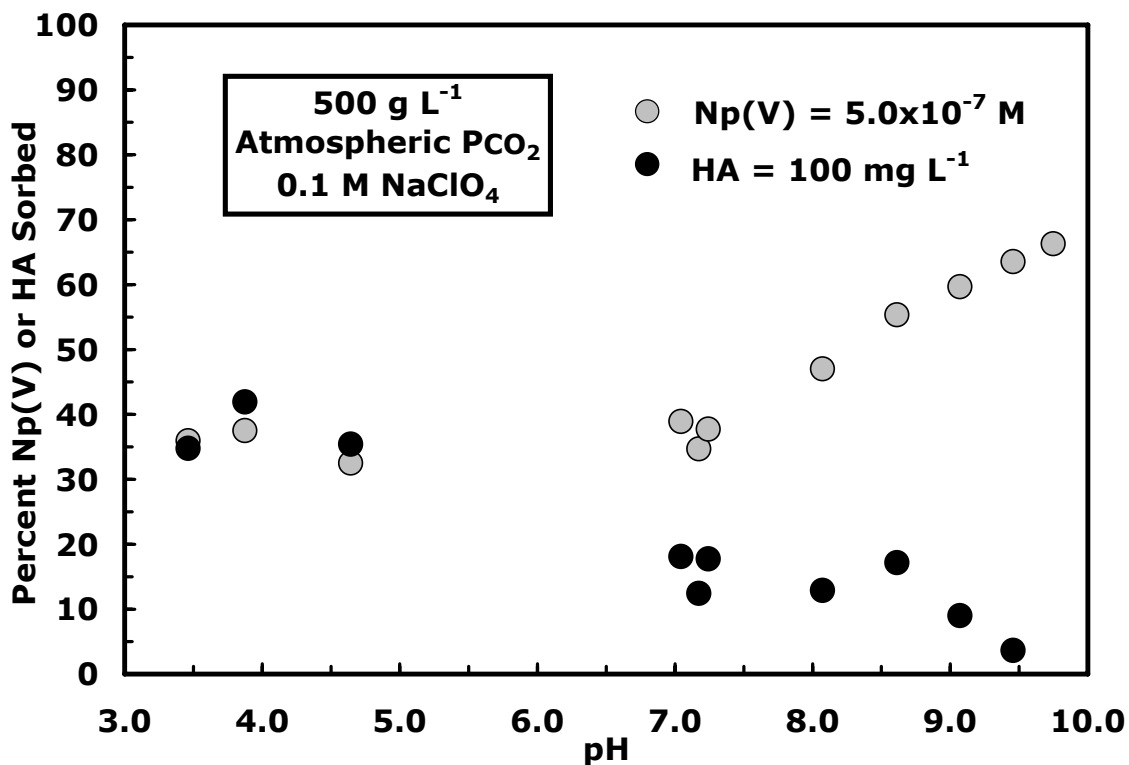


Figure 2.27a. Comparison of HA and Np(V) sorption edges using 100 mg L⁻¹ HA, 5.0x10⁻⁷ M Np(V), 500 g L⁻¹ treated NABS in 0.1 M NaClO₄ at atmospheric PCO₂.

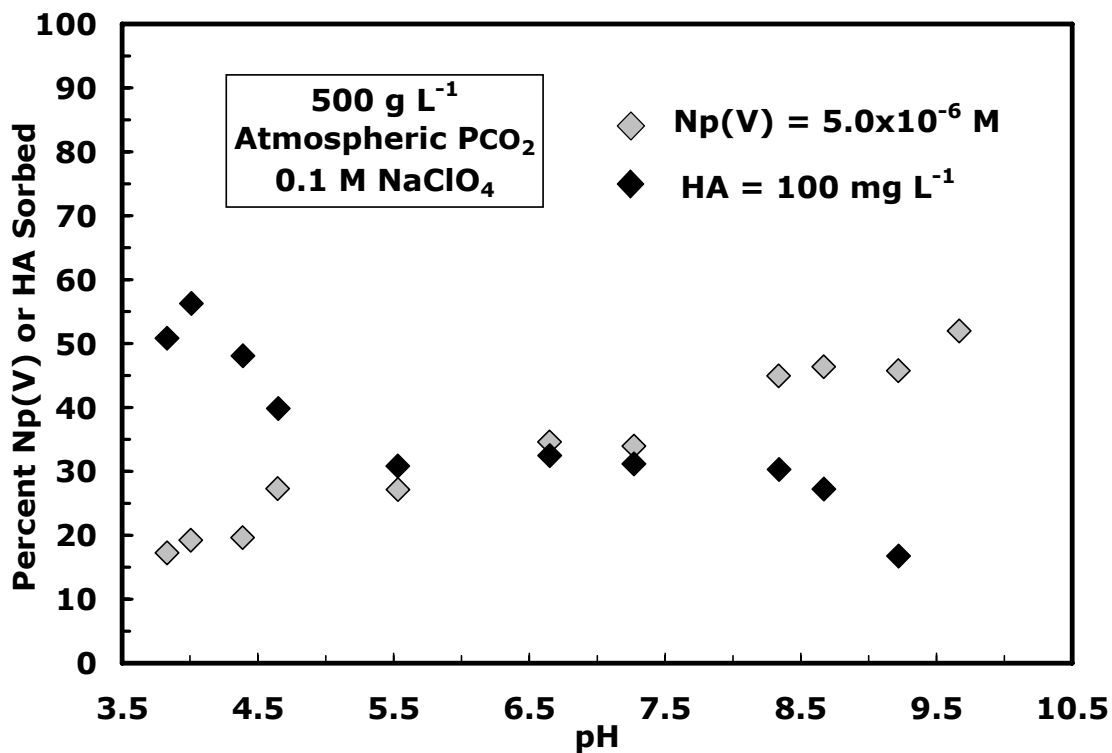


Figure 2.27b. Comparison of HA and Np(V) sorption edges using 100 mg L⁻¹ HA, 5.0x10⁻⁶ M Np(V), 500 g L⁻¹ treated NABS in 0.1 M NaClO₄ at atmospheric PCO₂.

2.3 Surface Complexation Modeling of Neptunium(V) Sorption in Natural Systems

2.3.1 Introduction

Performance assessments assist in evaluating the long-term safety of underground nuclear waste repositories. Generally, transport calculations within performance assessments account for sorption to mineral surfaces using distribution coefficients, K_d values (Bethke and Brady, 2000). However, changing geochemical conditions, such as pH, PCO_2 and mineral surface properties can substantially alter K_d values, resulting in inaccurate transport simulations (Glynn, 2003). Surface complexation models (SCMs) of the water/mineral interface have the capability of more accurately describing metal-ion sorption over a range of system conditions. Few SCMs have been developed to describe sorption to complex geomeia; this is in part due to difficulties in describing the electric double layer (EDL) of the water/mineral interface and in identifying specifically which minerals are involved in sorption (Davis et al., 1998). However, successful model simulations will foster the assimilation of SCMs into reactive transport models. In order to facilitate this transition, Curtis et al. (2006) recently demonstrated that incorporation of an SCM within a reactive transport calculation leads to an acceptable model for U(VI) transport through a shallow alluvial aquifer.

As illustrated in Table 2.13, a number of studies show that SCMs can accurately simulate Np(V) sorption to pure mineral phases over a range of system conditions characteristic of geochemical environments (e.g. Girvin et al., 1991; Kohler et al., 1999; Del Nero et al., 2004). An extensive literature review showed that SCMs have yet to be used to describe Np(V) sorption to complex geomeia. The goal of the current study is to test the ability of SCMs to describe Np(V) sorption to an alluvial aquifer sediment under a range of geochemical conditions.

2.3.2 Generalized Composite Modeling Approach

To date, GC modeling of sorption to complex geomeia has been accomplished without explicit correction for electrostatic interactions. The choice to use a non-electrostatic model (NEM) in this study is due to the difficulty in obtaining EDL information for the study sediment. However, an 'effective' point of zero charge (pH_{pzc}) was determined in Section 2.3.3.1 for treated (carbonate mineral-removed) Naturita alluvial background sediment (NABS), allowing surface reactions to be derived to describe the protonation and deprotonation of treated NABS surface sites.

Np(V) sorption was simulated using FITEQL (version 4.0), a nonlinear, least-squares optimization program (Herbelin and Westall, 1999). The extent of agreement between model results and experimental data, the goodness-of-fit, was established graphically and/or using the weighted sum of the squares of the residuals divided by the degrees of freedom (WSOS/DF) (Cernik et al., 1995). Valid WSOS/DF values are obtained when realistic error estimates are input into the model calculations.

Thermodynamic surface speciation models, such as the component additivity (CA) SCM developed by Honeyman (1984), require spectroscopic evidence to substantiate surface reactions and electric double layer properties (Hiemstra and van Riemsdijk, 1999). In contrast, the GC SCM does not require validation by spectroscopy, but instead is based on chemically plausible surface reactions. If possible, it is preferable to develop a GC model based on molecular level information. Few studies are available that explore the surface complexation behavior of Np(V) on a molecular scale. The Combes et al. (1992) study used X-ray absorption fine structure spectroscopy (EXAFS) to elucidate the surface coordination of Np(V) at the goethite ($\alpha\text{-FeOOH}$) surface. Their work showed that NpO_2^+ sorbs to the goethite surface as a mononuclear inner-sphere complex at pH 7.2, 7×10^{-7} M Np(V), $I = 0.08$ M NaNO_3 and 1 g L^{-1} goethite. However, Combes and coworkers acknowledged that the presence

Table 2.13 Surface Complexation Modeling Studies of Np(V) Sorption to Pure Mineral Phases

Reference Mineral Phase	Surface Reaction	Log K	Np(V) (M)	PCO ₂ (Atm)	I (M)	EDL	Source of SCM: Source of Experimental Data
Alumina (α -Al ₂ O ₃)	$\text{AlOH} + \text{H}^+ = \text{AlOH}_2^+$ $\text{AlOH} = \text{AlO}^- + \text{H}^+$ $\text{AlOH} + \text{NpO}_2^+ = \text{AlONpO}_2 + \text{H}^+$ $\text{AlOH} + \text{NpO}_2^+ = \text{AlOHNpO}_2^+$ $\text{AlOH} + \text{NpO}_2^+ + \text{H}_2\text{O} = \text{AlONpO}_2\text{OH}^- + 2\text{H}^+$ $\text{AlOH} + \text{NpO}_2^+ + \text{H}_2\text{O} = \text{AlOHNpO}_2\text{OH} + \text{H}^+$ $\text{AlOH}_2^+ + \text{NpO}_2^+ + \text{H}_2\text{O} = \text{AlOH}_2\text{NpO}_2\text{OH}^+ + \text{H}^+$ $2\text{AlOH} + \text{NpO}_2^+ = (\text{AlO})_2\text{NpO}_2^- + 2\text{H}^+$	DDL 7.29 DDL -8.93 DDL -4.26 DDL 5.07 DDL -13.37 DDL -4.26 DDL 5.07 DDL -7.99	6.0x10 ⁻⁶	<10 ^{-3.5}	0.1	CCM, DDL, TLM	Turner (1995); Nakayama and Sakamoto (1991)
Alumina	$\text{AlOH} + \text{H}^+ = \text{AlOH}_2^+$ $\text{AlOH} = \text{AlO}^- + \text{H}^+$ $\text{AlOH} + \text{NpO}_2^+ = \text{AlONpO}_2 + \text{H}^+$ $\text{AlOH} + \text{NpO}_2^+ + \text{H}_2\text{O} = \text{AlOHNpO}_2\text{OH}^- + 2\text{H}^+$	8.33 -9.73 -2.52 to -4.86 -12.44 to -14.29	1.9x10 ⁻⁷ , 1.9x10 ⁻⁹ , 1.0x10 ⁻⁶ , 6.0x10 ⁻⁶	10 ^{-3.5} , 0.05 M	0.01, 0.1	NEM	Zavarin and Bruton (2004a) and Turner (1995); Bertetti et al. (1998) and Nakayama and Sakamoto (1991) and Allard et al. (1982)
Alumina	$\text{AlOH} + \text{H}^+ = \text{AlOH}_2^+$ $\text{AlOH} = \text{AlO}^- + \text{H}^+$ $2\text{AlOH} + \text{NpO}_2^+ = (\text{AlO})_2\text{NpO}_2^- + 2\text{H}^+$	8.33 -9.73 -8.23	6.0x10 ⁻⁶	<10 ^{-3.5}	0.1*	DDL	Wang et al. (2001); Nakayama and Sakamoto (1991) and Tochiyama et al. (1996)

AlOH = aluminum oxide surface hydroxyl groups, FeOH= iron oxide surface hydroxyl groups, IX= ion exchange surface site, I =0.1 M NaNO₃, NaClO₄ or where noted with * tris(hydroxymethyl)amino-methane + 2-morpholinoethane sulfonic acid, M= mol L⁻¹

Table 2.13 (continued). Surface Complexation Modeling Studies of Np(V) Sorption to Pure Mineral Phases

Reference Mineral Phase	Surface Reaction	Log K	Np(V) (M)	PCO ₂ (Atm)	I (M)	EDL	Source of SCM: Source of Experimental Data
Alumina	$\text{AlOH} + \text{H}^+ = \text{AlOH}_2^+$ $\text{AlOH} = \text{AlO}^- + \text{H}^+$ $\text{AlOH} + \text{NpO}_2^+ = \text{AlONpO}_2 + \text{H}^+$ $\text{AlOH} + \text{NpO}_2^+ + \text{H}_2\text{O} = \text{AlOHNpO}_2\text{OH}^- + 2\text{H}^+$	8.33 -9.73 -2.18 to -2.49 -10.19 to -13.65	10^{-14} and 6.0×10^{-6}	$10^{-3.5}$, 0.05 M	0.1	NEM	Zavarin and Bruton (2004a) and Turner (1995); Bertetti et al. (1998) and Nakayama and Sakamoto (1991) and Righetto et al. (1988) and Righetto et al. (1991)
Alumina ($\gamma\text{-Al}_2\text{O}_3$)	$\text{AlOH} + \text{H}^+ = \text{AlOH}_2^+$ $\text{AlOH} = \text{AlO}^- + \text{H}^+$ $\text{AlOH} + \text{NpO}_2^+ + \text{H}_2\text{O} = \text{AlONpO}_2\text{OH}^- + 2\text{H}^+$	6.85 -9.05 -10.93	10^{-14}	0	0.1	DDL	Wang et al. (2001); Righetto et al. (1988)
Amorphous Al Silicates (Si/Al = 4.3 -10)	$\text{SiOH} + \text{H}^+ = \text{SiOH}_2^+$ $\text{SiOH} = \text{SiO}^- + \text{H}^+$ $\text{AlOH} + \text{H}^+ = \text{AlOH}_2^+$ $\text{AlOH} = \text{AlO}^- + \text{H}^+$ $\text{AlOH} + \text{NpO}_2^+ = \text{AlONpO}_2 + \text{H}^+$ $\text{SiOH} + \text{NpO}_2^+ = \text{SiOHNpO}_2^+$	1.0 -7.0 7.5 -10.2 -2.9 0.44	$6 \times 10^{-6} - 1 \times 10^{-9}$	0, $10^{-3.5}$	0.001, 0.1	DDL	Del Nero et al. (2004) and Sverjensky and Sahai (1996) and Bonnissel-Gissinger et al. (1999); Del Nero et al. (2004)
Amorphous Fe Silicates (Si/Al = 2.3 -10)	$\text{SiOH} + \text{H}^+ = \text{SiOH}_2^+$ $\text{SiOH} = \text{SiO}^- + \text{H}^+$ $\text{FeOH} + \text{H}^+ = \text{FeOH}_2^+$ $\text{FeOH} = \text{FeO}^- + \text{H}^+$ $\text{FeOH} + \text{NpO}_2^+ = \text{FeONpO}_2 + \text{H}^+$ $\text{SiOH} + \text{NpO}_2^+ = \text{SiOHNpO}_2^+$	1.0 -7.0 7.29 -8.93 -2.9 0.44	$1 \times 10^{-6} - 1 \times 10^{-9}$	0, $10^{-3.5}$	0.01, 0.1	DDL	Del Nero et al. (2004); Del Nero et al. (2004)

Table 2.13 (continued). Surface Complexation Modeling Studies of Np(V) Sorption to Pure Mineral Phases

Reference Mineral Phase	Surface Reaction	Log K	Np(V) (M)	P _{CO₂} (Atm)	I (M)	EDL	Source of SCM: Source of Experimental Data
Amorphous SiO ₂	$\text{SiOH} = \text{SiO}^- + \text{H}^+$ $\text{SiOH} + \text{NpO}_2^+ = \text{SiONpO}_2 + \text{H}^+$ $\text{SiOH} + \text{NpO}_2^+ = \text{SiOHNpO}_2^+$ $\text{SiOH} + \text{NpO}_2^+ + \text{H}_2\text{O} = \text{SiONpO}_2\text{OH}^- + 2\text{H}^+$ $\text{SiOH} + \text{NpO}_2^+ + \text{H}_2\text{O} = \text{SiOHNpO}_2\text{OH}^0 + \text{H}^+$ $\text{SiOH}_2^+ + \text{NpO}_2^+ + \text{H}_2\text{O} = \text{SiOH}_2\text{NpO}_2\text{OH}^+ + \text{H}^+$ $2\text{SiOH} + \text{NpO}_2^+ = (\text{SiO})_2\text{NpO}_2^- + 2\text{H}^+$	DDL -7.20 DDL -5.39 DDL 1.30 DDL -11.89 DDL -5.39 DDL 1.30 DDL -12.53	10 ⁻¹⁴	0	0.1	CCM, DDL, TLM	Turner (1995); Righetto et al. (1991)
Amorphous SiO ₂	$\text{SiOH} = \text{SiO}^- + \text{H}^+$ $\text{SiOH} + \text{NpO}_2^+ + \text{H}_2\text{O} = \text{SiONpO}_2\text{OH}^- + 2\text{H}^+$	-7.20 12.54	1.0x10 ⁻¹⁴	0	0.1	DDL	Wang et al. (2001) and Turner and Sassman (1996); Righetto et al. (1991)
Biotite (Si/Al = 3)	$\text{AlOH} + \text{H}^+ = \text{AlOH}_2^+$ $\text{AlOH} = \text{AlO}^- + \text{H}^+$ $\text{SiOH} = \text{SiO}^- + \text{H}^+$ $\text{SiOH} + \text{NpO}_2^+ = \text{SiONpO}_2 + \text{H}^+$ $\text{AlOH} + \text{NpO}_2^+ + \text{H}_2\text{O} = \text{AlONpO}_2\text{OH}^- + 2\text{H}^+$ $\text{SiOH} + \text{NpO}_2^+ + \text{H}_2\text{O} = \text{SiONpO}_2\text{OH}^- + 2\text{H}^+$	8.33 -9.73 -7.20 -4.15 -12.39 -11.58	6.0x10 ⁻⁶	0	0.1	DDL	Turner and Sassman (1996); Nakayama and Sakamoto (1991)
Biotite (Si/Al = 3)	$\text{AlOH} + \text{H}^+ = \text{AlOH}_2^+$ $\text{AlOH} = \text{AlO}^- + \text{H}^+$ $\text{SiOH} = \text{SiO}^- + \text{H}^+$ $\text{SiOH} + \text{NpO}_2^+ = \text{SiONpO}_2 + \text{H}^+$ $\text{AlOH} + \text{NpO}_2^+ + \text{H}_2\text{O} = \text{AlONpO}_2\text{OH}^- + 2\text{H}^+$	8.33 -9.73 -7.20 -4.17 -11.50	6.0x10 ⁻⁶	0	0.1	DDL	Wang et al. (2001) and Turner and Sassman (1996); Nakayama and Sakamoto (1991)

Table 2.13 (continued). Surface Complexation Modeling Studies of Np(V) Sorption to Pure Mineral Phases

Reference Mineral Phase	Surface Reaction	Log K	Np(V) (M)	PCO ₂ (Atm)	I (M)	EDL	Source of SCM: Source of Experimental Data
Boehmite (γ -AlOOH)	$\text{AlOH} + \text{H}^+ = \text{AlOH}_2^+$ $\text{AlOH} = \text{AlO}^- + \text{H}^+$ $\text{AlOH} + \text{NpO}_2^+ = \text{AlONpO}_2 + \text{H}^+$ $\text{AlOH} + \text{NpO}_2^+ = \text{AlOHNpO}_2^+$ $\text{AlOH} + \text{NpO}_2^+ + \text{H}_2\text{O} = \text{AlONpO}_2\text{OH}^- + 2\text{H}^+$ $\text{AlOH} + \text{NpO}_2^+ + \text{H}_2\text{O} = \text{AlOHNpO}_2\text{OH} + \text{H}^+$ $\text{AlOH}_2^+ + \text{NpO}_2^+ + \text{H}_2\text{O} = \text{AlOH}_2\text{NpO}_2\text{OH}^+ + \text{H}^+$ $2\text{AlOH} + \text{NpO}_2^+ = (\text{AlO})_2\text{NpO}_2^- + 2\text{H}^+$	DDL 6.85 DDL -9.05 DDL -3.36 DDL 4.09 DDL -10.84 DDL -3.36 DDL 4.09 DDL -7.60	6.0×10^{-6}	$<10^{-3.5}$	0.1	CCM, DDL, TLM	Turner (1995); Nakayama and Sakamoto (1991)
Boehmite	$\text{AlOH} + \text{H}^+ = \text{AlOH}_2^+$ $\text{AlOH} = \text{AlO}^- + \text{H}^+$ $\text{AlOH} + \text{NpO}_2^+ = \text{AlOHNpO}_2^+$ $\text{AlOH} + \text{NpO}_2^+ = \text{AlONpO}_2 + \text{H}^+$	6.85 -9.05 3.89 -4.50	6×10^{-6}	$<10^{-3.5}$	0.1	DDL	Wang et al. (2001) and Turner and Sassman (1996); Nakayama and Sakamoto (1991)
Calcite (CaCO ₃)	$\text{IX} + \text{Ca}^{2+} = \text{IXCa}^{2+}$ $\text{IX} + 2\text{NpO}_2^+ = \text{IX}(\text{NpO}_2^+)_2$ $\text{CO}_3\text{H} + \text{NpO}_2^+ = \text{CO}_3\text{HNpO}_2^+$ $\text{CO}_3\text{H} + \text{Ca}^{2+} = \text{CO}_3\text{Ca}^+ + \text{H}^+$ $\text{CaOH} + \text{NpO}_2^+ + \text{H}_2\text{O} = \text{CaONpO}_2\text{OH}^- + 2\text{H}^+$ $\text{CaOH} + \text{NpO}_2^+ + \text{CO}_3^{2-} = \text{CaOHNpO}_2\text{CO}_3$	IX 2.4 IX 12.05 CC 8.6 CC -1.9 CC -9.6 CC 12.4	1.6×10^{-6}	$10^{-3.5}$	~0.1 to 0.6	CCM, IX	Bertetti (2002); Bertetti (2002)
Calcite	$>\text{Ca}^{2+} + \text{NpO}_2^+ = >\text{NpO}_2^+ + \text{Ca}^{2+}$	1.46	$\sim 10^{-7}$	$10^{-3.5}$	0.1	NEM	Zavarin and Bruton (2004b); Zavarin and Bruton (2004b)

Table 2.13 (continued). Surface Complexation Modeling Studies of Np(V) Sorption to Pure Mineral Phases

Reference Mineral Phase	Surface Reaction	Log K	Np(V) (M)	PCO ₂ (Atm)	I (M)	EDL	Source of SCM: Source of Experimental Data
Clinoptilolite	$\text{AlOH} + \text{H}^+ = \text{AlOH}_2^+$ $\text{AlOH} = \text{AlO}^- + \text{H}^+$ $\text{SiOH} = \text{SiO}^- + \text{H}^+$ $\text{SiOH} + \text{NpO}_2^+ = \text{SiOHNpO}_2^+$ $\text{AlOH} + \text{NpO}_2^+ + \text{H}_2\text{O} = \text{AlONpO}_2\text{OH}^- + 2\text{H}^+$	8.33 -9.73 -7.20 3.27 -13.20	1×10^{-6}	0	0	DDL	Wang et al. (2001) and Turner and Sassman (1996): Bertetti et al. (1996)
Clinoptilolite	$\text{AlOH} + \text{H}^+ = \text{AlOH}_2^+$ $\text{AlOH} = \text{AlO}^- + \text{H}^+$ $\text{AlOH} + \text{NpO}_2^+ = \text{AlONpO}_2 + \text{H}^+$ $\text{AlOH} + \text{NpO}_2^+ + \text{H}_2\text{O} = \text{AlONpO}_2\text{OH}^- + 2\text{H}^+$	8.33 -9.73 Average - 4.67 Average - 14.26	1.0×10^{-6}	0, $10^{-3.5}$	0.01, 0.1	NEM	Zavarin and Bruton (2004a): Bertetti et al. (1998)
Diaspore (α -AlOOH)	$\text{AlOH} + \text{H}^+ = \text{AlOH}_2^+$ $\text{AlOH} = \text{AlO}^- + \text{H}^+$ $\text{AlOH} + \text{NpO}_2^+ = \text{AlONpO}_2 + \text{H}^+$ $\text{AlOH} + \text{NpO}_2^+ = \text{AlOHNpO}_2^+$ $\text{AlOH} + \text{NpO}_2^+ + \text{H}_2\text{O} = \text{AlONpO}_2\text{OH}^- + 2\text{H}^+$	8.33 -9.73 -3.62 5.50 -13.10	5.5×10^{-13}	0	0.1*	DDL	Wang et al. (2001) and Turner and Sassman (1996): Tochiyama et al. (1996)
Ferrihydrite ($\text{Fe}_2\text{O}_3 \cdot \text{H}_2\text{O}$)	$\text{FeOH} + \text{H}^+ = \text{FeOH}_2^+$ $\text{FeOH} = \text{FeO}^- + \text{H}^+$ $\text{FeOH} + \text{Na}^+ = \text{FeO}^- \text{--} \text{Na}^+ + \text{H}^+$ $\text{FeOH} + \text{H}^+ + \text{NO}_3^- = \text{FeOH}_2^+ \text{--} \text{NO}_3^-$ $\text{FeOH} + \text{NpO}_2^+ = \text{FeONpO}_2 + \text{H}^+$ $\text{FeOH} + \text{NpO}_2^+ + \text{H}_2\text{O} = \text{FeOHNpO}_2\text{OH} + \text{H}^+$	5.4 -10.4 -8.6 7.5 5.6 -3.2	4.7×10^{-12}	$10^{-3.5}$	0.1	TLM	Girvin et al. (1991): Girvin et al. (1991)
Ferrihydrite	$\text{FeOH} + \text{H}^+ = \text{FeOH}_2^+$ $\text{FeOH} = \text{FeO}^- + \text{H}^+$ $\text{FeOH} + \text{NpO}_2^+ = \text{FeONpO}_2 + \text{H}^+$	7.29 -8.93 -2.72	4.7×10^{-12}	$10^{-3.5}$	0.1	DDL	Wang et al. (2001) and Turner and Sassman (1996): Girvin et al. (1991)

Table 2.13 (continued). Surface Complexation Modeling Studies of Np(V) Sorption to Pure Mineral Phases

Reference Mineral Phase	Surface Reaction	Log K	Np(V) (M)	PCO ₂ (Atm)	I (M)	EDL	Source of SCM: Source of Experimental Data
Ferrihydrite	$\text{FeOH} + \text{H}^+ = \text{FeOH}_2^+$ $\text{FeOH} = \text{FeO}^- + \text{H}^+$ $\text{FeOH} + \text{NpO}_2^+ = \text{FeONpO}_2 + \text{H}^+$ $\text{FeOH} + \text{NpO}_2^+ = \text{FeOHNpO}_2^+$ $\text{FeOH} + \text{NpO}_2^+ + \text{H}_2\text{O} = \text{FeONpO}_2\text{OH}^- + 2\text{H}^+$ $\text{FeOH} + \text{NpO}_2^+ + \text{H}_2\text{O} = \text{FeOHNpO}_2\text{OH} + \text{H}^+$ $\text{FeOH}_2^+ + \text{NpO}_2^+ + \text{H}_2\text{O} = \text{FeOH}_2\text{NpO}_2\text{OH}^+ + \text{H}^+$ $2\text{FeOH} + \text{NpO}_2^+ = (\text{FeO})_2\text{NpO}_2^- + 2\text{H}^+$	DDL 7.29 DDL -8.93 DDL -3.02 DDL 5.04 DDL-11.08 DDL -3.02 DDL 5.04 DDL -8.28	4.7x10 ⁻¹²	10 ^{-3.5}	0.1	CCM, DDL, TLM	Turner (1995): Girvin et al. (1991)
Ferrihydrite	$\text{FeOH} + \text{H}^+ = \text{FeOH}_2^+$ $\text{FeOH} = \text{FeO}^- + \text{H}^+$ $\text{FeOH} + \text{NpO}_2^+ = \text{FeOHNpO}_2^+$ $\text{FeOH} + \text{NpO}_2^+ + \text{H}_2\text{O} = \text{FeONpO}_2\text{OH}^- + 2\text{H}^+$	Average 7.29 Average -8.93 Average 4.32 Average -11.26	4.7x10 ⁻¹²	10 ^{-3.5}	0.1	NEM	Zavarin and Bruton (2004b): Girvin et al. (1991)
Gibbsite (γ-Al(OH) ₃)	$\text{AlOH} + \text{H}^+ = \text{AlOH}_2^+$ $\text{AlOH} = \text{AlO}^- + \text{H}^+$ $\text{AlOH} + \text{NpO}_2^+ = \text{AlNpO}_2 + \text{H}^+$ $\text{AlOH} + \text{NpO}_2^+ = \text{AlOHNpO}_2^+$	6.85 -9.05 -3.53 4.95	5.5x10 ⁻¹³	0	0.1*	DDL	Wang et al. (2001) and Turner and Sassman (1996): Tochiyama et al. (1996)
Goethite (α-FeOOH)	$\text{FeOH} + \text{H}^+ = \text{FeOH}_2^+$ $\text{FeOH} = \text{FeO}^- + \text{H}^+$ $\text{FeOH} + \text{Na}^+ = \text{FeO}^- \text{--} \text{Na}^+ + \text{H}^+$ $\text{FeOH} + \text{H}^+ + \text{ClO}_4^- = \text{FeOH}_2^+ \text{--} \text{ClO}_4^-$ $\text{FeOH} + \text{NpO}_2^+ = \text{FeONpO}_2^+ + \text{H}^+$ $\text{FeOH} + \text{NpO}_2^+ + \text{H}^+ + \text{CO}_3^{2-} = \text{FeONpO}_2(\text{HCO}_3)^{2-}$	7.9 -9.9 -8.76 8.89 -1.57 22.81	1.2x10 ⁻⁷	0, 10 ^{-3.5} , 10 ^{-2.7}	0.1	TLM	Kohler et al. (1999): Kohler et al. (1999) and van Geen et al. (1994)

Table 2.13 (continued). Surface Complexation Modeling Studies of Np(V) Sorption to Pure Mineral Phases

Reference Mineral Phase	Surface Reaction	Log K	Np(V) (M)	PCO ₂ (Atm)	I (M)	EDL	Source of SCM: Source of Experimental Data
Goethite (α -FeOOH)	$\text{FeOH} + \text{H}^+ = \text{FeOH}_2^+$ $\text{FeOH} = \text{FeO}^- + \text{H}^+$ $\text{FeOH} + \text{NpO}_2^+ = \text{FeOHNpO}_2^+$ $\text{FeOH} + \text{NpO}_2^+ + \text{H}_2\text{O} = \text{FeONpO}_2\text{OH}^- + 2\text{H}^+$	7.35 -9.17 6.03 -12.0	6.0×10^{-6} , 1.2×10^{-12}	0	0.1	DDL	Wang et al. (2001) and Turner and Sassman (1996); Nakayama and Sakamoto (1991) and Tochiyama et al. (1995)
Goethite	$\text{FeOH} + \text{NpO}_2^+ = \text{FeONpO}_2 + \text{H}^+$ $\text{FeOH} + \text{H}^+ + \text{CO}_3^{2-} = \text{FeOH}_2\text{CO}_3^-$ $\text{FeOH} + 2\text{H}^+ + \text{CO}_3^{2-} = \text{FeOH}_2\text{HCO}_3$	0.8 16.5 21.5	4×10^{-7} - 6×10^{-6}	$10^{-3.5}$	0.1	CCM	Fujita et al. (1995); Fujita et al. (1995)
Goethite	$\text{FeOH} + \text{H}^+ = \text{FeOH}_2^+$ $\text{FeOH} = \text{FeO}^- + \text{H}^+$ $\text{FeOH} + \text{NpO}_2^+ = \text{FeONpO}_2 + \text{H}^+$ $\text{FeOH} + \text{NpO}_2^+ = \text{FeOHNpO}_2^+$ $\text{FeOH} + \text{NpO}_2^+ + \text{H}_2\text{O} = \text{FeONpO}_2\text{OH}^- + 2\text{H}^+$ $\text{FeOH} + \text{NpO}_2^+ + \text{H}_2\text{O} = \text{FeOHNpO}_2\text{OH} + \text{H}^+$ $\text{FeOH}_2^+ + \text{NpO}_2^+ + \text{H}_2\text{O} = \text{FeOH}_2\text{NpO}_2\text{OH}^+ + \text{H}^+$ $2\text{FeOH} + \text{NpO}_2^+ = (\text{FeO})_2\text{NpO}_2^- + 2\text{H}^+$	DDL 7.35 DDL -9.17 DDL -2.54 DDL 5.21 DDL -10.39 DDL -2.54 DDL 5.21 DDL -5.96	6.0×10^{-6}	0	0.1	CCM, DDL, TLM	Turner (1995); Nakayama and Sakamoto (1991)
Goethite	$\text{FeOH} + \text{H}^+ = \text{FeOH}_2^+$ $\text{FeOH} = \text{FeO}^- + \text{H}^+$ $\text{FeOH} + \text{NpO}_2^+ = \text{FeOHNpO}_2^+$ $\text{FeOH} + \text{NpO}_2^+ + \text{H}_2\text{O} = \text{FeONpO}_2\text{OH}^- + 2\text{H}^+$	Average 7.29 Average - 8.93 Average 4.32 Average - 11.26	6.0×10^{-6} , 1.2×10^{-12}	0	0.1	NEM	Zavarin and Bruton (2004b) and Turner (1995); Nakayama and Sakamoto (1991)
Hematite (α -Fe ₂ O ₃)	$\text{FeOH} + \text{H}^+ = \text{FeOH}_2^+$ $\text{FeOH} = \text{FeO}^- + \text{H}^+$ $\text{FeOH} + \text{Na}^+ = \text{FeO}^- \text{--} \text{Na}^+ + \text{H}^+$ $\text{FeOH} + \text{H}^+ + \text{ClO}_4^- = \text{FeOH}_2^+ \text{--} \text{ClO}_4^-$ $\text{FeOH} + \text{NpO}_2^+ = \text{FeO-NpO}_2^+ + \text{H}^+$ $\text{FeOH} + \text{NpO}_2^+ + \text{H}^+ + \text{CO}_3^{2-} = \text{FeO-NpO}_2(\text{HCO}_3)^{2-}$	8.4 -10.4 -8.55 10.33 -2.09 24.62	1.2×10^{-7} - 1.3×10^{-6}	0, $10^{-3.5}$, $10^{-2.7}$	0.005, 0.01, 0.05, 0.1	TLM	Kohler et al. (1999); Kohler et al. (1999)

Table 2.13 (continued). Surface Complexation Modeling Studies of Np(V) Sorption to Pure Mineral Phases

Reference Mineral Phase	Surface Reaction	Log K	Np(V) (M)	PCO ₂ (Atm)	I (M)	EDL	Source of SCM: Source of Experimental Data
Hematite	$\text{FeOH} + \text{H}^+ = \text{FeOH}_2^+$ $\text{FeOH} = \text{FeO}^- + \text{H}^+$ $\text{FeOH} + \text{NpO}_2^+ = \text{FeOHNpO}_2^+$ $2\text{FeOH} + \text{NpO}_2^+ = (\text{FeO})_2\text{NpO}_2^- + 2\text{H}^+$	7.35 -9.17 12.07 -6.79	6.0×10^{-6} , 1.2×10^{-12}	0	0.1	DDL	Wang et al. (2001) and Turner and Sassman (1996); Nakayama and Sakamoto (1991) and Tochiyama et al. (1995)
Hydrargilite ($\alpha\text{-Al(OH)}_3$)	$\text{AlOH} + \text{H}^+ = \text{AlOH}_2^+$ $\text{AlOH} = \text{AlO}^- + \text{H}^+$ $\text{AlOH} + \text{NpO}_2^+ = \text{AlONpO}_2 + \text{H}^+$	5.8 9.5 -3.4	$\approx 10^{-13}$	0, 10^{-4} M HCO_3^-	0.1, 0.01	NEM	Del Nero et al. (1997); Del Nero et al. (1997)
Hydrargilite	$\text{AlOH} + \text{H}^+ = \text{AlOH}_2^+$ $\text{AlOH} = \text{AlO}^- + \text{H}^+$ $\text{AlOH} + \text{NpO}_2^+ = \text{AlONpO}_2 + \text{H}^+$	5.7 -9.4 -3.6	$\approx 10^{-13}$	0, 10^{-4} M HCO_3^-	0.1	NEM	Del Nero et al. (1998); Del Nero et al. (1998)
Hydrargilite	$\text{AlOH} + \text{H}^+ = \text{AlOH}_2^+$ $\text{AlOH} = \text{AlO}^- + \text{H}^+$ $\text{AlOH} + \text{NpO}_2^+ = \text{AlONpO}_2 + \text{H}^+$	8.33 -9.73 -2.81	5.5×10^{-14} - 1.0×10^{-13}	0, 10^{-3} , 10^{-2}	0.1*	DDL	Wang et al. (2001) and Turner and Sassman (1996); Del Nero et al. (1997) and Del Nero et al. (1998)
Kaolinite (Si/Al = 1.0)	$\text{AlOH} + \text{H}^+ = \text{AlOH}_2^+$ $\text{AlOH} = \text{AlO}^- + \text{H}^+$ $\text{SiOH} = \text{SiO}^- + \text{H}^+$ $\text{AlOH} + \text{NpO}_2^+ = \text{AlONpO}_2 + \text{H}^+$ $\text{SiOH} + \text{NpO}_2^+ = \text{SiOHNpO}_2^+$	8.33 -9.72 -7.20 -4.04 4.09	7.0×10^{-6}	0	0.1	DDL	Wang et al. (2001) and Turner and Sassman (1996); Niitsu et al. (1997)

Table 2.13 (continued). Surface Complexation Modeling Studies of Np(V) Sorption to Pure Mineral Phases

Reference Mineral Phase	Surface Reaction	Log K	Np(V) (M)	PCO ₂ (Atm)	I (M)	EDL	Source of SCM: Source of Experimental Data
Lepidocrocite (γ -FeOOH)	$\text{FeOH} + \text{H}^+ = \text{FeOH}_2^+$ $\text{FeOH} = \text{FeO}^- + \text{H}^+$ $\text{FeOH} + \text{NpO}_2^+ = \text{FeONpO}_2 + \text{H}^+$ $\text{FeOH} + \text{NpO}_2^+ = \text{FeOHNpO}_2^+$ $\text{FeOH} + \text{NpO}_2^+ + \text{H}_2\text{O} = \text{FeONpO}_2\text{OH}^- + 2\text{H}^+$ $\text{FeOH} + \text{NpO}_2^+ + \text{H}_2\text{O} = \text{FeOHNpO}_2\text{OH} + \text{H}^+$ $\text{FeOH}_2^+ + \text{NpO}_2^+ + \text{H}_2\text{O} = \text{FeOH}_2\text{NpO}_2\text{OH}^+ + \text{H}^+$ $2\text{FeOH} + \text{NpO}_2^+ = (\text{FeO})_2\text{NpO}_2^- + 2\text{H}^+$	DDL 7.35 DDL -9.17 DDL -3.53 DDL 4.51 DDL -11.51 DDL -3.53 DDL 4.51 DDL -7.52	6.0×10^{-6}	$<10^{-3.5}$	0.1	CCM, DDL, TLM	Turner (1995): Nakayama and Sakamoto (1991)
Lepidocrocite	$\text{FeOH} + \text{H}^+ = \text{FeOH}_2^+$ $\text{FeOH} = \text{FeO}^- + \text{H}^+$ $\text{FeOH} + \text{NpO}_2^+ = \text{FeOH-NpO}_2^+$ $\text{AlOH} + \text{NpO}_2^+ + \text{H}_2\text{O} = \text{AlONpO}_2\text{OH}^- + 2\text{H}^+$	7.35 -9.17 4.25 -12.83	6.0×10^{-6}	$<10^{-3.5}$	0.1	DDL	Wang et al. (2001): Nakayama and Sakamoto (1991)
Magnetite (Fe ₃ O ₄)	$\text{FeOH} + \text{NpO}_2^+ = \text{FeONpO}_2 + \text{H}^+$ $\text{FeOH} + \text{H}^+ + \text{CO}_3^{2-} = \text{FeOH}_2\text{CO}_3^-$ $\text{FeOH} + 2\text{H}^+ + \text{CO}_3^{2-} = \text{FeOH}_2\text{HCO}_3$	1.7 20.3 24.9	4×10^{-7} - 6×10^{-6}	$10^{-3.5}$	0.1	CCM	Fujita et al. (1995): Fujita et al. (1995)
Magnetite	$\text{FeOH} + \text{H}^+ = \text{FeOH}_2^+$ $\text{FeOH} = \text{FeO}^- + \text{H}^+$ $\text{FeOH} + \text{NpO}_2^+ = \text{FeONpO}_2 + \text{H}^+$ $\text{FeOH} + \text{NpO}_2^+ = \text{FeOHNpO}_2^+$ $\text{FeOH} + \text{NpO}_2^+ + \text{H}_2\text{O} = \text{FeONpO}_2\text{OH}^- + 2\text{H}^+$ $\text{FeOH} + \text{NpO}_2^+ + \text{H}_2\text{O} = \text{FeOHNpO}_2\text{OH} + \text{H}^+$ $\text{FeOH}_2^+ + \text{NpO}_2^+ + \text{H}_2\text{O} = \text{FeOH}_2\text{NpO}_2\text{OH}^+ + \text{H}^+$ $2\text{FeOH} + \text{NpO}_2^+ = (\text{FeO})_2\text{NpO}_2^- + 2\text{H}^+$	DDL 6.72 DDL -6.37 DDL -3.42 DDL 3.55 DDL -10.53 DDL -3.42 DDL 3.55 DDL -4.82	1.0×10^{-6}	$<10^{-3.5}$	0.1	CCM, DDL, TLM	Turner (1995): Nakayama and Sakamoto (1991)

Table 2.13 (continued). Surface Complexation Modeling Studies of Np(V) Sorption to Pure Mineral Phases

Reference Mineral Phase	Surface Reaction	Log K	Np(V) (M)	PCO ₂ (Atm)	I (M)	EDL	Source of SCM: Source of Experimental Data
Magnetite	$\text{FeOH} + \text{H}^+ = \text{FeOH}_2^+$ $\text{FeOH} = \text{FeO}^- + \text{H}^+$ $\text{FeOH} + \text{NpO}_2^+ + 2\text{H}_2\text{O} = \text{FeONpO}_2(\text{OH})_2^{2-} + 3\text{H}^+$ $2\text{FeOH} + \text{NpO}_2^+ = (\text{FeO})_2\text{NpO}_2^- + 2\text{H}^+$	6.72 -6.37 -18.57 -5.11	1.0×10^{-6} , 1.0×10^{-12}	0	0.1	DDL	Wang et al. (2001) and Turner and Sassman (1996); Nakayama and Sakamoto (1991)
Montmorillonite	$\text{Na-mont.} + \text{NpO}_2^+ = \text{NpO}_2\text{-mont.} + \text{Na}^+$ $\text{AlOH} + \text{NpO}_2^+ = \text{AlONpO}_2 + \text{H}^+$ $\text{AlOH} + \text{NpO}_2^+ + \text{H}_2\text{O} = \text{AlOHNpO}_2\text{OH}^- + 2\text{H}^+$	1.1 -2.0 -12	$<10^{-13}$	$10^{-3.5}$	0.01 and 0.1	IX and NEM	Bradbury and Baeyens (2006)
Montmorillonite	$\text{AlOH} + \text{H}^+ = \text{AlOH}_2^+$ $\text{AlOH} = \text{AlO}^- + \text{H}^+$ $\text{AlOH} + \text{NpO}_2^+ = \text{AlONpO}_2 + \text{H}^+$ $\text{AlOH} + \text{NpO}_2^+ + \text{H}_2\text{O} = \text{AlOHNpO}_2\text{OH}^- + 2\text{H}^+$	8.33 -9.73 -2.52 to -4.86 -12.44 to -14.29	9×10^{-7}	0, $10^{-3.5}$	0.1	NEM	Zavarin and Bruton (2004a) and Turner (1995); Turner et al. (1998)
Montmorillonite (Si/Al = 1.2)	$\text{AlOH} + \text{H}^+ = \text{AlOH}_2^+$ $\text{AlOH} = \text{AlO}^- + \text{H}^+$ $\text{SiOH} = \text{SiO}^- + \text{H}^+$ $\text{AlOH} + \text{NpO}_2^+ + \text{H}_2\text{O} = \text{AlONpO}_2\text{OH}^- + 2\text{H}^+$ $\text{SiOH} + \text{NpO}_2^+ + \text{H}_2\text{O} = \text{SiOHNpO}_2^+ + \text{H}^+$	8.33 -9.73 -7.20 -13.72 3.04	1×10^{-6}	0	0.1	DDL	Wang et al. (2001) and Turner and Sassman (1996); Bertetti et al. (1996)
Montmorillonite	$\text{AlOH} + \text{H}^+ = \text{AlOH}_2^+$ $\text{AlOH} = \text{AlO}^- + \text{H}^+$ $\text{SiOH} = \text{SiO}^- + \text{H}^+$ $\text{AlOH} + \text{NpO}_2^+ + \text{H}_2\text{O} = \text{AlONpO}_2\text{OH}^- + 2\text{H}^+$ $\text{SiOH} + \text{NpO}_2^+ = \text{SiOHNpO}_2^+$	8.33 -9.73 -7.20 -13.79 4.05	8.79×10^{-7}	0, $10^{-3.5}$	0.1	DDL	Turner et al (1998); Turner et al. (1998) and Turner and Sassman (1996)

Table 2.13 (continued). Surface Complexation Modeling Studies of Np(V) Sorption to Pure Mineral Phases

<p>Quartz (SiO₂)</p>	<p>$\text{SiOH} = \text{SiO}^- + \text{H}^+$ $\text{SiOH} + \text{NpO}_2^+ = \text{SiONpO}_2 + \text{H}^+$ $\text{SiOH} + \text{NpO}_2^+ + \text{H}_2\text{O} = \text{SiOHNpO}_2\text{OH}^- + 2\text{H}^+$</p>	<p>-7.20 -3.56 to -5.31 -11.59 to -12.90</p>	<p>1×10^{-14}, 1×10^{-7}, 1×10^{-6}</p>	<p>0, $10^{-3.5}$</p>	<p>0.1</p>	<p>NEM</p>	<p>Zavarin and Bruton (2004a) and Turner (1995); Bertetti et al. (1998) and Righetto et al. (1991)</p>
<p>Quartz</p>	<p>$\text{SiOH} + \text{H}^+ = \text{SiOH}_2^+$ $\text{SiOH} = \text{SiO}^- + \text{H}^+$ $\text{SiOH} + \text{Na}^+ = \text{SiO}^- \text{--} \text{Na}^+ + \text{H}^+$ $\text{SiOH} + \text{H}^+ + \text{ClO}_4^- = \text{SiOH}_2^+ \text{--} \text{ClO}_4^-$ $\text{SiOH} + \text{NpO}_2^+ = \text{SiONpO}_2^+ + \text{H}^+$</p>	<p>-2.3 -6.8 -7.1 -6.4 -6.93</p>	<p>1.2×10^{-7}</p>	<p>0</p>	<p>0.1</p>	<p>TLM</p>	<p>Kohler et al. (1999) and Dove and Elston (1992); Kohler et al. (1999)</p>

of sorbed neptunyl hydroxo or carbonato complexes could not be ruled out. Recently, Arai et al. (2007) gave evidence for the presence of bidentate mononuclear inner-sphere neptunyl biscarbonato complexation and outer-sphere neptunyl tricarbonato complexation at the hematite surface. Interestingly, the study conducted by the Arai group found that sorption of free neptunyl was not observed under the study conditions, specifically atmospheric PCO_2 , pH 7.0, 8.2 and 8.8, 4 – 5 μM Np(V) , 0.1 M NaClO_4 and 0.3 g L^{-1} hematite. The resulting reactions determined by spectroscopy as well as some chemically feasible reactions are presented in Table 2.14.

The total site concentrations were calculated using an average site density of 2.31 sites nm^{-2} (3.84 $\mu\text{mol m}^{-2}$) recommended by Davis and Kent (1990) and BET surface area measurements determined by Davis et al. (2004) for unmodified NABS (5.15 $\text{m}^2 \text{g}^{-1}$) and by Sanpawanitchakit (2002) for treated NABS (4.47 $\text{m}^2 \text{g}^{-1}$). Site concentrations were only varied as described above and were otherwise considered nonadjustable. Initial model simulations were conducted using a single site type. The use of a two-site type model is consistent with the approach of Dzombak and Morel (1990) for modeling cation binding to

hydrous iron oxides. Slight improvements in the fits were obtained by adding a second site type having a higher sorption affinity. Therefore, a two-site type model using 99% weak affinity sites and 1% strong sites was chosen to model Np(V) sorption. This site type distribution was selected based on best fits to preliminary model simulations using a range of site distributions (0.01-10% strong sites).

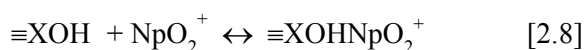
Sanpawanitchakit (2002) obtained excellent model simulations of U(VI) sorption to treated NABS under atmospheric and 2% PCO_2 using a two-site type GC SCM with 0.8% strong sites. In addition, Davis et al. (2004) used a GC SCM with 99.89% weak (YOH), 0.1% strong (SOH) and 0.01% very strong (SSOH) site types to describe U(VI) sorption to unmodified NABS. For this study, a noticeable improvement in model fits was not observed during the initial model simulations and therefore a third site type was excluded from any further model calculations. Finally, a maximum of 3 surface reactions were considered in order to minimize the model fitting parameters.

To begin, model simulations for 5.0×10^{-7} M Np(V) sorption to treated NABS in AGW-A were obtained for individual data sets as a

Table 2.14 Plausible Np(V) Surface Reactions Considered in Models

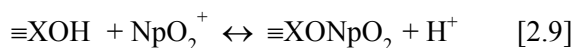
1	$\equiv\text{XOH} + \text{NpO}_2^+$	\rightleftharpoons	$\equiv\text{XOHNpO}_2^+$	
2	$\equiv\text{XOH} + \text{NpO}_2^+$	\rightleftharpoons	$\equiv\text{XONpO}_2$	$+ \text{H}^+$
3	$\equiv\text{XOH} + \text{NpO}_2^+ + \text{H}_2\text{O}$	\rightleftharpoons	$\equiv\text{XONpO}_2\text{OH}^-$	$+ 2\text{H}^+$
4	$\equiv\text{XOH} + \text{NpO}_2^+ + \text{H}_2\text{CO}_3^*$	\rightleftharpoons	$\equiv\text{XONpO}_2\text{CO}_3^{2-}$	$+ 3\text{H}^+$
5	$\equiv\text{XOH} + \text{NpO}_2^+ + \text{H}_2\text{CO}_3^*$	\rightleftharpoons	$\equiv\text{XOHNpO}_2\text{CO}_3^-$	$+ 2\text{H}^+$
6	$\equiv\text{XOH} + \text{NpO}_2^+ + \text{H}_2\text{CO}_3^*$	\rightleftharpoons	$\equiv\text{XONpO}_2\text{HCO}_3^-$	$+ 2\text{H}^+$
7	$\equiv\text{XOH} + \text{NpO}_2^+ + 2\text{H}_2\text{CO}_3^*$	\rightleftharpoons	$\equiv\text{XONpO}_2(\text{HCO}_3)_2^{2-}$	$+ 3\text{H}^+$
8	$\equiv\text{XOH} + \text{NpO}_2^+ + 2\text{H}_2\text{CO}_3^*$	\rightleftharpoons	$\equiv\text{XOHNpO}_2(\text{HCO}_3)_2^-$	$+ 2\text{H}^+$
9	$\equiv\text{XOH} + \text{NpO}_2^+ + 2\text{H}_2\text{CO}_3^*$	\rightleftharpoons	$\equiv\text{XONpO}_2(\text{CO}_3)_2^{4-}$	$+ 5\text{H}^+$
10	$\equiv\text{XOH} + \text{NpO}_2^+ + 2\text{H}_2\text{CO}_3^*$	\rightleftharpoons	$\equiv\text{XOHNpO}_2(\text{CO}_3)_2^{3-}$	$+ 4\text{H}^+$
11	$\equiv\text{XOH} + \text{NpO}_2^+ + \text{H}_2\text{O} + \text{H}_2\text{CO}_3^*$	\rightleftharpoons	$\equiv\text{XONpO}_2\text{OH}(\text{CO}_3)^{3-}$	$+ 4\text{H}^+$

function of pH at fixed solid-solution ratios. These initial model calculations, though part of a range finding exercise, give some valuable insight into the process of obtaining an acceptable GC model fit. In addition, a single site type was used for the initial model fits. A summary of the reactions used, optimized log K values and WSOS/DF values for the initial model simulations are given in Table 2.15. Figures 2.28a and b contain the model simulation using the following surface reaction,



with 50 and 125 g L⁻¹, respectively. In these simulations constant Np(V) sorption is expected below approximately pH 8.0 as a result of the pH independence of reaction 2.8, while a steady decrease in sorption is shown as aqueous neptunyl carbonate complexes begin to dominate. The models are unable to fit the slight pH dependence at low pH and overestimate the reduction in sorption at high pH. In contrast, model simulations using the

following reaction show that proton release results in rapid Np(V) uptake (Figures 2.29a and b).



Similar to reaction 2.8, a rapid decrease in sorption is observed as pH increases past 8.2. Of all the single reaction model simulations, reactions 2.8 and 2.9 give the best fits, although these fits are clearly poor. Reaction 2.9 is one of the most commonly used surface reactions to simulate Np(V) sorption to pure mineral phases (see Table 2.13). This is in part due to the spectroscopic evidence supporting the species (see Combes et al., 1992). However, it is also based on observation, since the strong pH dependence of Np(V) sorption seen in many experimental systems is well fit using a surface reaction that also exhibits strong pH dependence. For example, Wang et al. (2001) successfully simulated the experimental data from the Girvin et al. (1991) study of Np(V) sorption to ferrihydrite at 3 different solid-

Table 2.15 Summary of Adjustable Parameters and Goodness-Of-Fit: One-Site Models (5x10⁻⁷ M Np(V) with 50 or 125 g L⁻¹ in AGW-A at atmospheric PCO₂)

Figure #/solid-solution ratio Np(V) concentration/solution	Surface Complexes	*Log K	WSOS/DF
2.28a/50 g L ⁻¹ 5x10 ⁻⁷ M/ AGW-A	≡XOHNpO ₂ ⁺	2.72	300
2.28b/125 g L ⁻¹ 5x10 ⁻⁷ M/ AGW-A	≡XOHNpO ₂ ⁺	2.66	197
2.29a/50 g L ⁻¹ 5x10 ⁻⁷ M/ AGW-A	≡XONpO ₂	-4.85	500
2.29b/125 g L ⁻¹ 5x10 ⁻⁷ M/ AGW-A	≡XONpO ₂	-5.09	365
2.30a/50 g L ⁻¹ 5x10 ⁻⁷ M/ AGW-A	≡XOHNpO ₂ ⁺ ≡XONpO ₂	2.25 -5.07	68
2.30b/125 g L ⁻¹ 5x10 ⁻⁷ M/ AGW-A	≡XOHNpO ₂ ⁺ ≡XONpO ₂	2.14 -5.31	53
2.31a/50 g L ⁻¹ 5x10 ⁻⁷ M/ AGW-A	≡XOHNpO ₂ ⁺ ≡XONpO ₂ ≡XONpO ₂ (HCO ₃) ₂ ²⁻	2.51 -5.36 -13.4	14
2.31b/125 g L ⁻¹ 5x10 ⁻⁷ M/ AGW-A	≡XOHNpO ₂ ⁺ ≡XONpO ₂ ≡XONpO ₂ (HCO ₃) ₂ ²⁻	2.42 -5.62 -13.7	13

*Binding constants for a single site type model

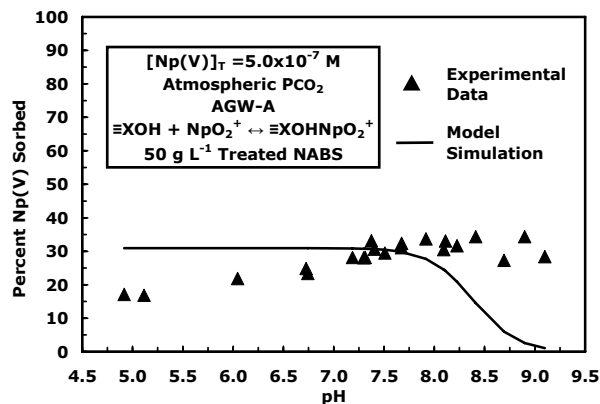


Figure 2.28a. Model calibration with a single surface species ($\equiv\text{XOHNpO}_2^+$) and a single data set; 5×10^{-7} M Np(V), 50 g L^{-1} treated NABS in AGW-A at atmospheric PCO_2 .

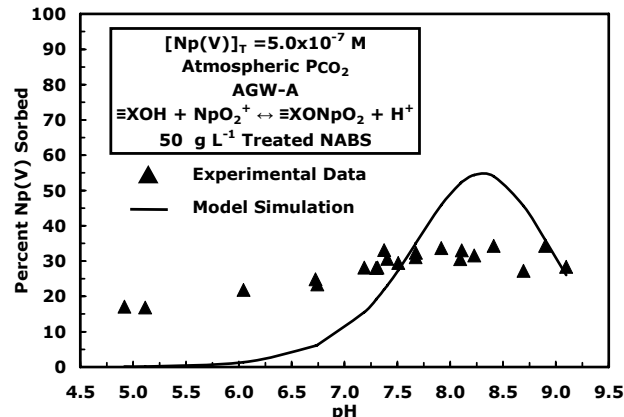


Figure 2.29a Model calibration with a single surface species ($\equiv\text{XONpO}_2$) and a single data set; 5×10^{-7} M Np(V), 50 g L^{-1} treated NABS in AGW-A at atmospheric PCO_2 .

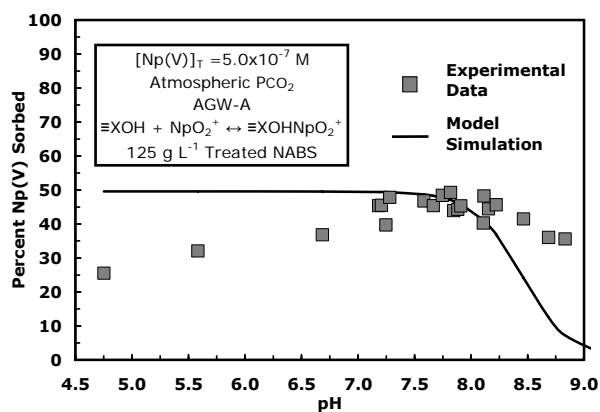


Figure 2.28b. Model calibration with a single surface species ($\equiv\text{XOHNpO}_2^+$) and a single data set; 5×10^{-7} M Np(V), 125 g L^{-1} treated NABS in AGW-A at atmospheric PCO_2 .

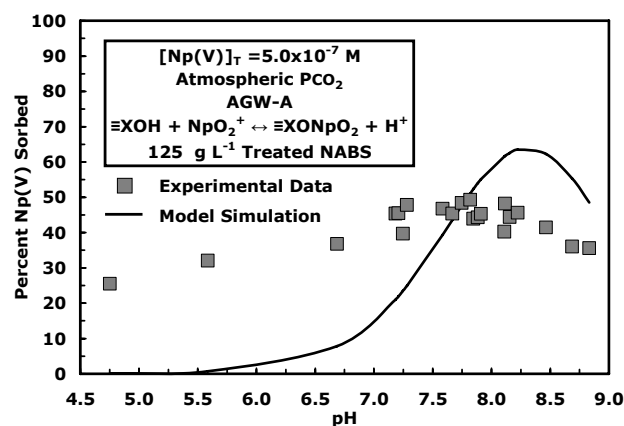
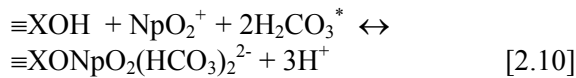


Figure 2.29b. Model calibration with a single surface species ($\equiv\text{XONpO}_2$) and a single data set; 5×10^{-7} M Np(V), 125 g L^{-1} treated NABS in AGW-A at atmospheric PCO_2 .

solution ratios using reaction 2.9 and a DDL SCM. The sorption of Np(V) to ferrihydrite shows an increase in sorption from approximately 0 to 100% between pH 4 and 7 using 4.7×10^{-7} M Np(V), 0.89 g L^{-1} , 0.1 M NaNO_3 and atmospheric PCO_2 . Similarly, Del Nero et al. (1997) used a NEM SCM with surface protolysis reactions and reaction 2.9 to effectively model 10^{-13} M Np(V) sorption to 10 g L^{-1} hydrargilite in 0.01 and 0.1 M NaClO_4 using CO_2 -free conditions. The variation in Np(V) sorption from approximately 10% to 95%

between pH 6 and 9 was well fit using the $\equiv\text{XONpO}_2$ surface complex. The strong pH dependence of the sorption data from Girvin et al. (1991) and Del Nero et al. (1997) is consistent with numerous studies of Np(V) sorption to monomineralic phases (e.g. Nakayama and Sakamoto, 1991; Niitsu et al., 1997; Kohler et al. 1999). In contrast, the sorption data from this study is only minimally pH dependent under the conditions studied. Therefore, reaction 2.9 alone cannot successfully simulate the sorption data.

The model fit is greatly improved by combining reactions 2.8 and 2.9 and re-optimizing the associated log K values (Figures 2.30a and b). Compared to the single reaction models, the minimal pH dependence of the experimental data is better fit by the 2-reaction model below approximately pH 7.5. In addition, the fits improve substantially in the alkaline pH range. However, the 2-reaction model continues to inadequately simulate the experimental data above approximately pH 7.5 by showing decreasing sorption at high pH that is inconsistent with the experimental data. Addition of a third reaction, based on the formation of a ternary neptunyl carbonate surface complex, greatly improves the model fit to both data sets. Figures 2.31a and b show the single data set simulations obtained by adding the following reaction,



Using the above approach to model multiple data sets gives further insight into the models ability to simulate Np(V) sorption to treated NABS. Figure 2.32a shows the model fit when both data sets are modeled simultaneously using a single site type. Although the weak pH dependence for these data sets is well simulated, the model generally overestimates the 125 g L⁻¹ data and slightly underestimates the 50 g L⁻¹ data. In order to obtain a better model fit, a two site type model containing 1% strong sites was used to produce the model fit in Figure 2.32b.

The model simulations presented above do not explicitly incorporate protolysis reactions for surface sites. From the batch salt titration results, an approximate value of pH_{pzc} ≈ 7 was chosen to obtain approximate acidity constants for the surface protolysis reactions, log K₋ and log K₊, using the following equation,

$$\text{pH}_{\text{pzc}} = \frac{1}{2} [\log K_+ - \log K_-] \quad [2.11]$$

The difference between the log K values (Δlog K = 1.4) for the surface protonation and deprotonation reactions was chosen based on the

Turner and Sassmann (1996) acidity constants for clay and aluminum oxide surfaces, log K₋ = -9.73 and log K₊ = 8.33, determined using a DDL SCM. Using equation 2.11, the estimated acidity constants for protolysis of NABS surface sites are as follows:

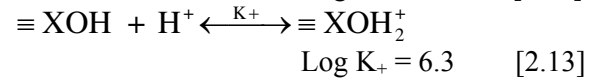
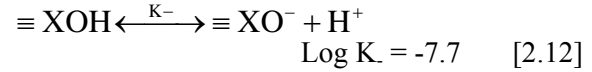


Figure 2.32c shows the result of incorporating the surface protolysis reactions (reactions 2.12 and 2.13) into the best fit model (Figure 2.32b) for the AGW-A data sets using 5.0x10⁻⁷ M Np(V) with 50 and 125 g L⁻¹ treated NABS at atmospheric PCO₂ (WSOS/DF = 126). At low pH, the model is unable to simulate the weak pH dependence. The sorption data is better fit as the pH increases, but the sorption is overestimated for the 125 g L⁻¹ data set and underestimated for the 50 g L⁻¹ data set at pH greater than approximately 6.5. The initial model simulation in Figure 2.32b follows a similar trend but fits the experimental data better (WSOS/DF = 31). Incorporation of the surface protolysis reactions decreases the pH at which the maximum sorption is simulated. For example, in Figure 2.32b maximum sorption is calculated to occur at approximately pH 8.2 while the maximum Np(V) uptake occurs at approximately pH 7.2 when the surface protolysis reactions are included.

Ultimately the true test of the usefulness of the model may be its transferability to experimental data at other experimental conditions. Ideally, the model parameters are transferable to conditions and substrates other than those used to develop the initial model. In general, the transferability of GC models is expected to be limited to conditions within the model calibration range (Payne et al., 2004). The model simulations presented in Figure 2.33a are based on the best fit model without further optimization, but applied to the data sets with 5.0x10⁻⁶ M Np(V) under otherwise similar conditions. The model appropriately captures the increase in Np(V) sorption for both solid-

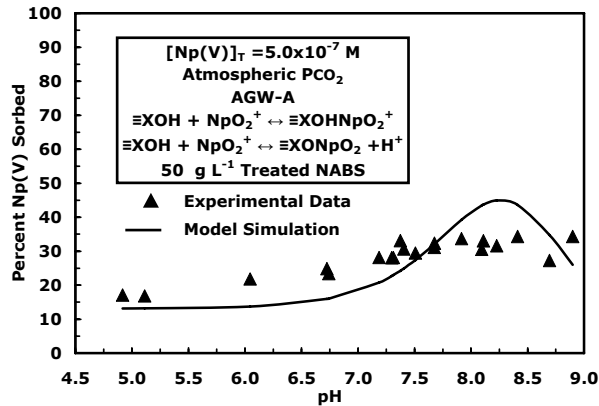


Figure 2.30a. Model calibration with two surface species ($\equiv\text{XOHNpO}_2^+$ and $\equiv\text{XONpO}_2$) and a single data set; 5×10^{-7} M Np(V), 50 g L^{-1} treated NABS in AGW-A at atmospheric PCO_2 .

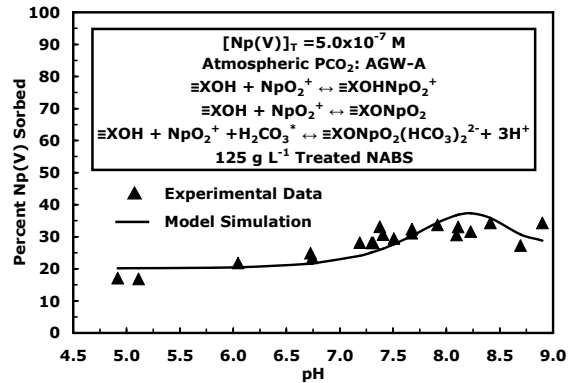


Figure 2.31a. Model calibration including a neptunyl carbonato ternary surface complex ($\equiv\text{XONpO}_2(\text{HCO}_3)_2^{2-}$) and a single data set; 5×10^{-7} M Np(V), 50 g L^{-1} treated NABS in AGW-A at atmospheric PCO_2 .

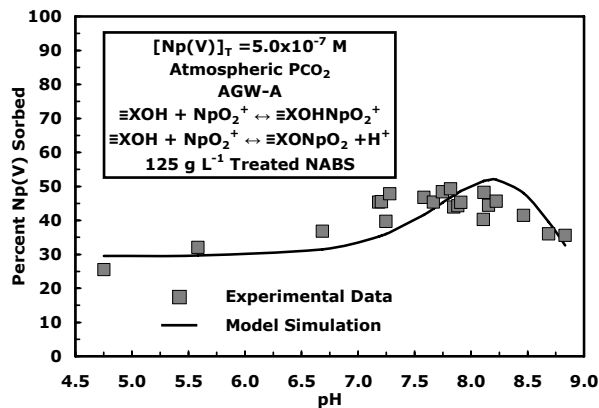


Figure 2.30b. Model calibration with two surface species ($\equiv\text{XOHNpO}_2^+$ and $\equiv\text{XONpO}_2$) and a single data set; 5×10^{-7} M Np(V), 125 g L^{-1} treated NABS in AGW-A at atmospheric PCO_2 .

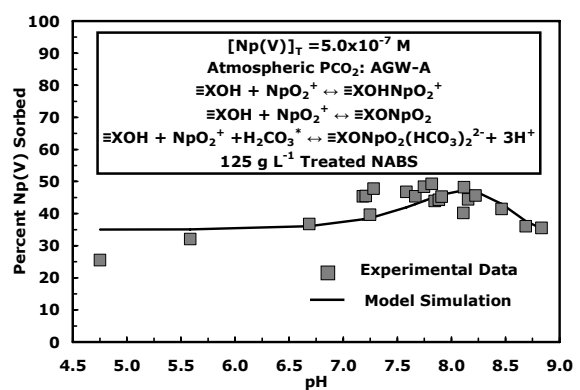


Figure 2.31b. Model calibration including a neptunyl carbonato ternary surface complex ($\equiv\text{XONpO}_2(\text{HCO}_3)_2^{2-}$) and a single data set; 5×10^{-7} M Np(V), 125 g L^{-1} treated NABS in AGW-A at atmospheric PCO_2 .

solution ratios but the $\text{WSOS/DF} = 76$ indicates a less than adequate fit. Optimizing the log K values results in a slightly more acceptable fit considering the relatively limited amount of experimental data collected at 5.0×10^{-6} M (Figure 2.33b). However, the slight reduction in sorption at higher Np(V) concentrations observed for sorption when pH is varied is not well captured by the calibration model. A summary of the surface species employed, log K values and WSOS/DF values for the model

simulations in Figures 2.32 and 2.33 are given in Table 2.16.

The next step to examining model transferability is to apply the best fit model (Figure 2.32b) to the isotherm experimental data sets using treated NABS. This is tested using the model to simulate Np(V) sorption to 125 g L^{-1} treated NABS using a maximum range of Np(V) from 2.0×10^{-7} M to 3.0×10^{-6} M, in AGW-3 (pH 8.0 ± 0.1) at atmospheric PCO_2 and in AGW-6 (pH 6.8 ± 0.1) at 8% PCO_2 . Figure 2.34a shows the

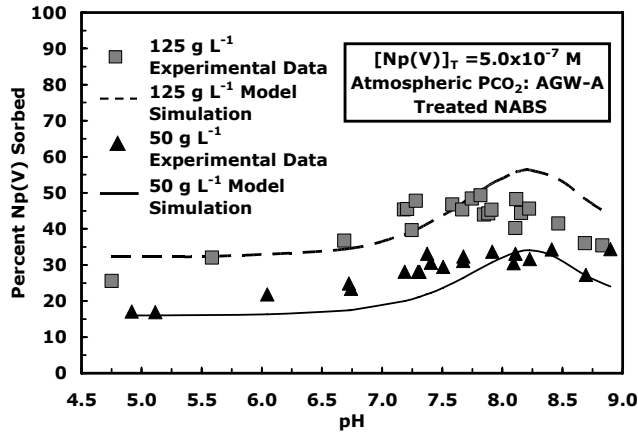


Figure 2.32a. Model calibration with both AGW-A data sets, 5×10^{-7} M Np(V), 50 and 125 g L^{-1} treated NABS at atmospheric PCO_2 , using a 1-site type model.

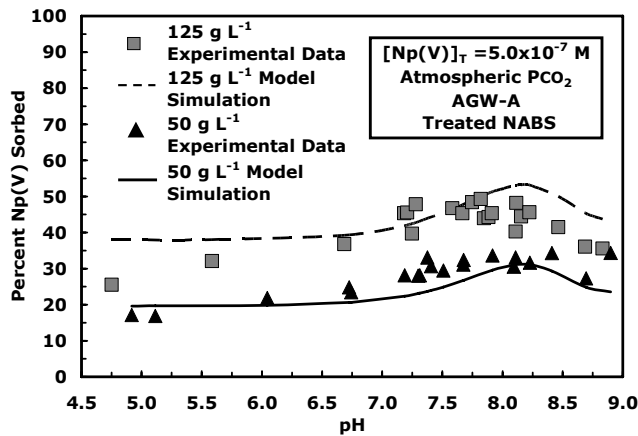


Figure 2.32b. Model calibration with both AGW-A data sets, 5×10^{-7} M Np(V), 50 and 125 g L^{-1} treated NABS at atmospheric PCO_2 , 2-site type model with 99% weak sites and 1% strong sites.

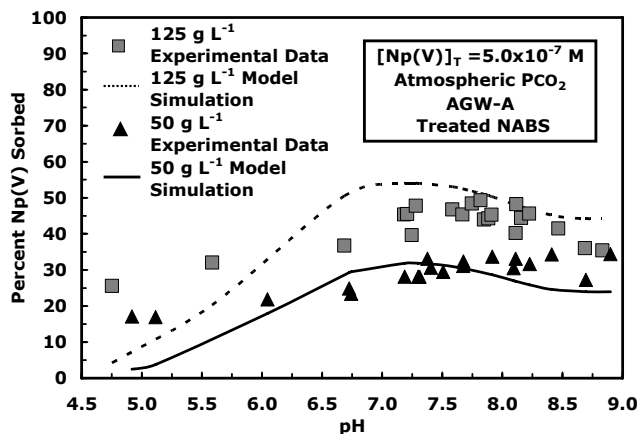


Figure 2.32c. Model calibration with both AGW-A data sets; specifically 5×10^{-7} M Np(V), 50 and 125 g L^{-1} treated NABS at atmospheric PCO_2 with incorporation of surface protolysis reactions. Surface species include $\equiv XOHNPo_2^+$, $\equiv XONPo_2$ and $\equiv XONPo_2(HCO_3)_2^{2-}$.

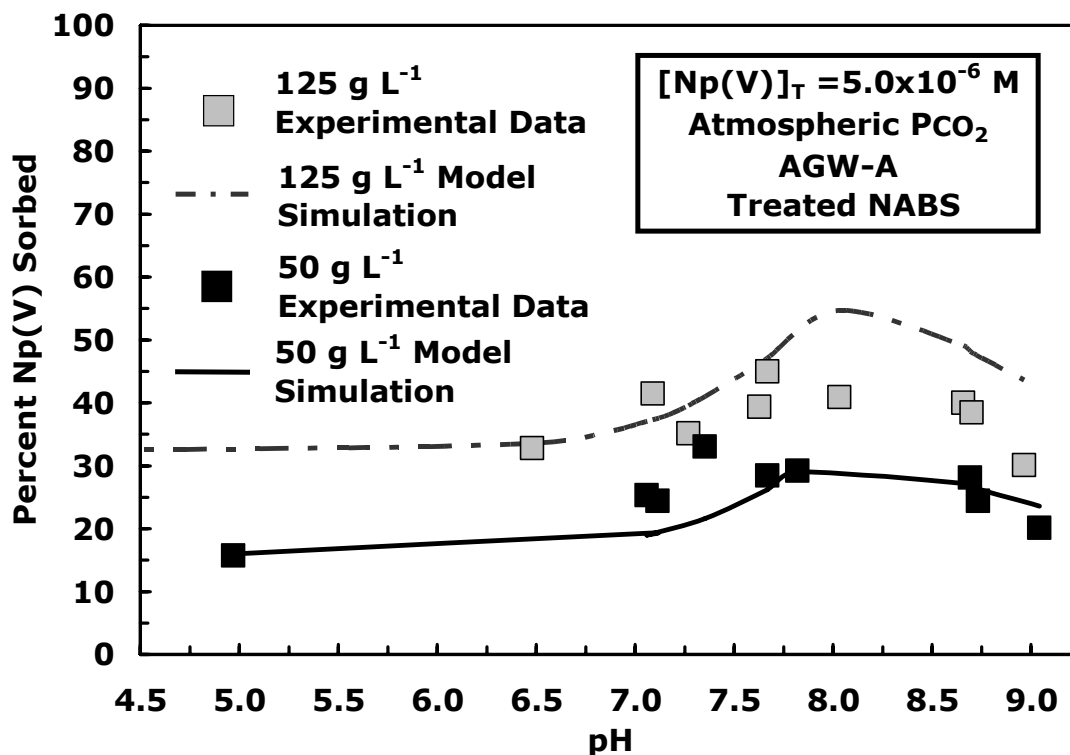


Figure 2.33a. Test of model performance for the higher Np(V) concentration AGW-A data sets without additional parameter optimization.

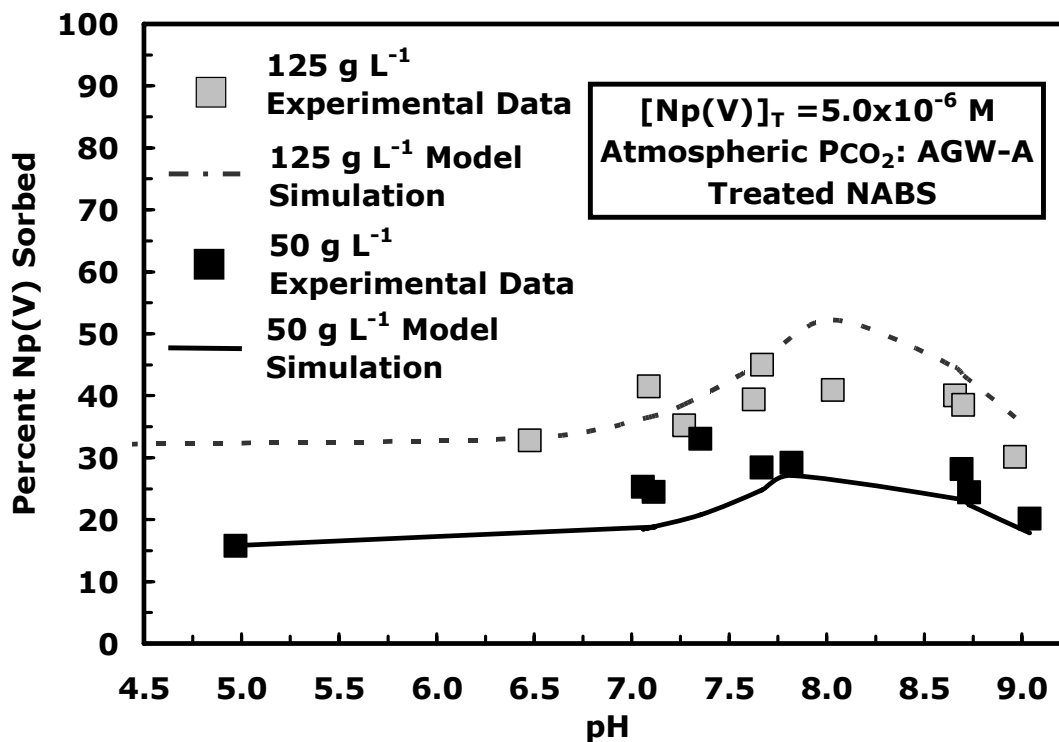


Figure 2.33b. Test of model performance for the higher Np(V) concentration AGW-A data sets with additional log K optimization.

Table 2.16 Summary of Adjustable Parameters and Goodness-Of-Fit: Two-Site Models (5×10^{-7} M Np(V) with 50 or 125 g L⁻¹ in AGW-A at atmospheric PCO₂)

Figure #/solid-solution ratio Np(V) concentration /solution	Surface Complexes	Log K _s	Log K _w	WSOS/DF
2.32a/50 and 125 g L ⁻¹ 5.0x10 ⁻⁷ M / AGW-A	≡XOHNpO ₂ ⁺ ≡XONpO ₂ ≡XONpO ₂ (HCO ₃) ₂ ²⁻	Log K		28
		2.47	-5.45 -13.6	
2.32b/50 and 125 g L ⁻¹ 5.0x10 ⁻⁷ M / AGW-A	≡XOHNpO ₂ ⁺ ≡XONpO ₂ ≡XONpO ₂ (HCO ₃) ₂ ²⁻	4.18	2.17	31
		-3.64	-5.92	
		-11.5	-14.4	
2.32c/50 and 125 g L ⁻¹ 5.0x10 ⁻⁷ M / AGW-A	≡XOHNpO ₂ ⁺ ≡XONpO ₂ ≡XONpO ₂ (HCO ₃) ₂ ²⁻	4.76	1.90	126
		-3.06	-5.92	
		-9.88	-14.2	
2.33a/50 and 125 g L ⁻¹ 5.0x10 ⁻⁶ M / AGW-A	≡XOHNpO ₂ ⁺ ≡XONpO ₂ ≡XONpO ₂ (HCO ₃) ₂ ²⁻	4.18	2.17	76
		-3.64	-5.92	
		-11.5	-14.4	
2.33b/50 and 125 g L ⁻¹ 5.0x10 ⁻⁶ M / AGW-A	≡XOHNpO ₂ ⁺ ≡XONpO ₂ ≡XONpO ₂ (HCO ₃) ₂ ²⁻	3.85	2.18	66
		-3.51	-5.92	
		-11.9	-14.4	

initial model simulations without parameter optimization from the best fit model. In Figure 2.34a the sorption is overestimated for both isotherms and the goodness-of-fit is poor (WSOS/DF = 88). Optimization of the log K values for each surface reaction results in a very good fit to both the atmospheric and 8% PCO₂ data (Figure 2.34b). Sorption pH edge data required the formation of 3 surface species, specifically ≡XONpO₂, ≡XOHNpO₂⁺ and ≡XONpO₂(HCO₃)₂²⁻, in order to obtain reasonable model fits over the entire pH range. To illustrate this point, Figure 2.34c shows the calculated sum of the surface speciation and the surface species distribution of 5.0x10⁻⁷ M Np(V) sorption to 125 g L⁻¹ treated NABS at atmospheric PCO₂ given in Figure 2.31b. This surface species distribution shows that at pH 8.0 and atmospheric PCO₂, the contribution of the ≡XOHNpO₂⁺ species (≡SOHNpO₂⁺ and ≡YOHNpO₂⁺) are becoming less important compared to the neutral species, ≡XONpO₂. Figure 2.34d shows the re-calibrated experimental data with additional log K optimization following removal of the

≡XOHNpO₂⁺ species. Removal of ≡XOHNpO₂⁺ species results in a similar fit to the experimental data as the 3 surface reaction fit shown in Figure 2.34b. Therefore, the number of fitting parameters can be reduced when modeling Np(V) sorption at fixed pH while varying other conditions such as Np(V) concentration, solid-solution ratio and PCO₂. The resulting model simulation fits the experimental data at both atmospheric and 8% PCO₂ very well (WSOS/DF = 8). Table 2.17 summarizes the log K values, surface species and goodness-of-fit values for simulations of all isotherm data.

The same steps used to test the transferability of the model to Np(V) sorption isotherms using treated NABS were followed to explore model performance in describing Np(V) sorption to the unmodified sediment at atmospheric and 8% PCO₂ (WSOS/DF = 54). The primary change to the initial model was an increase in surface site concentration due to the higher BET surface area of unmodified NABS. Figure 2.35a shows the model fit without additional parameter optimization beyond the increase in site concentration. The model overestimates the

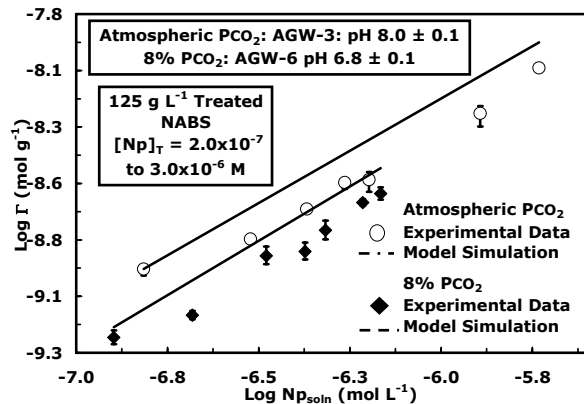


Figure 2.34a. Test of model performance to Np(V) sorption isotherm data sets without additional parameter optimization using the best fit model (Figure 2.32b). Experimental data includes Np(V) sorption isotherms with a range of total Np(V) concentration from 2×10^{-7} M to 3×10^{-6} M, 125 g L^{-1} treated NABS, in AGW-3 (pH 8) at atmospheric PCO_2 or in AGW-6 (pH 6.8) at 8% PCO_2 .

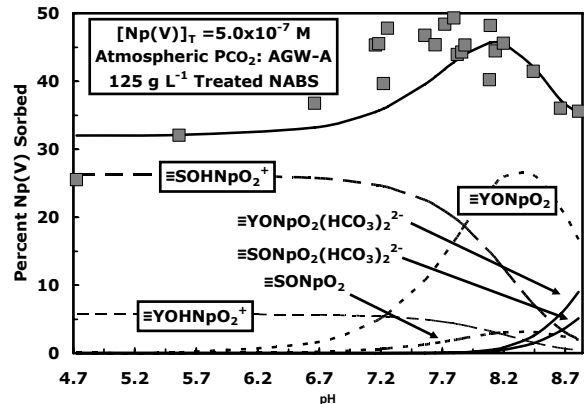


Figure 2.34c. Np(V) surface species distribution for the model simulation presented in Figure 2.31b with the 5×10^{-7} M Np(V), 125 g L^{-1} treated NABS in AGW-A at atmospheric PCO_2 data set.

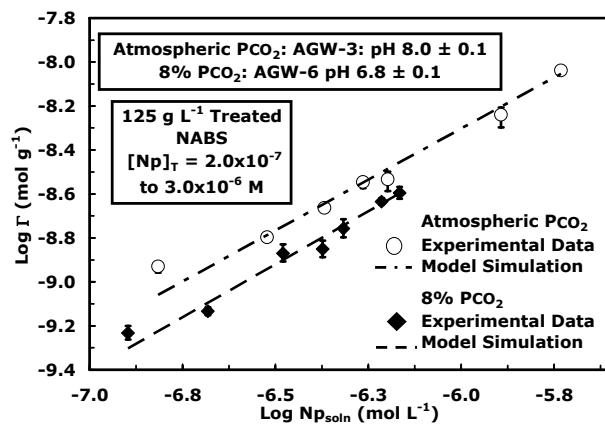


Figure 2.34b. Test of model performance to Np(V) sorption isotherm data sets with additional log K optimization. Experimental data includes Np(V) sorption isotherms with a range of total Np(V) concentration from 2×10^{-7} M to 3×10^{-6} M, 125 g L^{-1} treated NABS, in AGW-3 (pH 8) at atmospheric PCO_2 or in AGW-6 (pH 6.8) at 8% PCO_2 .

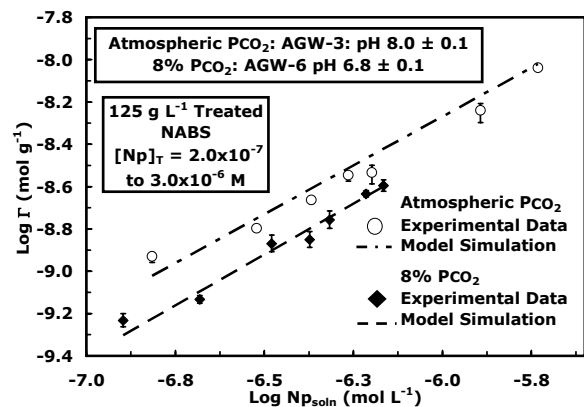


Figure 2.34d. Model calibration for the Np(V) sorption isotherms using $\equiv\text{XONpO}_2$ and $\equiv\text{XONpO}_2(\text{HCO}_3)_2^{2-}$ with a range of total Np(V) concentrations from 2×10^{-7} M to 3×10^{-6} M, 125 g L^{-1} treated NABS, in AGW-3 (pH 8) at atmospheric PCO_2 or in AGW-6 (pH 6.8) at 8% PCO_2 .

Table 2.17 Summary of Adjustable Parameters and Goodness-Of-Fit: Isotherm Data (50 or 125 g L⁻¹ in AGW-3 at atmospheric PCO₂ and AGW-6 at 8% PCO₂)

Figure #/solid-solution ratio solution	Surface Complexes	Log K _s	Log K _w	WSOS/DF
2.34a/125 g L ⁻¹ treated/ AGW-3 (atm PCO ₂) and AGW-6 (8% PCO ₂)	≡XOHNPo ₂ ⁺	4.18	2.17	88
	≡XONPo ₂	-3.64	-5.92	
	≡XONPo ₂ (HCO ₃) ₂ ²⁻	-11.5	-14.4	
2.34b/125 g L ⁻¹ treated/ AGW-3 (atm PCO ₂) and AGW-6 (8% PCO ₂)	≡XOHNPo ₂ ⁺	3.90	2.17	8.1
	≡XONPo ₂	-4.88	-5.98	
	≡XONPo ₂ (HCO ₃) ₂ ²⁻	-12.0	-14.4	
2.34d/125 g L ⁻¹ treated/ AGW-3 (atm PCO ₂) and AGW-6 (8% PCO ₂)	≡XONPo ₂	-3.53	-5.92	7.6
	≡XONPo ₂ (HCO ₃) ₂ ²⁻	-11.1	-14.4	
2.35a/125 and 500 g L ⁻¹ unmodified /AGW-3 (atm PCO ₂), AGW-6 (8% PCO ₂)	≡XOHNPo ₂ ⁺	4.18	2.17	54
	≡XONPo ₂	-3.64	-5.92	
	≡XONPo ₂ (HCO ₃) ₂ ²⁻	-11.5	-14.4	
2.35b/125 and 500 g L ⁻¹ / unmodified /AGW-3 (atm PCO ₂), AGW-6 (8% PCO ₂)	≡XOHNPo ₂ ⁺	4.03	2.17	9.2
	≡XONPo ₂	-5.59	-5.98	
	≡XONPo ₂ (HCO ₃) ₂ ²⁻	-11.7	-14.4	
2.35c/125 and 500 g L ⁻¹ / unmodified /AGW-3 (atm PCO ₂), AGW-6 (8% PCO ₂)	≡XONPo ₂	-3.48	-5.98	13
	≡XONPo ₂ (HCO ₃) ₂ ²⁻	-11.0	-14.2	

sorption at atmospheric PCO₂ using both 125 and 500 g L⁻¹ but gives a good fit to the 8% PCO₂ data. The un-optimized model simulations more closely represent untreated NABS experimental data at fixed pH and variable Np(V) concentration than the model fits to treated NABS data (see Figure 2.34a). Re-optimization of log K values gives a very good model fit to the data (WSOS/DF = 9) (Figure 2.35b). Figure 2.35c shows that an acceptable fit to the experiment data (WSOS/DF = 13) is also obtained by removing the ≡XOHNPo₂⁺ followed by log K re-optimization. These results confirm that the initial model developed for pH sorption edges needs to be adjusted by either log K value optimization and/or modification of the surface speciation to successfully fit experimental isotherm data for Np(V) sorption to unmodified NABS.

Figure 2.36a shows that the original best-fit model (Figure 2.32b) inadequately models pH sorption edge data sets at higher ionic strength (0.1 M) using 50, 125 and 500 g L⁻¹ treated NABS even *after* log K re-optimization

(WSOS/DF = 95). FITEQL did not converge on a solution when data above approximately pH 10 were included, likely due to the increase in sorption at high pH that the original 3-reaction model, calibrated between pH 4.5 and 9.0, is unable to capture. The ternary NpO₂⁺-carbonate surface complex initially postulated is relatively weak, and therefore as pH increases the model simulation deviates significantly from the experimental data. The original 3-reaction model simulates very weak pH dependence over the entire pH range studied. Therefore, the slightly stronger pH dependence of Np(V) sorption to treated NABS in 0.1 M NaClO₄ is inadequately described by the original model developed using AGW-A. It is desirable to obtain an acceptable model fit to the 500 g L⁻¹ treated NABS data in 0.1 M NaClO₄ at atmospheric PCO₂, since similar conditions are employed for the Np(V)-HA sorption experiments discussed below. For simplicity as well as consistency with the HA sorption models (Moran, 2007), a single site type model was employed to describe Np(V) sorption in Figure 2.36b. Substantial improvements in the model

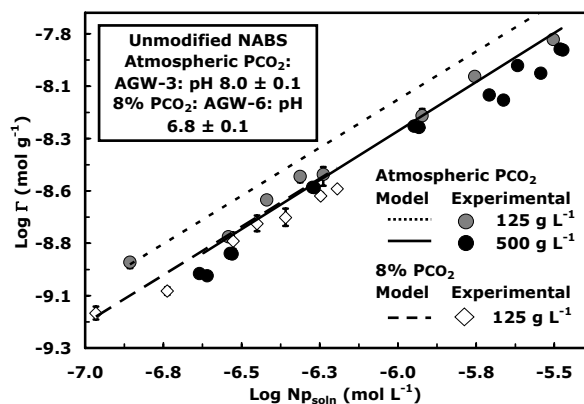


Figure 2.35a. Test of model performance to Np(V) sorption isotherm data sets without additional parameter optimization. Experimental data includes Np(V) sorption isotherms with a range of total Np(V) concentration from 3×10^{-7} M to 5×10^{-6} M, 125 and 500 g L^{-1} unmodified NABS, in AGW-3 (pH 8) at atmospheric PCO_2 and 125 g L^{-1} unmodified NABS in AGW-6 (pH 6.8) at 8% PCO_2 .

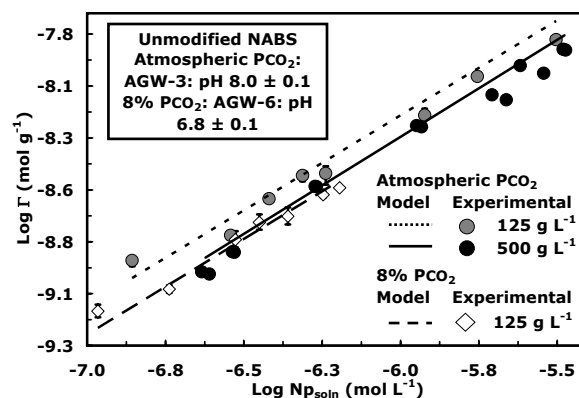


Figure 2.35c. Test of model performance to Np(V) sorption isotherm data sets with additional parameter optimization and exclusion of a $\equiv\text{XOHNpO}_2^+$ surface species. Experimental data includes the Np(V) sorption isotherms with a range of total Np(V) concentration from 3×10^{-7} M to 5×10^{-6} M, 125 g L^{-1} unmodified NABS, in AGW-3 (pH 8) at atmospheric PCO_2 or in AGW-6 (pH 6.8) at 8% PCO_2 .

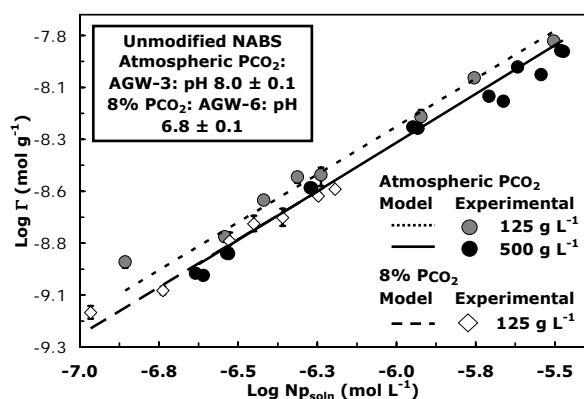


Figure 2.35b. Test of model performance to Np(V) sorption isotherm data sets with additional log K optimization. Experimental data includes Np(V) sorption isotherms with a range of total Np(V) concentration from 3×10^{-7} M to 5×10^{-6} M, 125 and 500 g L^{-1} unmodified NABS, in AGW-3 (pH 8) at atmospheric PCO_2 and 125 g L^{-1} unmodified NABS in AGW-6 (pH 6.8) at 8% PCO_2 .

fit are not achieved using the 2-site type model. The simulation of the 500 g L^{-1} data set alone produces a better goodness-of-fit than seen for the multiple data set simulations as expected, but the model highly overestimates Np(V) uptake between pH 7.0 and 9.5. Figure 2.36b also shows that the model can more closely match the shape of the sorption envelope by increasing the strength of the ternary neptunyl carbonate surface complex. A summary of the surface species employed, log K values and WSOS/DF values for the model simulations in Figures 2.36a and b are given in Table 2.18.

2.3.3 Effect of Humic Acid Presence

It is clear from the experimental data presented in Figures 2.24-2.25 that Np(V) sorption to treated NABS in the presence of HA is impacted to varying degrees depending on the concentration of HA. For example, sorption of both 5.0×10^{-6} M and 5.0×10^{-7} M Np(V) to 500 g L^{-1} treated NABS is substantially decreased in the presence of 100 mg L^{-1} Suwannee River HA whereas addition of 10 mg L^{-1} HA had an insignificant impact on sorption of Np(V) at

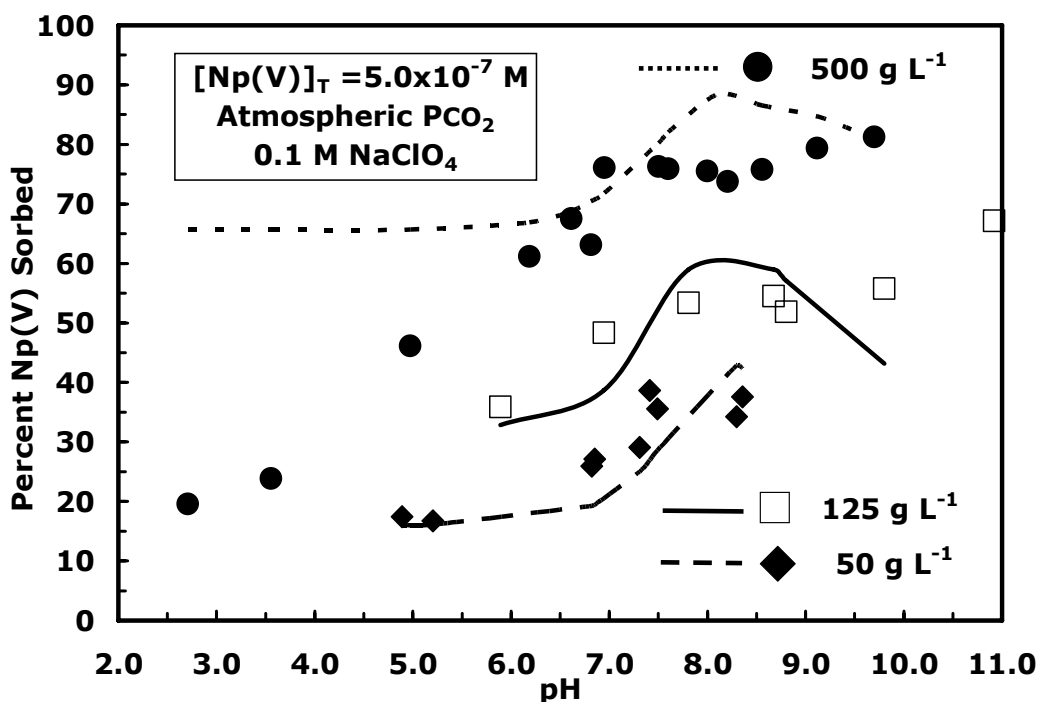


Figure 2.36a. Test of model performance for the 5×10^{-7} M Np(V) data sets using 50, 125 and 500 g L^{-1} treated NABS in 0.1 M NaClO_4 with additional log K optimization.

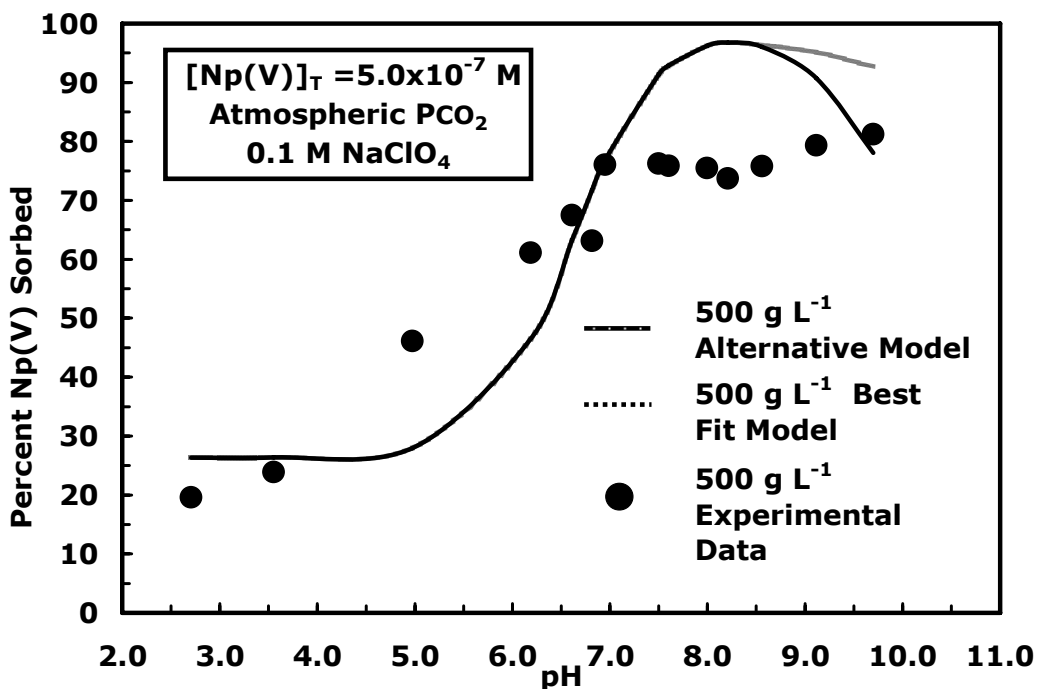


Figure 2.36b. Test of model performance for the 5×10^{-7} M Np(V) data set using 500 g L^{-1} treated NABS in 0.1 M NaClO_4 with additional log K optimization and an additional fit showing the effect of increasing the importance of the ternary neptunyl carbonate surface species.

Table 2.18 Summary of Adjustable Parameters and Goodness-Of-Fit: NaClO₄ Solution (5x10⁻⁷ M Np(V) with 125 or 500 g L⁻¹ in 0.1M NaClO₄ at atmospheric PCO₂)

Figure #/solid-solution ratio Np(V) concentration/solution	Surface Complexes	Log K _s	Log K _w	WSOS/DF
2.36a/50, 125 and 500 g L ⁻¹ 5.0x10 ⁻⁷ M / 0.1 M NaClO ₄	≡XOHNpO ₂ ⁺	4.18	2.17	95.3
	≡XONpO ₂	-3.64	-5.92	
	≡XONpO ₂ (HCO ₃) ₂ ²⁻	-11.5	-14.4	
2.36b/ 500 g L ⁻¹ 5.0x10 ⁻⁷ M / 0.1 M NaClO ₄	≡XOHNpO ₂ ⁺ ≡XONpO ₂ ≡XONpO ₂ (HCO ₃) ₂ ²⁻	Log K		55
		1.62		
		-4.4	-13.6	

both Np(V) concentrations studied. The likely processes that decrease Np(V) sorption in the presence of 100 mg L⁻¹ HA include complexation of Np(V) with HA and sorption of HA to the NABS surface. In all likelihood these processes are acting in tandem and therefore any SCM must take into account both aqueous complexation with HA and surface complexation in order to successfully simulate the data.

To begin, model simulations of Np(V) sorption to treated NABS in the presence of HA are obtained by combining the GC SCM discussed above with the discrete ligand modeling approach for Np(V)-HA complexation (Moran, 2007). The polyfunctionality and heterogeneous nature of HA is captured using a suite of 5 hypothetical ligands with monoprotic acidic functional groups having pK_a values of 2, 4, 6, 8 and 10. Table 2.19 shows the concentration of each ligand determined by fitting the discrete ligand model to potentiometric titration data of Suwannee River HA at 0.004 and 0.04 M NaClO₄ (Moran, 2007). The discrete ligand approach is expanded upon in order to describe both HA complexation with NpO₂⁺ as well as surface complexation of HA with treated NABS. The hypothetical ligands (L₁-L₅) are assumed to sorb to NABS surface sites independently.

The relevant binding constants for the sorption of 100 mg L⁻¹ HA to treated NABS at atmospheric PCO₂ without Np(V) present (binary system) are obtained using ligand

exchange reactions between the NABS surface sites and the discrete ligands L₁-L₄ and the “electrostatic-type” reaction for L₅ with NABS (Figure 2.37a). Although the goodness-of-fit value is low (WSOS/DF = 88), likely due to scatter in the data, the model captures the trend in HA sorption behavior relatively well. The sorption of HA to treated NABS in the presence of Np(V) (ternary system) is well simulated (WSOS/DF = 14) using only the ligand exchange reactions between NABS surface sites and ligands L₁-L₄ (Figure 2.37b). This is consistent with the obvious trend towards minimal HA sorption in the ternary system at high pH, which is less apparent in the binary HA system (Moran, 2007). The high goodness-of-fit was obtained by removing any dependence of the HA sorption on the sorption of 5x10⁻⁷ M Np(V). Much less acceptable model fits are obtained from simulations using 10 mg L⁻¹ HA, due to higher variability in the sorption data resulting from variability in the concentration of desorbed organic carbon (TOC) (Moran, 2007). Therefore, the systems containing 10 mg L⁻¹ HA were not explored in depth. The log K values for the HA surface reactions are given in Table 2.20.

Combining the models discussed above in an additive manner in an attempt to simulate Np(V) sorption in the presence of HA results in limited success. This ternary system model only allows for a small concentration of Np(V) to sorb to treated NABS in the presence of 100 mg L⁻¹ HA. Rather, in order to produce a somewhat adequate

Table 2.19 Humic Acid Solution Reactions*

Reactions	HL _i concentration (mmol g ⁻¹)	Log K (I = 0)
HL ₁ = L ₁ ⁻ + H ⁺	0.608	-2
HL ₂ = L ₂ ⁻ + H ⁺	1.65	-4
HL ₃ = L ₃ ⁻ + H ⁺	1.46	-6
HL ₄ = L ₄ ⁻ + H ⁺	0.578	-8
HL ₅ = L ₅ ⁻ + H ⁺	0.678	-10
Na ⁺ + L _i ⁻ = NaL _i		-2.34
NpO ₂ ⁺ + L _i ⁻ = NpO ₂ L _i ⁰		4.4

*Total HA = 4.97 mmol g⁻¹ as determined by model fit to potentiometric titration data

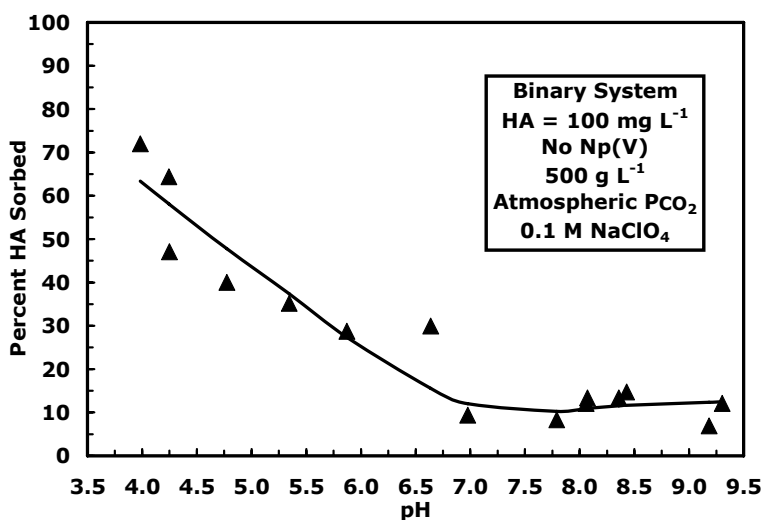


Figure 2.37a. Model simulation of 100 mg L⁻¹ HA sorption to 500 g L⁻¹ treated NABS at atmospheric PCO₂ in 0.1 M NaClO₄ without Np(V) present.

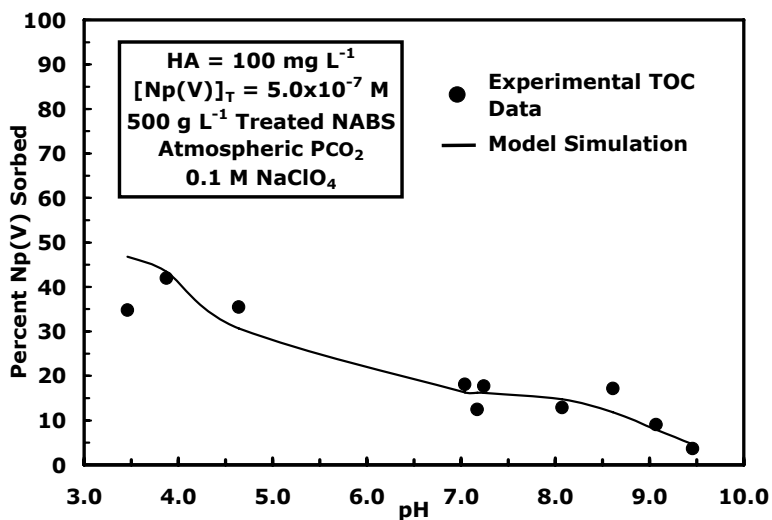


Figure 2.37b. Model simulation of 100 mg L⁻¹ HA sorption to 500 g L⁻¹ treated NABS at atmospheric PCO₂ in 0.1 M NaClO₄ with 5x10⁻⁷ M Np(V) present.

Table 2.20 Humic Acid Surface Reactions

Reactions	Binary System Log K (I = 0)	Ternary System Log K (I = 0)
$\equiv\text{XOH} + \text{HL}_1 \leftrightarrow \equiv\text{XL}_1 + \text{H}_2\text{O}$	20.2	21.5
$\equiv\text{XOH} + \text{HL}_2 \leftrightarrow \equiv\text{XL}_2 + \text{H}_2\text{O}$	15.6	13.9
$\equiv\text{XOH} + \text{HL}_3 \leftrightarrow \equiv\text{XL}_3 + \text{H}_2\text{O}$	15.0	14.1
$\equiv\text{XOH} + \text{HL}_4 \leftrightarrow \equiv\text{XL}_4 + \text{H}_2\text{O}$	14.2	13.7
$\equiv\text{XOH} + \text{HL}_5 \leftrightarrow \equiv\text{XOHL}_5^- + \text{H}^+$	6.29	–

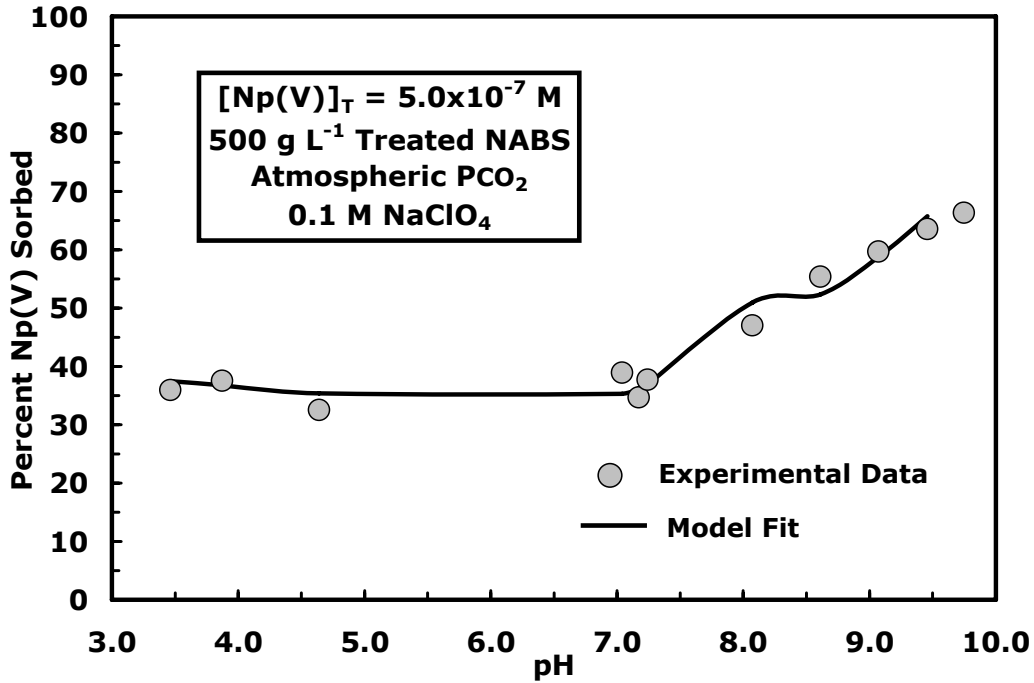


Figure 2.38. Model simulation of 5×10^{-7} M Np(V) to 500 g L^{-1} treated NABS in the presence of 100 mg L^{-1} HA sorption at atmospheric PCO_2 in 0.1 M NaClO_4 .

fit to the data (WSOS/DF= 58), the strength of all the Np(V) surface complexes must be increased substantially in order to compete with HA sorption (Figure 2.38). A good model fit is limited to below pH 9.5, the highest pH for which the ternary system samples were analyzed for TOC (Moran, 2007).

2.3.4 Summary of Np(V) Surface Complexation Modeling

Np(V) sorption to 50 and 125 g L^{-1} treated NABS in AGW at atmospheric PCO_2 was well simulated using a 3-reaction, 2 site-type GC SCM. Transferability of this model to other system conditions met with limited success. In

most cases, good model transferability is possible when surface reaction log K values are re-optimized. For example, the model transfers exceptionally well to isotherm experimental data at atmospheric and 8% PCO_2 once the strengths of the surface complexes are adjusted. Incorporation of surface protolysis reactions results in shifts in the maximum simulated sorption to lower pH and additional pH dependence, both results being inconsistent with the experimental data.

3 DEVELOPMENT OF A SURFACE COMPLEXATION MODEL FOR URANIUM(VI) SORPTION ONTO FORTY MILE WASH (NEVADA) AQUIFER SEDIMENTS

3.1 Materials and Methods

3.1.1 Sediments

Sediments from the saturated zone of the Forty Mile Wash aquifer, Nye County, Nevada, were collected for this study. Dry and moist sediment samples were obtained from Borehole NC-EWDP 19PB, ranging in depth from 350 to 587 feet. Sediments were air dried in the laboratory and sieved through a 3 mm mesh. The Forty Mile Wash composite sample (FMW-COMP) is a mixture of the <3 mm individual depth fractions, weighted according to their mass per depth ratio. FMW-COMP was well mixed and N₂-BET specific surface area measurements were made on a Tristar Micromeritics analyzer. X-ray diffraction results for samples from this site indicate that quartz, cristobalite, alkali feldspars, plagioclase, zeolites and clays are present in the sediments (P. Bertetti, personal communication). The total uranium content of FMW-COMP, assessed by γ -spectrometry, is 3.6 ppm.

3.1.2 Artificial Groundwater Solutions

An artificial groundwater was developed with a composition that reflected an average groundwater composition of 37 quarternary alluvium aquifer water samples from the area near where the aquifer sediment sample was collected. The composition of the Forty Mile Wash artificial groundwater (referred to as FMW-2) was as follows: $[Ca^{2+}] = 5.50 \cdot 10^{-4} M$, $[Mg^{2+}] = 1.00 \cdot 10^{-4} M$, $[K^+] = 1.70 \cdot 10^{-4} M$, $[Na^+] = 2.50 \cdot 10^{-3} M$, $[HCO_3^-] = 2.50 \cdot 10^{-3} M$, $[SO_4^{2-}] = 5.50 \cdot 10^{-4} M$ and $[ClO_4^-] = 3.70 \cdot 10^{-4} M$. Its calcite saturation index is 0.24 at atmospheric levels of CO₂ (=373ppm). Modifications to the groundwater composition were made in order to increase alkalinity (by adding NaHCO₃), to increase the level of pCO₂ (by adding NaHCO₃ and H₂SO₄), or to increase the ionic strength to approximately 0.1M (by adding 0.1M NaClO₄).

Addition of chloride ion to the artificial groundwater was avoided because of interference with the method for determining dissolved uranium(VI) by kinetic phosphorescence analysis (KPA). To avoid the addition of chloride anion, perchlorate and/or sulfate salts were used to prepare the artificial groundwater solutions. Target partial pressures of carbon dioxide gas (pCO₂) for sorption experiments ranged from atmospheric (ca. 400 ppm) to approximately 2%. For higher ionic strength experiments, the concentration of NaClO₄ was simply increased from $1.7 \cdot 10^{-4} M$ in FMW-2 to 0.1M (FMW-2I), keeping the other components unchanged.

3.1.3 Sodium Carbonate Extractions

Extractions were performed on FMW-COMP at a solid to liquid ratio of 100 g/L with a solution composed of $1.44 \cdot 10^{-2} M$ NaHCO₃ and $2.8 \cdot 10^{-3} M$ Na₂CO₃. The extraction solution had an alkalinity of 20 meq/L and a pH of 9.45 under atmospheric pCO₂ and was previously proved to desorb labile U(VI) (Davis et al., 2006; Kohler et al., 2004; USNRC, 2003). The extraction time was 3 weeks.

3.1.4 Uranium(VI) Sorption Experiments

Prior to sorption experiments, aliquots of the FMW-COMP sample were equilibrated for several days (2-6 days) with artificial groundwater solution at a solid to liquid ratio of 200 g/L. Aliquots of 4 and 8 g of solid were weighed into centrifuge tubes and 20 or 40 mL of artificial groundwater were added, respectively. Centrifuge tubes were rotated during the equilibration time. At the end of this pretreatment (PT), the pH was measured, and the samples were centrifuged at 7000 rpm for 15 minutes. After PT, 0.45 μm filtered samples from each centrifuge tube were taken for alkalinity measurements (Gran titrations), for U(VI) analysis by kinetic phosphorescence analysis (KPA), and for the determination of

major ions by inductively-coupled argon plasma optical emission spectrometry (ICAP-OES). The samples were weighed to determine the amount of PT solution remaining with the sediment, and fresh groundwater was added to the solids prior to spiking the samples with 120 to 400 μL of U(VI) stock solution (concentration of the stock solution was usually about 100 times greater than the experimental target concentration).

The background uranium(VI) adsorbed on the sediments (0.253 nanomoles U(VI)/g) was determined by the sodium carbonate extraction method described in the section above. Desorption of a portion of the background adsorbed U(VI) occurred during PT and was accounted for in mass balance calculations. The total U(VI) concentrations added in the experiments were $1 \cdot 10^{-7}$, $3 \cdot 10^{-7}$, $1 \cdot 10^{-6}$, $3 \cdot 10^{-6}$, and $1 \cdot 10^{-5}$ M. For calculations of the uranium(VI) K_d values (or percent adsorbed), the total U(VI) concentrations in the experiments were calculated to be equal to the U(VI) added to the experiments plus the remaining background adsorbed U(VI) associated with the sediments after the PT. The inclusion of the remaining background adsorbed U(VI) impacted K_d values at the lowest two total U(VI) concentrations. At the three higher total U(VI) concentrations, the background U(VI) was negligible. Samples were rotated for a sorption time of 6 days and processed as described above. In kinetic experiments, supernatant samples were taken after 2 hours and up to 4 weeks.

3.2 Results

The BET surface area of the FMW-COMP sample was measured as $19.15 \text{ m}^2/\text{g}$.

3.2.1 Uranium(VI) Sorption Kinetics onto Forty-Mile Wash Sediments

Figure 3.1 shows the results of U(VI) sorption onto 200 g/L the FMW-COMP sample as a function of time at a total U(VI) concentration of 10^{-6} M and at low ionic strength of (5.1 ± 0.1) mM. Duplicate samples were taken for each time point. The errors in percent adsorbed reflect

analytical uncertainties of 3% in the analysis of dissolved U(VI) (and their propagation). The points shown as open squares illustrate that lowering the amount of solid per sample, while keeping the same solid/solution ratio, had no measurable effect on the uptake of U(VI) within experimental error. In addition, U(VI) uptake by sediment samples pretreated three times was the same as samples pretreated only once (diamonds vs. circles, respectively). U(VI) uptake reached a plateau after approximately one week. For all other experiments in this system, a standard method was adopted with a single pretreatment time of 2 days and a sorption period of 6 days.

3.2.2 Uranium(VI) Sorption onto Forty-Mile Wash Sediments at Variable pH and Alkalinity

Figure 3.2 shows the results of 6-day sorption experiments at low ionic strength (4.9 to 15 mM) for a solid/liquid ratio of 200 g/L in isotherm format. Different sets of symbols reflect different total U(VI) concentrations in the systems. Each data point reflects a set of parameters, consisting of pH, alkalinity and pCO_2 . The latter can be calculated from the former two values via the Henry's Law constant and the acidity constants for carbonic acid. Data points illustrated by the open symbols reflect conditions for a small pH range of 8.53 to 8.56, alkalinities between 2.46 and 2.51 meq/L, and calculated pCO_2 values of 400 to 440 ppm. Because of the relatively narrow range in each of these parameters, the data set can be considered as approximating an adsorption isotherm. In double logarithmic representation, the data describe a non-linear isotherm with a slope of 0.750 (linear regression analysis) and a correlation coefficient of 1.000.

Figures 3.3 and 3.4 illustrate the same data as in Figure 3.2 plus additional batch data, while representing the data as $\log K_d$ values for U(VI) sorption or percent U(VI) adsorbed.

The results for a corresponding series of experiments at higher ionic strength (0.1M NaClO_4) are shown in Figures 3.5 through 3.7. Again, the different symbols reflect different

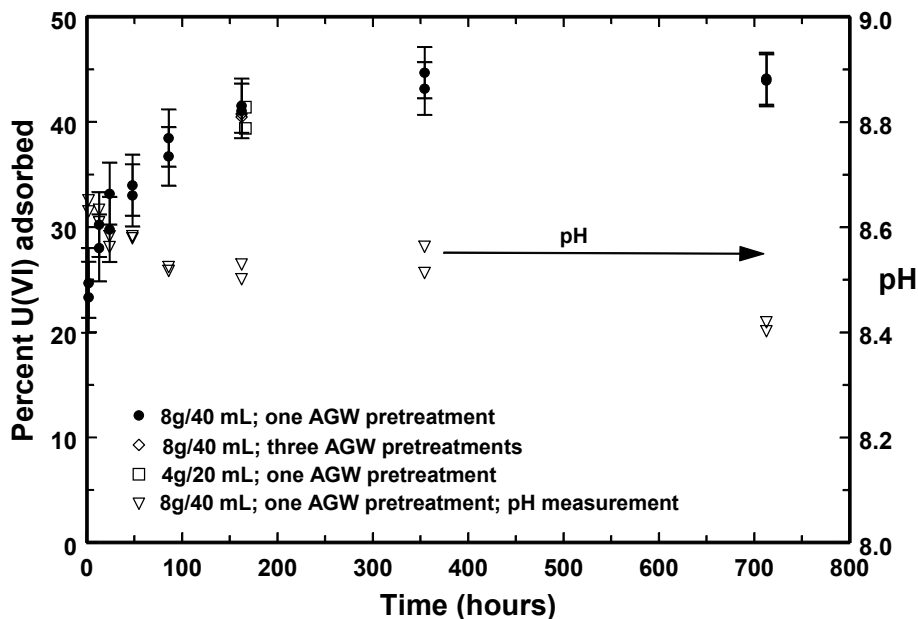


Figure 3.1. Kinetics of U(VI) adsorption on the composite sample of Forty-Mile Wash subsurface sediments (FMW-COMP) in artificial groundwater solution (FMW-2). Circles show percent of 1 μM total U(VI) adsorbed; triangles show pH values.

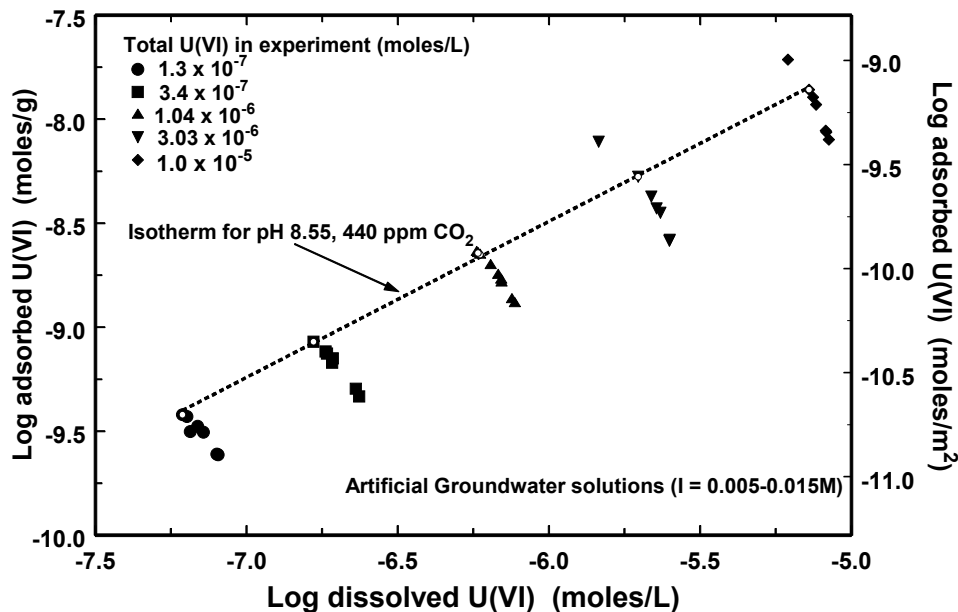


Figure 3.2. U(VI) sorption data on the composite sample of Forty Mile Wash subsurface sediments (FMW-COMP) in artificial groundwater solutions at low ionic strength. 6-day equilibration time was used for U(VI) sorption following one pretreatment of the sediments with artificial groundwater solution. The open symbols represent data with nearly identical conditions for pH (8.53-8.56), alkalinity (2.46-2.51 meq/L), and pCO_2 (400-440 ppm), meaning that these data approximately represent a traditional isotherm.

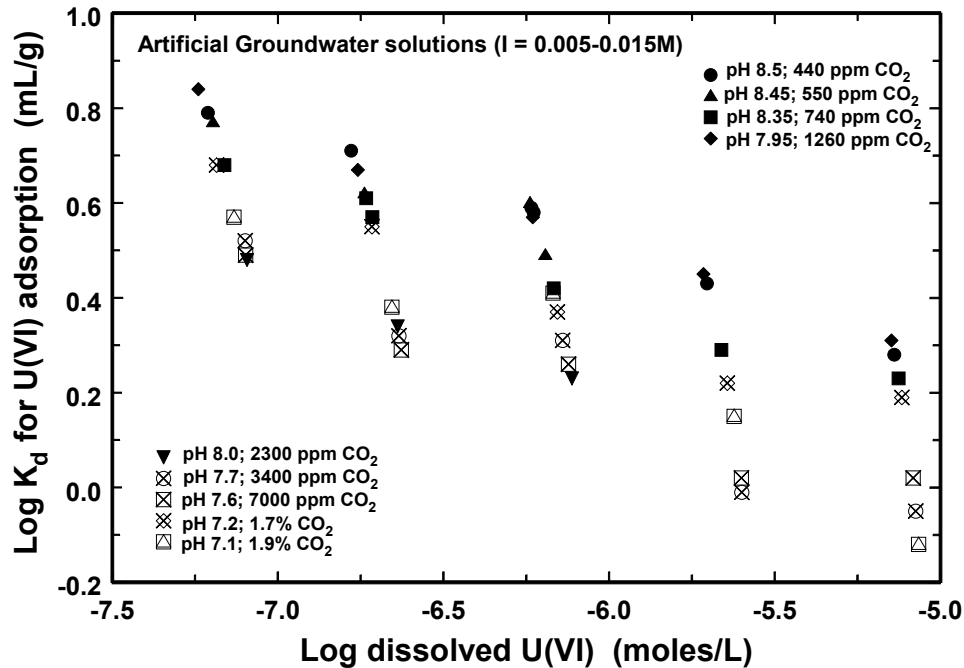


Figure 3.3. U(VI) sorption data on the composite sample of Forty Mile Wash subsurface sediments (FMW-COMP) in artificial groundwater solutions at low ionic strength as a function of dissolved U(VI) and PCO₂. Data expressed as log K_d for U(VI) sorption versus log dissolved U(VI) concentration.

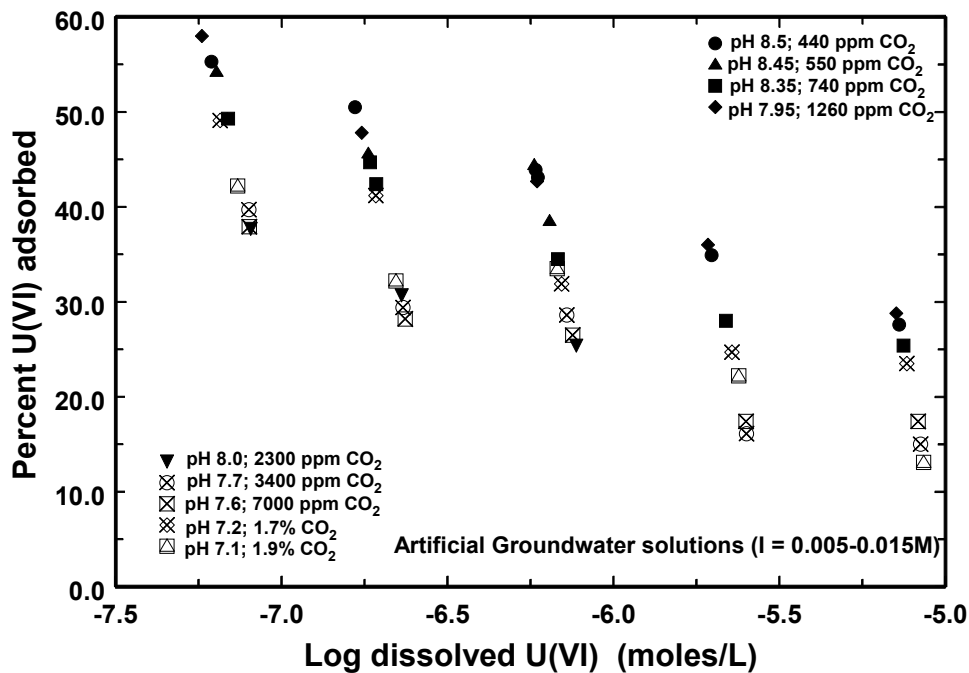


Figure 3.4. U(VI) sorption data on the composite sample of Forty Mile Wash subsurface sediments (FMW-COMP) in artificial groundwater solutions at low ionic strength as a function of dissolved U(VI) and PCO₂. Data expressed as percent U(VI) adsorbed versus log dissolved U(VI) concentration.

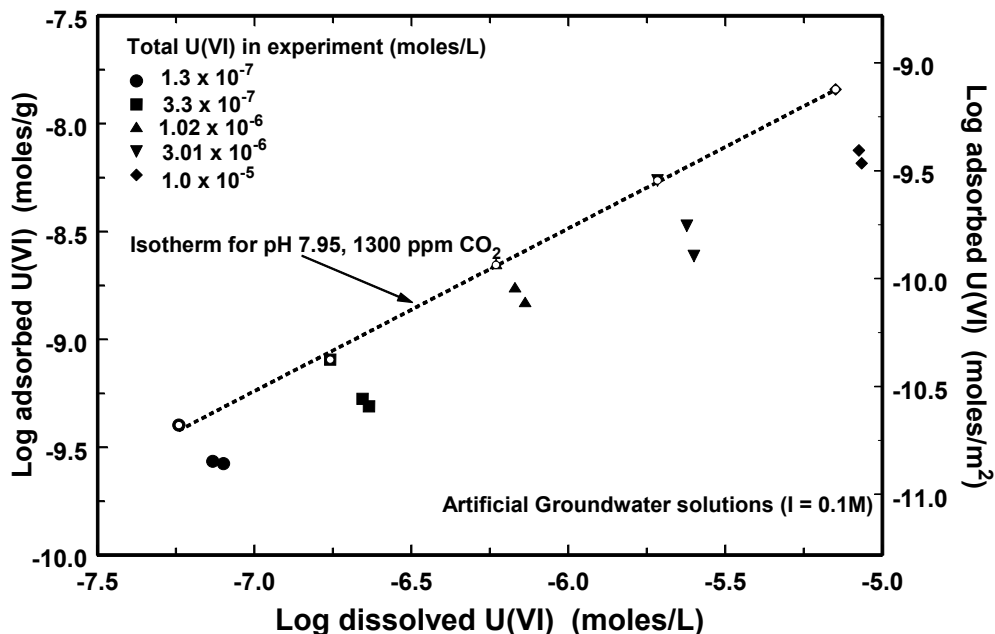


Figure 3.5. U(VI) sorption data on the composite sample of Forty Mile Wash subsurface sediments (FMW-COMP) in artificial groundwater solution at ionic strength of 0.1M. 6-day equilibration time was used for U(VI) sorption following one pretreatment of the sediments with the artificial groundwater solution. The open symbols represent data with nearly identical conditions for pH (7.94-7.96), alkalinity (2.19-2.32 meq/L), and pCO₂ (1240-1310 ppm), meaning that these data approximately represent a traditional isotherm.

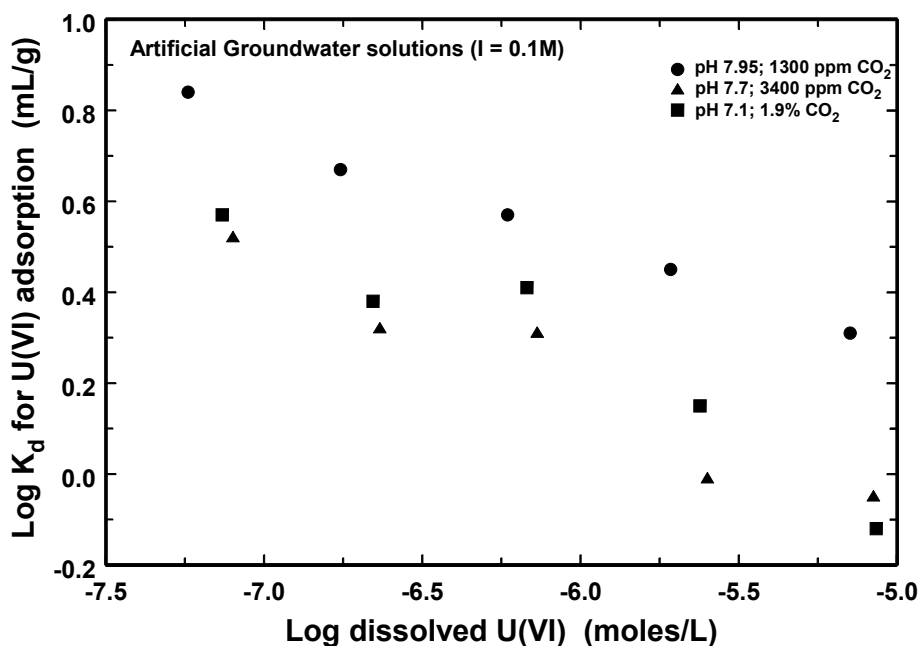


Figure 3.6. U(VI) sorption data on the composite sample of Forty Mile Wash subsurface sediments (FMW-COMP) in artificial groundwater solution at ionic strength of 0.1M as a function of dissolved U(VI) and PCO₂. Data expressed as log K_d for U(VI) sorption versus log dissolved U(VI) concentration.

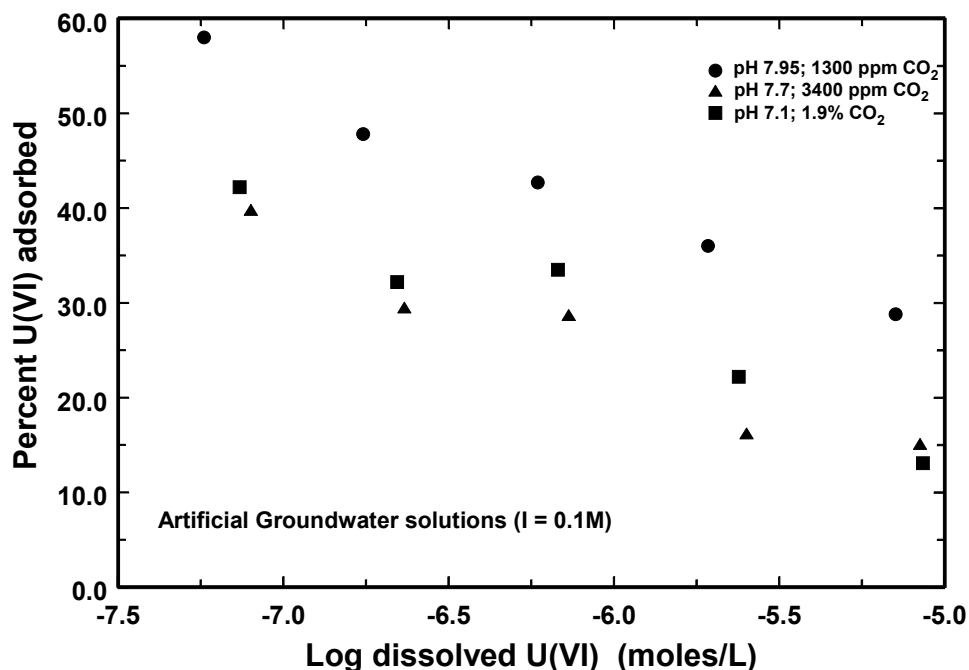


Figure 3.7. U(VI) sorption data on the composite sample of Forty Mile Wash subsurface sediments (FMW-COMP) in artificial groundwater solution at ionic strength of 0.1M as a function of dissolved U(VI) and PCO₂. Data expressed as percent U(VI) adsorbed versus log dissolved U(VI) concentration.

total U(VI) concentrations and the open symbols in Figure 3.5 shows conditions in which the parameters pH (7.94 to 7.96), alkalinity (2.19 to 2.32 meq/L) and pCO₂ (1240-1310 ppm) varied over a relatively narrow range. A linear regression line through these data had a slope of 0.755 with a correlation coefficient of 0.999.

3.3 Uranium(VI) Surface Complexation Modeling for Forty-Mile Wash Sediments

3.3.1 Introduction

There is considerable experimental data for U(VI) adsorption in systems with one mineral phase, and surface complexation models (SCM) have been developed to accurately describe these data (e.g., Arnold et al., 2001; Pabalan et al., 1998; Waite et al., 1994). Nevertheless, the application of SCM to the mixtures of minerals in soils and sediments is difficult because of the presence of secondary mineral and organic coatings (USNRC, 2003; Penn et al. 2001,

Padmanabhan and Mermut, 1996; Coston et al., 1995) that affect the stoichiometry and coulombic correction factors of surface complexation reactions. There are two major approaches for applying the SCM concept to soils and sediments: the Component Additivity (CA) and Generalized Composite (GC) approaches (Davis et al., 2004; 1998).

In the CA approach, it is assumed that a mineral assemblage is composed of one or more reference phases, whose surface chemical reactions are known from independent studies of each phase (e.g., Arnold et al., 2001; Prikryl et al., 2001; Turner et al., 1996; Cowan et al., 1992). Then, based on a measurement of the relative amounts or surface areas of each mineral present in the soil or sediment, adsorption by the mixture of phases can be *predicted* by an equilibrium calculation, without any fitting of experimental data for the mixture (Honeyman, 1984). CA model predictions are sometimes made by assuming that one mineral component dominates adsorption (Barnett et al., 2002;

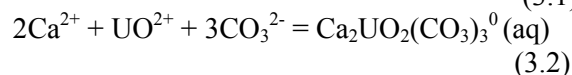
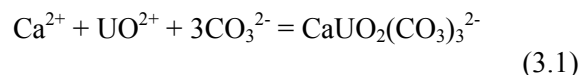
Waite et al., 2000; Schmeide et al., 2000; Davis et al., 1998), allowing a straightforward equilibrium calculation if the exposed surface area of that mineral component in the soil or sediment can be quantified.

In the GC approach, the surface of the mineral assemblage is considered too complex to be quantified in terms of the contributions of individual phases to adsorption. The complexity is caused, in part, by the difficulties in quantifying the electrical field and proportions of surface functional groups at the mineral-water interface in the mixture of mineral phases and associated surface coatings. In the GC approach it is assumed that adsorption can be described by mass laws written with “generic” surface functional groups, with the stoichiometry and formation constants for each mass law determined by fitting experimental data for the mineral assemblage as a whole (Davis et al., 2004; Davis et al., 2002; Davis et al., 1998; Westall et al., 1998; van Benschoten et al., 1998). GC model calculations are presented in this section to simulate U(VI) adsorption by subsurface sediments collected from Forty-Mile Wash aquifer (Nye County, Nevada).

3.3.2 Modeling Calculations and Approach

FITEQL 4.0 (Herbelin and Westall, 1999) was used to determine the best fit of various U(VI) surface reactions or combinations of reactions to the experimental U(VI) adsorption data in the GC model calculations. The Davies equation was used for activity correction of aqueous species only. Relative errors of 1% in the concentrations of surface sites, total U(VI), and adsorbed U(VI), and relative errors of 5% in $\log [H^+]$ and $\log [H_2CO_3]$ were used as FITEQL inputs. Thermodynamic data used in the modeling are consistent with the most recent NEA database for uranium (Guillaumont et al., 2003), except the aqueous species, $CaUO_2(CO_3)_3^{2-}$ and $Ca_2UO_2(CO_3)_3^0(aq)$ (Kalmykov and Choppin, 2000; Bernhard et al., 2001) were also included. Corrected to zero ionic strength, Bernhard et al. (2001) estimated values of 25.4 ± 0.3 and 30.6 ± 0.3 for the log of

the formation constants for reactions (3.1) and (3.2), respectively, and Kalmykov and Choppin (2000) estimated a value of 29.8 ± 0.7 for reaction (3.2):



To be consistent with the new NEA database (Guillaumont et al., 2003), the log K values for reactions (3.1) and (3.2) were corrected upwards by 0.24 log unit (Fox et al., 2006). For reaction (3.2), the value of Kalmykov and Choppin (2000) was chosen for modeling calculations because it gave a better prediction of the experimental data for U(VI) sorption on quartz in the presence of Ca (Fox et al., 2006).

The GC model was developed based on a semi-empirical fit to the experimental data for U(VI) adsorption by the Forty-Mile Wash aquifer sediments. In the GC approach, laboratory experiments are conducted with sediments from the field site to be modeled, and mass law relationships are derived that describe the change in metal ion adsorption with variations in groundwater chemical conditions observed or anticipated in the aquifer (Davis et al., 2004; 2002; 1998). Because no electrostatic information was available for the charge and potential on Forty-Mile Wash sediment surfaces, a non-electrostatic GC model was used. In principle, potentiometric titration can be used to determine the surface proton balance of soils and sediments (Charlet and Sposito, 1987), as is commonly done to determine surface charge on pure, insoluble mineral phases, such as goethite (Lützenkirchen et al., 2002). However, the interpretation of the titration data is complex in the case of soils and sediments, because the consumption of titrant is often dominated by the dissolution of mineral phases, the release of organic acids, or other adsorption/desorption reactions.

In order to simplify the GC model further, the following decisions were made *a priori*: a) a total site density of $3.84 \mu\text{moles}/\text{m}^2$ was assumed (based on the recommended total site

density (Davis and Kent, 1990) of 3.84 $\mu\text{moles}/\text{m}^2$), b) at least two types of sites (strong and weak) were assumed to exist on the surface to account for the non-linear adsorption isotherms commonly observed for U(VI) adsorption (Davis, 2001; Waite et al., 1994), and as observed here for Forty-Mile Wash sediments (Figs. 3.2 and 3.5), and c) it was assumed that U(VI) adsorption could be described by three or less surface reactions. The latter constraint was arbitrary but was adopted to reduce the number of model fitting parameters. In general, a goal of the semi-empirical GC modeling approach is to develop the simplest model possible that describes the major features of adsorption as chemical conditions are varied over field-relevant ranges (Davis et al., 1998).

Based on previous work with U(VI) (Davis et al., 2004; USNRC, 2003), at least nine monomeric U(VI) surface reactions are possible in a uranyl/carbonate/oxide system (Table 3.1). Other U(VI) surface ternary complexes are plausible, including uranyl-phosphate and -silicate ternary complexes, but these were not considered because their existence has not yet been confirmed in model systems. Because of the excess of surface sites in comparison to the U(VI) concentrations in the experiments, combined with the assumption of a non-electrostatic model, it is not necessary to consider ionization reactions of the surface hydroxyl groups (Davis et al., 1998).

Initially the experimental data were fit with a one-site model. FITEQL calculations were completed to determine which single reaction (Table 3.1) would provide the best fit to the

experimental data. FITEQL output includes a goodness-of-fit parameter, WSOS/DF, the weighted sum of squares of the difference in value between model simulations and experimental data points, divided by the degrees of freedom (Herbelin and Westall, 1999). Lower values of WSOS/DF mean the proposed model is a better fit to the data; WSOS/DF will be referred to as a “fit value” below.

Representing the U(VI) adsorption data with a single reaction produced a reasonably good fit, with the best fits (fit values = 4.9 or 11.3) provided by reactions 2 or 4, respectively (Table 3.1). The second step in model development was to consider combinations of two reactions to represent the data. Unlike the case for modeling U(VI) adsorption on Naturita sediments (Davis et al., 2004; USNRC, 2003), the fit to the data was not improved by adding a second reaction; the best fits were still the single reactions 2 or 4. Further testing showed that the fit could be improved by adding a second site type, a strong-binding site. The site density of the strong-binding site was optimized by comparing the fits to the data as a function of the site density; this was done in separate calculation with only reaction 2 or 4 alone, and with a combination of reaction 2 and 4. The best overall fit to the experimental data occurred with reaction 2 alone and with a strong site density of 0.002% of total sites (fit = 1.17). The log K values for reaction 2 in the optimized fit to the experimental data were -0.541 and -5.761 for the strong-site and weak-site reactions, respectively. The fit of the GC model to experimental data is illustrated in Figures 3.8 through 3.10 and the model

Table 3.1. U(VI) Surface Reactions Considered for the Forty-Mile Wash GC Model

Number	Reaction
1	$\text{SOH} + \text{UO}_2^{2+} = \text{SOUO}_2^+ + \text{H}^+$
2	$\text{SOH} + \text{UO}_2^{2+} + \text{H}_2\text{O} = \text{SOUOOH} + 2\text{H}^+$
3	$\text{SOH} + \text{UO}_2^{2+} + \text{H}_2\text{CO}_3 = \text{SOUO}_2\text{HCO}_3 + 2\text{H}^+$
4	$\text{SOH} + \text{UO}_2^{2+} + \text{H}_2\text{CO}_3 = \text{SOUO}_2\text{CO}_3^- + 3\text{H}^+$
5	$\text{SOH} + \text{UO}_2^{2+} + \text{H}_2\text{CO}_3 + \text{H}_2\text{O} = \text{SOUO}_2\text{OHCO}_3^{2-} + 4\text{H}^+$
6	$\text{SOH} + \text{UO}_2^{2+} + 2\text{H}_2\text{CO}_3 = \text{SOUO}_2(\text{HCO}_3)_2^- + 3\text{H}^+$
7	$\text{SOH} + \text{UO}_2^{2+} + 2\text{H}_2\text{CO}_3 = \text{SOUO}_2(\text{CO}_3\text{HCO}_3)^{2-} + 4\text{H}^+$
8	$\text{SOH} + \text{UO}_2^{2+} + 2\text{H}_2\text{CO}_3 = \text{SOUO}_2(\text{CO}_3)_2^{3-} + 5\text{H}^+$
9	$\text{SOH} + \text{UO}_2^{2+} + 2\text{H}_2\text{CO}_3 + \text{H}_2\text{O} = \text{SOUO}_2\text{OH}(\text{CO}_3)_2^{4-} + 6\text{H}^+$

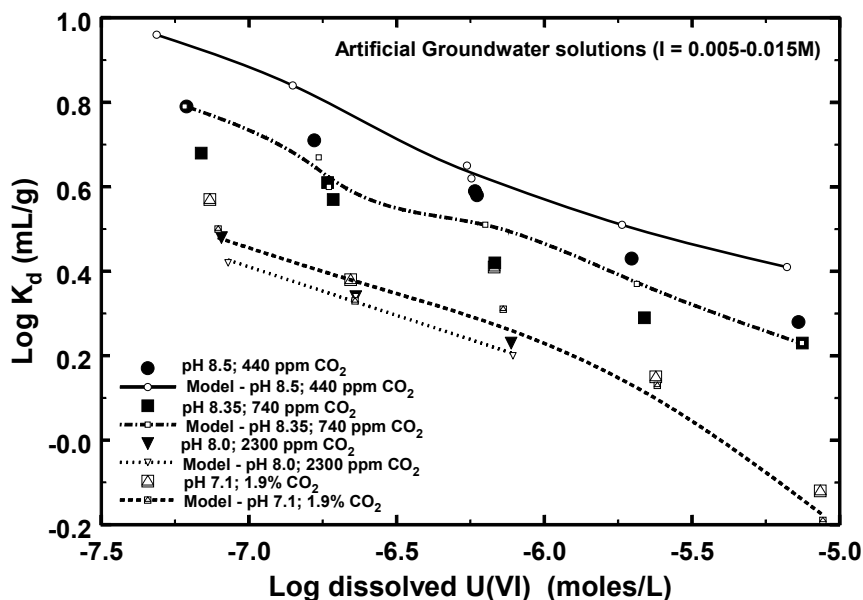


Figure 3.8a. Comparison of U(VI) sorption data and surface complexation model calculations for the composite sample of Forty Mile Wash subsurface sediments (FMW-COMP) in artificial groundwater solutions at low ionic strength as a function of dissolved U(VI) and PCO_2 . Data expressed as $\log K_d$ for U(VI) sorption versus \log dissolved U(VI) concentration and shown with large symbols. Model calculations shown as curved splines, with individual model points shown with small symbols.

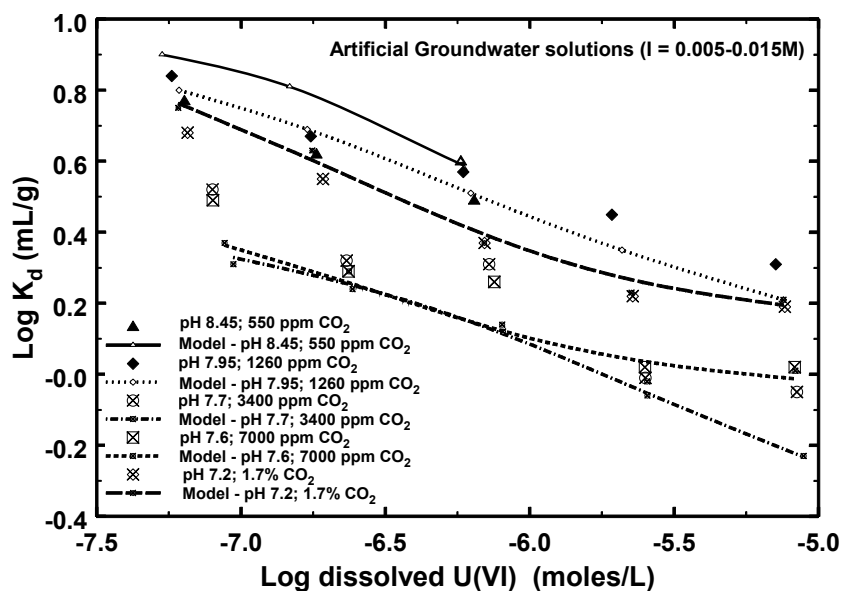


Figure 3.8b. Comparison of U(VI) sorption data and surface complexation model calculations for the composite sample of Forty Mile Wash subsurface sediments (FMW-COMP) in artificial groundwater solutions at low ionic strength as a function of dissolved U(VI) and PCO_2 . Data expressed as $\log K_d$ for U(VI) sorption versus \log dissolved U(VI) concentration and shown with large symbols. Model calculations shown as curved splines, with individual model points shown with small symbols.

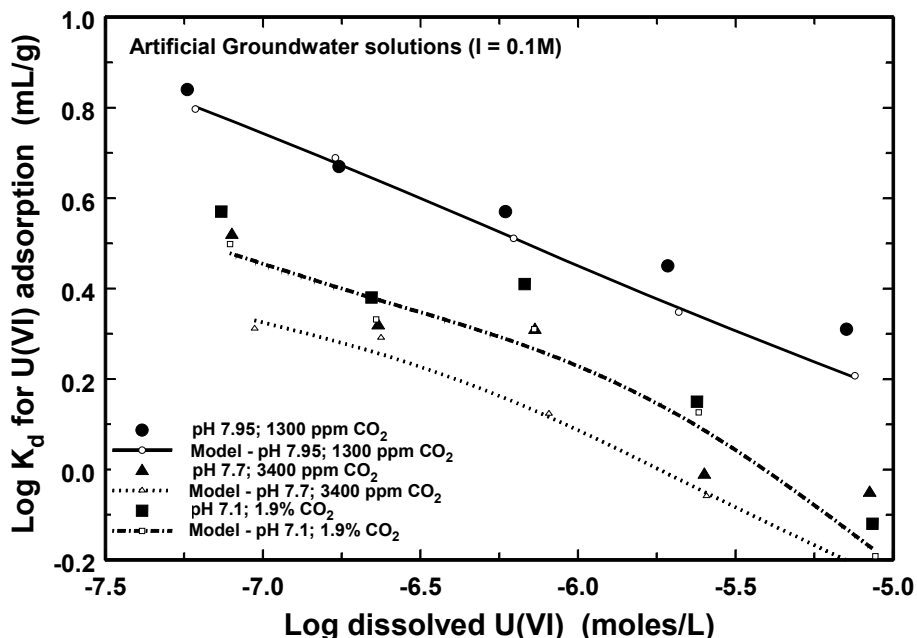


Figure 3.9. Comparison of U(VI) sorption data and surface complexation model calculations for the composite sample of Forty Mile Wash subsurface sediments (FMW-COMP) in artificial groundwater solutions at an ionic strength of 0.1M as a function of dissolved U(VI) and PCO_2 . Data expressed as $\log K_d$ for U(VI) sorption versus \log dissolved U(VI) concentration and shown with large symbols. Model calculations shown as curved splines, with individual model points shown with small symbols.

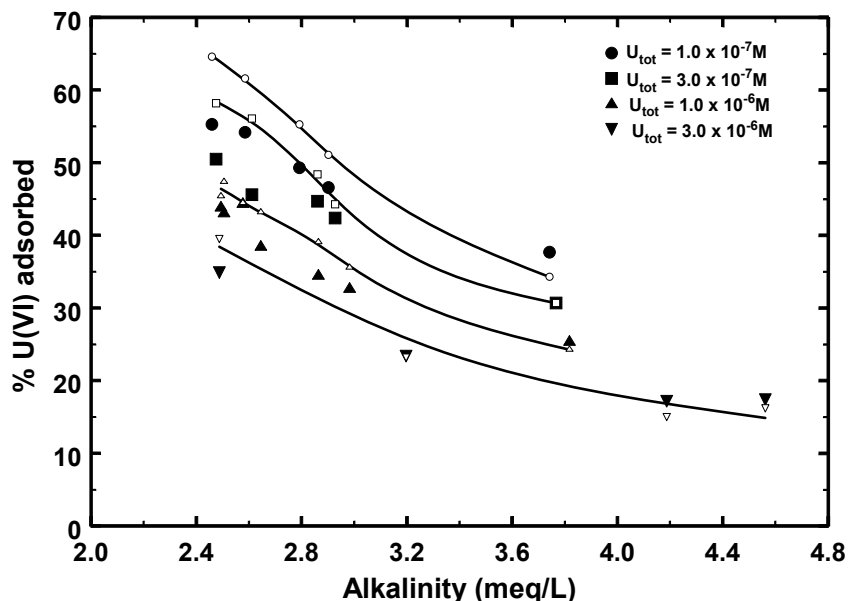


Figure 3.10. Comparison of selected U(VI) sorption data and surface complexation model calculations for the composite sample of Forty Mile Wash subsurface sediments (FMW-COMP) in artificial groundwater solutions at low ionic strength. Data expressed as percent U(VI) adsorbed versus alkalinity and shown with large symbols. Model calculations shown as curved splines, with individual model points shown with small symbols.

describes the data quite well. The fits are shown for the variation of log Kd value as a function of dissolved U(VI) concentration and PCO2 at low ionic strength (Fig. 3.8) and high ionic strength (Fig. 3.9). Figure 3.10 shows the fit of a portion of the dataset with the data expressed as percent

U(VI) adsorbed versus the alkalinity in the artificial groundwater solution. The experimental data are shown as large symbols in the figures; model simulations are shown as smooth curves, with the individual model calculations shown as small symbols.

4 DEVELOPMENT OF A SURFACE COMPLEXATION MODEL FOR NICKEL SORPTION ONTO CAPE COD (MASSACHUSETTS) AQUIFER SEDIMENTS

4.1 Materials and Methods

4.1.1 Preparation of an Aquifer Sediment Composite Sample

Aquifer sediment was collected in 1994 along a transect two meters east of the multilevel sampler array at the USGS research site at Cape Cod, Massachusetts (Davis et al., 2000), using a wireline-piston core barrel and plastic core liners approximately 1.5 meters in length. Sufficient core material was collected from the suboxic zone to make three composites of the sediments, one of which was used in the following experiments (suboxic composite #2). Cores were frozen immediately after collection and stored frozen until processing in the USGS laboratory in Menlo Park, CA.

Each core was sectioned at 10 cm intervals, dried under a laminar flow hood at room temperature, and then sieved to remove grains >1000 microns in diameter. A sample of <1000 micron sediment from the core section was then leached with 0.25 hydroxylamine hydrochloride solution in 0.25 M HCl (HH) at 50°C for 30 minutes; the solid to solution ratio in the extractions was 200 g/L. The supernatants of the extractions were measured by inductively-coupled argon plasma optical emission spectrometry (ICAP-OES) using single point external calibration standards (Coston et al. 1998). Analysis of the extraction solutions was used to determine the amount of zinc (Zn) extracted in each subsample. The amount of zinc was used to determine where the Zn-contaminated transition zone was in each core (Rea et al. 1991, Coston et al. 1995, Kent et al., 2000), in order to prepare a composite of suboxic material that was located beneath the Zn-contaminated transition zone. BET surface areas were measured by nitrogen gas adsorption for the composite sand sample, using methods previously discussed in Coston et al. (1995).

4.1.2 Nickel Sorption Experiments

Batch experiments were conducted using the same suboxic artificial groundwater solution (SAGW) used in previous experiments by Coston et al. (1995). The pH was controlled by addition of 2-N-morpholinoethane sulfonic acid buffer (MES) to the artificial groundwater solution. MES is known to be an extremely weak chelator of metals and is used in biochemical studies of metal binding by amino acids and peptides (Coston et al., 1995). SAGW was adjusted within the pH range 4.5-6.7. All salts used to make primary solutions were trace metal grade. Since the sediment was dried, these experiments included a pretreatment procedure using the SAGW. A solid/solution ratio of 400 g of sediment per L of artificial groundwater solution was used in all nickel (Ni) sorption experiments.

4.2 Results

Preliminary experiments demonstrated that there was no significant interference of the MES buffer with Ni sorption. The surface area of the Cape Cod aquifer composite sample was 0.33 m²/g.

Figures 4.1 and 4.2 show the adsorption of Ni(II) at total concentrations of 1, 18 and 29 µM with increasing pH, and Ni sorption isotherms at pH 5.4 and 6.1. As expected, Ni adsorption increases with increasing pH and the slope of the isotherms (log-log scale) is less than one, indicating that the average Ni adsorption bond is weaker with increasing Ni concentration.

Sodium carbonate solution extractions of the Cape Cod sand composite showed that reactive phosphate concentrations averaged 0.0046 milligrams of P per gram of sand. 1M hydrochloric acid extractions of the sand yielded 0.02 milligrams of P per gram of solid. Sorption experiments were carried out to determine the

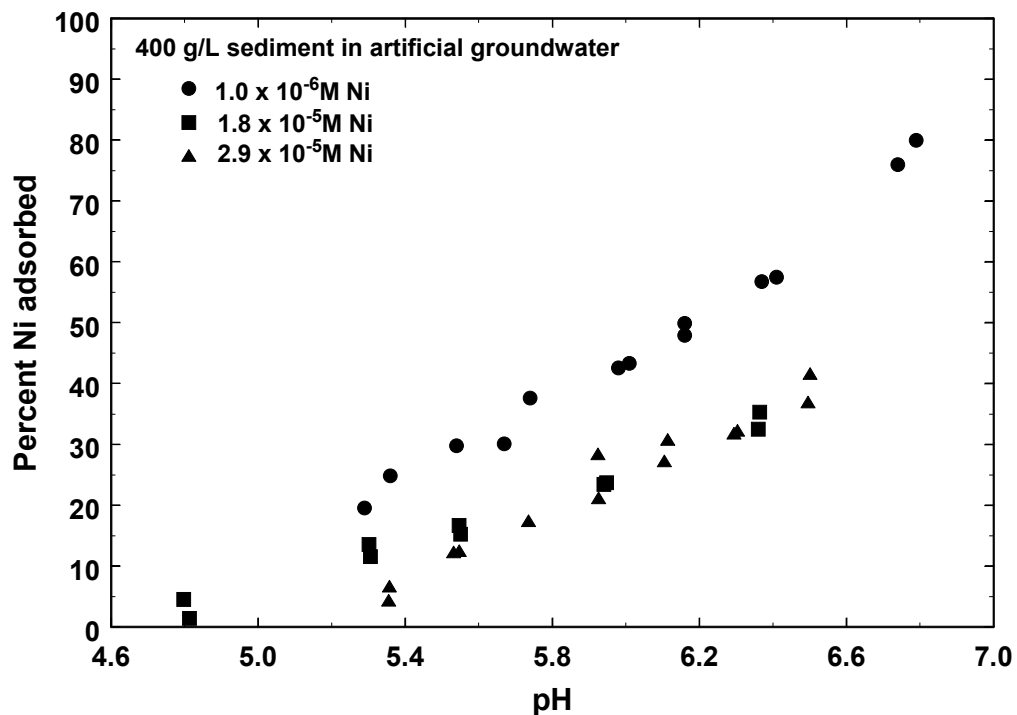


Figure 4.1. Percent Ni adsorbed as a function of pH and total Ni concentration for suspensions with 400 g/L of Cape Cod aquifer sand composite in artificial groundwater solution.

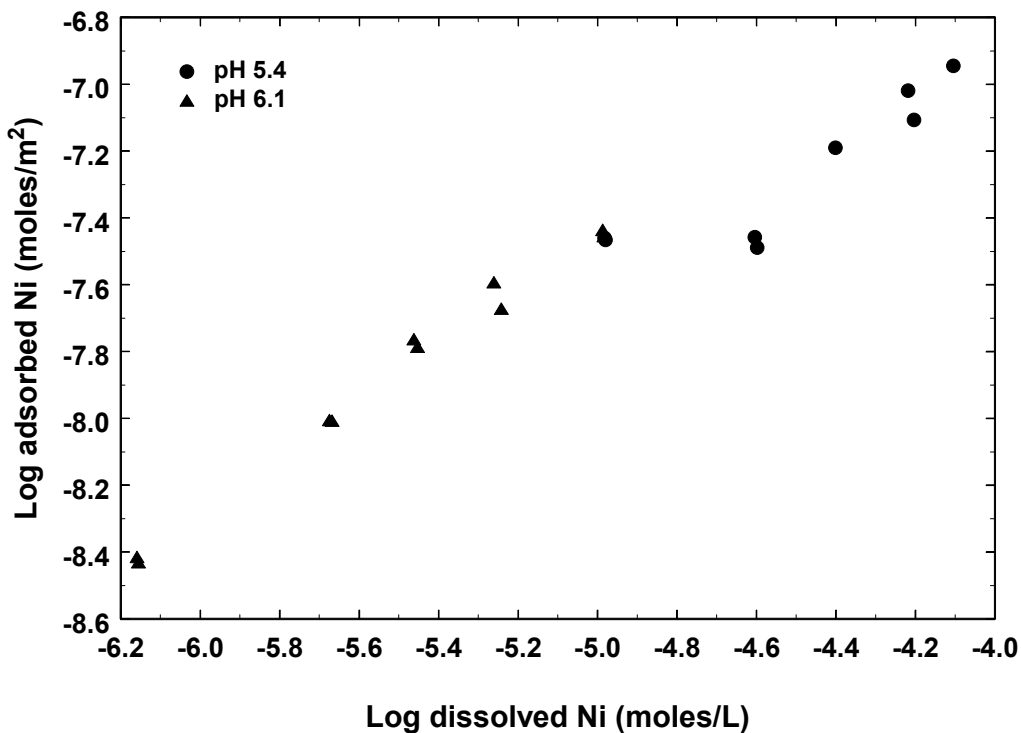


Figure 4.2. Ni adsorption isotherms for Cape Cod aquifer sand composite in artificial groundwater solution at pH 5.4 and 6.1.

possible effects of phosphorus sorption on Ni(II) sorption. Phosphate concentrations of both 400 and 700 micromolar P had no observable effect on 20 micromolar Ni sorption at pH 6.25.

4.3 Surface Complexation Model Development for Nickel Adsorption

FITEQL 4.0 (Herbelin and Westall, 1999) was used to determine the best fit of various Ni surface reactions or combinations of reactions to the experimental Ni adsorption data in GC model calculations. The Davies equation was used for activity correction of aqueous species only. Relative errors of 1% in the concentrations of surface sites, total Ni, and adsorbed Ni, and relative errors of 5% in $\log [H^+]$ and $\log [H_2CO_3]$ were used as FITEQL inputs. Thermodynamic data used in the modeling are consistent with the data given in Smith and Martell (1981).

The GC model was developed based on a semi-empirical fit to the experimental data for Ni adsorption by the Cape Cod aquifer sediments. As in the case for U(VI) sorption on Forty-Mile Wash sediments (section 3), a non-electrostatic GC model was used. In order to simplify the GC model further, the following decisions were made *a priori*: a) a total site density of 3.84 $\mu\text{moles/m}^2$ was assumed (based on the recommended total site density by Davis and Kent, 1990), b) at least two types of sites (strong and weak) were assumed to exist on the surface to account for the non-linear adsorption isotherms observed (Fig. 4.2), and c) it was assumed that Ni adsorption could be described by two or less surface reactions. Table 4.1 shows the two Ni surface reactions considered in the GC modeling.

Initially it was attempted to fit the experimental data with a one-site model. FITEQL calculations were completed to determine which single reaction (Table 4.1) would provide the best fit to the experimental data. FITEQL output includes a goodness-of-fit parameter, WSOS/DF, the weighted sum of squares of the difference in value between model simulations and experimental data points, divided by the degrees of freedom (Herbelin and Westall, 1999). Lower values of WSOS/DF mean the proposed model is a better fit to the data; WSOS/DF will be referred to as a “fit value” below. Neither reaction 1 or 2 or a combination of the two (Table 4.1) could produce a good fit of the data with a one-site model.

Representing the Ni adsorption data with reaction 1 (Table 4.1) produced a reasonably good fit with a two-site model. No improvement in the fit could be achieved by adding reaction 2 to the model. The site density of the strong-binding site was optimized by comparing the fits to the data as a function of the site density; the best overall fit to the experimental data occurred with reaction 1 alone and with a strong site density of 1% of total sites (fit = 14.8). The log K values for reaction 1 in the optimized fit to the experimental data were -0.675 and -3.331 for the strong-site and weak-site reactions, respectively.

The fit of the GC model to experimental data is illustrated in Figures 4.3 and 4.4 and the model describes the data reasonably well. The fits are shown for the percent Ni adsorbed as a function of pH and total Ni concentration (Fig. 4.3) and for the Ni adsorption isotherms at pH 5.4 and 6.1 (Fig. 4.4).

Table 4.1. Ni Surface Reactions Considered for the Cape Cod GC Model

Number	Reaction
1	$\text{SOH} + \text{Ni}^{2+} = \text{SONi}^+ + \text{H}^+$
2	$\text{SOH} + \text{Ni}^{2+} + \text{H}_2\text{O} = \text{SONiOH} + 2\text{H}^+$

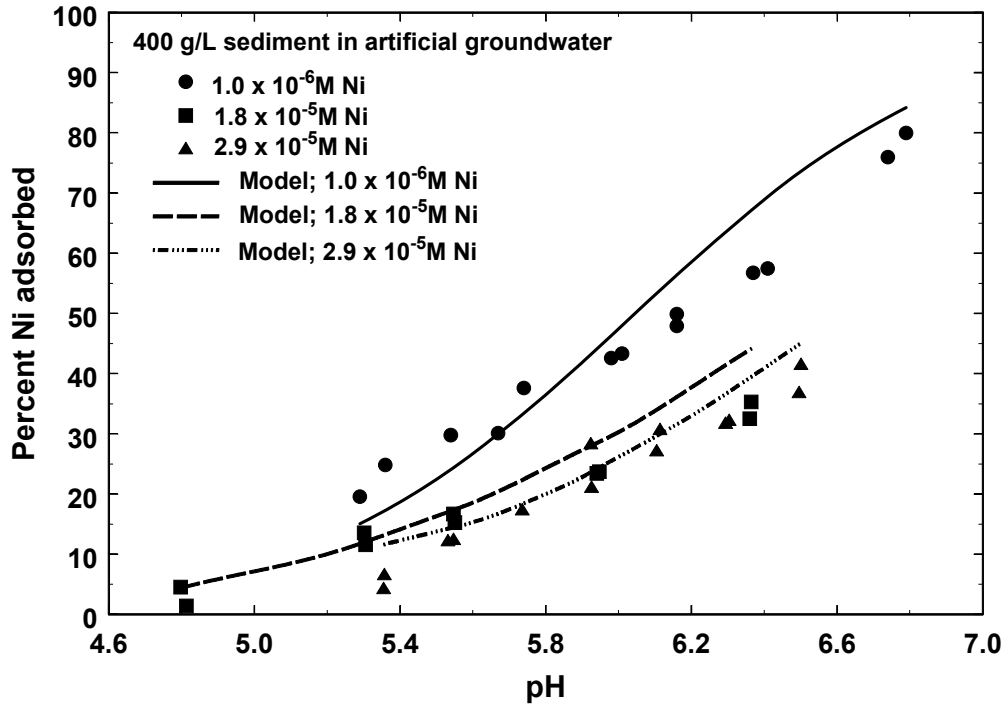


Figure 4.3. Comparison of GC model simulation and experimental data for percent Ni adsorbed as a function of pH and total Ni concentration, for suspensions with 400 g/L of Cape Cod aquifer sand composite in artificial groundwater solution.

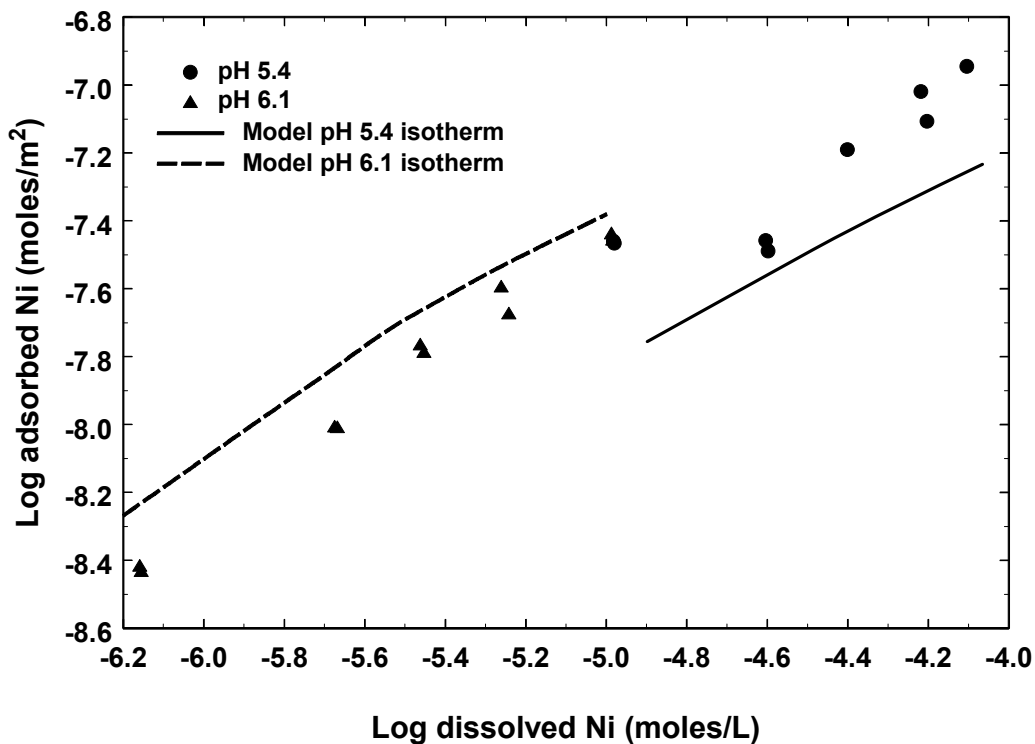


Figure 4.4. Comparison of GC model simulations and experimental data for Ni adsorption isotherms for Cape Cod aquifer sand composite in artificial groundwater solution at pH 5.4 and 6.1.

5 CONCLUDING REMARKS AND SUMMARY

Prior to this investigation, the Generalized Composite (GC) modeling approach to surface complexation model development had been tested at the field scale in two other studies (Curtis et al., 2006; USNRC, 2003; Kent et al., 2000) and in a small number of laboratory investigations. The objective of the current study was to demonstrate the GC modeling approach for a number of different sorbing radionuclides and geomaterials. Geomaterials chosen for the study included the Naturita and Cape Cod aquifer sediments because these materials have been well characterized in the literature (Davis et al., 2004; USNRC, 2003; Kohler et al., 2004; Davis et al., 1998; Coston et al., 1995). In addition, it was desired to demonstrate the GC model for uranium(VI) on a new geomaterial; the Forty-Mile Wash aquifer was chosen for that purpose. Most previous GC model studies have been done with uranium(VI); in this work GC models were developed for Np(V) and Ni to expand the number of radionuclides for which adsorption has been modeled with this approach.

It is known from studies of pure mineral phases that dissolved carbonate concentration and pH are significant aqueous chemical variables that influence the adsorption of U(VI) and Np(V) (Davis et al., 2004; Waite et al., 1994; Kohler et al., 1999). As expected, adsorption of U(VI) by the Forty-Mile Wash sediments was strongly influenced by the carbonate concentration (Section 3), however, the influence of carbonate and humic acids on Np(V) sorption by Naturita sediments was much weaker (Section 2). For Ni, pH is the main variable that influences its sorption (Section 4).

In the literature, at least three types of adsorption modeling approaches can be distinguished: 1) empirical partitioning relationships (Davis and Kent, 1990), 2) thermodynamic surface speciation models that describe the molecular details of chemical species formation at mineral surfaces (Hiemstra and van Riemsdijk, 1999; Sahai and Sverjensky, 1997), and 3) semi-empirical site-binding models that utilize

concepts from the first two model types (Davis et al., 2004; Davis et al., 2002; Borkovec et al., 1998; Davis et al., 1998).

In the first approach, empirical relationships such as K_d values, sorption isotherms, and partitioning equations are used to predict adsorption as a function of aqueous concentration variables (Davis and Kent, 1990). K_d values are defined as:

$$K_d = RN_{ads} / RN_{aq}$$

where RN_{ads} refers to the quantity of radionuclide sorbed and RN_{aq} refers to the dissolved concentration of the same radionuclide. The relationship implies that a constant ratio is obtained between these two quantities, as in a linear isotherm.

There are many types of non-linear adsorption isotherms. The most common, the Langmuir isotherm can be represented as (Davis and Kent, 1990):

$$K_L = RN_{ads} / (RN_{aq})(\Gamma_{free})$$

where K_L is a constant and Γ_{free} refers to the quantity (or concentration) of available surface sites. The Langmuir isotherm accounts for the decrease in K_d values that occurs as an adsorbing surface becomes partially saturated with adsorbed species (Davis and Kent, 1990). The relationship is usually determined for a specific set of constant chemical and physical conditions while a radionuclide concentration is varied.

K_d values for radionuclides have been determined experimentally on a wide variety of geological solids (Altmann et al., 2001; USEPA, 1999), and the variability of K_d values with chemical conditions has been the subject of several studies (Waite et al., 1994; Davis et al., 2002; USEPA, 1999; Pabalan et al., 1998; Altmann et al., 2001; Turner and Sassman, 1996; Prikryl et al., 2001; Barnett et al., 2002). For example, it has been shown that K_d values for

adsorption of U(VI) on sediments and pure mineral phases may vary by more than 8 orders of magnitude over a wide range of chemical conditions in which U(VI) aqueous speciation changes significantly (e.g., pH 4-10) (USEPA, 1999). This is in agreement with other reports that show that K_d values are highly sensitive to chemical conditions (Curtis et al., 2004; USNRC, 2003, Davis et al., 2002; Bethke and Brady, 2000; Kent et al., 2000; USNRC, 2001).

For the second and third approaches, surface complexation models (SCM) use mass action laws analogous to aqueous phase reactions to describe adsorption (USNRC, 2001; Davis and Kent, 1990) as a function of aqueous chemical conditions, thus taking into account changes in chemical speciation, competitive adsorption, and other multi-solute interactive chemical effects. The possible advantages of applying the surface complexation concept to describe radionuclide sorption in nuclear waste performance assessment (PA) include the following factors:

- 1) the modeling approach provides a thermodynamic framework to describe adsorption reactions of radionuclides,
- 2) the stability constants for the adsorption reactions can be included as part of an overall network of chemical reactions in geochemical equilibrium or coupled reactive transport models, and thus coupled with thermodynamic databases for radionuclide aqueous speciation and solubilities, such as the NEA thermodynamic database (Guillaumont et al., 2003),
- 3) the modeling approach allows predictive calculations for a range of chemical conditions without adjustment of the values of the model parameters, as chemical conditions are varied in space or time, unlike the condition-dependent empirical relationships,
- 4) the modeling approach can be included efficiently in transport simulations (or PA scenarios) in which there are chemical gradients in space or time.

The thermodynamic surface speciation and GC modeling approaches represent two extremes of surface complexation modeling (Davis et al., 2004; Davis et al., 1998). Table 5.1 compares the modeling approaches and their data requirements. In thermodynamic surface speciation models (Weerasoriya et al., 2001; Hiemstra and van Riemsdijk, 1999), the surface species postulated must be supported with spectroscopic evidence (e.g., Arai et al., 2007; Bargar et al., 2000, 1999). Thermodynamic surface speciation models typically include electrical double layer terms in the mass law equations, and hence, adsorption predictions with these models are sensitive to the double layer parameters, as has been shown for U(VI) adsorption on hematite (USNRC, 2003).

The sensitivity to electrostatic terms illustrates a significant practical problem in extending thermodynamic surface speciation models directly to simulate radionuclide adsorption on complex mineral assemblages in the environment. Mineral surfaces in the environment are typically coated with poorly crystalline secondary mineral coatings, as has been shown for the Naturita and Cape Cod aquifer sediments (Davis et al., 2004; USNRC, 2003; Sanpawanitchakit, 2002). The coatings make it extremely difficult to assess the electrostatic contribution to the free energy of adsorption quantitatively. In the literature one finds the frequently made assumption (e.g., Barnett et al., 2002; Arnold et al., 2001) that the electrical double layer properties of pure mineral phases studied in the laboratory are the same in a mineral assemblage in the environment. It seems highly unlikely that this assumption is valid given the fact that coatings of various materials on mineral surfaces are very prevalent in soils and sediments. In addition to the fact that coatings drastically change the electrical double layer at surfaces, the Component Additivity modeling approach is difficult to apply because the site densities of the mineral and organic phases in the coatings that are contributing to radionuclide adsorption are unknown (Davis et al., 2004; Davis et al., 2002; Sanpawanitchakit, 2002; Davis et al., 1998).

Table 5.1. Characteristics of Surface Complexation Modeling Approaches for Environmental Adsorbents

	Thermodynamic Surface Speciation Modeling¹	Semi-Empirical (GC) Modeling
A	Adsorption is predicted from thermodynamic constants and known (confirmed) surface species	Adsorption data are simulated (fit) using site-specific adsorbent samples, using chemically plausible surface reactions
B	Surface sites are unique and defined for each specific mineral phase present in environmental samples	Generic surface sites are assumed, with average chemical characteristics
C	Surface site densities are quantified by detailed characterization of the surface of environmental samples	Surface site densities are quantified by the measurement of specific surface area or by fitting adsorption data of environmental samples
D	Apparent stability constants and reaction stoichiometries are obtained from studies of adsorption by reference mineral phases present in environmental samples	Apparent stability constants and reaction stoichiometries are fit to experimental adsorption data for environmental samples
E	Overall adsorption is predicted by the sum of adsorption calculated for each specific mineral phase present in environmental samples	Numbers of surface site types and chemical reactions are increased as necessary to achieve good model simulations and to meet modeling objectives

¹ Thermodynamic surface speciation models that are developed by predicting adsorption as the sum of contributions from individual mineral phases are called Component Additivity models (Davis et al., 2004; Davis et al., 2002; Sanpawanitchakit, 2002; Davis et al., 1998; Honeyman, 1984). Characteristics D and E for thermodynamic surface speciation modeling in Table 5.1 apply to the Component Additivity modeling approach.

Thus, the challenge in applying the surface complexation concept in the environment is to simplify the adsorption model, such that predicted adsorption is still calculated with mass laws that are coupled with aqueous speciation, while lumping parameters that are difficult to characterize in the environment in with other parameters. This modeling approach can be achieved with the semi-empirical, site-binding (GC) modeling approach used in this report and elsewhere (Davis et al., 2004; Davis et al., 2002; Borkovec et al., 1998; Davis et al., 1998).

While a thermodynamic surface speciation model must be validated with spectroscopic evidence and other detailed data to confirm surface speciation and electrical double layer

properties (Hiemstra and van Riemsdijk, 1999), the GC modeling approach is more easily applied and less experimental data need to be collected. The range of applicability of a GC model with respect to chemical variation is determined by the type and amount of experimental data collected. GC model parameters are calibrated by fitting a simple surface speciation model such that the major features of radionuclide adsorption are simulated as chemical conditions are varied over field-relevant ranges (Curtis et al., 2004; Kohler et al., 2004; Davis et al., 2004; Davis et al., 1998).

An important limitation of the GC approach is that adsorption predictions should not be extrapolated to conditions outside of the range

for which data were collected for model calibration. However, a GC model can be used for predictive calculations that interpolate within the range of chemical conditions studied.

While the GC modeling approach has not been widely used to date, we believe it is a practical approach in terms of data collection needs and the capability to predict radionuclide distributions and transport over a range of chemical conditions at field sites (Curtis et al., 2006; Kent et al., 2000). The GC modeling approach is also an important compromise between the simple constant K_d approach and the most complex SCM, the thermodynamic surface speciation models (Hiemstra and van Riemsdijk, 1999). In order to be applied by solute transport modelers and within PA applications, the complexity of the adsorption model needs to be balanced with the goal of using the simplest model possible that is consistent with observed data. Historically, solute transport modelers have lacked the necessary expertise to apply the SCM modeling approach and many have believed that the SCM approach is too complex to be applied. While it is true that the thermodynamic surface speciation models are currently difficult to apply, it has been demonstrated in Curtis et al. (2006), USNRC (2003), and Kent et al. (2000) that the GC modeling approach can be easily applied to simulations of radionuclide transport at the field scale.

The GC models developed here for U(VI), Np(V) and Ni adsorption by aquifer sediments did not correct the mass laws with terms that estimate electrostatic attraction or repulsion of surface species by average surface charge. In USNRC (2003) it was shown that transport simulations were not sensitive to the use of non-electrostatic adsorption models by comparing simulations with and without explicit consideration of surface charge.

A limitation of the GC approach is that the mass action equations and associated stability constants are valid only for site-specific materials; a database that is transferable to other mineral assemblages is not expected. However, the GC approach is preferable to completely

empirical approaches, such as the constant K_d model or adsorption isotherms, because the important linkage between surface and aqueous species (and associated thermodynamic data) is retained in the modeling through the coupling of mass action equations.

Our current understanding and models for adsorption are well advanced at the molecular scale (Arai et al., 2007; Bargar et al., 2000), but our understanding and models become increasingly uncertain as the physical scale increases. The observed adsorption of radionuclides by aquifer sediments is ultimately controlled by sorptive phases with dimensions on the order of tens of nanometers. This inherent heterogeneity of environmental samples makes application of thermodynamic surface speciation models difficult at present, even at the microscale level. However, in the authors' opinion, the current operational paradigm that employs constant- K_d values for individual radionuclides introduces more uncertainty than is necessary in our predictions of radionuclide retardation during transport. This uncertainty could be reduced in the future with the use of site-binding (GC-SCM) models, such as described in this study. To reduce uncertainty, more emphasis needs to be placed on site-specific characterization of natural mineral assemblages that are expected to be encountered along major flowpaths away from disposal sites or other source areas. From a practical point of view, a limiting factor in applying any type of SCM is the knowledge of the spatial and temporal variation in aqueous chemical conditions and mineral surfaces exposed along flow paths in PA scenarios.

6 REFERENCES

- Al Mahamid I., Novak C. F., Becraft K. A., Carpenter S. A. and Hakem N. "Solubility of Np(V) in K-Cl-CO₃ and Na-K-Cl-CO₃ Solutions to High Concentrations: Measurements and Thermodynamic Model Predictions" *Radiochimica Acta*. 81, 93-101, 1998.
- Allard B., Olofsson U., Torstenfelt B., Kipatsi H. and Andersson K. "Sorption of Actinides in Well-defined Oxidation States on Geologic Media" *In Scientific Basis for Radioactive Waste Management - V*. Elsevier. Amsterdam. pp. 775-782, 1982.
- Altmann, S.A., J. Bruno, and C. Tweed, *Using Thermodynamic Sorption Models for Guiding Radioelement Distribution Coefficient (K_d) Investigations for Performance Assessment – A Status Report*, Nuclear Energy Agency, Paris, 2001.
- Arai Y., Moran P. B., Davis J. A. and Honeyman B. D. "In Situ Spectroscopic Evidence for Neptunium(V)-Carbonate Inner-Sphere and Outer-Sphere Ternary Surface Complexes on Hematite Surfaces" *Environmental Science and Technology*, 41, 3940-3944, 2007.
- Arnold, T. et al., "Sorption Behavior of U(VI) on Phyllite: Experiments and Modeling," *Journal of Contaminant Hydrology*, Vol. 47, No. 2, 219-231, 2001.
- Artinger R., Marquardt C. M., Kim J. I., Seibert A., Trautmann N. and Kratz J. V. "Humic Colloid-Borne Np Migration: Influence of the Oxidation State" *Radiochimica Acta*. 88, 609-612, 2000.
- Baes, C.F. and R.D. Sharp, "A Proposal for Estimation of Soil Leaching and Leaching Constants for Use in Assessment Models," *J. Environ. Quality*, Vol. 12, 17-28, 1983.
- Bargar, J.R., R. Reitmeyer, and J.A. Davis, "Spectroscopic Confirmation of Uranium(VI)-Carbonate Adsorption Complexes on Hematite," *Environmental Science & Technology*, Vol. 33, No. 14, 2481, 1999.
- Bargar, J.R. et al., "Characterization of U(VI)-Carbonate Ternary Complexes on Hematite: EXAFS and Electrophoretic Mobility Measurements," *Geochim. Cosmochim. Acta*, Vol. 64, No. 16, 2737-2749, 2000.
- Barnett, M.O., P.M. Jardine, and S.C. Brooks, "U(VI) Adsorption to Heterogeneous Subsurface Media: Application of a Surface Complexation Model," *Environmental Science and Technology*, Vol. 36, 937-942, 2002.
- Beall G. W. and Allard B. *Chapter 10: Sorption of Actinides from Aqueous Solutions Under Environmental Conditions*. In *Adsorption from Aqueous Solutions*. Plenum Press. New York, NY. pp 193-212, 1981.
- Bernhard, G., et al., "Uranyl(VI) carbonate complex formation: Validation of the Ca₂UO₂(CO₃)₃ (aq) species", *Radiochim. Acta*, Vol. 89, 511-518, 2001.
- Berry, J.A., "A Review of Sorption of Radionuclides under Near- and Far-Field Conditions of an Underground Radioactive Waste Repository: Parts I, II, and III," Oxfordshire, United Kingdom, Her Majesty's Inspectorate of Pollution/Department of the Environment, Harwell Laboratory, DOE/HMIP/RR/92/061, 1992.

Bertetti P. F., Pabalan R. T. and Turner D. R. "Neptunium(V) Sorption Behavior on Clinoptilolite, Quartz and Montmorillonite" *Materials Research Society Symposium Proceedings*. 412, 631-638, 1996.

Bertetti F. P., Pabalan R. T. and Almendarez M. G. "Studies on Neptunium(V) Sorption on Quartz, Clinoptilolite, Montmorillonite, and α -Alumina" *In Adsorption of Metals by Geomedia*. Academic Press. San Diego, CA. pp. 131- 148, 1998.

Bertetti F. P. *Laboratory and Modeling Studies of Neptunium Uptake on Calcite*. Center for Nuclear Waste Regulatory Analyses. Center for Nuclear Waste Regulatory Analyses, Southwest Research Institute, San Antonio, TX. U. S. Nuclear Regulatory Commission. Contract NRC-02-97-009, 2002.

Bertetti F. P., Werling B. and Roberts M. M. *Retention of Neptunium in the Saturated Alluvial Sediments of Fortymile Wash, Nye County, Nevada*. Center for Nuclear Waste Regulatory Analyses, Southwest Research Institute, San Antonio, TX, 2006.

Bethke C. M. and Brady P. V. "How the Kd Approach Undermines Ground Water Cleanup" *Ground Water*, Vol. 38, 435-443, 2000.

Bidoglio G., Offermann P. and Saltelli A. "Neptunium Migration in Oxidizing Clayey Sand" *Applied Geochemistry*. 2, 275-284, 1987.

Bonnissel-Gissinger P., Alnot M., Lickes J.-P., Ehrhardt I.-J., Behra P. "Modeling the Adsorption of Mercury(II) on (Hydr)oxides. II: α -FeOOH (Goethite) and Amorphous Silica" *Journal of Colloid and Interfacial Science*. 215, 312 – 322, 1999.

Borkovec, M., U. Rusch, and J.C. Westall, "Modeling of Competitive Ion Binding to Heterogeneous Materials with Affinity Distribution," *Adsorption of Metals by Geomedia*, Academic Press, 467-482, 1998.

Bradbury M. H. and Baeyens B. "Modelling Sorption Data for the Actinides Am(III), Np(V) and Pa(V) on Montmorillonite" *Radiochimica Acta*. 94, 619-625, 2006.

Burney G. A. and Harbour R. M. *Radiochemistry of Neptunium*. U. S. Atomic Energy Commission. Oak Ridge, TN, 1974.

Cernik M., Borkovec M. and Westall J. C. "Regularized Least-squares Methods for the Calculation of Discrete and Continuous Affinity Distributions for Heterogeneous Sorbents" *Environmental Science and Technology*. 29, 413-425, 1995.

Charlet, L. and Sposito, G. "Monovalent ion adsorption by an oxisol" *Soil Sci.Soc.Amer. J.*, 51, 1155-1160, 1987.

Choppin G. R. and Unrein P. J. "Thermodynamics Study of Actinide Fluorine Complexation. *In* Transplutonium Elements" North Holland, Amsterdam. pp. 97-107, 1976.

Choppin G. R. "Actinide Solution Chemistry" *Radiochimica Acta*. Vol. 32, 43-53, 1983.

Chunli L., Yuee Y., Zhiming W., Shushen L., Zede G., Bing L., Ling J., Hong J., Ling W., Dan L. and Zhongde D. "Influence of Humic Substances on the Migration of ^{237}Np , ^{238}Pu and ^{241}Am in a Weak Loess Aquifer" *Radiochimica Acta*. 89, 387-391, 2001.

- Clark D. L., Hobart D. E. and Neu M. P. "Actinide Carbonate Complexes and Their Importance in Actinide Environmental Chemistry" *Chemical Reviews*. Vol. 95, 25-48, 1995.
- Clark D. L., Conradson S. D., Ekberg S. A., Hess N. J., Neu M. P., Palmer P. D., Runde W. and Tait C. D. "EXAFS Studies of Pentavalent Neptunium Carbonate Complexes. Structural Elucidation of the Principle Constituents of Neptunium in Groundwater Environments" *Journal of the American Chemical Society*. 118, 2089-2090, 1996.
- Combes J., Chisholm-Brause C. J., Brown G. E., Parks G. A., Conradson S. D., Eiler P. G., Triay I. R., Hobart D. E. and Meljer A. "EXAFS Spectroscopic Study of Neptunium(V) Sorption at the α -FeOOH/Water Interface" *Environmental Science & Technology*. 26, 376-382, 1992.
- Coston, J.A., C.C. Fuller, and J.A. Davis, "Pb²⁺ and Zn²⁺ Adsorption by a Natural Aluminum- and Iron-bearing Surface Coating on an Aquifer Sand," *Geochim. Cosmochim. Acta*, Vol. 59, No. 17, 3535-3547, 1995.
- Cowan, C.E., Zachara, J.M, Smith, S.C., and Resch, C.T. "Individual sorbent contributions to cadmium sorption on ultisols of mixed mineralogy" *Soil Sci.Soc.Amer. J.*, 56, 1084-1094, 1992.
- Crowley, K.D. and J.F. Ahearne, "Managing the Environmental Legacy of U.S. Nuclear Weapons Production," *American Scientist*, Vol. 90, 514-523, 2002.
- Curtis, G.P., Fox, P., Kohler, M., and Davis, J. A. "Comparison of field uranium K_d values with a laboratory determined surface complexation model" *Applied Geochemistry*, Vol. 19, 1643-1653, 2004.
- Curtis G. P., Davis J. A. and Naftz D. L. "Simulation of Reactive Transport of Uranium(VI) in Groundwater with Variable Chemical Conditions" *Water Resources Research*. Vol. 42, W04404, 2006.
- Dahlman R. C., Bondietti E. A. and Eyman L. D. *Biological Pathways and Chemical Behavior of Plutonium and Other Actinides in the Environment*. In Actinides in the Environment. ACS Symposium Series No. 35, American Chemical Society, Washington, DC, 1976.
- Davis, J.A. and J.O. Leckie, "Effect of Adsorbed Complexing Ligands on Trace Metal Uptake by Hydrous Oxides," *Environ. Sci. Technol.*, Vol. 12, 1309-1315, 1978.
- Davis J. A. and Kent D. B. "Surface Complexation Modeling in Aqueous Geochemistry. Mineral-Water Interface Geochemistry" *Reviews in Mineralogy Series. Mineralogical Society of America*. Vol. 23, 177-260, 1990.
- Davis J. A., Coston J. A., Kent D. B., and Fuller C. C. "Application of the Surface Complexation Concept to Complex Mineral Assemblages" *Environmental Science and Technology*. Vol. 32, 2820-2828, 1998.
- Davis, J.A., Curtis, G.P., Wilkins, M.J., Kohler, M., Fox, P.M., Naftz, D.L., and Lloyd, J.R., "Processes affecting transport of uranium in a suboxic aquifer" *Physics and Chemistry of the Earth*, 31, 548-555, 2006.
- Davis, J.A., Kent, D.B., Coston, J.A., Hess, K.M., and Joye, J.L., "Multispecies reactive tracer test in an aquifer with spatially variable chemical conditions" *Water Resources Research*, Vol.. 36, 119-134, 2000.

Davis J.A., Meece D. E., Kohler M. and Curtis G. P. "Approaches to Surface Complexation Modeling of Uranium(VI) Adsorption on Aquifer Sediments" *Geochimica et Cosmochimica Acta*. Vol. 68, 3621-3641, 2004.

Davis J A., T.E. Payne, and T.D. Waite, "Simulating the pH and pCO₂ Dependence of Uranium(VI) Adsorption by a Weathered Schist with Surface Complexation Models," *Geochemistry of Soil Radionuclides*, Soil Science Society America, Madison, Chap. 4, p. 61-86, 2002.

Del Nero M., Madé B., Bontems G. and Clément A. "Adsorption of Neptunium(V) on Hydrargillite. Application of the Non-Electrostatic Model" *Radiochimica Acta*. 76, 219-228, 1997.

Del Nero M., Saïd B. K., Madé B., Clément A. and Bontems G. "Effect of pH and Carbonate Concentration in Solution on the Sorption of Neptunium(V) by Hydrargillite. Application of the Non-Electrostatic Model" *Radiochimica Acta*. 81, 133-141, 1998.

Del Nero M., Assada A., Madé B., Barillon R. and Duplâtre G. "Surface Charge and Np(V) Sorption on Amorphous Al and Fe Silicates" *Chemical Geology*. 211, 15-45, 2004.

Dove P. M. and Elston S. F. "Dissolution Kinetics of Quartz in Sodium Chloride Solutions: Analysis of Existing Data and a Rate Model for 25°C" *Geochimica et Cosmochimica Acta*. 56, 4147-4156, 1992.

Dozol M. and Hagemann R. "Radionuclide Migration in Groundwaters: Review of the Behaviour of Actinides" *International Union of Pure and Applied Chemistry*. 65, 1081-1102, 1993.

Dzombak D. A. and Morel F. M. M. *Surface Complexation Modeling: Hydrous Ferric Oxide*. John Wiley and Sons. New York, NY, 1990.

Eckhardt R. C. "Yucca Mountain: Looking Ten Thousand Years into the Future" *Los Alamos Science*. 26, 464-489, 2000.

Efurd D. W., Runde W., Banar J. C., Janecky D. R., Kaszuba J. P., Palmer P. D., Roensch F. R. and Tait C. D. "Neptunium and Plutonium Solubilities in a Yucca Mountain Groundwater" *Environmental Science and Technology*. 32, 3893-3900, 1998.

Fox, P.M., Davis, J.A., and Zachara, J.M, "The effect of calcium on aqueous uranium (VI) speciation and adsorption to ferrihydrite and quartz" *Geochimica et Cosmochimica Acta*, 70, 1379-1387, 2006.

Fujita T., Tsukamoto M., Ohe T., Nakayama S. and Sakamoto Y. "Modeling of Neptunium (V) Sorption Behavior onto Iron-containing Minerals" *Materials Research Society Symposium Proceedings*. 353, 965-972, 1995.

Girvin D. C., Ames L. L., Schwab A. P. and McGarrah J. E. "Neptunium Adsorption on Synthetic Amorphous Iron Oxyhydroxide" *Journal of Colloid and Interfacial Science*. 141, 67-78, 1991.

Glynn P. D. "Modeling Np and Pu Transport with a Surface Complexation Modeling and Spatially Variant Sorption Capacities: Implications for Reactive Transport Modeling and Performance Assessments of Nuclear Waste Disposal Sites" *Computers and Geosciences*. 29, 331-349, 2003.

Grenthe, I. et al., *Chemical Thermodynamics of Uranium*, Elsevier, Amsterdam, 1992.

- Grenthe I., Robouch P. and Vitorge P. "Chemical Equilibria in Actinide Carbonate Systems" *Journal of Less Common Minerals*. 122, 225-231, 1986.
- Grossman C. J., Field R. A., Coates J. T. and Elzerman A. W. "The Sorption of Selected Radionuclides in Sedimentary Interbed Soils from the Snake River Plain" INEEL/EXT-01-01106. Idaho National Engineering and Environmental Laboratory, Idaho Falls, ID, 2001.
- Guillaumont R., Fanghänel T., Fuger J., Grenthe I., Neck V., Palmer D. A. and Rand M. H. *Update on Chemical Thermodynamics of Uranium, Neptunium, Plutonium, Americium and Technetium*. Elsevier. Amsterdam, 2003.
- Hagan P. G. and Cleveland J. M. "The Absorption Spectra of Neptunium Ions in Perchloric Acid Solutions" *Journal of Inorganic Nuclear Chemistry*. 28, 2905-2909, 1966.
- Herbelin A.L. and Westall J. C. FITEQL 4.0: A Computer Program for Determination of Chemical Equilibrium Constants from Experimental Data; Report 99-01. Department of Chemistry, Oregon State University. Corvallis, Oregon, 1999.
- Hiemstra T. and van Riemsdijk W. H. "Surface Structural Ion Adsorption Modeling of Competitive Binding of Oxyanions by Metal (Hydr)oxides" *Journal of Colloid and Interfacial Science*. 210, 182-193, 1999.
- Honeyman B. D. Cation and Anion Adsorption at the Oxide/Solution Interface in Systems Containing Binary Mixtures of Adsorbents: An Investigation of the Concept of Adsorptive Additivity. Ph.D. Thesis. Stanford University. Stanford, California, 1984.
- Horrocks D. L. *Applications of Liquid Scintillation Counting*. Academic Press. New York, NY, 1976.
- Isherwood, D. "Geoscience Data Base Handbook for Modeling a Nuclear Waste Repository," U. S. Nuclear Regulatory Commission, NUREG/CR-0912, Vol. 1, 1981.
- Kalmykov, S.N. and Choppin, G.R., "Mixed $\text{Ca}^{2+}/\text{UO}_2^{2+}/\text{CO}_3^{2-}$ complex formation at different ionic strengths", *Radiochim. Acta*, Vol. 88, 603-606, 2000.
- Kantar C., Gillow J. B., Harper-Arabie R., Honeyman B. D. and Francis A. J. "Determination of Stability Constants of U(VI)-Fe(III)-Citrate Complexes" *Environmental Science and Technology*. 39, 2161-2168, 2005.
- Kaplan D. I and Serne R. J. Distribution Coefficient Values Describing Iodine, Neptunium, Selenium, Technetium, and Uranium Sorption to Hanford Sediments. PNL-10379. Pacific Northwest National Laboratory. Richland, WA, 1995.
- Katz J. J., Seaborg G. T. and Morss L. R. *The Chemistry of Actinide Elements*. Chapman and Hall. New York, NY, 1986.
- Keeney-Kennicutt W. L. and Morse J. W. "The Interaction of Np(V)O_2^{2+} with Common Mineral Surfaces in Dilute Aqueous Solutions and Seawater" *Marine Chemistry*. 15, 133-150, 1984.
- Kent D. B., Abrams R. H., Davis J. A., Coston J. A. and LeBlanc D. R. "Modeling the Influence of Variable pH on the Transport of Zinc in a Contaminated Aquifer using Semiempirical Surface Complexation Modeling" *Water Resources Research*. Vol. 36, 3411-3425, 2000.

- Kohler, M. et al., "Experimental Investigation and Modeling of Uranium(VI) Transport under Variable Chemical Conditions," *Water Resour. Res.*, Vol. 32, No. 12, 3539-3551, 1996.
- Kohler, M., Meece, D.M., Curtis, G.P., and Davis, J.A., "Methods for estimating adsorbed uranium(VI) and distribution coefficients in contaminated sediments" *Environmental Science and Technology*, Vol. 38, 240-247, 2004.
- Kohler M., Honeyman B. D. and Leckie J. O. "Neptunium(V) Sorption of Hematite in Aqueous Suspension: The Effect of CO₂" *Radiochimica Acta*. 85, 33-48, 1999.
- Koretsky C. "The Significance of Surface Complexation Reactions in Hydrologic Systems: A Geochemist's Perspective" *Journal of Hydrology*. 230, 127-171, 2000.
- Kozai N., Ohnuki T. and Muraoka S. "Sorption Characteristics of Neptunium by Sodium-Smectite" *Journal of Nuclear Science and Technology*. 30, 1153-1159, 1993.
- Kozai N., Ohnuki T. and Muraoka S. "Sorption Behavior of Neptunium on Bentonite- Effect of Calcium Ion on the Sorption" *Materials Research Society Symposium Proceedings*. 353, 1021- 1028, 1995.
- Krupka, K.M., and J.R. Serne, "Input Vault and Sorption Values for Use in the NRC Low-Level Radioactive Waste Performance Assessment Test Case," Richland, Washington, Pacific NW Laboratory/Water and Land Resource. Dept., Task Order 1, Letter Rept., October 1, 1996.
- Kumata M. and Vandergraaf T. T. "Experimental Study on Neptunium Migration under In Situ Geochemical Conditions" *Journal of Contaminant Hydrology*. 35, 31-40, 1998.
- Kung K. S. and Triay I. R "Effect of Natural Organic Materials on Cadmium and Neptunium Sorption" LA-UR 94-3303. Los Alamos National Laboratory. Los Alamos, NM, 1994.
- Langmuir, D., *Aqueous Environmental Chemistry*, Prentice-Hall, Upper Saddle River, NJ, 1997.
- Leiser K. H. and Mühlenweg U. "Neptunium in the Hydrosphere and in the Geosphere. I. Chemistry of Neptunium in the Hydrosphere and Sorption of Neptunium from Groundwaters on Sediments under Aerobic and Anaerobic Conditions" *Radiochimica Acta*. 43, 27-35, 1988.
- Lemire R. J., Fuger J., Nitsche H., Potter P., Rand M. H., Rydberg J., Spahiu K., Sullivan J. C., Ullman W. J., Vitorge P. and Wanner H. *Chemical Thermodynamics of Neptunium and Plutonium*. Elsevier. Amsterdam, 2001.
- Lenhart J. J. *Application of Surface Complexation Modeling to the Adsorption of Uranium(VI) onto Hematite in the Presence of Humic and Fulvic Acid*, Ph.D. Thesis. Colorado School of Mines. Golden, Colorado, 1997.
- Lenhart J. J. and Honeyman B. D. "Reactions at the Solid/Solution Interface: Fe-Oxides and Hydroxides. Uranium(VI) Sorption to Hematite in the Presence of Humic Acid" *Geochimica et Cosmochimica Acta*. 63, 2891-2901, 1999.
- Lenhart J. J., Cabaniss S. E., MacCarthy P. and Honeyman B. D. "Uranium(VI) Complexation with Citric, Humic and Fulvic Acids" *Radiochimica Acta*. 88, 345-353, 2000.

Lierse C., Treiber W. and Kim J. I. "Hydrolysis Reactions of Neptunium (V)" *Radiochimica Acta*. 38, 27-28, 1985.

Livens F. R., Jones M. J., Hayes A. J., Charnock J. M., Mosselmans J. F. W., Hennig C., Steele H., Collison D., Vaughan D. J., Patrick R. A. D., Reed W. A. and Moyes L. N. "X-ray Absorption Spectroscopy Studies of Reactions of Technetium, Uranium and Neptunium with Mackinawite" *Journal of Environmental Radioactivity*. 74, 211-219, 2004.

Looney, B.B. et al., "Estimation of Geochemical Parameters for Assessing Subsurface Transport at the Savannah River Plant," Aiken, S.C, Savannah River Lab., DPST-85-904, 1987.

Lützenkirchen, J., Boily, J-F., Lövgren, L., and Sjöberg, S. "Limitations of the potentiometric titration technique in determining the proton active site density of goethite surfaces" *Geochimica et Cosmochimica Acta* 66, 3389-3396, 2002.

Maya L. "Hydrolysis and Carbonate Complexation of Dioxoneptunium(V) in 0.1 M NaClO₄ at 25°C" *Inorganic Chemistry*, 22, 2093-2095, 1983.

McCubbin D. and Leonard K. S. "Influence of Some Seawater Components on the Sorption Behavior of Neptunium(V)" *Radiochimica Acta*. 69, 97-102, 1995.

McCubbin D. and Leonard K. S. "Laboratory Studies to Investigate Short-Term Oxidation and Sorption Behavior of Neptunium in Artificial and Natural Seawater Solutions" *Marine Chemistry*. 56, 107-121, 1997.

McKinley G. and Scholtis A. "A Comparison of Radionuclide Sorption Databases Used in Recent Performance Assessment". *Journal of Contaminant Hydrology*. 13, 347-363, 1993.

Merli L. and Fuger J. "Thermochemistry of a Few Neptunium and Neodymium Oxides and Hydroxides" *Radiochimica Acta*. 66/67, 109-113, 1994.

Miller R. W. and Gardiner D. T. *Soils in Our Environment*. 8th Edition. Prentice-Hall Publishers. Upper Saddle River, NJ, 1998.

Mincher B. J., Fox R. V., Cooper D. C. and Groenewold G. S. "Neptunium and Plutonium Sorption to Snake River Plain, Idaho Soil" *Radiochimica Acta*. 91, 397-401, 2003.

Moran, P. B., *Neptunium(V) Sorption To An Alluvial Aquifer Sediment Under Environmentally Relevant Conditions: Applicability Of Surface Complexation Modeling*, PhD. Thesis, Colorado School of Mines, 2007.

Morrison, S.J. and L.S. Cahn, "Mineralogical Residence of Alpha-emitting Contamination and Implications for Mobilization from Uranium Mill Tailings," *J. Contam. Hydrol.*, 8, 1-21, 1991.

X Morse J. W. and Choppin G. R. "The Chemistry of Transuranic Elements in Natural Waters" *Reviews in Aquatic Sciences*. 4, 1-22, 1991

Moyes L. N., Jones M. J., Reed W. A., Livens F. R., Charnock J. M., Mosselmans F. W., Hennig C., Vaughan D. J. and Patrick R. A. D. "An X-Ray Absorption Study of Neptunium(V) Reactions with Mackinawite (FeS)" *Environmental Science and Technology*. 36, 179-183, 2002.

Nagasaki S., Tanaka S., Todoriki M. and Suzuki A. "Sorption Equilibrium and Kinetics of NpO_2^+ Uptake onto Illite" *Radiochimica Acta*. 82, 263-267, 1998.

Nagasaki S. and Tanaka S. « Sorption Equilibrium and Kinetics of NpO_2^+ on Dispersed Particles of Na-Montmorillonite » *Radiochimica Acta*. 88, 705-709, 2000.

Nakata K., Nagasaki S., Tanaka S., Sakamoto Y., Tanaka T. and Ogawa H. "Sorption and Desorption Kinetics of Np(V) on Magnetite and Hematite" *Radiochimica Acta*. 88, 453-457, 2000.

Nakata K., Nagasaki S., Tanaka S., Sakamoto Y., Tanaka T. and Ogawa H. "Sorption and Reduction of Neptunium(V) on the Surface of Iron Oxides" *Radiochimica Acta*. 90, 665-669, 2002.

Nakayama S. and Sakamoto Y. « Sorption of Neptunium on Naturally-Occurring Iron-Containing Minerals » *Radiochimica Acta*. 52/53, 153-157, 1991.

NEA, *NEA Sorption Project Phase II: Interpretation and Prediction of Radionuclide Sorption onto Substrates Relevant for Radioactive Waste Disposal Using Thermodynamic Sorption Models*, Nuclear Energy Agency, OECD Rept. 5992, Paris, 2005.

Neck V., Kim J. I. and Kanellakopoulos B. "Solubility and Hydrolysis Behavior of Neptunium(V)" *Radiochimica Acta*. 56, 25-30, 1992.

Neck V., Runde W., Kim J. I. and Kanellakopoulos B. "Solid-Liquid Equilibrium Reactions of Neptunium(V) in Carbonate Solution at Different Ionic Strength" *Radiochimica Acta*. 65, 29-37, 1994.

Neck V., Runde W. and Kim J. I. "Solid-Liquid Equilibria of Neptunium(V) in Carbonate Solutions of Different Ionic Strengths: II. Stability of the Solid Phases" *Journal of Alloys and Compounds*. 225, 295-302, 1995.

Niitsu Y., Sato S., Ohashi H., Sakamoto Y., Nagao S., Ohnuki T. and Muraoka S. "Effects of Humic Acid on the Sorption of Neptunium(V) on Kaolinite" *Journal of Nuclear Materials*. 248, 328-332, 1997.

Nishita H., Wallace A., Romney E. M and Schulz R. K. "Effect of Soil Type on the Extractability of Np-237 , Pu-239 , Am-241 , and CM-244 as a Function of pH" *Soil Science*. 132, 25-34, 1981.

Novak C. F., Al Mahamid I., Becraft K. A., Carpenter S. A., Hakem N. and Prussin T. "Measurement and Thermodynamic Modeling of Np(V) Solubility in Aqueous K_2CO_3 Solutions to High Concentrations" *Journal of Solution Chemistry*. 26, 681-697, 1997.

Pabalan, R.T. et al., "Uranium(VI) Sorption onto Selected Mineral Surfaces: Key Geochemical Parameters," *Adsorption of Metals by Geomedia*, Academic Press, p. 99-130, 1998.

Pabalan, R.T. and D.R. Turner, "Uranium(6+) Sorption on Montmorillonite: Experimental and Surface Complexation Modeling Study," *Aquatic Geochemistry*, Vol. 2, 203-226, 1996.

Padmanabhan, E. and A. R. Mermut, "Submicroscopic Structure of Fe-coatings on Quartz Grains in Tropical Environments," *Clays and Clay Minerals*, Vol. 44, 801-810, 1996.

Paulus J. M., Bontems G. and Schleiffer, J. J. "Neptunium (V and VI) Exchange between Silicate Gels and Aqueous Solutions" *Applied Clay Science*. 7, 71-78, 1992.

Payne T. E., Davis J. A., Ochs M., Olin M. and Tweed C. J. "Uranium Adsorption on Weathered Schist- Intercomparison of Modelling Approaches" *Radiochimica Acta*. 92, 651-661, 2004.

Penn, R.L. et al., "Iron Oxide Coatings on Sand Grains from the Atlantic Coastal Plain: High-resolution Transmission Electron Microscopy Characterization," *Geology*, Vol. 29, 843-846, 2001.

Prikryl, J.D. et al., "Uranium(VI) Sorption Behavior on Silicate Mineral Mixtures," *J. Contam. Hydrol.*, Vol. 47, 241-253, 2001.

Rea, B.A., Kent, D.B., LeBlanc, D.R., and Davis, J.A. "Mobility of Zn in a sewage-contaminated aquifer, Cape Cod, Massachusetts" in U. S. Geological Survey Toxic Substances Hydrology Program-- Proceedings of the Technical Meeting, Monterey, California, March 11-15, 1991 (G. E. Mallard and D. A. Aronson, eds., Water Resources Investigations Report 91-4304, p. 88-95, 1991.

Righetto L., Bidoglio G., Marcandalli B. and Bellobono I. R. "Surface Interactions of Actinides with Alumina Colloids" *Radiochimica Acta*. 44/45, 73-75, 1988.

Righetto L., Bidoglio G., Azimonti G. and Bellobono I. R. "Competitive Actinide Interactions in Colloidal Humic Acid Mineral Oxide Systems" *Environmental Science and Technology*. 25, 1913-1919, 1991.

Routson R. C., Jansen G. and Robinson A. V. "Sorption of Tc, Np and Am-241 on Two Subsoils From Differing Weathering Intensity Areas" BNWL-1889. Pacific Northwest Laboratories. Richland, WA, 1975.

Routson R. C., Jansen G. and Robinson A. V. ^{241}Am , ^{237}Np , and ^{99}Tc Sorption on Two United States Subsoils from Differing Weathering Intensity Areas. *Health Physics*. 33, 311-317, 1976.

Runde W. and Kim J. I. "Chemical Behavior of Tri- and Pentavalent Americium in Saltwater NaCl Solutions" University of Munich. Munich, Germany, 1995.

Runde W., Conradson S. D, Efurud E. W., Lu N-P., VanPelt C. E. and Tait C. D. "Solubility and Sorption of Redox-Sensitive Radionuclides (Np, Pu) in J-13 Water from the Yucca Mountain Site: Comparison Between Experiment and Theory" *Applied Geochemistry*. 17, 837-853, 2002.

Sahai, N. and D. A. Sverjensky, "Solvation and Electrostatic Model for Specific Electrolyte Adsorption," *Geochim. Cosmochim. Acta*, Vol. 61, 2827-2848, 1997.

Sakamoto Y., Nagao S., Ogawa H. and Rao R. R. "The Migration Behavior of Np(V) in Sandy Soil and Granite Media in the Presence of Humic Substances" *Radiochimica Acta*. 88, 651-656, 2000.

Sanpawanitchakit C. "The Application of Surface Complexation Modeling to the Adsorption of Uranium (VI) on Natural Composite Materials" Ph.D. Thesis. Colorado School of Mines. Golden, Colorado, 2002.

Schmeide, K., Pompe, S., Bubner, M., Heise, K.H., Bernhard, G. and Nitsche, H. "Uranium(VI) sorption onto phyllite and selected minerals in the presence of humic acid" *Radiochim. Acta*, 88, 723-728, 2000.

Serne R. J., Conca J. L., LeGore V. L., Cantrell K. J., Lindenmeier C. W., Cambell J. A., Amonette J. E. and Wood M. I. Solid-Waste Leach Characteristics and Contaminant Sediment Interactions. Volume 1: Batch Leach and Adsorption Tests and Sediment Characterization. PNL-8889. Pacific Northwest National Laboratory. Richland, WA, 1993.

Sheppard, M.I. and D.H. Thibault, "Default Soil Solid/Liquid Partition Coefficients, K_d s, for Four Major Soil Types: A Compendium," *Health Physics*, Vol. 59, 471-482, 1990.

Sherman C., Vial M., Plaue J., Noyes K., Czerwinski K., Hermes A. and Reed D. "Chemical Speciation of Neptunium in Spent Nuclear Fuel" Massachusetts Institute of Technology. DE-FG03-99SF21903. Cambridge, MA, 2000.

Siebert A., Mansel A., Marquardt C. M., Keller H., Kratz J. V. and Trautmann N. "Complexation Behavior of Neptunium with Humic Acid" *Radiochimica Acta*. 89, 505-510, 2001.

Silva R. J. and Nitsche H. "Actinide Environmental Chemistry" *Radiochimica Acta*. 70/71, 377-396, 1995.

Silva, R.J. et al., "Thermodynamics 2; Chemical Thermodynamics of Americium," with an appendix on "Chemical Thermodynamics of Uranium," Nuclear Energy Agency, OECD, North-Holland, Elsevier, 1995.

Sposito G. "On Points of Zero Charge" *Environmental Science and Technology*. 32, 2815 – 2819, 1998.

Sverjensky D. A. and Sahai N. "Theoretical Prediction of Single-site Surface-Protonation Equilibrium Constants for Oxides and Silicates in Water" *Geochimica Cosmochimica Acta*. 60, 3773 – 3797, 1996.

Ticknor K. V. "Actinide Sorption by Fracture-Infilling Minerals" *Radiochimica Acta*. 60, 33-42, 1993.

Tochiyama O., Endo S. and Inoue Y. Sorption of Neptunium(V) on Various Iron Oxides and Hydrous Iron Oxides. *Radiochimica Acta*. 68, 105-111, 1995.

Tochiyama O., Yamazaki H. and Mikami T. Sorption of Neptunium(V) on Various Aluminium Oxides and Hydrous Aluminium Oxides *Radiochimica Acta*. 73, 191-198, 1996.

Torstenfelt B., Rundberg R. S. and Mitchell A. J. "Actinide Sorption on Granites and Minerals as a Function of pH and Colloids/Pseudocolloids" *Radiochimica Acta*. 44/45, 111-117, 1988.

Triay I. R., Robinson B. A., Lopez R. M., Mitchell A. J. and Overly C. M. Neptunium Retardation with Tuffs and Groundwaters From Yucca Mountain. 1993 International High-Level Radioactive Waste Management Conference. Las Vegas, Nevada, April 26-30, 1993.

Triay I. R., Furlano A. C., Weaver S. C., Chipera S. J. and Bish D. L. Comparison of Neptunium Sorption Results Using Batch and Column Techniques, Yucca Mountain Site Characterization Program, Milestone 3041. LA-12958-MS. Los Alamos National Laboratory. Los Alamos, NM, 1996.

Turner, D., "A Uniform Approach to Surface Complexation Modeling of Radionuclide Sorption," CNWRA Rept. 95-001, Center for Nuclear Waste Regulatory Analyses, San Antonio, TX, 1995.

Turner D. R., Pabalan R. T. and Bertetti P. F. "Neptunium(V) Sorption of Montmorillonite: An Experimental and Surface Complexation Modeling Study" *Clays and Clay Minerals*. 43, 256-269, 1998.

- Turner D. R. and Sassman S. A. "Approaches to Sorption Modeling for High-level Waste Performance Assessment" *Journal of Contaminant Hydrology*. 21, 311-332, 1996.
- USEPA, "Soil Screening Guidance: User's Guide," EPA/540/R-96/018, Washington, D. C., 1996.
- USEPA, *Understanding Variation in Partition Coefficient, K_d, Values. Volume 1*. Report EPA 402-R-99 – 0044A. U. S. Environmental Protection Agency. Washington, DC, 1999.
- USNRC, *Critical Review: Radionuclide Transport, Sediment Transport and Water Quality Mathematical Modeling; and Radionuclide Adsorption/Desorption Mechanisms*. Report NUREG/CR-1322, U. S. Nuclear Regulatory Commission, Washington, DC, 1981.
- USNRC, *Surface Complexation Modeling of Uranium(VI) Adsorption on Natural Mineral Assemblages*, U.S. Nuclear Regulatory Commission, NUREG/CR-6708, 2001.
- USNRC, *Application of Surface Complexation Modeling to Describe Uranium(VI) Adsorption and Retardation at the Uranium Mill Tailings Site at Naturita, Colorado*. Report NUREG CR-6820. U. S. Nuclear Regulatory Commission, Rockville, MD, 2003.
- USNRC *Risk Insights Baseline Report*. U. S. Nuclear Regulatory Commission. Rockville, MD, 2004.
- van Benschoten, J. E., Young, W. H., Matsumoto, M. R., and Reed, B. E. "A nonelectrostatic surface complexation model for lead sorption on soils and mineral surfaces" *J. Environ. Qual.* 27, 24-30, 1998.
- Van Geen A., Robertson A. P. and Leckie J. O. "Complexation of Carbonate Species at the Goethite Surface: Implications for Adsorption of Metal Ions in Natural Waters" *Geochimica et Cosmochimica Acta*. 58, 2073–2086, 1994.
- Waite, T.D. et al., "Uranium(VI) Adsorption to Ferrihydrite; Application of a Surface Complexation Model," *Geochim. Cosmochim. Acta*, Vol. 58, No. 24, 5465-5478, 1994.
- Waite, T.D. et al., "Approaches to Modelling Uranium(VI) Adsorption on Natural Mineral Assemblages," *Radiochim Acta*, Vol. 88, No. 9/11, 687-699, 2000.
- Wang, P., Anderko, A., and Turner, D. R., "Thermodynamic Modeling of the Adsorption of Radionuclides on Selected Minerals. I: Cations" *Ind. Eng. Chem. Res.* 40, 4428-4463, 2001.
- Weerasooriya R., D. Aluthpatabendi, and H.J. Tobschall, "Charge Distribution Multi-site Complexation (CD-MUSIC) Modeling of Pb(II) Adsorption on Gibbsite," *Colloids and Surfaces A-Physicochemical and Engineering Aspects*, Vol. 189, 131-144, 2001.
- Weijuan L. and Zuyi T. "Sorption and Desorption of Neptunium(V) on Calcareous Soil and its Solid Components: A Comparative Study" *Journal of Radioanalytical and Nuclear Chemistry*. 258, 659-664, 2003.
- Westall J. C., Jones J. D., Turner G. D. and Zachara J. M. "Models for the Association of Metal Ions with Heterogeneous Environmental Sorbents. 1. Complexation of Co(II) by Leonardite Humic Acid as a Function of pH and NaClO₄ Concentration" *Environmental Science and Technology*. 29, 951-959, 1995.

Westall, J. C., M. Cernik, and M. Borkovec, "Modeling metal speciation in aquatic systems", in *Metals in Surface Water*, Ann Arbor Press, p. 191-216, 1998.

Wilk P.A., Shaughnessy D. A., Wilson R. E. and Nitsche H. "Interfacial Interactions between Np(V) and Manganese Oxide Minerals Manganite and Hausmannite" *Environmental Science and Technology*. 39, 2608-2615, 2005.

Yamaguchi T., Nakayama S. and Yoshida T. "Interactions Between Anionic Complex Species of Actinides and Negatively Charged Mineral Surfaces" *Radiochimica Acta*. 92, 677 – 682, 2004.

Zavarin M. and Bruton C. J. *A Non-Electrostatic Surface Complexation Approach to Modeling Radionuclide Migration at the Nevada Test Site: II. Aluminosilicates*. UCRL-TR-208672. U.S. Department of Energy. Lawrence Livermore National Laboratory. Livermore, CA, 2004a

Zavarin M. and Bruton C. J. *A Non-Electrostatic Surface Complexation Approach to Modeling Radionuclide Migration at the Nevada Test Site: II. Aluminosilicates*. UCRL-TR-208672. U.S. Department of Energy. Lawrence Livermore National Laboratory. Livermore, CA, 2004b.

Zavarin M., Roberts S. K., Hakem N., Sawvel A. M. and Kersting A. B. "Eu(III), Sm(III), Np(V), Pu(V), and Pu(IV) Sorption to Calcite" *Radiochimica Acta*. 93, 93-102, 2005.